UNIVERSITY OF BIRMINGHAM

Polyion complex (PIC) nanoparticles for the targeted and passive delivery of antimicrobial polymers and peptides

by

Ignacio Insua López

A thesis submitted to the

University of Birmingham

for the degree of

DOCTOR OF PHILOSOPHY

School of Chemistry

College of Engineering and Physical Sciences

University of Birmingham

February 2017

Abstract

Antibiotic resistance is a serious worldwide threat. Alternative solutions to the limited pipeline of new antibiotics are urgently needed. Nanotechnology and drug delivery can be used to develop new therapies from old antimicrobials by controlling their distribution in the body.

The goal of this thesis was to investigate the formation and activity of polyion complex (PIC) nanoparticles as vehicles for the delivery of two cationic antibiotics: poly(ethylene imine), used as model to develop these nanomaterials, and the FDA-approved antimicrobial peptide polymyxin B. These antibiotics were combined with two types of polyanions to form PIC particles with distinct antimicrobial properties: 1) Anionic peptides, degradable by bacterial enzymes led to bacteria-targeted nanoparticles; 2) Acidic polymers assembled particles for passive release, which tuned the activity of the antibiotic in the absence of a specific trigger.

All the PIC particles prepared were characterised, and their physiological stability and antimicrobial properties evaluated. To improve the stability and activity of these nanoparticles, several characteristics of their anionic components were optimised: 1) their multivalency, as a function of the peptide's anionic residues and polymer's DP; 2) the acidity of the polymers; and 3) the number of cross-linking residues in the peptides.

This thesis is dedicated to my parents,

for their constant, endless and valuable support over the years.

Esta tesis está dedicada a mis padres,

por su constante, infinito y valioso apoyo durante los años.

“The saddest aspect of life right now is that science gathers knowledge faster than society gathers wisdom.” – Isaac Asimov.

Acknowledgements

I would like to start by thanking my supervisor, Dr Francisco Fernández-Trillo, for giving me the opportunity to work in, and actually start, his group. I have learnt a great deal about science and academic life from Paco, but more importantly, he has been a good counsellor in scientific and personal matters. I will miss your cheer-up sessions over coffee or beer when experiments didn't work.

Big thank you to my two other mentors during these years of PhD: my co-supervisor Dr Anna Peacock, and my microbiology tutor Dr Anne Marie Krachler.

Thank you to the rest of Paco's group, past and present, for creating an enjoyable work atmosphere, specially my UG/PG students (*a.k.a.* minions) Menisha and Marion, for their contribution to this thesis; the rest of minions I have mentored (Maria, Nico, Löic, Louise, Rob, Nada, Greg, Joel and Nathan), for enduring my supervision; Nico, for his coffee-breaks and help with bacterial work; Zelu, for his doses of "constructive" criticism; Adam and Oli, for the good times we had during this time in Birmingham (and Amsterdam); and Daniel, for the commutes to the lab and your help whenever I needed it.

To my brother from another mother, Xavi. This time in Birmingham would have never been the same without you. I don't realise now how much I will miss you, but I know for sure we'll still be good friends wherever we go. Thank you and Mariyuki for the time we lived together.

To my best friend, the person with this strange power that makes my worries disappear when I am with her. The person I have shared this time in Birmingham with. In the distance or presence, she was always there: my girlfriend Laura.

To my family (Papá, Mamá, Noe, Paulita y María), for making me feel like I never left home every time I visit you.

To all other people who have contributed to this thesis, both scientifically and personally: Dr Marie-Christine Jones for access to DLS, the O'Reilly group in Warwick, the analytical technicians in our school (Chi, Peter, Allen and Cécile), my friends in Chemistry: Dr Para, Edgar and Elsa, and to all the "puteros"!

Finally, I would like to acknowledge the editorial work done by the Royal Society of Chemistry and Elsevier on the published work presented in this thesis.

Table of contents

Abbreviations

Δ*lasAB*	*P. aeruginosa*; LasB-knockdown strain
+eV	Positive ion mode
a.k.a.	Also known as
a.u.	Arbitrary units
Ac_2O	Acetic anhydride
AcCN	Acetonitrile
ACF	Autocorrelation function
AFM	Atomic force microscopy
CFU	Colony forming unit
CMetC	Carboxymethyl cellulose
D	Diameter
DCM	Dichloromethane
D_H	Hydroynamic diameter
DIPEA	*N*,*N*-diisopropylethylamine
DLS	Dynamic light scattering
DMEM	Dulbecco's modified eagle medium
DMF	*N*,*N*-Dimethylformamide
DMSO	Dimethylsulfoxide
DOX	Doxorubicin
DP	Degree of polymerisation
DPBS	Dulbecco's phosphate-buffered saline
DTBN	5,5'-dithiobis(2-nitrobenzoic acid)
EDT	1,2-ethanedithiol
EDTA	Ethylenediaminetetraacetic acid
ESI	Electrospray ionisation
Et_2O	Diethylether
EtAcO	Ethyl acetate
FACS	Fluorescence-activated cell sorting
FDA	Food and Drug Administration (USA)
Fmoc	Fluorenylmethyloxycarbonyl
GPC	Gel permeation chromatography
HBTU	*N*,*N*,*N*',*N*'-tetramethyl-*O*-(1*H*-benzotriazol-1-yl)uranium hexafluorophosphate
HEPES	4-(2-hydroxyethyl)piperazine-1-ethanesulfonic acid
HLE	Human leukocyte elastase
HPLC	High performance liquid chromatography
ISO	International Standards Organization (Geneva, Switzerland)
kcps	Kilocounts per second
L/B-PEI	Linear/Branched-poly(ehtylene imine)

LasB	Elastase B from *Pseudomonas aeruginosa*
LB	Luria Bertani (medium)
m/z	Mass/charge ratio
MALDI	Matrix-assisted laser desorption/ionisation
MeOH	Methanol
MS	Mass spectrometry
Mw	Molecular weight
MWCO	Molecular weight cut-off
NMR	Nuclear magnetic resonance
NMVA	*N*-methyl-*N*-vinylacetamide
NNLS	Non-negative least squares
OD	Optical density
PAA	Poly(acrylic acid)
PAH	Poly(allylamine)
PAO1V	*P. aeruginosa*; wild type strain
PBS	Phosphate-buffered saline
PDADMA	Poly(diallyldimethylammonium chloride)
PdI	Polydispersity index
pDNA	Plasmid DNA
PEG	Poly(ethylene glycol)
PIC	Polyion complex
PLL	Poly(L-lysine)
Pol-B	Polymyxin B
PSS	Poly(styrene sulfonate)
PVAm	Poly(vinylamine)
r.f.u	Relative fluorescence units
R_g	Radius of gyration
R_H	Hydrodynamic radius
RP	Reverse phase
SAXS	Small angle X-ray scattering
SC	Succinyl casein
SD	Standard deviation
siRNA	Small interfering RNA
SLS	Static light scattering
^{t}Bu	*Tert*-butyl
TEM	Transmission electron microscopy
TFA	Trifluoroacetic acid
TIPS	Triisopropylsilane
TOF	Time-of-flight
Trt / Trityl	Triphenylmethane
UV-Vis	Ultraviolet-visible

Dynamic Light Scattering (DLS): data acquisition and interpretation

Overview [1,2]

DLS is a particle characterisation technique that correlates the fluctuations in the amount of light scattered by a particle suspension over time with particle size. Colloidal particles undergo Brownian motion as solvent molecules collide into them transferring kinetic energy, thus causing the particles to move in random directions. As such, the intensity of light scattered by a particle suspension will vary with time as particles in Brownian motion exit and enter the illuminated space in the sample (*i.e.* under analysis). As solvent collisions with smaller particles are more efficient, smaller particles undergo faster Brownian motion. On this basis, DLS correlates the frequency of the fluctuations in the light scattered by a particle suspension over time with the diffusion coefficient (*D*) of the particles – the speed at which they move. The calculated value of *D* can then be transformed into a size parameter known as hydrodynamic diameter (D_H) using the Stokes-Einstein equation (*Eq. 1*); where K_B represents Boltzmann's constant, T is the absolute temperature and η is the viscosity of the solution:

$$D = \frac{K_B \, \mathrm{T}}{3 \, \pi \, \eta \, D_H} \qquad (Eq. 1)$$

The D_H of a particle is defined as the diameter of a theoretical sphere that diffuses in the same fashion as the particle under analysis (*i.e.* has the same *D*). DLS therefore gives a theoretical size value for the particles under analysis inferred from the speed at which they diffuse.

The analysis of particle size by DLS offers a rapid, controlled and non-destructive methodology to probe for differences in nanoparticle formulations and their stability. For this reason, it has been used throughout this thesis as first characterisation point for the study of nanoparticles.

It is not the aim of this overview to introduce the fundamentals of DLS, but rather to give a basic understanding of the acquisition and processing of DLS data to guide the discussion below. The reader is referred to specialised literature for more information about DLS.[1-4]

Instrumentation and analysis parameters

All DLS data presented in this thesis was acquired on Zetasizer Nano instruments (Malvern Instruments Ltd.), using either models ZS or ZSP as indicated in the experimental section of each chapter. All samples described in this thesis were analysed under the same conditions regardless of the instrument used: temperature = 37 °C, solvent's viscosity = 0.6687,[5] solvent's refractive index = 1.330,[5] particles' refractive index = 1.450,[6] particles' absorption = 0.001,[6] measuring angle = 173° (non-invasive backscatter), run duration = 60 s, fixed measurement position = 4.65 mm, and automatic attenuation – unless monitoring average scattering intensities (kcps) while studying the enzymatic degradation of nanoparticles, where the attenuator was fixed to the value automatically set by the instrument at the start of the experiments –.

At this stage, it must be noted that NaCl was added to nanoparticle samples for physiological stability experiments, which causes an increase in viscosity that was not accounted for during DLS analysis. The addition of NaCl to a 154 mM concentration should increase the viscosity of the medium by 2.3 %, having a negligible effect on its refractive index (0.15 %).[7] Therefore, and given the inverse correlation between viscosity and D_H in the Stokes-Einstein equation (*Eq. 1*), the actual D_H values measured in the presence of 154 mM NaCl are 2.3% smaller than what is reported in this Thesis. Nevertheless, given that all samples analysed under these conditions have the same error, thus making the data comparable, and since during physiological stability assays we studied stability trends, and not absolute changes in size, the impact of this error in the interpretation of the data presented in this thesis is of little significance.

Data interpretation [2-4]

Three steps are required to obtain a particle's D_H by DLS: i) First, the instrument records the fluctuations in the intensity of light scattered by a particle suspension over time. ii) The instrument then produces an autocorrelation function (ACF), or correlogram, which is a single exponential decay function for monodisperse particles that contains information about their diffusion. iii) Finally, the ACF must be deconvoluted into a diffusion coefficient using an algorithm. Two main types of fits can be used in the deconvolution of ACF curves: Cumulants and non-negative least squares (NNLS) algorithms. Care should be taken when choosing a model for ACF fitting, as each model has its own limitations and may produce misleading results if not suitable for a particular ACF.

The Cumulants algorithm is the ISO recommended interpretation of monomodal particle samples and applies a single exponential fit to the ACF. The D_H extracted by Cumulants is called Z-Average size, and it is the most stable and comparable parameter produced by DLS. The Cumulants fit also produces a width parameter for the size population known as polydispersity index (PdI), which is dimensionless and directly proportional to the broadness of the size distribution. The Cumulants fit is hence the standard for DLS interpretation, but it provides no information about the modality of the size distribution. As such, the Cumulants algorithm assumes a single particle size family, and is therefore unsuitable for the analysis of samples with multiple particle size groups.

On the other hand, NNLS algorithms apply multi-exponential fits to ACFs for the extraction of several size populations, thus giving a more complete picture of the particle size distribution. There is a range of available NNLS algorithms for DLS analysis, all characterised by a different fitting roughness. In practice, the best NNLS algorithm to use will depend on the type of sample, the working range of the DLS instrument, and most importantly the noise-to-signal ratio in the ACF. Regardless of the algorithm, NNLS fits produce a Size-Intensity distribution proportional to the scattering intensity of each particle family, which are Gaussian distributions characterised by a mean size value and a standard deviation.

All the nanoparticles described in this thesis were analysed using Malvern's Zetasizer software,[5] which can simultaneously apply the Cumulants and a NNLS fit to ACF curves. Only Malvern's *General Purpose* algorithm was used as NNLS fit to analyse the particles presented in this thesis, chosen for having an intermediate level of roughness with a moderate estimate of noise, which provides an average resolution. As such, all samples analysed for this work count with both a Z-Average and intensity-weighed mean size, calculated by Cumulants and NNLS *General Purpose* algorithms, respectively (**Figure 1**).

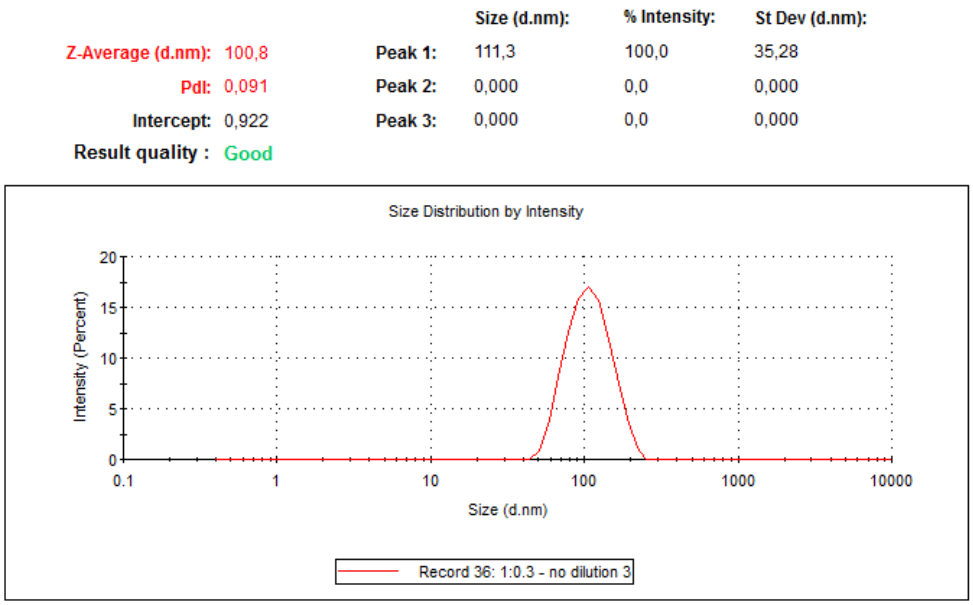

Figure 1 Data obtained by DLS for PIC particles prepared from B-PEI$_{25}$ and **P1$_{SH}$** at a [N:COOH] ratio of 1:0.3 (see Chapter 2, Fig 2a). The mean size of Gaussian distribution found in the Size-Intensity plot and its standard deviation are reported on the top-right area (Peak 1), and were obtained using Malvern's *General Purpose* NNLS algorithm. In addition, the Z-Average size and PdI obtained by Cumulants are also reported on the top-left corner.

At this stage, we must clarify that **all D_H values reported in this thesis correspond to the mean size found in Size-Intensity distributions obtained using Malvern's *General Purpose* NNLS algorithm, and never indicate the Z-Average size of the particles**. The mean Size-Intensity value was chosen over Z-Average to report D_H for the latter being unsuitable for multimodal samples, which appeared during the physiological stability experiments described in this thesis.

For this reason, and to keep the parameters of D_H analysis constant throughout the thesis, Z-Average values were disregarded. **All plots describing particle D_H represent the mean value ± one standard deviation (SD) of the only size population found in their Size-Intensity plots obtained by NNLS *General Purpose* analysis. Additionally, a polydispersity index (PdI) is reported in the supplementary information of each chapter, which does not correspond to that obtained by Cumulants, but was rather obtained by applying the formula below to the SD and mean size obtained by NNLS *General Purpose* fit:**[4]

$$PdI = \left(\frac{SD}{Mean}\right)^2 \qquad (Eq. 2)$$

All PIC nanoparticles reported in this thesis displayed a single Size-Intensity population when analysed by DLS immediately after their preparation. As such, these nanomaterials can be accurately described with their mean size ± SD values obtained through NNLS *General Purpose* analysis. However, during physiological stability assays the nanoparticles increased in size, and in some cases, more than one Size-Intensity population was fitted by the software (*e.g.* Chapter 2, Fig. S11 or Chapter 4, Fig. 3A-B). This evolution of the size of PIC nanoparticles into two or more distinct size populations justifies the choice of NNLS algorithms for DLS analysis.

In Chapters 2 and 3, the relative change in the size of PIC nanoparticles under simulated physiological conditions is reported as a single size value ± error *versus* time (Chapter 2, Fig. 3 and Chapter 3, Fig. 3). The values plotted in these graphs correspond to the average D_H of three DLS measurements performed on the same sample (*i.e.* technical replicates) ± the SD of this average. All the samples studied in these experiments presented a single Size-Intensity population at all times, with the exception of one single sample and time point: $\mathbf{P1_{SH}}$ at a 1:0.3 ratio after 1 hour (Chapter 2, Fig. S11); This sample was represented in Fig. 3 of that same Chapter only considering its larger size population, assuming the

smaller size mode was an intermediate in the process of these nanoparticles becoming larger, as suggested by the disappearance of the smaller population over time (Chapter 2, Fig. S11).

Finally, the reader should also note that **all plots reporting both the D_H and ζ-potential of PIC particles (*e.g.* Figure 2), indicate the values for these two parameters calculated for the same sample, which is denoted by its charge ratio (*e.g.* [N:COOH]) in the X axis.**

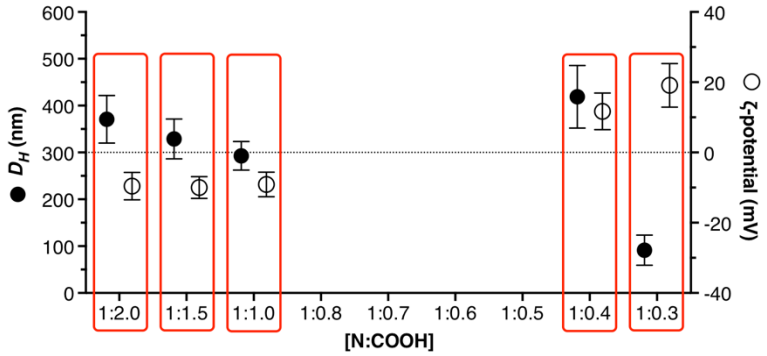

Figure 2 Representation of PIC nanoparticle characterisation for different formulations (*i.e.* [N:COOH] values): The two dots contained inside each rectangle represent the D_H (left axis) and ζ-potential (right axis) of the same sample, denoted by the [N:COOH] value enclosed in the same rectangle. This example was taken from Chapter 3, Fig. 2A.

References and notes

1 Malvern Instruments Ltd., *Dynamic Light Scattering: An Introduction in 30 Minutes*, Technical Note Malvern, 2014.

2 Malvern Instruments Ltd., *Dynamic light scattering - common terms defined*, Whitepaper Malvern, 2014.

3 Malvern Instruments Ltd., *Application of Dynamic Light Scattering (DLS) to Protein Therapeutic Formulations: Principles, Measurements and Analysis - 1. Basic Principles*, Whitepaper Malvern, 2014.

4 Malvern Instruments Ltd., *Application of Dynamic Light Scattering (DLS) to Protein Therapeutic Formulations: Principles, Measurements and Analysis - 3. DLS Deconvolution Algorithms*, Whitepaper Malvern, 2014.

5 The solvent's viscosity and refractive index used for DLS analysis were calculated using the Zetasizer software (v 7.11) by Malvern Instruments Ltd., and were the values obtained for a 5 mM tris(hydroxymethyl)aminomethane (Tris) solution in water at 37 °C.

6 Particles' refractive index and absorption set from the default values given by Malvern's Zetasizer software for protein-based materials.

7 5 mM Tris in water + 154 mM NaCl showed a calculated viscosity of 0.6840 cP and a refractive index of 1.332 at 37 °C according to the Zetasizer software.

CHAPTER 1

Polyion complex (PIC) particles: preparation and biomedical applications

Format: Review article.

Information: I. Insua, A. Wilkinson and F. Fernández-Trillo, *Eur. Polym. J.*, 2016, 81, 198–215. DOI: 10.1016/j.eurpolymj.2016.06.003.

Overview: In this Chapter, we give an introduction to PIC particles covering their composition, their behaviour in solution and the key factors that affect their self-assembly. In addition, the biomedical applications of PIC particles described in the literature are reviewed in the last two sections, gene delivery being the most thoroughly described application due to the prevalence of PIC particles in current gene therapy research, but also covering the delivery of other charged therapeutics such as proteins and antineoplastics.

In this thesis, PIC particles were selected as the ideal nanomaterial to prepare the target antibiotic vehicles, given the simplicity of their preparation and for being a modular system, whose properties can be easily tuned during their assembly by using different polyelectrolyte structures and mixtures. As such, PIC particles are the common theme in all the Chapters of this thesis, so the parameters described in this Chapter that affect their self-assembly and stability help understand and justify the observations described throughout the thesis. Likewise, the explanations given in this Chapter about the affinity and binding between oppositely charged polyelectrolytes guided the modifications of the polyanions explored in this thesis, and thus the optimisation of the initial PIC particles designed.

At the end of this Chapter, the current need for new antimicrobial therapies is introduced, covering the current state of the art in polymer-based antimicrobial nanotechnologies with a focus on PIC nanoparticles, presenting the recent developments and challenges ahead in this area.

Contributions: FFT wrote section 1, II wrote sections 2 and 4 and AW and FFT wrote section 3 of this review. All authors revised the manuscript and contributed to the final version.

European Polymer Journal 81 (2016) 198–215

Contents lists available at ScienceDirect

European Polymer Journal

journal homepage: www.elsevier.com/locate/europolj

Polyion complex (PIC) particles: Preparation and biomedical applications

Ignacio Insua, Andrew Wilkinson, Francisco Fernandez-Trillo *

School of Chemistry, University of Birmingham, B15 2TT, UK

ARTICLE INFO

Article history:
Received 1 April 2016
Received in revised form 1 June 2016
Accepted 3 June 2016
Available online 6 June 2016

ABSTRACT

Oppositely charged polyions can self-assemble in solution to form colloidal polyion complex (PIC) particles. Such nanomaterials can be loaded with charged therapeutics such as DNA, drugs or probes for application as novel nanomedicines and chemical sensors to detect disease markers. A comprehensive discussion of the factors affecting PIC particle self-assembly and their response to physical and chemical stimuli in solution is described herein. Finally, a collection of key examples of polyionic nanoparticles for biomedical applications is discussed to illustrate their behaviour and demonstrate the potential of PIC nanoparticles in medicine.

1. Introduction

Macromolecules carrying multiple charges (*a.k.a.* polyelectrolytes) are ubiquitous in nature and include nucleic acids, proteins or polysaccharides. The presence of these charges often dictates the physical properties of these biopolymers, including their self-assembly or their solubility in physiological environments. More importantly, charge-charge interactions often mediate relevant biological processes, from the package of DNA around histones [1], to the initial adhesion of microbes to surfaces and hosts [2]. It is not surprising then that researchers have tried to imitate these important polyionic interactions to develop synthetic systems that can interact with biology. As such, polyionic complexes (PIC), *a.k.a.* polyelectrolyte complexes (PECs) [3] or interpolyelectrolyte complexes (IPECs) [4], have been investigated as novel platforms to stabilise and deliver drugs [5,6], proteins [7,8] or nucleic acids [9–11].

The morphology of the complexes formed depends on the topology of the polyelectrolytes employed and the way these are assembled. For instance, ionic-hydrophilic block copolymers have been used for the preparation of PIC micelles [12,13] and PIC vesicles (PICsomes) [14], while the sequential assembly of polyelectrolytes on surfaces and colloidal templates has been exploited for the preparation of layer-by-layer films [15] and capsules [16] respectively.

In this review we will focus on the preparation and biomedical applications of PIC particles, formed by the neutralisation of non-stoichiometric mixtures of polyelectrolytes. Other morphologies and their biomedical applications have been extensively reviewed elsewhere and interested readers are encouraged to read that literature [12–17].

2. Self-assembly of PIC nanoparticles

The preparation of PIC particles was first reported by Fuoss and Sadek in the late 1940's as a straightforward turbidimetric study of polyion condensation [18]. Over the last decades, more sophisticated instrumentation has allowed a deeper

* Corresponding author.
E-mail address: f.fernandez-trillo@bham.ac.uk (F. Fernandez-Trillo).

http://dx.doi.org/10.1016/j.eurpolymj.2016.06.003
0014-3057/

understanding of PIC particle assembly. It is now well established that non-stoichiometric mixtures of oppositely charged polyions lead to the formation of PIC particles, which consist of a neutral core entrapping 1:1 mixtures of oppositely charged polymers surrounded by a shell of excess polyion chains (Fig. 1) [19,20]. The charged corona stabilises the coacervate by repelling other PIC particles in solution. In contrast, stoichiometric mixtures of polyions lead to unstable shell-deficient PIC particles, which flocculate due to the hydrophobic attraction between neutral coacervates [21,22].

General models rationalise that PIC formation is primarily based on the electrostatic attraction between oppositely charged polyions [3,18,23,24]. However, it has been demonstrated that the increase in entropy upon counterion release from polyelectrolytes is the main driving force in PIC particle self-assembly [25,26].

PIC particles are often polydisperse systems with diameters comprised between 10 nm and 1 μm. Particle size is usually measured from indirect techniques, mainly static and dynamic light scattering, which maintain the integrity of the nanoparticles in solution. Imaging techniques are often used to support the results from light scattering, but it must be noted that in this case the size of PIC particles can be affected during sample preparation and analysis (especially in the case of drying and staining) [27].

The self-assembly of PIC particles is a reversible process where nanoparticles coexist in equilibrium with free polyions in solution (Fig. 1) [26,28]. This dynamic nature of PIC particles inherently compromises their integrity upon dilution and addition of other charged species, which can cause electrostatic shielding and polyion exchange from these nanomaterials [29]. As a result, the stability of PIC particles can be seriously compromised in biological settings, where high concentrations of small electrolytes and charged proteins can be found [30]. However, PIC particles can be easily stabilised by cross-linking of the polyelectrolyte components, minimising this way the exchange with free polymers in solution (see Section 2.7). On the other hand, the structural damage caused by physiological electrolytes to PIC particles can be beneficial, for example by increasing the permeability of these nanomaterials thus triggering the release of preloaded cargos [31,32].

Finally, it must be highlighted that only certain polyelectrolytes, mixed under suitable conditions, lead to disperse and stable PIC particles. Several factors need to be optimised during the formulation of these nanomaterials, in particular molecular weight, concentration and charge density of the polyelectrolytes, pH and ionic strength of the (aqueous) media, or relative ratio and mixing order of both polyelectrolytes. These parameters are normally interdependent, and have to be optimised in parallel. Often, stable colloidal PIC particles are therefore prepared at high dilution and low ionic strength, with an excess of one of the polyions, ideally with weak ionic groups in one of the polymers and a considerable mismatch in their molecular weights [28,33]. Under different conditions, coacervates separate from solution and coalesce into dense materials known as *compact polyelectrolyte complexes*, which have also shown great potential in some biomedical applications such as synthetic cartilage and enzymatically active biocomposites [34]. To give the reader a deeper understanding of the variables affecting the complexation of polyelectrolytes, we will now describe how these factors affect PIC particle formation, explaining their fundamentals and influence on the characteristics of PIC particles.

2.1. Charge density, molecular weight and topology

The binding properties of polyions to other charged species show a strong dependency on the density and number of charged groups in the polyelectrolyte's structure. As a result of the cooperative nature of polyelectrolyte binding, polymers with higher charge densities show stronger avidity for charged substrates.

The simplest way to increase charge density is to increase the polyelectrolyte's molecular weight. Given the partially entangled conformation of polymers in solution [35], higher molecular weight leads to larger polyelectrolyte cores. This molecular weight dependency was nicely demonstrated by Fischer et al. with a comparative study on the preparation of DNA polyplexes from poly(diallyldimethylammonium chloride) (PDADMA) of four different molecular weights (5–244 KDa) [36]. Higher charge densities, corresponding to higher PDADMA molecular weights, formed more stable polyplexes as indicated by the higher tolerance of complexed DNA to ultrasonication and enzymatic digestion. The authors explained these results from the possible rearrangement of polyions with low charge densities, weakly bound to the polyplex. It has been rationalised that the stability of PIC particles is influenced by the number of charged groups per

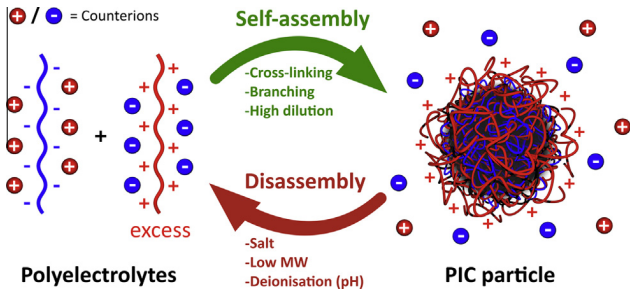

Fig. 1. Representation of polyion self-assembly into PIC nanoparticles and subsequent counterion release (charged spheres). In this example, the excess of polycation in the mixture leads to the formation of a neutral core surrounded by the excess of cationic material.

polymer chain (*i.e.* multivalency), and above an 'upper critical length' polyions can form stable complexes [37]. Nonetheless, a significant difference in the molecular weight of the polyions is often required for the colloidal stability of PIC particles [38].

Alternatively, charge density can be "diluted" by the addition of neutral monomers to the polyelectrolyte. Dautzenberg et al. evaluated the formation and stability of PIC particles from poly(styrene sulfonate) (PSS) and four PDADMA copolymers of comparable molecular weight, which contained increasing amounts (0, 25, 47 and 76%) of neutral *N*-methyl-*N*-vinylacetamide (p(DADMA)-co-(NMVA)) [21]. As the NMVA content in the copolymers increased (lower charge density), bigger particles formed with up to twice the size of those from 100% PDADMA. In addition, the destabilising effect of NaCl on PIC particles was significantly reduced with higher PDADMA contents. Nanoparticles prepared from pure PDADMA remained unaffected by concentrations of NaCl twice higher than those causing particles with weaker charge densities to swell. These results reinforce the direct correlation between charge density and the binding avidity of polyelectrolytes.

The topology of polyelectrolytes can also have a profound effect on their charge density. It is known that branched and dendritic polyelectrolytes show increased binding affinities to charged surfaces compared to their linear analogues [24]. This effect is due to the higher spatial density of monomers in branched structures and thus results in an increase in avidity. As such, branched polyelectrolytes can electrostatically cross-link multiple counter-polyion chains, creating tighter polymeric networks [39]. Dunlap et al. showed that, under the same conditions, whereas linear poly(ethylene imine) (PEI) formed polyplexes of 20–50 nm and left uncomplexed DNA fragments, branched PEI of similar molecular weight fully condensed DNA and formed significantly larger complexes (100–200 nm), probably due to interparticular condensation as a result of its higher binding capacity than linear PEI [40]. The high charge density of branched PEI is responsible for its remarkable capacity to tightly complex DNA, thus setting a benchmark for other transfection agents [41].

Although challenging due to their low charge density, PIC particles have been successfully prepared from small molecules bearing certain motifs that aid the nucleation process. For example, the Behr group studied the self-assembly of small cationic detergents with DNA into lipidic polyplexes or lipoplexes [42]. The authors prepared a dimerisable detergent ($C_{14}CO$) that could condense DNA despite its low charge density, aided by the hydrophobic interactions between aliphatic chains (Fig. 2). After the initial aggregation of $C_{14}CO$ with plasmid DNA, the oxidative dimerisation of this detergent into $(C_{14}CO)_2$ caused a drop in its critical micellar concentration, thus increasing the packing and stability of the complex.

2.2. Polyelectrolyte concentration

Recent work by Starchenco and co-workers rationalised the mechanism of PIC particle self-assembly as the sequential nucleation of polyions as primary molecular complexes, which then aggregate into colloidal complexes (Fig. 3A) [44]. The authors explained this behaviour by the increase in the Debye length of the nanoparticles as they become bigger, thus creating more intense repulsive electrostatics between the "secondary" complexes. In this article, the size of PIC particles from PSS/PDADMA was studied as a function of polyelectrolyte concentration. As shown in Fig. 3B, a linear correlation was found between polymer concentration and complex size, regardless of the molecular weight of PSS used (4.6–1132 KDa). It was observed that, at the lowest concentration of polyions tested (50 μM), particles with a radius of 23 and 50 nm were found when using the lowest and highest PSS molecular weight, respectively. As observed here, the size of PIC particles can be finely tuned by a combination of polyion length and concentration.

Often during the assembly of PIC particles, high concentrations of the starting polyelectrolytes lead to the formation of micron-sized complexes with poor colloidal stability [28,33]. As a consequence, it can be generalised that dispersed PIC nanoparticles can only form in polyelectrolyte mixtures below a critical concentration, above which the system flocculates or precipitates (ca. <1 mg/mL) [3]. The concentration restraints during PIC particle preparation can be a limitation when it is required to prepare concentrated dispersions of these complexes. Nevertheless, Müller et al. showed that it was possible to

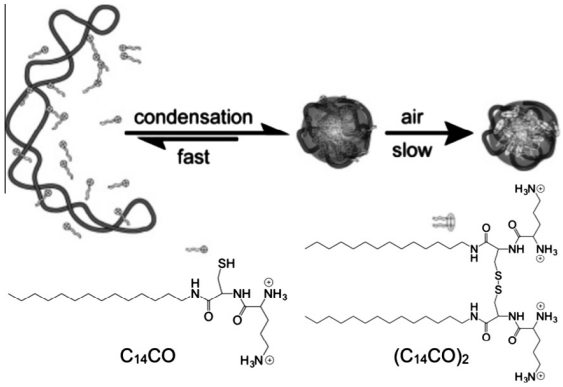

Fig. 2. Plasmid DNA is condensed into monomolecular particles with a thiol-containing cationic detergent. The particles are stabilised by spontaneous oxidation of the detergent. Adapted from Ref. [43].

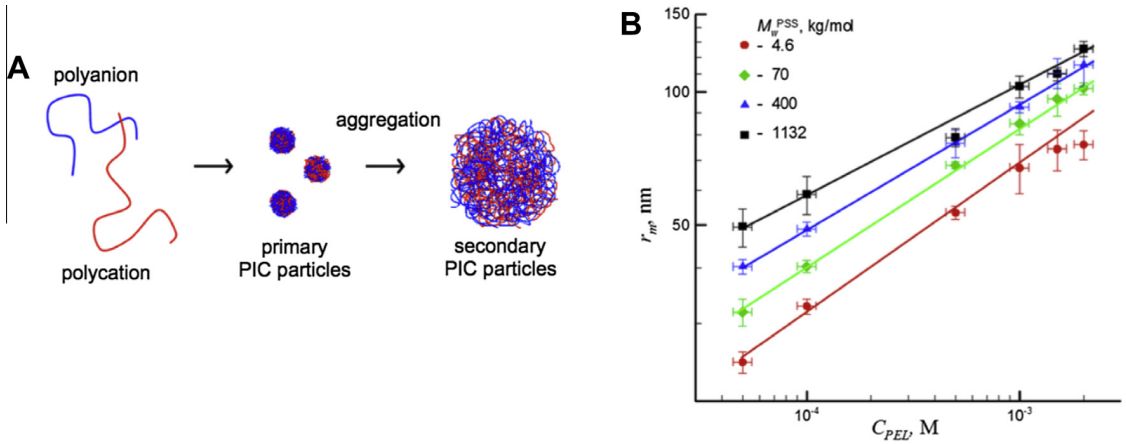

Fig. 3. (A) Schematic presentation of the processes occurring during mixing of polyelectrolytes and formation of PIC particles. (B) PIC particle size (r_m) dependence on polyelectrolyte concentration (C_{PEL}) using different PSS molecular weight with PDADMA. n−/n+ = 1.5. Adapted with permission from Ref. [44].

centrifuge and redisperse PIC particles from PDADMA and poly(maleic acid-*alt*-α-methylstyrene), and that consecutive centrifugation cycles allowed to refine the polydispersity of the complexes, ultimately achieving monomodal size distributions without affecting their initial size during the process [45]. Ouyang et al. found the same effect on PSS/PDADMA complexes of 318 nm in diameter and polydispersity index (PDI) = 0.38 [46]. After one centrifugation, the size of these complexes dropped to 250 nm, showing a much narrower size distribution (PDI = 0.06). After a second centrifugation, particle size was maintained (251 nm) and the PDI could be narrowed further down to 0.04. As such, it is possible to obtain concentrated PIC particles dispersions by centrifugation, although the final morphology of the complexes may be affected.

2.3. pH

From a biomedical perspective, polyelectrolytes can be classified as either weak or strong whether they undergo partial or full ionisation at physiological pH, respectively [35]. As a result, as opposed to strong polyelectrolytes, the charge density of weak polyions will strongly depend on the pH found in different tissues and organelles (4.5–7.4) [47]. Variations within this pH range can lead to significant changes in polyelectrolyte binding and PIC particle stability from the loss or gain of valency (*i.e.* charges per molecule). A good example of this pH-responsive behaviour of polyion complexes was reported by Han et al., where the authors studied a system comprised of a strong poly(allylamine) (PAH) and weak poly(acrylic acid) (PAA) polyelectrolytes at different pHs (Fig. 4) [48]. At low pH (2.0–2.5), PAA is only deprotonated to a small extent so that more swollen and loose complexes are formed as a consequence of its low charge density. However, at higher pH (3.5–5.5) the PAA chains are more ionised, and thus more packed complexes form with PAH from an increase in the number of electrostatic cross-links.

Weak polyions can therefore change their (de)protonation degree and charge density with changes in biological pH. In addition, the different chemical environments and sterics result in a range of different pK_a values for the same monomer in different positions of the polyelectrolyte. This is specially the case for branched polymers and translates into broad

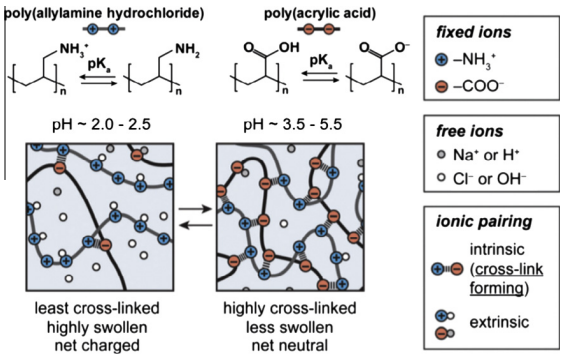

Fig. 4. Illustration of the pH-dependent binding between poly(allylamine hydrochloride) and poly(acrylic acid). Adapted from Ref. [48].

buffering capacity. As such, the changes in pH found in different physiological settings have been exploited to trigger the release of drugs and DNA from PIC particles by changes in the ionisation of the complexing polyions. A classic example of this behaviour is the so-called 'proton sponge' effect displayed by PEI, which allows polyplexes to escape the acidic endosome after cellular uptake (Section 3). For example, branched PEI (B-PEI) displays a wide buffering window from approximately pH 2–10 regardless of its molecular weight (Fig. 5) [49,50], and can therefore buffer the influx of protons into the endosome, ultimately causing an increase in osmotic pressure that causes the organelle to burst and release the polyplex into the cytosol.

Other relevant examples of pH-responsive PIC particles include enzyme [51] and antimicrobial [52] delivery, which are based on nanoparticle disassembly or swelling upon polyion (de)protonation, respectively. As shown by Sui et al., reversible pH-responsive PIC particles can be prepared by blending a weak polyacid (PAA) with a strong polybase (PDADMA) into PDADMA-*co*-PAA [53]. Mixing this copolymer with PSS at pH 4.1 led to the formation of PIC particles, which dissolved at pH > 5.7 due to the deprotonation of PAA in the copolymer and subsequent repulsion between PSS and this partially anionic copolymer. When the solution was acidified again, PIC particles reformed at pH 4.5–5.5, thus demonstrating the reversibility of the process.

Similarly, the pH chosen to self-assemble two polyions can affect their charge densities and therefore the final characteristics of the resulting nanoparticles. Feng et al. studied the effect of pH during PIC particle preparation from carboxymethyl cellulose (CMetC) and poly(vinylamine) (PVAm) in different proportions (*i.e.* mixing ratios) [22]. The authors observed a mixing ratio-dependent effect that originated more positive or negative PIC particles from more acidic or basic pH, respectively (Fig. 6A). This result is consistent with the higher (de)protonation of polyions at higher pH values. However, lower CMetC (weaker polyion) contents led to less pronounced changes in PIC particle charge, as expected from the higher pH-sensitivity of CMetC over PVAm. Size-wise, although an increase in one unit of pH led to a 4-fold increase in size at a 10/20 ratio (CMetC/PVAm), PIC particle size was not very sensitive to changes in pH above their isoelectric points (Fig. 6B).

2.4. Ionic strength

The addition of small electrolytes can aid the self-assembly of PIC particles by shielding the intramolecular charge repulsions of polyions, thus increasing the flexibility of the polymers and their ability to self-assemble [54]. On the other hand, high salt concentrations can lead to strong electrostatic screening between polyelectrolytes and quench the nucleation of PIC particles [3]. Therefore, the ionic strength of the medium must be carefully selected to successfully assemble PIC particles.

To this end, Dautzenberg et al. studied the effect of NaCl during the assembly of PIC particles from PSS and p(DADMA)-co-(NMVA) copolymers (Fig. 7A–C) [21]. In general, the sizes of PIC particles decreased when the polyions were mixed in the presence of higher concentrations of NaCl, probably due to a better packing of more flexible polyelectrolytes. The difference

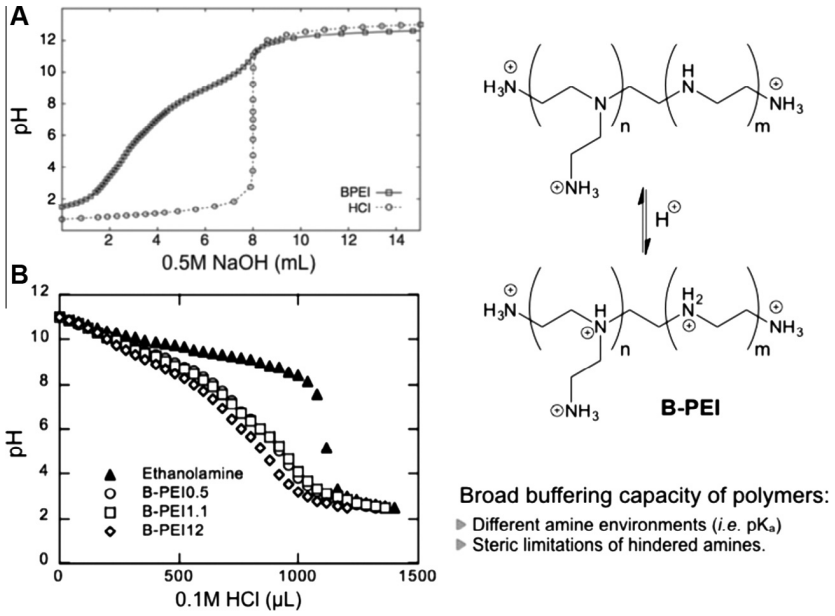

Fig. 5. Buffering capacity of branched poly(ethylene imine) (B-PEI). (A) Titration of 25 KDa B-PEI acidified with HCl (also titrated in the same concentration as control). (B) Potentiometric titration of 0.5, 1.1 and 12 KDa B-PEIs, compared to that of ethanolamine as control for a small monofunctional amine. Adapted from Refs. [49,50].

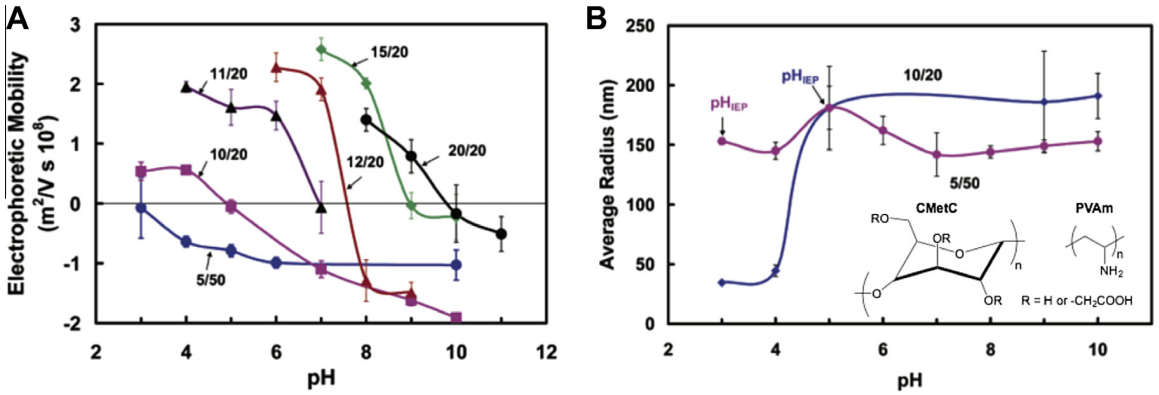

Fig. 6. Effect of pH during preparation of PIC particles from carboxymethyl cellulose (CMetC) and poly(vinylamine) (PVAm) at different mixing ratios (labels: CMetC/PVAm) on their charge (A) and size (B). Adapted from Ref. [22].

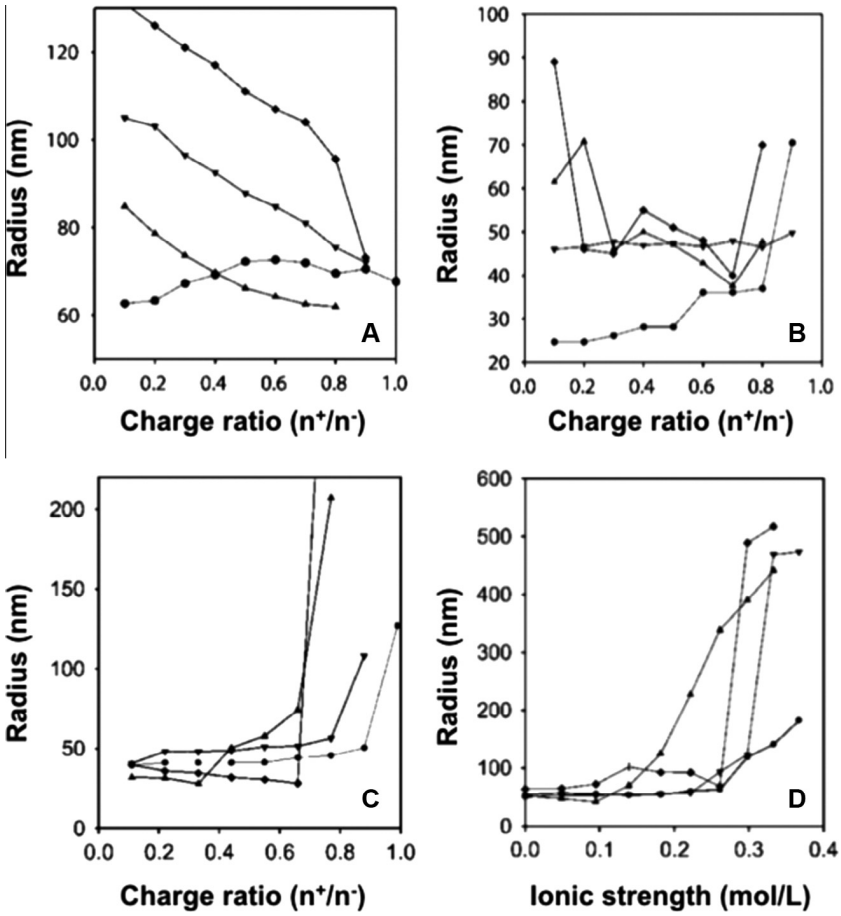

Fig. 7. Size of PIC particles prepared from PSS and p(DADMA)-co-(NMVA) with 100% (●), 75% (▼), 53% (▲) and 24% (◆) of PDADMA (*i.e.* cationic) content in pure water (A), 10 mM (B) and 100 mM (C) NaCl. (D) Swelling of PIC particles prepared in water at increasing NaCl concentrations. Adapted from Ref. [21].

in sizes found between copolymers in water decreased in 10 mM NaCl, ultimately forming particles of the same size at 100 mM NaCl. Overall, polyions with stronger charge densities (*i.e.* lower NMVA content) were more tolerant to NaCl during PIC particle preparation. The authors also observed that particles prepared in pure water swelled from 100 nm up to 1 μm in diameter when exposed to NaCl once assembled (Fig. 7D) [21]. This post-assembly effect of NaCl is due to its infiltration within the core of the complexes, thus neutralising the electrostatic cross-links between polyelectrolytes and subsequently

causing pre-formed complexes to swell. In later work, the same group studied the kinetics and mechanism of salt-induced PIC particle swelling by static light scattering [19]. The authors observed that the increase in size occurs quickly after the addition of NaCl (ca. < 10 min) as a combination of swelling and subsequent aggregation of swollen complexes. Once again, copolymers with higher charge density (*i.e.* PDADMA content) showed improved tolerance to the swelling effect caused by NaCl due to their higher avidity, requiring in some cases twice the concentration of NaCl to swell compared to less charged copolymers (Fig. 7D).

Wang et al. studied the effect of increasing concentrations of KBr on complexes made from PDADMA and PSS [55]. The authors found dense PIC particles in the absence of KBr, which started swelling with increasing amounts of KBr (doping) due to electrostatic shielding. Higher KBr concentrations (ca. 1.5 M) led to disperse colloidal PIC particles, which dissolved above 1.8 M KBr. It is noteworthy that the dilution of concentrated KBr samples with water re-assembled PIC particles, evidencing the reversible nature of salt doping effects. Also the high molecular weights of the polymers used in this study (200 KDa PSS and 400 KDa PDADMA) required higher concentrations of KBr to shield such multivalent interactions and trigger these phase transitions. It is expected that PIC particles made from shorter polyelectrolytes with weaker avidities would require lower doping levels to undergo similar structural changes: *e.g.* particles in Fig. 7D from 66 KDa PSS and 100 KDa PDADMA required only about 0.35 M NaCl to swell twice in size.

Physiological electrolytes may also cause swelling and compromise the functionality and stability of PIC particles in biological settings. If salt-tolerant particles are required, the assembled chains of polyelectrolytes can be covalently cross-linked to maintain the complex together even after the weaker electrostatic forces have been screened with salt [56,57]. Nevertheless, the swelling of PIC particles with small electrolytes has been exploited to release entrapped drugs from within the complex as a result of its increased permeability [31,32].

2.5. Mixing ratio

This is the proportion of positive and negative charges in the polyelectrolytes that are mixed. Mixing ratio not only affects the final size and charge of PIC particles, but also their biological activity. It must be pointed out that, as seen in the previous section, the degree of ionisation of polyelectrolytes is pH-dependent, and therefore the 'effective' mixing ratio will vary for the same mixture of polyions at different pH values [6]. Mixing ratios are denoted regardless of the pH by the fraction or percentage of acidic and basic monomers in solution (*e.g.* 'N:P' ratios are normally used in polyplex formulations to indicate the 'N' number of amine monomers complexed with 'P' phosphate groups in the nucleic acid).

Non-stoichiometric mixing ratios are necessary to give colloidal PIC particles a stabilising shell of the polyion in excess (Fig. 1). On this basis, and as long as other variables such as pH, ionic strength and the polyions structure are kept constant, the absolute value and variations in ζ potential of PIC particles can be predicted from changes in their mixing ratio.

Given the strong dependency of numerous PIC particle systems on mixing ratio, it is always necessary to assess a range of ratios in order to draw consistent and representative conclusions of PIC particle behaviour. The range of mixing ratios usually evaluated varies from very positive-rich mixtures in polyplexes (up to 50 in N:P) [58] whereas other systems just explore values closer to equimolarity (*e.g.* 0.2–1.8 [59] or 0.5–2.0 [4] in n−/n+).

A thorough mixing ratio study was conducted by Drogoz et al., who studied the formation of PIC particles from mixtures of chitosan and dextran sulphate two orders magnitude above and below equimolarity [54]. Firstly, the authors observed that the absolute charge of the complex was that of the polyion in excess. Secondly, the size of the nanoparticles was distributed in three ranges of $[NH_3^+]/[SO_4^-]$ ratios: above 10 (420 nm), between 10 and 1 (250 nm) and below 1 (200 nm) (Fig. 8). The authors explained these three particle sizes from the different nucleation mechanisms taking place in excess of either polymer. At mixing ratios close to neutrality, unstable complexes formed and flocculated. The authors also found that at high excess of either polyion (5-fold and above), more than 70% of this polymer stays uncomplexed free in solution. Comparing this to other examples in the literature, whereas mixing ratio has the same effect on the ζ potential for other PIC

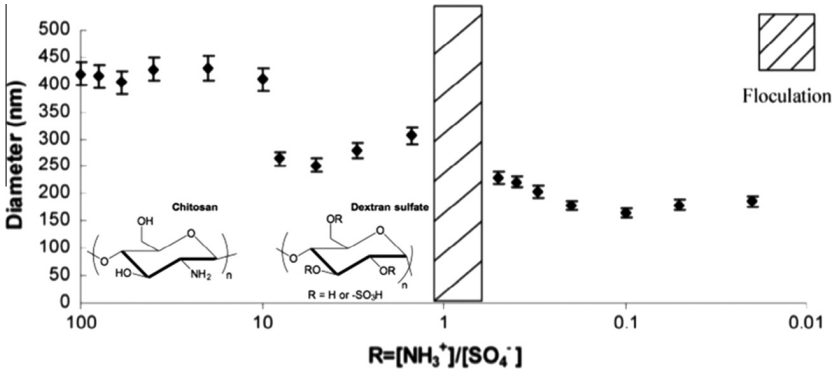

Fig. 8. Average hydrodynamic diameter of PIC particles from chitosan and dextran sulphate at different $[NH_3^+]/[SO_4^-]$ ratios. Adapted from Ref. [54].

particles, its influence in size is not consistent and seems to be influenced by other variables (*e.g.* molecular weight and strength of the polyions) [56,60,61].

2.6. Mixing order

The order in which polyelectrolytes are mixed together will dictate what polyion is in excess at the beginning of the assembling process. It is very important to notice that for the preparation of non-stoichiometric PIC particles, for example at $[n+/n-] = 2$, if the polyanion is added to the polycation there is always an excess of positive charge in the complexes, and repulsive forces between them help maintain colloidal stability. However, if the same polymer mixture is prepared by addition of polycation (in excess) to polyanion, the negative charge of the initial coacervates will reach a neutral value half way through the addition of polycation. As a result, neutral particles can flocculate if polyelectrolytes are mixed in the wrong order. Therefore, it is suggested that the polyion in deficit is added to the one in excess, which results in different nucleation dynamics depending on the nature of the polyelectrolytes [54].

The effects of the order of addition become evident when titrating mixing ratios of polyelectrolytes. For example, Dautzenberg et al. observed that the mixing order of polyelectrolytes not only affected the size of the resulting nanoparticles, causing up to a 2-fold change in size, but also the stability of these complexes to NaCl, probably due to a different packing of the polymers [21]. Other studies in the literature have shown rather dissimilar results, finding either a strong dependency or almost negligible effect on the final morphology of the complexes [3,62]. Discrepancies between studies should be attributed to the effects of other variables (*e.g.* molecular weight and polyion strength), and therefore each case should be evaluated individually.

2.7. PIC particle cross-linking

PIC nanoparticles, in particular those prepared from low molecular weight polymers, partially ionised polyions or when exposed to high salt concentrations, are in equilibrium with free polyions in solution [28]. This equilibrium can be displaced towards the release of polyions from the nanoparticles in circumstances that weaken their electrostatic binding (Fig. 1). As a result, PIC particles can disassemble when diluted or exposed to other charged species [29].

Alternatively, the stability of PIC particles can be greatly enhanced by covalently cross-linking the complexed polyions, thus preventing the detachment of polymer chains from the nanoparticle. In essence, cross-linking works by 'polymerising' polyelectrolyte chains, thus dramatically increasing the overall molecular weight of the polymer and consequently its binding affinity (see Section 2.1.). To this end, polyelectrolytes can be cross-linked during or after particle self-assembly, depending on whether the polyelectrolytes carry cross-linking groups in their structure or if a third component that cross-links pre-assembled complexes is added to the system, respectively.

An illustrative example of PIC particle post-cross-linking was reported by Hsieh et al., who prepared nanoparticles from poly(acrylic acid) (PAA) and poly(L-lysine) (PLL) cross-linked at their core and/or shell [56]. The amines or carboxylic acids found in the shell of these PIC particles were cross-linked using genipin or cystamine, respectively. PLL chains in the core were cross-linked by silica deposition using orthosilicic acid as precursor. These cross-linked particles tolerated up to a 150-fold dilution.

The post-assembly cross-linking of PIC particles has the advantage of not requiring the functionalisation of the polymers with cross-linking groups, thus being applicable to virtually any polyelectrolyte with the suitable functional group (*e.g.* amines or carboxylic acids in the case described). Given the wide application of polyamines in gene delivery, other amine cross-linkers have been applied to polyplex preparation, including glutaraldehyde [63], citric acid [64], carboximidates and *N*-hydroxysuccinimide esters [65].

Alternatively, functionalised polyelectrolytes allow to cross-link the PIC particles as they are formed. By far, the most used group to functionalise and cross-link the polyions in PIC particles are thiols, given their mild reaction conditions and reversible cross-link into disulphide bridges. For example, McKenzie et al. described the preparation of disulphide cross-linked polyplexes from plasmid DNA and PLL decorated with cysteine residues [66]. Polyplexes prepared from a difunctional Cys-PLL-Cys (Fig. 9A) did not show an increase in stability compared to a control PLL of the same molecular weight. However, when three cysteines were incorporated to PLL (Cys-PLL-Cys-PLL-Cys), the resulting nanoparticles tolerated 2.5 times the maximum concentration of salts Cys-PLL-Cys polyplexes could stand. The effect of this extra cysteine can be explained from the cross-linking of PLL into branched structures (Fig. 9B), leading to a higher charge density as discussed in Section 2.1. However, a dramatic increase in particle size was observed for Cys-PLL-Cys-PLL-Cys polyplexes (1.4 μm) compared to the analogous Cys-PLL-Cys (52 nm), an effect the authors attributed to inter-particle cross-linking by the former polyion. When exposed to reducing conditions, the disulphide cross-links in these polyplexes broke, leading to a sudden loss in the PLL's apparent molecular weight and thus triggering the disassembly of the nanoparticle and DNA release (Fig. 9A).

As described, cross-linking short polyions through labile cross-linkers allows the preparation of stimuli-responsive PIC particles, which can breakdown in the presence of agents that degrade such labile linkers, thus causing a sudden loss of charge density and binding affinity between polyions. As so, the reducing conditions found in the cytosol have been exploited to trigger intracellular drug and nucleic acid delivery through the reduction of disulphide cross-linked vehicles [67].

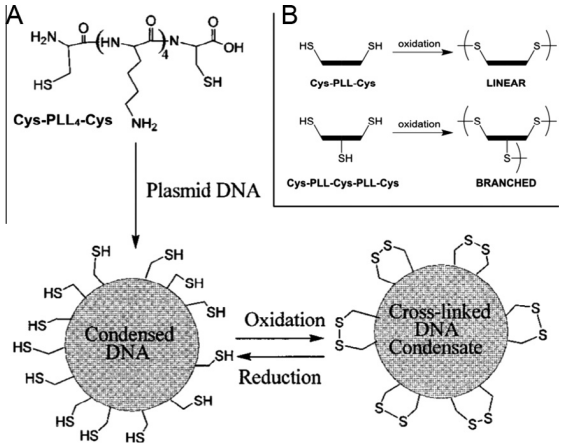

Fig. 9. (A) Formation of cysteine-containing PLL/plasmid DNA nanoparticles. The thiol groups in cysteine (Cys) residues can cross-link PLL molecules through oxidation into disulphide bridges. These cross-links will break under reducing conditions (*e.g.* human cytosol), destabilising the nanoparticles and thus allowing the release of DNA. (B) Schematic representation of the linear and branched cross-linking of these polyplexes that forms upon oxidation of PLL containing two and three Cys residues, respectively. Adapted from Ref. [66].

Our group combined two different labile linkers to develop dual-stimuli-responsive PIC particles, which disassembled in the presence of enzymes and reducing agents [68]. In this system, PEI was complexed with a short anionic peptide bearing two cysteine residues to allow their oxidative cross-linking (**P1$_{SH}$**, Fig. 10), endowing PIC particles with redox-responsive properties like those in the previous example. In addition, the amino acid sequence in those peptides could be specifically degraded by a bacterial elastase (LasB), thus providing another point to cleave the cross-linked peptide chains and ultimately the PIC particles themselves.

As just illustrated, the integrity of the cross-links in such particles is of paramount importance to ensure particle stability, but at the same time, labile cross-links can be designed as sacrificial groups that trigger particle disassembly and release of their cargo when cleaved.

3. Application of PIC particles in gene therapy

Possibly the widest application of PIC particles in biomedicine has been the non-viral delivery of nucleic acids [69–71]. Nucleic acids are strong polyelectrolytes that present one negative charge per nucleotide at neutral pH. This high negative charge density in nucleic acids poses a big challenge when trying to deliver them across negatively charged cellular and nuclear membranes to enable gene therapy (Fig. 11). Moreover, foreign nucleic acids will be readily degraded in biological environments, thus compromising their half-life *in vitro* and *in vivo*. In natural systems, this is often compensated by pro-

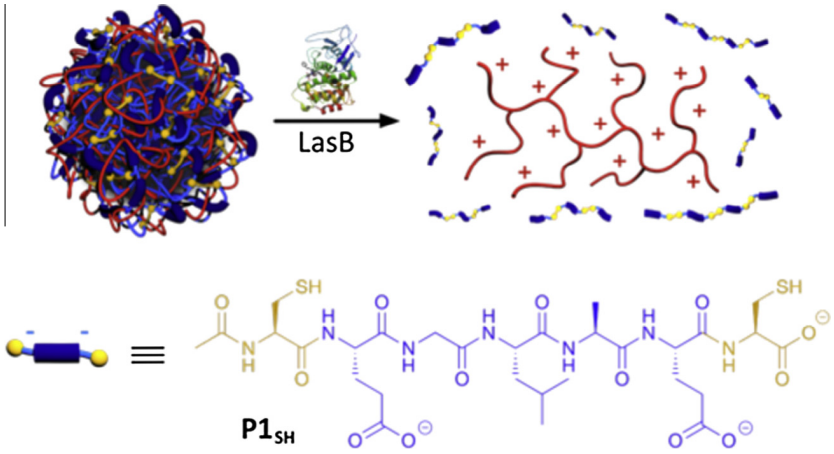

Fig. 10. LasB-triggered disassembly of responsive PIC particles prepared from branched PEI (red polycation) and anionic peptide **P1$_{SH}$**. The cysteine residues allowed peptide cross-link (in yellow) and the -GLA- amino acid sequence in the peptide (dark blue) hydrolysed by LasB. Adapted from Ref. [68]. (For interpretation of the references to colour in this figure legend, the reader is referred to the web version of this article.)

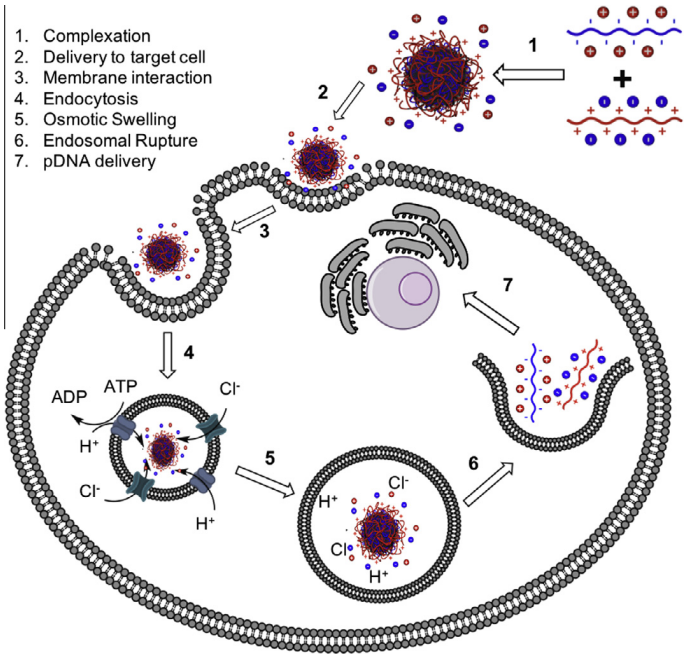

Fig. 11. Schematic representation of the uptake of polyplexes into cells, illustrating the different challenges faced in the development of PIC particles for gene delivery.

tecting the nucleic acids by complexation with positively charged proteins, such as histones [72], or within viral capsids [73]. Not surprisingly, the gene delivery community has placed its attention into mimicking nature's strategy using positively charged polyelectrolytes [69–71].

Often, it has been argued that PIC particles made with nucleic acids and cationic polyelectrolytes, *a.k.a.* polyplexes, can address some of the limitations observed in viral gene delivery (*i.e.* immunogenicity and scalability). However, as will be explained in the following sections, synthetic polyplexes developed so far for non-viral delivery have been found to have separate issues on their own that need to be overcome including stability, toxicity, cellular uptake, endosomal escape and for nucleic acids, delivery to the nuclei.

3.1. Toxicity

Most of the polymers employed in non-viral gene delivery are strong cationic polyelectrolytes, such as PEI, PLL or chitosan. However, it has been long established that most cationic polymers are cytotoxic and cause damage to cells [74,75]. The mechanism for this toxicity though is still widely debated. PEI and other polycations can cause disruption of lipidic bilayers. This is thought to be driven by electrostatic (and possibly hydrophobic) interactions between the negatively charged lipidic membrane and these polyelectrolytes, which often results in depolarisation of the membrane and the formation of pores [76]. This is further evidenced by the release of cytosolic contents such as lactate dehydrogenase [77].

Yet it is also postulated that cationic polyelectrolytes (*i.e.* PEI) can trigger cell apoptosis [78] by release of cytochrome *c* from mitochondria upon intracellular interaction of the polymer with organelles. A similar interaction may be expected here where interaction of PEI with the anionic organelle membrane leads to pore formation and release of the organelle contents [79]. Even if these two mechanisms are working in isolation or cooperatively towards cell death, this toxicity does need to be considered in the future development of PIC particles for gene delivery.

Several strategies have been reported to minimise the toxicity of these polyplexes. For instance, Zhao et al. found that inclusion of chitosan in a PEI/DNA complex significantly reduced the toxicity when compared to the PEI/DNA complex alone [58]. The authors argued that this decrease in cytotoxicity was related to the lower toxicity of chitosan, due to its increased steric hindrance and charge shielding ability.

The simplest way to reduce toxicity of cationic polymers though is reducing the molecular weight of the polyelectrolyte used [74,80]. In depth studies have demonstrated that both PEI and PLL have lower toxicity when the molecular weight is reduced [77,80]. However, as mentioned in the previous section, reducing the molecular weight of the polyelectrolytes has a dramatic effect on the stability of the PIC particles formed. With gene delivery, this is often translated into a lower transfection efficiency [81]. As such, much work has focused in the application of cross-linkers that can reversibly increase the polyelectrolyte molecular weight (Section 2.7) [82].

Disulphide formation has often been the preferred method of cross-linking. Of relevance to the delivery of nucleic acids is the ability of these cross-linkers to be cleaved in the presence of reducing media. This is what happens upon entry into the cell, where the concentration of glutathione is increased up to 100-fold when compared to the extracellular environment [83]. Using this strategy, transfection efficiencies with cross-linked 1.8 KDa PEI are equivalent to that of PIC particles made with 25 KDa PEI [84].

It was thought until recently that dendritic polymers could have reduced toxicity compared to linear analogues [85,86]. However a comprehensive study had not been completed on a comparison of the toxicities of linear vs. dendritic PLL. Klok et al. found that dendritic equivalents of PLL and hyper-branched versions have improved transfection efficiencies compared to their linear analogues (Fig. 12) [87]. However, when carrying out a toxicity study it was found that dendritic and hyper-branched PLL has greater cytotoxicity compared to an equivalently sized linear analogue [88]. The key factors that were highlighted for this increase in cytotoxicity were osmotic shock and cell membrane damage. Osmotic shock causes initial disruption to cells which leads to a marked decrease in EC_{50} values for dendritic and hyper-branched structures. Whilst the membrane disruption characteristics show that the dendritic and hyper-branched structures also cause cell apoptosis due to their interaction with mitochondria which leads to the release of cytochrome *c* as discussed previously [78]. What is interesting to note for the studies by Kadlecova is that although there is increased cytotoxicity seen for both the dendritic and hyper-branched forms of PLL, the hyper-branched structure is much simpler in its synthesis however, and has almost identical effects in terms of toxicity and transfection.

Finally, it is worth mentioning that conjugation of PEG to one of the polyelectrolytes is another strategy to minimise toxicity of the polyplexes. This strategy results in the formation of PIC micelles [12,13], which are stabilised by a PEGylated corona. It is thought that the reduction in toxicity is achieved thanks to the formation of a hydration shell around the polymer reducing interactions with the membrane during delivery [89,90]. This strategy has been used successfully, for example when coupled to PEI, to reduce the toxicity of the polyplexes used for *in vitro* delivery studies [91,92]. Further examples can be found in specialised reviews [12,13,93].

3.2. Transfection efficiency

The other key factor to consider when developing a non-viral gene delivery vehicle is transfection efficiency. How efficiently a gene is expressed (or knocked-down for small interfering RNA) is normally a consequence of several factors, including circulation half-life, uptake, endosomal escape and transfer to the nuclei in the case of plasmid DNA [94,95]. Representative examples of the effect of these factors over transfection efficiency will be described in the next sections.

3.2.1. Circulation half-life

As mentioned earlier, nucleic acids when introduced in biological environment (*i.e.* the body or serum) have a very poor circulation half-life. This is because nucleic acids are quickly degraded by extracellular nucleases, which are responsible for the elimination of any foreign genetic material [96]. Complexation of these nucleic acids in polyplexes is thus the first step to improve their circulation half-life. Normally, polycations are added in excess and nucleic acids are therefore contained within the neutral core, protected this way by the cationic corona from the action of these nucleases.

However, as described in the first section, the stability of the formed polyplexes would strongly depend on several factors. Assuming that parameters such as concentration, pH and ionic strength can be maintained constant when comparing different polyelectrolytes in the same application, factors such as polyelectrolyte molecular weight and topology dictate the stability of the formed polyplexes. This is often the case when comparing pDNA (normally over one thousand base pairs) to oligonucleotides such as siRNA, which have a significantly smaller size (20–25 base pairs). This was nicely illustrated by

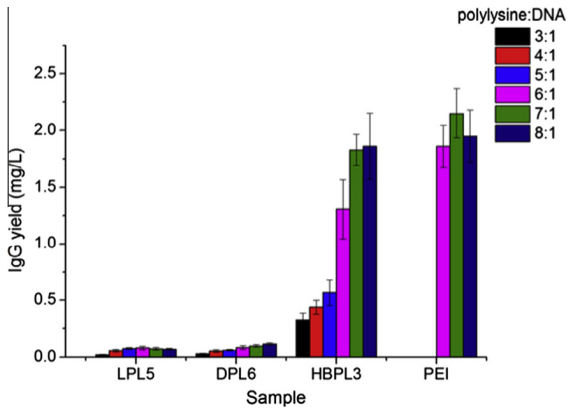

Fig. 12. Comparison of the percentage of eGFP positive cells obtained after 24 h transfection with polylysine analogues of comparable molecular weight. Reproduced from [87].

Seymour et al. with their reducible polycation-based system [97]. While a weight ratio of 5:1 (N:P 1.9:1) was enough to achieve complete retention of pDNA in an agarose gel, weight ratios of up to 20 (N:P 7.5:1) were insufficient to fully conjugate all of the siRNA employed. As expected, polyplex formation in the absence of other salts, resulted in full conjugation of the siRNA with the 20:1 weight ratios, highlighting once again the role of ionic strength in the formation and stability of PIC particles.

Another explanation for the reduced half-life of polyplexes is opsonisation, whereby soluble proteins (opsonins) bind to the surface of complexes leading to their targeted destruction through phagocytosis and subsequent removal from circulation [98]. This process is thought to occur due to the non-specific binding of serum proteins to the positively charged polymer [99].

It is commonly understood that circulation half-life of drugs in the body can be improved through the attachment of hydrophilic residues [100]. Again, in gene delivery this is often achieved through the introduction of PEG residues within the polymeric structure [12,13,89,93]. Kissel et al. evaluated the effect of PEGylation on the pharmacokinetic study carried *in vivo* of PEI polyplexes [101]. Less than 1%/mL of the injected dose (ID) was detected after 2 hours, following injection of polyplexes containing 1.5 μg of pDNA. However, over 20% was still in blood when these polyplexes were PEGylated (Fig. 13).

3.2.2. Uptake

To be transfected, polyplexes have to be efficiently taken up by the cell. This is normally facilitated by the excess of positive charge in the corona of the polyplex. This has been demonstrated for instance using PEI [102], where transfection efficiency was increased with increasing amount of PEI (*i.e.* N/P ratios) (Fig. 14). However, increasing PEI content in the PIC particle also resulted in an increase in cytotoxicity, and thus transfection efficiency eventually was compromised.

Alternatively targeting ligands, that are recognised by the cell surface thus promoting binding and endocytosis of the polyplexes, can be employed to improve transfection efficiency. For instance, Behr and co-workers demonstrated that the use of glycosylated or RGD PEI derivatives, resulted in higher transfection efficiencies when compared to polyplexes prepared with "pristine" PEI [103]. Typically, transfection efficiencies increased by 1–2 orders of magnitude for the targeted PIC particles. Other targeting ligands such as antibodies, folic acid or prostaglandins have been [104] or could be employed [105] in the development of targeted polyplexes.

3.2.3. Endosomal escape

One of the key barriers that polyplexes need to overcome to mediate efficient transfection is the endosome. Uptake normally results in polyplexes trapped within the endosome, where the cell will try to either digest them or recycle the contents [106]. However, nucleic acids need to be transported into the cytosol, where they can carry out their function (*e.g.* siRNA) or be further trafficked into the nuclei (pDNA).

Part of the reason why PEI has garnered more interest than other polycations is because of its inherent ability to act as a buffer within the endosome (Fig. 5), causing osmotic swelling and potential leakage of the endosome contents ('The proton sponge effect') [107]. Behr et al. hypothesised that the reason for endosomal rupture is the protonation of the amine groups in PEI which subsequently leads to an influx of Cl^- counterions and water. It is known that protons can be pumped against the electrochemical gradient that is formed due to the presence of ATPase V type pumps, which helps support this hypothesis [108]. This influx then leads to osmotic swelling, eventually rupturing the endosome.

However, there is still debate as to whether this is the method for endosomal release. Benjaminsen et al. recently found that PEI complexes reach lysosomes to a high extent, but do not cause a change in lysosomal pH [49]. Instead Benjaminsen states that the failure of the 'proton sponge model' is that the swelling caused by this process would not cause rupture. This opinion directly contradicts computational calculations that have been made which support the proton sponge effect

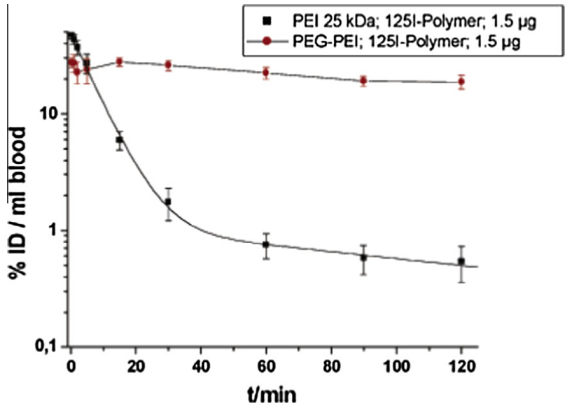

Fig. 13. Pharmacokinetic study showing the effect of PEGylation on circulation half-life as measured by radioactive isotopes ^{125}I. Reproduced from [101].

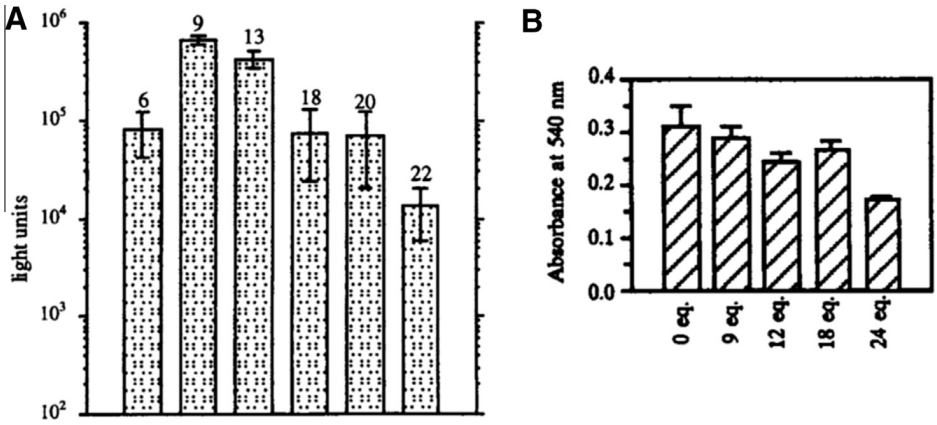

Fig. 14. Transfection efficiency (A) of PEI/pDNA increases with increasing equivalents of PEI, and has its maximum at 9–13.5 equivalents when toxicity towards 3T3 cells (B) starts to be apparent. Reproduced from [102].

[109,110]. Here it has been modelled that osmotic swelling is highly dependent on polymer pK_a as protonation needs to be caused by entry into the endosome.

In line with Benjaminsen's observations, some have argued that the sponge effect should result in an increase in pH [111]. However this doesn't have to be the case because if enough ATP is present in the cytosol, the lysosome could counteract PEI buffering with the influx of more protons. Even if the pH is not changed, osmotic swelling should occur upon the recruitment of protons to neutralise the endosomal pH. An alternative explanation to the proton sponge effect is that complexes are released from lysosomes through small membrane damage, and that the lysosome in fact stays intact [112]. Overall, whatever the actual mechanism of this 'sponge effect' polymers with high buffering capacity, such as PEI have a beneficial effect on endosomal escape.

Other common polycations such as PLL lack this ability to facilitate endosomal escape [113]. One way of addressing this issue is through the introduction of lysosomotropic reagents such as chloroquine to DNA polyplexes [114]. This method has successfully increased the transfection efficiency of PLL based delivery systems [115,116]. However, it has been found that these lysosomotropic reagents are also toxic [117], possibly due to the increased membrane permeabilisation that they cause [118]. As such, this method of delivery is limited in its application.

An alternative strategy to improve endosomal escape is through the introduction of histidine residues to the polymer [119]. It is thought that histidine can successfully increase transfection efficiency acting again as a proton sponge within the polyplex. This is due to the imidazole present in histidine that has a pK_a of ~6 meaning that in slightly acidic media of the endosome it is will become protonated. Evidence for the success of this process can be seen through its escape from negatively charged liposomes in acidic media [120].

Niidome et al. employed this strategy to prepare novel PLL dendrimers. While no beneficial effect was observed for histidine capped-PLL polyplexes prepared at neutral pH, a significant increase in their transfection efficiency was observed when the histidine containing polyplexes where prepared at pH 5. The authors demonstrated that the latter polyplexes were more stable upon incubation in buffer, demonstrating the role of histidine protonation in polyplex formation.

4. Other biomedical applications of PIC particles

While gene delivery has been possibly the field where PIC particles have made the biggest impact, there are other areas where these particles have had a significant contribution [17]. In this section we will describe representative examples of the application of PIC particles for the encapsulation and delivery of proteins and small molecules. Interested readers are referred to specialised reviews [5–8].

Proteins and polysaccharides are other biomacromolecules that often present multiple charges in their backbone. Chitosan, alginate or hyaluronic acid are charged polysaccharides that have been commonly employed as biocompatible polyelectrolytes in the formulation of PIC particles [121]. They often play a passive/structural role, although their enzymatic degradation has been exploited to trigger the release of encapsulated materials [122]. Proteins however tend to have an active role and researchers have been interested in the application of PIC particles to protect and deliver 'functional' proteins such as enzymes [51]. When compared to polysaccharides and nucleic acids, proteins normally present a lower density of charges. Moreover, the presence of positively and negatively charged residues complicates things further and the overall charge of the protein will depend on their isoelectric point and the pH at which the formulation has to be prepared.

A good example of the challenges in the preparation of PIC particles from functional proteins has been described by Giannotti et al., who prepared PIC particles from *N*-trimethyl chitosan and the anionic lysosomal enzyme α-galactosidase A (α-GalA) [51]. These complexes only formed at pH values between 7.3 and 8.0, whereas no particles formed at pH

4.5–5.5, as expected from the neutralisation of α-GalA at pH values close to its isoelectric point (pI ~ 5.7). Similarly, these nanoparticles disassembled at acidic pH, which could be exploited to trigger enzyme release inside the lysosomes, where the authors found these complexes are accumulated *in vitro*. Although a fair 62% of the initial activity of α-GalA was retained after complexation into PIC particles, there is still room for improving this result and develop complexes that do not affect the complexed enzyme and maintain its full activity.

More challenging is the encapsulation of small peptides, which very often have few charge residues and thus weak charge densities, making their complexation into PIC particles particularly unfavourable (see Section 2.1). This is the case for insulin, whose molecular weight is almost 15 times smaller than that of the enzyme α-GalA discussed above. Despite this intrinsic limitation, Jintapattanakit et al. complexed acidic insulin with *N*-trimethyl chitosan into PIC particles, which they evaluated as potential vehicles for the oral delivery of insulin [123]. The oral administration of peptides is limited by their degradation by endogenous proteases. However, the authors found that the stability of free insulin to digestion by trypsin, used as a model gastric protease, was almost doubled when the peptide was complexed inside PIC particles. However, a recent report highlights how despite increasing the stability to proteases, it is the release and subsequent absorption of insulin in the gastrointestinal tract that currently limits the efficacy of PIC particles for this application [124]. Alternative ways of stabilising and administering such complexes must be explored to circumvent this limitation.

The complexation of short charged peptides with very few charges can be facilitated by the addition of cross-linkers, which allow peptide polymerisation and thus increase their binding affinity (Section 2.7). Our group has recently exploited this strategy for the targeted delivery of antimicrobial PEI (Fig. 10) [68]. Incorporation of cysteine residues into a short peptide sequence allowed self-assembly with as little as three negative charges per peptide, otherwise not possible. The peptides were designed to incorporate a short sequence that was cleavable by *Pseudomonas aeruginosa*'s elastase. When these nanoparticles were exposed to the bacterial elastase, the cross-linked peptides were hydrolysed, reducing this way charge density, thus causing particles to disassemble and release the PEI. PIC particles were stable in the absence of this bacterial elastase, and were not able to elicit an antimicrobial effect on a *P. aeruginosa* mutant that was unable to produce this enzyme.

More challenging is the complexation of singly charged molecules such as the chemotherapeutic doxorubicin (DOX) that presents a single amine group in its structure. Hsieh et al. prepared DOX-loaded PIC particle system from PAA/PLL blends, cross-linking the amines in PLL with genipin [56]. In this paper, the authors illustrate how the release kinetics of DOX (or virtually any loaded drug) could be tuned by changing the degree of cross-linking, thus changing the permeability of the nanoparticles. In addition, the weak polyelectrolyte PAA endowed PIC particles with pH-responsive behaviour, accelerating the release of DOX under acidic conditions.

Alternatively, PIC particles can have a "passive" role in the delivery of small molecules, where electrostatic interactions between the polyelectrolytes and the drug to be delivered do not play a role in the encapsulation. For example, non-ionic chemotherapeutic paclitaxel has been encapsulated into the hydrophobic core of PIC particles prepared in this case from hyaluronic acid and styrylpyridinium [125]. The UV cross-linking of styrylpyridinium in the core stabilised the assembled particle, which was then loaded with paclitaxel. High cellular uptake and sustained drug release were achieved from these nanoparticles, proving the utility of PIC particles as vehicles for non-charged drugs as well.

5. Conclusions and outlook

This review gives an overview of the preparation and biomedical applications of PIC particles. A comprehensive description of the factors affecting PIC particle self-assembly has been included: Here, we highlight the effect of polyelectrolyte molecular weight, concentration and charge density, pH and ionic strength of the (aqueous) media, or relative ratio and mixing order of both polyelectrolytes, in particle preparation and stability. Understanding how to optimise PIC particle preparation and stability is of key importance for the development of biomedical application of these nanomaterials. Representative examples of their application in gene, protein and small molecule delivery have been included to illustrate the particular challenges faced in these applications, in particular the issues surrounding toxicity and transfection efficiency in gene delivery. Selected examples of the use of targeted and responsive delivery systems have been included, which highlight how polymer synthesis and characterisation can allow the field of PIC particles, as well as other polyelectrolyte complex nanomaterials, to eventually develop truly mimics of natural delivery systems.

Acknowledgements

F. F-T. thanks the University of Birmingham for the John Evans Fellowship and the Wellcome Trust (177ISSFPP) for funding. II and AW thank the University of Birmingham for PhD studentships.

References

[1] K. Luger, A.W. Mäder, R.K. Richmond, D.F. Sargent, T.J. Richmond, Crystal structure of the nucleosome core particle at 2.8 A resolution, Nature 389 (1997) 251–260, http://dx.doi.org/10.1038/38444.
[2] A.M. Krachler, K. Orth, Targeting the bacteria-host interface: strategies in anti-adhesion therapy, Virulence 4 (2013) 284–294, http://dx.doi.org/10.4161/viru.24606.
[3] H. Dautzenberg, Polyelectrolyte complex formation in highly aggregating systems. 1. Effect of salt: polyelectrolyte complex formation in the presence of NaCl, Macromolecules 30 (1997) 7810–7815, http://dx.doi.org/10.1021/ma970803f.

[4] E.S. Dragan, S. Schwarz, Polyelectrolyte complexes. VI. Polycation structure, polyanion molar mass, and polyion concentration effects on complex nanoparticles based on poly(sodium 2-acrylamido-2-methylpropanesulfonate), J. Polym. Sci., Part A: Polym. Chem. 42 (2004) 2495–2505, http://dx.doi.org/10.1002/pola.20110.
[5] V. Vergaro, F. Scarlino, C. Bellomo, R. Rinaldi, D. Vergara, M. Maffia, et al, Drug-loaded polyelectrolyte microcapsules for sustained targeting of cancer cells, Adv. Drug Delivery Rev. 63 (2011) 847–864, http://dx.doi.org/10.1016/j.addr.2011.05.007.
[6] M. Müller, Sizing, shaping and pharmaceutical applications of polyelectrolyte complex nanoparticles, in: Polyelectrolyte Complexes in the Dispersed and Solid State II, Springer Berlin Heidelberg, Berlin, Heidelberg, 2012, pp. 197–260 10.1007/12_2012_170.
[7] C.L. Cooper, P.L. Dubin, A.B. Kayitmazer, S. Turksen, Polyelectrolyte–protein complexes, Curr. Opin. Colloid Interface Sci. 10 (2005) 52–78, http://dx.doi.org/10.1016/j.cocis.2005.05.007.
[8] A.B. Kayitmazer, D. Seeman, B.B. Minsky, P.L. Dubin, Y. Xu, Protein–polyelectrolyte interactions, Soft Matter 9 (2013) 2553–2583, http://dx.doi.org/10.1039/C2SM27002A.
[9] C.M. Jewell, D.M. Lynn, Multilayered polyelectrolyte assemblies as platforms for the delivery of DNA and other nucleic acid-based therapeutics, Adv. Drug Delivery Rev. 60 (2008) 979–999, http://dx.doi.org/10.1016/j.addr.2008.02.010.
[10] M. Soliman, S. Allen, M.C. Davies, C. Alexander, Responsive polyelectrolyte complexes for triggered release of nucleic acid therapeutics, Chem. Commun. 46 (2010) 5421–5433, http://dx.doi.org/10.1039/c0cc00794c.
[11] H. Yin, R.L. Kanasty, A.A. Eltoukhy, A.J. Vegas, J.R. Dorkin, D.G. Anderson, Non-viral vectors for gene-based therapy, Nat. Rev. Genet. 15 (2014) 541–555, http://dx.doi.org/10.1038/nrg3763.
[12] K. Miyata, R.J. Christie, K. Kataoka, Reactive & functional polymers, React. Funct. Polym. 71 (2011) 227–234, http://dx.doi.org/10.1016/j.reactfunctpolym.2010.10.009.
[13] D.V. Pergushov, A.H.E. Müller, F.H. Schacher, Micellar interpolyelectrolyte complexes, Chem. Soc. Rev. 41 (2012) 6888–6901, http://dx.doi.org/10.1039/C2CS35135H.
[14] A. Kishimura, Development of polyion complex vesicles (PICsomes) from block copolymers for biomedical applications, Polym. J. 45 (2013) 892–897, http://dx.doi.org/10.1038/pj.2013.33.
[15] P.T. Hammond, Building biomedical materials layer-by-layer, Mater Today 15 (2012) 196–206, http://dx.doi.org/10.1016/S1369-7021(12)70090-1.
[16] W. Tong, X. Song, C. Gao, Layer-by-layer assembly of microcapsules and their biomedical applications, Chem. Soc. Rev. 41 (2012) 6103, http://dx.doi.org/10.1039/c2cs35088b.
[17] H. Yoon, E.J. Dell, J.L. Freyer, L.M. Campos, W.-D. Jang, Polymeric supramolecular assemblies based on multivalent ionic interactions for biomedical applications, Polymer 55 (2014) 453–464, http://dx.doi.org/10.1016/j.polymer.2013.12.038.
[18] R.M. Fuoss, H. Sadek, Mutual interaction of polyelectrolytes, Science 110 (1949) 552–554, http://dx.doi.org/10.1126/science.110.2865.552.
[19] H. Dautzenberg, G. Rother, Response of polyelectrolyte complexes to subsequent addition of sodium chloride: time-dependent static light scattering studies, Macromol. Chem. Phys. 205 (2004) 114–121, http://dx.doi.org/10.1002/macp.200350083.
[20] H.-M. Buchhammer, M. Mende, M. Oelmann, Formation of mono-sized polyelectrolyte complex dispersions: effects of polymer structure, concentration and mixing conditions, Colloids Surf. A: Physicochem. Eng. Aspects 218 (2003) 151–159, http://dx.doi.org/10.1016/S0927-7757(02)00582-4.
[21] H. Dautzenberg, W. Jaeger, Effect of charge density on the formation and salt stability of polyelectrolyte complexes, Macromol. Chem. Phys. 203 (2002) 2095–2102, http://dx.doi.org/10.1002/1521-3935(200210)203:14<2095::AID-MACP2095>3.0.CO;2-9.
[22] X. Feng, R. Pelton, M. Leduc, S. Champ, Colloidal complexes from poly(vinyl amine) and carboxymethyl cellulose mixtures, Langmuir 23 (2007) 2970–2976, http://dx.doi.org/10.1021/la0628064.
[23] K. Ueno, H. Ueno, T. Sato, Colloidal polyion complexation from sodium poly(acrylate) and poly(vinyl ammonium) chloride in aqueous solution, Polym. J. 44 (2011) 59–64, http://dx.doi.org/10.1038/pj.2011.65.
[24] I. Szilagyi, G. Trefalt, A. Tiraferri, P. Maroni, M. Borkovec, Polyelectrolyte adsorption, interparticle forces, and colloidal aggregation, Soft Matter 10 (2014) 2479, http://dx.doi.org/10.1039/c3sm52132j.
[25] C.B. Bucur, Z. Sui, J.B. Schlenoff, Ideal mixing in polyelectrolyte complexes and multilayers: entropy driven assembly, J. Am. Chem. Soc. 128 (2006) 13690–13691, http://dx.doi.org/10.1021/ja064532c.
[26] J. Fu, J.B. Schlenoff, Driving forces for oppositely charged polyion association in aqueous solutions: enthalpic, entropic, but not electrostatic, J. Am. Chem. Soc. 138 (2016) 980–990, http://dx.doi.org/10.1021/jacs.5b11878.
[27] J.P. Patterson, M.P. Robin, C. Chassenieux, O. Colombani, R.K. O'Reilly, The analysis of solution self-assembled polymeric nanomaterials, Chem. Soc. Rev. 43 (2014) 2412–2425, http://dx.doi.org/10.1039/c3cs60454c.
[28] A. Zintchenko, G. Rother, H. Dautzenberg, Transition highly aggregated complexes soluble complexes via polyelectrolyte exchange reactions: kinetics, structural changes, and mechanism, Langmuir 19 (2003) 2507–2513, http://dx.doi.org/10.1021/la0265427.
[29] Z. Sui, D. Salloum, J.B. Schlenoff, Effect of molecular weight on the construction of polyelectrolyte multilayers: stripping versus sticking, Langmuir 19 (2003) 2491–2495, http://dx.doi.org/10.1021/la026531d.
[30] P.R. Dash, M.L. Read, L.B. Barrett, M.A. Wolfert, L.W. Seymour, Factors affecting blood clearance and in vivo distribution of polyelectrolyte complexes for gene delivery, Gene Ther. 6 (1999) 643–650, http://dx.doi.org/10.1038/sj.gt.3300843.
[31] H. Cai, C. Ni, L. Zhang, Preparation of complex nano-particles based on alginic acid/poly[(2-dimethylamino) ethyl methacrylate] and a drug vehicle for doxorubicin release controlled by ionic strength, Eur. J. Pharm. Sci. 45 (2012) 43–49, http://dx.doi.org/10.1016/j.ejps.2011.10.020.
[32] W.S. Cheow, K. Hadinoto, Self-assembled amorphous drug-polyelectrolyte nanoparticle complex with enhanced dissolution rate and saturation solubility, J. Colloid Interface Sci. 367 (2012) 518–526, http://dx.doi.org/10.1016/j.jcis.2011.10.011.
[33] M. Mende, H.-M. Buchhammer, S. Schwarz, G. Petzold, W. Jaeger, The stability of polyelectrolyte complex systems of poly(diallydimethyl-ammonium chloride) with different polyanions, Macromol. Symp. 211 (2004) 121–134, http://dx.doi.org/10.1002/masy.200450709.
[34] P. Schaaf, J.B. Schlenoff, Saloplastics: processing compact polyelectrolyte complexes, Adv. Mater. 27 (2015) 2420–2432, http://dx.doi.org/10.1002/adma.201500176.
[35] F. Oosawa, Polyelectrolytes, Marcel Dekker, New York, 1971.
[36] D. Fischer, H. Dautzenberg, K. Kunath, T. Kissel, Poly(diallyldimethylammonium chlorides) and their N-methyl-N-vinylacetamide copolymer-based DNA-polyplexes: role of molecular weight and charge density in complex formation, stability, and in vitro activity, Int. J. Pharm. 280 (2004) 253–269, http://dx.doi.org/10.1016/j.ijpharm.2004.05.018.
[37] N. Karibyants, H. Dautzenberg, Preferential binding with regard to chain length and chemical structure in the reactions of formation of quasi-soluble polyelectrolyte complexes, Langmuir 14 (1998) 4427–4434, http://dx.doi.org/10.1021/la980301a.
[38] A. Shovsky, I. Varga, R. Makuška, P.M. Claesson, Formation and stability of water-soluble, molecular polyelectrolyte complexes: effects of charge density, mixing ratio, and polyelectrolyte concentration, Langmuir 25 (2009) 6113–6121, http://dx.doi.org/10.1021/la804189w.
[39] M. Xu, J.A. Lewis, Phase behavior and rheological properties of polyamine-rich complexes for direct-write assembly, Langmuir 23 (2007) 12752–12759, http://dx.doi.org/10.1021/la702249u.
[40] D.D. Dunlap, A. Maggi, M.R. Soria, L. Monaco, Nanoscopic structure of DNA condensed for gene delivery, Nucleic Acids Res. 25 (1997) 3095–3101, http://dx.doi.org/10.1093/nar/25.15.3095.
[41] K. Nam, S. Jung, J.-P. Nam, S.W. Kim, Poly(ethylenimine) conjugated bioreducible dendrimer for efficient gene delivery, J. Controlled Release 220 (2015) 447–455, http://dx.doi.org/10.1016/j.jconrel.2015.11.005.
[42] E. Dauty, J.-S. Remy, T. Blessing, J.-P. Behr, Dimerizable cationic detergents with a low cmc condense plasmid DNA into nanometric particles and transfect cells in culture, J. Am. Chem. Soc. 123 (2001) 9227–9234, http://dx.doi.org/10.1021/ja015867r.

[43] C. Chittimalla, L. Zammut-Italiano, G. Zuber, J.-P. Behr, Monomolecular DNA nanoparticles for intravenous delivery of genes, J. Am. Chem. Soc. 127 (2005) 11436–11441, http://dx.doi.org/10.1021/ja0522332.
[44] V. Starchenko, M. Müller, N. Lebovka, Sizing of PDADMAC/PSS complex aggregates by polyelectrolyte and salt concentration and PSS molecular weight, J. Phys. Chem. B. 116 (2012) 14961–14967, http://dx.doi.org/10.1021/jp3095243.
[45] M. Müller, B. Keßler, S. Richter, Preparation of monomodal polyelectrolyte complex nanoparticles of PDADMAC/poly(maleic acid-alt-alpha-methylstyrene) by consecutive centrifugation, Langmuir 21 (2005) 7044–7051, http://dx.doi.org/10.1021/la050716d.
[46] W. Ouyang, M. Müller, Monomodal polyelectrolyte complex nanoparticles of PDADMAC/poly(styrenesulfonate): preparation and protein interaction, Macromol. Biosci. 6 (2006) 929–941, http://dx.doi.org/10.1002/mabi.200600143.
[47] N.M. Moore, C.L. Sheppard, T.R. Barbour, S.E. Sakiyama-Elbert, The effect of endosomal escape peptides on in vitro gene delivery of polyethylene glycol-based vehicles, J. Gene Med. 10 (2008) 1134–1149, http://dx.doi.org/10.1002/jgm.1234.
[48] B. Han, D.R. Chery, J. Yin, X.L. Lu, D. Lee, L. Han, Soft Matter, Soft Matter 12 (2016) 1158–1169, http://dx.doi.org/10.1039/C5SM01430A.
[49] R.V. Benjaminsen, M.A. Mattebjerg, J.R. Henriksen, S.M. Moghimi, T.L. Andresen, The possible "proton sponge" effect of polyethylenimine (PEI) does not include change in lysosomal pH, Mol. Ther. 21 (2013) 149–157, http://dx.doi.org/10.1038/mt.2012.185.
[50] K.A. Gibney, I. Sovadinova, A.I. Lopez, M. Urban, Z. Ridgway, G.A. Caputo, et al, Poly(ethylene imine)s as antimicrobial agents with selective activity, Macromol. Biosci. 12 (2012) 1279–1289, http://dx.doi.org/10.1002/mabi.201200052.
[51] M.I. Giannotti, O. Esteban, M. Oliva, M.F. García-Parajo, F. Sanz, PH-Responsive polysaccharide-based polyelectrolyte complexes as nanocarriers for lysosomal delivery of therapeutic proteins, Biomacromolecules 12 (2011) 2524–2533, http://dx.doi.org/10.1021/bm2003384.
[52] F. Bigucci, B. Luppi, T. Cerchiara, M. Sorrenti, G. Bettinetti, L. Rodriguez, et al, Chitosan/pectin polyelectrolyte complexes: selection of suitable preparative conditions for colon-specific delivery of vancomycin, Eur. J. Pharm. Sci. 35 (2008) 435–441, http://dx.doi.org/10.1016/j.ejps.2008.09.004.
[53] Z. Sui, J.A. Jaber, J.B. Schlenoff, Polyelectrolyte complexes with pH-tunable solubility, Macromolecules 39 (2006) 8145–8152, http://dx.doi.org/10.1021/ma061098q.
[54] A. Drogoz, L. David, C. Rochas, A. Domard, T. Delair, Polyelectrolyte complexes from polysaccharides: formation and stoichiometry monitoring, Langmuir 23 (2007) 10950–10958, http://dx.doi.org/10.1021/la7008545.
[55] Q. Wang, J.B. Schlenoff, The polyelectrolyte complex/coacervate continuum, Macromolecules 47 (2014) 3108–3116, http://dx.doi.org/10.1021/ma500500q.
[56] Y.-H. Hsieh, Y.-T. Hsiao, J.-S. Jan, Shell and core cross-linked poly(l-lysine)/poly(acrylic acid) complex micelles, Soft Matter 10 (2014) 9568–9576, http://dx.doi.org/10.1039/C4SM02033B.
[57] J.-G. Piao, J.-J. Yan, M.-Z. Wang, D.-C. Wu, Y.-Z. You, A new method to cross-link a polyplex for enhancing in vivo stability and transfection efficiency, Biomater. Sci. 2 (2014) 390–398, http://dx.doi.org/10.1039/C3BM60204D.
[58] Y.H. Kim, J.H. Park, M. Lee, Y.-H. Kim, T.G. Park, S.W. Kim, Polyethylenimine with acid-labile linkages as a biodegradable gene carrier, J. Controlled Release 103 (2005) 209–219, http://dx.doi.org/10.1016/j.jconrel.2004.11.008.
[59] S. Schwarz, W. Jaeger, S. Bratskaya, J. Bohrisch, T. Schimmel, M. Mende, et al, Formation of polyelectrolyte complexes in a polycarboxybetaine/weak polyanion system, Colloids Surf. A: Physicochem. Eng. Aspects 276 (2006) 65–71, http://dx.doi.org/10.1016/j.colsurfa.2005.10.017.
[60] C. Schatz, J.-M. Lucas, C. Viton, A. Domard, C. Pichot, T. Delair, Formation and properties of positively charged colloids based on polyelectrolyte complexes of biopolymers, Langmuir 20 (2004) 7766–7778, http://dx.doi.org/10.1021/la049460m.
[61] M.A. Hubbe, S.M. Moore, S.Y. Lee, Effects of charge ratios and cationic polymer nature on polyelectrolyte complex deposition onto cellulose, Ind. Eng. Chem. Res. 44 (2005) 3068–3074, http://dx.doi.org/10.1021/ie048902m.
[62] M. Müller, B. Keßler, J. Fröhlich, S. Poeschla, B. Torger, Polyelectrolyte complex nanoparticles of poly(ethyleneimine) and poly(acrylic acid): preparation and applications, Polymers 3 (2011) 762–778, http://dx.doi.org/10.3390/polym3020762.
[63] R.C. Adami, K.G. Rice, Metabolic stability of glutaraldehyde cross-linked peptide DNA condensates, J. Pharm. Sci. 88 (1999) 739–746, http://dx.doi.org/10.1021/js990042p.
[64] M.D. Giron-Gonzalez, R. Salto-Gonzalez, F.J. Lopez-Jaramillo, A. Salinas-Castillo, A.B. Jodar-Reyes, M. Ortega-Muñoz, et al, Polyelectrolyte complexes of low molecular weight PEI and citric acid as efficient and nontoxic vectors for in vitro and in vivo gene delivery, Bioconjugate Chem. 27 (2016) 549–561, http://dx.doi.org/10.1021/acs.bioconjchem.5b00576.
[65] M.A. Gosselin, W. Guo, R.J. Lee, Efficient gene transfer using reversibly cross-linked low molecular weight polyethylenimine, Bioconjugate Chem. 12 (2001) 989–994, http://dx.doi.org/10.1021/bc0100455.
[66] D.L. McKenzie, E. Smiley, K.Y. Kwok, K.G. Rice, Low molecular weight disulfide cross-linking peptides as nonviral gene delivery carriers, Bioconjugate Chem. 11 (2000) 901–909, http://dx.doi.org/10.1021/bc000056i.
[67] R. Cheng, F. Feng, F. Meng, C. Deng, J. Feijen, Z. Zhong, Glutathione-responsive nano-vehicles as a promising platform for targeted intracellular drug and gene delivery, J. Controlled Release 152 (2011) 2–12, http://dx.doi.org/10.1016/j.jconrel.2011.01.030.
[68] I. Insua, E. Liamas, Z. Zhang, A.F.A. Peacock, A.M. Krachler, F. Fernandez-Trillo, Enzyme-responsive polyion complex (PIC) nanoparticles for the targeted delivery of antimicrobial polymers, Polym. Chem. 7 (2016) 2684–2690, http://dx.doi.org/10.1039/C6PY00146G.
[69] T. Hashimoto, T. Yamaoka, Polymeric gene carriers, in: Non-Viral Gene Therapy, Springer-Verlag, Tokyo, 2005, pp. 35–50, http://dx.doi.org/10.1007/4-431-27879-6_4.
[70] T. Wang, J.R. Upponi, V.P. Torchilin, Design of multifunctional non-viral gene vectors to overcome physiological barriers: dilemmas and strategies, Int. J. Pharm. 427 (2012) 3–20, http://dx.doi.org/10.1016/j.ijpharm.2011.07.013.
[71] E. Wagner, Polymers for nucleic acid transfer—an overview, in: L. Huang, D. Liu, E. Wagner (Eds.), Nonviral Vectors for Gene Therapy Lipid- and Polymer-Based Gene Transfer, Academic Press, 2014, pp. 231–261, http://dx.doi.org/10.1016/B978-0-12-800148-6.00008-0.
[72] W. Fischle, Y. Wang, C.D. Allis, Histone and chromatin cross-talk, Curr. Opin. Cell Biol. 15 (2003) 172–183.
[73] J.A. Speir, J.E. Johnson, Nucleic acid packaging in viruses, Curr. Opin. Struct. Biol. 22 (2012) 65–71, http://dx.doi.org/10.1016/j.sbi.2011.11.002.
[74] M.A. Wolfert, P.R. Dash, O. Nazarova, D. Oupický, L.W. Seymour, S. Smart, et al, Polyelectrolyte vectors for gene delivery: influence of cationic polymer on biophysical properties of complexes formed with DNA, Bioconjugate Chem. 10 (1999) 993–1004, http://dx.doi.org/10.1021/bc990025r.
[75] S. Kawakami, Y. Ito, P. Charoensit, F. Yamashita, M. Hashida, Evaluation of proinflammatory cytokine production induced by linear and branched polyethylenimine/plasmid DNA complexes in mice, J. Pharmacol. Exp. Ther. 317 (2006) 1382–1390, http://dx.doi.org/10.1124/jpet.105.100669.
[76] P.R. Leroueil, S.A. Berry, K. Duthie, G. Han, V.M. Rotello, D.Q. McNerny, et al, Wide varieties of cationic nanoparticles induce defects in supported lipid bilayers, Nano Lett. 8 (2008) 420–424, http://dx.doi.org/10.1021/nl0722929.
[77] S. Choksakulnimitr, S. Masuda, H. Tokuda, Y. Takakura, M. Hashida, In-vitro cytotoxicity of macromolecules in different cell-culture systems, J. Controlled Release 34 (1995) 233–241, http://dx.doi.org/10.1016/0168-3659(95)00007-U.
[78] B.I. Florea, C. Meaney, H.E. Junginger, G. Borchard, Transfection efficiency and toxicity of polyethylenimine in differentiated Calu-3 and nondifferentiated COS-1 cell cultures, Aaps Pharmsci. 4 (2002).
[79] S.M. Moghimi, P. Symonds, J.C. Murray, A.C. Hunter, G. Debska, A. Szewczyk, A two-stage poly(ethylenimine)-mediated cytotoxicity: implications for gene transfer/therapy, Mol. Ther. 11 (2005) 990–995, http://dx.doi.org/10.1016/j.mythe.2005.02.010.
[80] D. Fischer, T. Bieber, Y. Li, H.P. Elsässer, T. Kissel, A novel non-viral vector for DNA delivery based on low molecular weight, branched polyethylenimine: effect of molecular weight on transfection efficiency and cytotoxicity, Pharm. Res. 16 (1999) 1273–1279, http://dx.doi.org/10.1023/A:1014861900478.
[81] W.T. Godbey, K.K. Wu, A.G. Mikos, Poly(ethylenimine) and its role in gene delivery, J. Controlled Release 60 (1999) 149–160, http://dx.doi.org/10.1016/S0168-3659(99)00090-5.
[82] C. Alexander, F. Fernandez-Trillo, Bioresponsive polyplexes and micelleplexes, in: C. Alvarez-Lorenzo, A. Concheiro (Eds.), Smart Materials for Drug Delivery, first ed., Royal Society of Chemistry, 2013, pp. 256–282, http://dx.doi.org/10.1039/9781849736800-00256.

[83] A. Meister, M.E. Anderson, Glutathione, Annu. Rev. Biochem. 52 (1983) 711–760, http://dx.doi.org/10.1146/annurev.bi.52.070183.003431.
[84] S. Choi, K.-D. Lee, Enhanced gene delivery using disulfide-crosslinked low molecular weight polyethylenimine with listeriolysin o-polyethylenimine disulfide conjugate, J. Controlled Release 131 (2008) 70–76, http://dx.doi.org/10.1016/j.jconrel.2008.07.007.
[85] M. Ohsaki, T. Okuda, A. Wada, T. Hirayama, T. Niidome, H. Aoyagi, In vitro gene transfection using dendritic poly(L-lysine), Bioconjugate Chem. 13 (2002) 510–517, http://dx.doi.org/10.1021/bc015525a.
[86] T. Okuda, A. Sugiyama, T. Niidome, H. Aoyagi, Characters of dendritic poly((L)-lysine) analogues with the terminal lysines replaced with arginines and histidines as gene carriers in vitro, Biomaterials 25 (2004) 537–544, http://dx.doi.org/10.1016/S0142-9612(03)00542-8.
[87] Z. Kadlecova, Y. Rajendra, M. Matasci, L. Baldi, D.L. Hacker, F.M. Wurm, et al, DNA delivery with hyperbranched polylysine: a comparative study with linear and dendritic polylysine, J. Controlled Release 169 (2013) 276–288, http://dx.doi.org/10.1016/j.jconrel.2013.01.019.
[88] Z. Kadlecova, L. Baldi, D. Hacker, F.M. Wurm, H.-A. Klok, Comparative study on the in vitro cytotoxicity of linear, dendritic, and hyperbranched polylysine analogues, Biomacromolecules 13 (2012) 3127–3137, http://dx.doi.org/10.1021/bm300930j.
[89] F.M. Veronese, G. Pasut, PEGylation, successful approach to drug delivery, Drug Discovery Today 10 (2005) 1451–1458, http://dx.doi.org/10.1016/S1359-6446(05)03575-0.
[90] R.E.B. Fitzsimmons, H. Uludağ, Specific effects of PEGylation on gene delivery efficacy of polyethylenimine: interplay between PEG substitution and N/P ratio, Acta Biomater 8 (2012) 3941–3955, http://dx.doi.org/10.1016/j.actbio.2012.07.015.
[91] S.-J. Sung, S.H. Min, K.Y. Cho, S. Lee, Y.-J. Min, Y.I. Yeom, et al, Effect of polyethylene glycol on gene delivery of polyethylenimine, Biol. Pharm. Bull. 26 (2003) 492–500.
[92] Z. Zhong, J. Feijen, M.C. Lok, W.E. Hennink, L.V. Christensen, J.W. Yockman, et al, Low molecular weight linear polyethylenimine-b-poly(ethylene glycol)-b-polyethylenimine triblock copolymers: synthesis, characterization, and in vitro gene transfer properties, Biomacromolecules 6 (2005) 3440–3448, http://dx.doi.org/10.1021/bm050505n.
[93] Y. Bae, H. Cabral, K. Kataoka, Block copolymer micelles for drug delivery in nanoscience, in: M. Lazzari, G. Liu, S. Lecommandoux (Eds.), Block Copolymers in Nanoscience, Wiley-VCH Verlag GmbH & Co. KGaA, Weinheim, Germany, 2006, pp. 73–89, http://dx.doi.org/10.1002/9783527610570.ch4.
[94] K. Miyata, N. Nishiyama, K. Kataoka, Rational design of smart supramolecular assemblies for gene delivery: chemical challenges in the creation of artificial viruses, Chem. Soc. Rev. 41 (2012) 2562–2574, http://dx.doi.org/10.1039/c1cs15258k.
[95] C.H. Jones, C.-K. Chen, A. Ravikrishnan, S. Rane, B.A. Pfeifer, Overcoming nonviral gene delivery barriers: perspective and future, Mol. Pharmaceutics. 10 (2013) 4082–4098, http://dx.doi.org/10.1021/mp400467x.
[96] M.J. Roberts, M.D. Bentley, J.M. Harris, Chemistry for peptide and protein PEGylation, Adv. Drug Delivery Rev. 54 (2002) 459–476.
[97] M. Stevenson, V. Ramos-Perez, S. Singh, M. Soliman, J.A. Preece, S.S. Briggs, et al, Delivery of siRNA mediated by histidine-containing reducible polycations, J. Controlled Release 130 (2008) 46–56, http://dx.doi.org/10.1016/j.jconrel.2008.05.014.
[98] C. Plank, K. Mechtler, F.C. Szoka, E. Wagner, Activation of the complement system by synthetic DNA complexes: a potential barrier for intravenous gene delivery, Hum. Gene Ther. 7 (1996) 1437–1446, http://dx.doi.org/10.1089/hum.1996.7.12-1437.
[99] M. Ogris, S. Brunner, S. Schüller, R. Kircheis, E. Wagner, PEGylated DNA/transferrin-PEI complexes: reduced interaction with blood components, extended circulation in blood and potential for systemic gene delivery, Gene Ther. 6 (1999) 595–605, http://dx.doi.org/10.1038/sj.gt.3300900.
[100] C. Monfardini, F.M. Veronese, Stabilization of substances in circulation, Bioconjugate Chem. 9 (1998) 418–450, http://dx.doi.org/10.1021/bc970184f.
[101] T. Merdan, K. Kunath, H. Petersen, U. Bakowsky, K.H. Voigt, J. Kopeček, et al, PEGylation of poly(ethylene imine) affects stability of complexes with plasmid DNA under in vivo conditions in a dose-dependent manner after intravenous injection into mice, Bioconjugate Chem. 16 (2005) 785–792, http://dx.doi.org/10.1021/bc049743q.
[102] O. Boussif, F. Lezoualc'h, M.A. Zanta, M.D. Mergny, D. Scherman, B. Demeneix, et al, A versatile vector for gene and oligonucleotide transfer into cells in culture and in vivo: polyethylenimine, Proc. Natl. Acad. Sci. U. S. A. 92 (1995) 7297–7301. http://www.pnas.org/content/92/16/7297.abstract.
[103] L. Poulain, C. Ziller, C.D. Muller, P. Erbacher, T. Bettinger, J.F. Rodier, et al, Ovarian carcinoma cells are effectively transfected by polyethylenimine (PEI) derivatives, Cancer Gene Ther. 7 (2000) 644–652, http://dx.doi.org/10.1038/sj.cgt.7700170.
[104] E. Wagner, Polymers for siRNA delivery: inspired by viruses to be targeted, dynamic, and precise, Acc. Chem. Res. 45 (2012) 1005–1013, http://dx.doi.org/10.1021/ar2002232.
[105] M. Somiya, S. Kuroda, Development of a virus-mimicking nanocarrier for drug delivery systems: the bio-nanocapsule, Adv. Drug Delivery Rev. 95 (2015) 77–89, http://dx.doi.org/10.1016/j.addr.2015.10.003.
[106] T. Taguchi, Emerging roles of recycling endosomes, J. Biochem. 153 (2013) 505–510, http://dx.doi.org/10.1093/jb/mvt034.
[107] J.-P. Behr, The proton sponge: a trick to enter cells the viruses did not exploit, Chimia 51 (1997) 34–36. http://www.ingentaconnect.com/content/scs/chimia/1997/00000051/f0020001/art00026.
[108] A.R. Graves, P.K. Curran, C.L. Smith, J.A. Mindell, The Cl(−)/H(+) antiporter ClC-7 is the primary chloride permeation pathway in lysosomes, Nature 453 (2008) 788–792, http://dx.doi.org/10.1038/nature06907.
[109] E.C. Freeman, L.M. Weiland, W.S. Meng, Modeling the proton sponge hypothesis: examining proton sponge effectiveness for enhancing intracellular gene delivery through multiscale modeling, J. Biomater. Sci. Polym. Ed. 24 (2013) 398–416, http://dx.doi.org/10.1080/09205063.2012.690282.
[110] S. Yang, S. May, Release of cationic polymer-DNA complexes from the endosome: a theoretical investigation of the proton sponge hypothesis, J. Chem. Phys. 129 (2008), http://dx.doi.org/10.1063/1.3009263.
[111] W.T. Godbey, M.A. Barry, P. Saggau, K.K. Wu, A.G. Mikos, Poly(ethylenimine)-mediated transfection: a new paradigm for gene delivery, J. Biomed. Mater. Res. 51 (2000) 321–328, http://dx.doi.org/10.1002/1097-4636(20000905)51:3<321::Aid-Jbm5>3.0.Co;2-R.
[112] T. Bieber, W. Meissner, S. Kostin, A. Niemann, H.P. Elsasser, Intracellular route and transcriptional competence of polyethylenimine-DNA complexes, J. Controlled Release 82 (2002) 441–454, http://dx.doi.org/10.1016/S0168-3659(02)00129-3.
[113] T. Merdan, K. Kunath, D. Fischer, J. Kopeček, T. Kissel, Intracellular processing of poly(ethylene imine)/ribozyme complexes can be observed in living cells by using confocal laser scanning microscopy and inhibitor experiments, Pharm. Res. 19 (2002) 140–146, http://dx.doi.org/10.1023/A:1014212630566.
[114] C.W. Pouton, P. Lucas, B.J. Thomas, A.N. Uduehi, D.A. Milroy, S.H. Moss, Polycation-DNA complexes for gene delivery: a comparison of the biopharmaceutical properties of cationic polypeptides and cationic lipids, J. Controlled Release 53 (1998) 289–299.
[115] K. Ciftci, R.J. Levy, Enhanced plasmid DNA transfection with lysosomotropic agents in cultured fibroblasts, Int. J. Pharm. 218 (2001) 81–92, http://dx.doi.org/10.1016/S0378-5173(01)00623-8.
[116] C. Wong-Baeza, I. Bustos, M. Serna, A. Tescucano, V. Alcantara-Farfan, M. Ibanez, et al, Membrane fusion inducers, chloroquine and spermidine increase lipoplex-mediated gene transfection, Biochem. Biophys. Res. Commun. 396 (2010) 549–554, http://dx.doi.org/10.1016/j.bbrc.2010.04.143.
[117] A.M. Funhoff, C.F. Van Nostrum, M.C. Lok, J.A.W. Kruijtzer, D.J.A. Crommelin, W.E. Hennink, Cationic polymethacrylates with covalently linked membrane destabilizing peptides as gene delivery vectors, J. Controlled Release 101 (2005) 233–246, http://dx.doi.org/10.1016/j.jconrel.2004.06.023.
[118] A.M.V. Giraldo, H. Appelqvist, T. Ederth, K. Ollinger, Lysosomotropic agents: impact on lysosomal membrane permeabilization and cell death, Biochem. Soc. Trans. 42 (2014) 1460–1464, http://dx.doi.org/10.1042/Bst20140145.
[119] C. Pichon, C. Gonçalves, P. Midoux, Histidine-rich peptides and polymers for nucleic acids delivery, Adv. Drug Delivery Rev. 53 (2001) 75–94, http://dx.doi.org/10.1016/S0169-409X(01)00221-6.
[120] P.S. Uster, D.W. DEAMER, pH-dependent fusion of liposomes using titratable polycations, Biochemistry 24 (1985) 1–8.
[121] Y. Luo, Q. Wang, Recent development of chitosan-based polyelectrolyte complexes with natural polysaccharides for drug delivery, Int. J. Biol. Macromol. 64 (2014) 353–367, http://dx.doi.org/10.1016/j.ijbiomac.2013.12.017.
[122] Y. Wu, Y. Long, Q.-L. Li, S. Han, J. Ma, Y.-W. Yang, et al, Layer-by-layer (LBL) self-assembled biohybrid nanomaterials for efficient antibacterial applications, ACS Appl. Mater. Interfaces 7 (2015) 17255–17263, http://dx.doi.org/10.1021/acsami.5b04216.

[123] A. Jintapattanakit, V.B. Junyaprasert, S. Mao, J. Sitterberg, U. Bakowsky, T. Kissel, Peroral delivery of insulin using chitosan derivatives: a comparative study of polyelectrolyte nanocomplexes and nanoparticles, Int. J. Pharm. 342 (2007) 240–249, http://dx.doi.org/10.1016/j.ijpharm.2007.05.015.
[124] K. Al Rubeaan, M. Rafiullah, S. Jayavanth, Oral insulin delivery systems using chitosan-based formulation: a review, Expert Opin. Drug Deliv. 13 (2016) 223–237, http://dx.doi.org/10.1517/17425247.2016.1107543.
[125] Y. Tao, J. Xu, M. Chen, H. Bai, X. Liu, Core cross-linked hyaluronan-styrylpyridinium micelles as a novel carrier for paclitaxel, Carbohydr. Polym. 88 (2012) 118–124, http://dx.doi.org/10.1016/j.carbpol.2011.11.075.

Ignacio Insua graduated from the University of Santiago de Compostela (Spain) in 2012 with a BSc in Pharmacy. He obtained his MSc degree in industry at InKemia-IUCT (Spain) in 2013. Later in 2013, he joined the laboratory of Dr. Francisco Fernandez-Trillo at the University of Birmingham (UK), where he is currently a PhD candidate studying bacteria-responsive nanomaterials and polyelectrolyte self-assembly.

Andrew Wilkinson graduated from the University of Birmingham in 2015 with a MSci in Chemistry. He carried out his final year project in the synthesis and characterisation of polyacetylenes. Since 2015, he has been a PhD student working on the development of novel gene delivery techniques in the groups of Dr Robert Neely and Dr Francisco Fernandez-Trillo.

Francisco Fernandez-Trillo (Paco) is the John Evans Fellow of Nanotechnology at the University of Birmingham (UK) developing Biomedical Applications of Nanomaterials. Prior to this he received his PhD in Organic Chemistry in 2004 from the University of Santiago de Compostela (Spain). This was followed by post-doctoral positions, both in the UK (Durham and Nottingham) and Spain (Santiago de Compostela) working on polymeric nanomaterials for biocatalysis, cell recognition and synthetic biology. Paco now leads a diverse research group working at the interface between organic chemistry, polymer science and nanotechnology.

1.2. Nanotechnology for antimicrobial delivery – PIC nanoparticles

Since the first clinical application of antibiotics in the 1940s, microorganisms have developed different mechanisms to resist and survive the antimicrobial agents we use.[1,2] The development of drug resistance is a normal evolutionary process for microorganisms, but it has been accelerated by the excessive use and misuse of antibiotics.[3] The current situation is very concerning: in developed countries worldwide, over 50% of diagnosed infections by common human pathogens display resistance to commonly used antibiotics,[3] and an estimated impact of €1.5 billion and 25,000 deaths is caused by multidrug-resistant infections in the European Union yearly.[4] In this regard, the limited pipeline of new antibiotics cannot supply new drugs to treat these drug-resistant infections at the required pace,[3,5,6] and alternative methods to tackle infection that go beyond the conventional use of antibiotics are urgently needed.[5] Two main alternative antimicrobial therapies are currently under study:

i) The clinical use of new antimicrobial agents with novel mechanisms of action (*e.g.* antibodies, enzymes, bacteriophages, nucleic acids, *etc.*).[6]
ii) The formulation of 'traditional' antibiotics as nanomaterials for drug delivery, to improve their therapeutic action *via* three complimentary mechanisms:[7-9]
    a. Targeted delivery and accumulation at infected sites for higher efficiency.
    b. Controlled and/or burst release to maintain antimicrobial drug concentrations for long periods, thus maximising treatment efficacy and preventing sub-antimicrobial drug levels to induce antimicrobial resistance.
    c. Reduced toxicity to the host by minimising undesired drug-cell interactions.

This Thesis aims to expand the knowledge on the second approach by exploring PIC nanoparticles as drug delivery vehicles for antimicrobial therapy. Therefore, and to put this Thesis in context, an overview of the recent developments in antimicrobial nanotherapy will be now discussed, pointing out the current challenges in the field and highlighting the examples of PIC nanoparticles for antimicrobial delivery. Given the focus of this Thesis on polymeric PIC nanoparticles, and due to the extensive literature about antimicrobial nanotechnology, only polymer-

based nanomaterials for antibiotic delivery will be covered in this section. The reader is referred to specialised reviews for information about other nanomaterials explored in antimicrobial application.[7-10]

Considering **polymers** in solution as structurally disorganised nanomaterials, these are the simplest platforms that have been exploited for antimicrobial delivery though nanotechnology. The covalent conjugation of polymers to antibiotics has shown to protect these drugs from inactivation by bacterial enzymes (*i.e.* β-lactamases) and thus overcome this mechanism of drug resistance in bacteria.[11] These antibiotic-polymer conjugates showed up to 20 times higher stability to β-lactamases and up to 350 times higher antimicrobial activity against β-lactamase-producing bacteria than pristine penicillin. The linker group connecting the polymer and antibiotic is critical to preserve the activity of the drug,[12] and these polymers can be modified with additional antimicrobial functionalities to work synergistically with the conjugated antibiotics.[11] Alternatively, polymers with pending cationic groups have also shown to electrostatically bind anionic β-lactam antibiotics (*e.g*. penicillin), also protecting them from degradation by bacterial β-lactamases, and releasing the complexed antibiotic in the presence of bacteria by exchange of polymer-drug pairs with anionic bacterial components.[13] This ion-paired conjugate was later improved by incorporation of a boronic acid derivative in the polymer to bind sugars present in bacterial membranes, which translated into a 2 to 3-fold increase in the antimicrobial activity of penicillin with low toxicity to the host.[14] Ferguson *et al*. covalently conjugated the antimicrobial peptide colistin, only used as last resort against multidrug-resistant infections due to its high toxicity,[15] with the polysaccharide dextrin to drive the accumulation of macromolecular colistin-polymer conjugates at infected parts of the body displaying enhanced permeability as a result of inflammation (**Figure 15**).[16] Once accumulated in the infected area, dextrin can be broken down by endogenous amylase to release and trigger the antimicrobial activity of colistin. Not only this drug-polymer system displayed comparable antimicrobial activity to that of the free drug, but also its *in vivo* evaluation on a murine model revealed prolonged circulation times

and decreased toxicity for the polymer-conjugated colistin, showing great potential for a clinical translation.

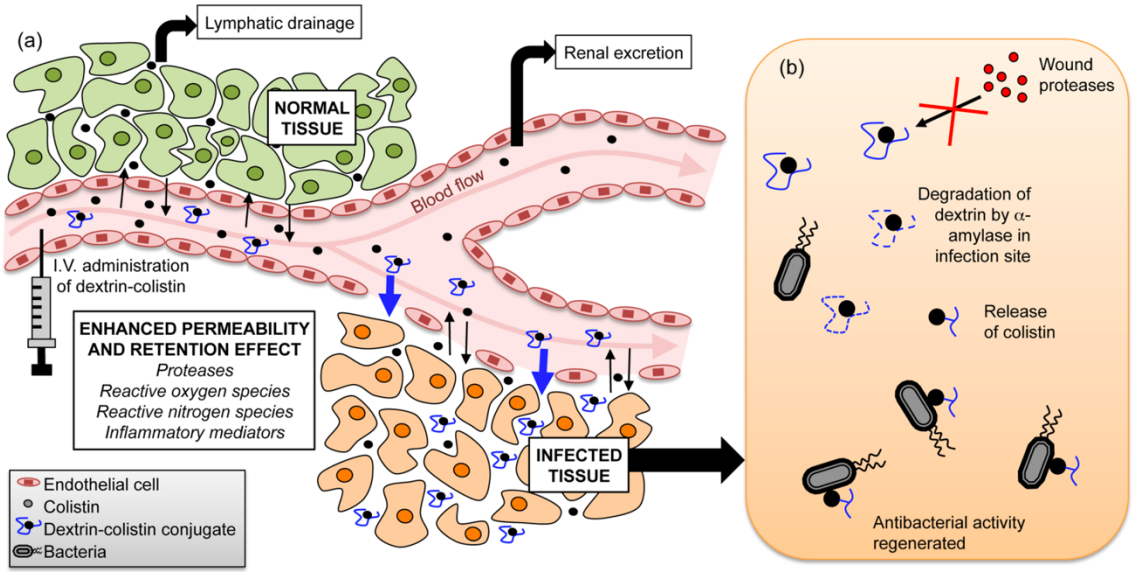

Figure 15 Proposed mechanism of action of dextrin-colistin conjugates: Polymer-drug conjugates cannot diffuse into normal tissue due to the tight junctions between endothelial cells around it, and only small amounts of free colistin, formed by systemic degradation of drug-polymer conjugates, can reach this non-infected tissue (a); Enhanced permeability between endothelial cells around infected tissue allow dextrin-polymer conjugates to diffuse through, where dextrin can be degraded by host amylase and thus the antimicrobial activity of colistin can be regenerated (b). Reprinted with permission from reference [16]. Copyright 2014 American Chemical Society.

Polymers, and derivatives thereof, have also been assembled into structurally-organised nanomaterials (*e.g.* particles, vesicles, *etc.*) for application as antibiotic delivery systems. These systems present void spaces or compartments where drug can be loaded to minimise undesired interactions between antimicrobial agents and healthy host cells, and engineered to tune the release of drug and thus control the antimicrobial action. **Nanogels** are one example of such materials, which consist of highly hydrated and cross-linked polymeric particles that can release pre-loaded drugs that diffuse out of their soft and porous structure. The sustained release of pre-loaded antibiotics from nanogels can be controlled by

adjusting the cross-linking degree of these materials, allowing to tune the antimicrobial effect while also reducing the toxicity of loaded antibiotics to host cells.[17,18] Nanogels loaded with the topical disinfectant chlorhexidine have also been applied as surface coatings for sustained antimicrobial release, with potential applications as coatings for biomedical devices (*e.g*. catheters) or in food packaging to prevent bacterial colonisation.[19]

Another type of polymeric nanomaterial studied in antibiotic delivery are **dendrimers**, which are hyperbranched polymers emerging from a central core that originate soft globular-shape nanoparticles.[20] Dendrimers have been used to increase the water solubility of hydrophobic antibiotics such as erythromycin[21] or sulfamethoxazole[22], working as soluble depots of drug that increased the antimicrobial activity of the drug by 2 to 3-fold.[21] Jain and co-workers developed a sugar-coated dendrimer loaded with the antifungal and antiprotozoal drug amphotericin B, which allowed the targeted uptake of these dendrimers by macrophages infected with the intracellular protozoan *Leishmania donovani*.[23] Macrophage targeting was achieved by recognition of sugar groups on the surface of dendrimers by membrane receptors expressed by these cells. These amphotericin B-loaded dendrimers not only displayed lower toxicity towards red blood cells and macrophages *in vitro* than two commercial formulations of this drug, including a nano-formulation of amphotericin B as liposomes (AmBisome®), but also showed superior anti-leishmanial activity *ex vivo* and *in vivo* than any of these two commercial preparations (**Figure 16**). This example is particularly relevant to demonstrate the potential of drug delivery to improve the activity of traditional antibiotics against intracellular pathogens (*e.g*. viruses, fungi, protozoa and bacteria), which are intrinsically more difficult to kill due to the limited access and accumulation of antibiotic inside host cells.[8,24,25]

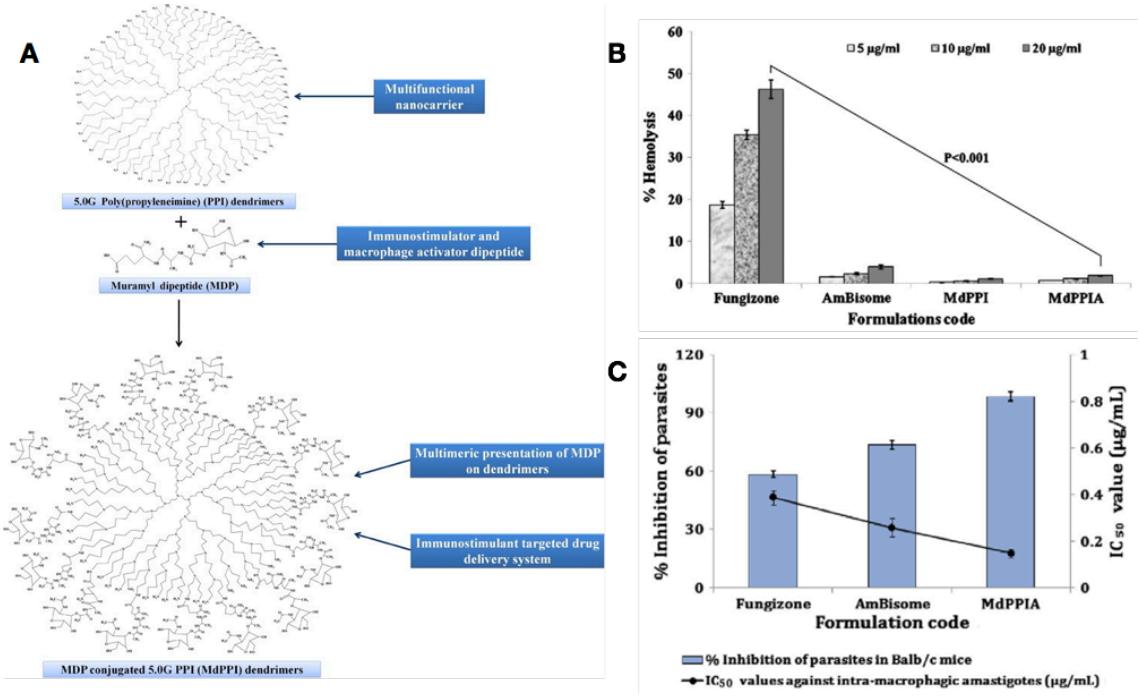

Figure 16 Structure of anti-leishmanial dendrimers, consisting of hyper-branched poly(propylene imine) cores conjugated with a glycosylated peptide (MDP) to give sugar-coated dendrimers, to be loaded with amphotericin B (A). Decreased hemolytic toxicity of 'empty' (MdPPI) and amphotericin B-loaded (MdPPIA) dendrimers compared to commercial formulations of amphotericin B (Fungizone® and AmBisome®) (B). Increased *ex vivo* (IC_{50}) and *in vivo* (inhibition of parasites) anti-leishmanial activity of MdPPIA compared to commercial amphotericin B fomulations (C). Reprinted from reference [23], with permission from Elsevier.

Polymers can also be assembled into hollow **nanocapsules** that contain an internal liquid compartment where drugs can be incorporated. For example, capsules loaded with the antibiotic imipenem and the adjuvant cilastatin, which protects imipenem from proteolytic inactivation, were prepared by coating an emulsified mixture of these drugs with poly(Ɛ-caprolactone).[26] These capsules displayed up to a 250-fold increase in antimicrobial activity against drug-resistant bacteria than the free drugs, protected imipenem from degradation by bacterial carbapenemases, reduced the formation of bacterial biofilms by *ca*. 75%, and sustained the release of imipenem for at least 7 days. This work is an excellent example of the potential of nanotechnology to redesign 'obsolete' antibiotics (*i.e.*

those to which bacteria have become resistant) into medicines with superior therapeutic performance.

Despite the study of **PIC particles** for drug delivery has mostly been focused on gene therapy, there are a few examples in the literature that apply these polymeric nanoparticles as vehicles for antimicrobial agents. Brocchini *et al*. complexed the monocationic antimicrobial amphotericin B with poly(glutamic acid) into PIC nanoparticles for evaluation against *L. donovani*.[27] It was found that these PIC nanoparticles could release amphotericin B in a sustained manner and kill this pathogen inside infected macrophages *in vitro* with the same activity as the free drug, while displaying less toxicity towards red blood and epithelial cells. As such, PIC particles increased the therapeutic index of amphotericin B (*i.e*. the ratio between the active and toxic dose of a drug), potentially allowing to administer higher doses of drug for stronger antimicrobial effects. Müller and collaborators developed a three-component PIC nanoparticle system consisting of poly(L-lysine) and cellulose sulphate complexes, which were then loaded with the antibiotic rifampicin to be applied as bone implant coatings for sustained drug release.[28] The authors demonstrated the influence of the pH and ionic strength of the medium on the release kinetics of rifampicin from films prepared by deposition of these PIC nanoparticles, but there was no antimicrobial evaluation reported on the article to assess the therapeutic potential of these films. Another ternary PIC nanoparticle for antimicrobial delivery was reported by Cerchiara *et al.,* prepared by simultaneous aggregation of chitosan, carboxymethylcellulose and the antibiotic vamcomycin.[29] These PIC nanoparticles were designed for drug delivery in the colon to tackle gastrointestinal pathogens, so the dose of vancomycin that reaches the colon after oral administration can be increased by loading the drug inside these nanoparticles, thus protecting vancomycin from acidic degradation in the stomach and systemic absorption in the intestine. The sustained release of drug was affected by the polyelectrolyte composition of the PIC particles and the medium's pH. One formulation was identified that displayed significantly faster drug release at pH 7.4 than 2.0, which respectively simulate the conditions in the colon and stomach – ideal for a localised drug release in the colon. Although this

particular formulation showed the same antimicrobial activity against *Staphylococcus aureus* than free vancomycin *in vitro*, it could surpass the traditional use of this antibiotic by preventing side effects derived from systemic drug absorption, and protect this peptide-based antibiotic from degradation by gastric proteases. Cavallaro and co-workers developed PIC nanoparticles by complexation of the cationic antimicrobial tobramycin with polypeptides bearing grafted glucuronic acid groups, and evaluated the formulation, drug release and antimicrobial action of these complexes towards their application in pulmonary infections (**Figure 17**).[30] It was found that these PIC nanoparticles could release of tobramycin in a controlled fashion, with *ca*. 50% of the loaded drug released after 6 hours. The authors further coated these tobramycin-loaded PIC nanoparticles with mannitol through spray-drying, which led to microparticles of 1-4 μm in diameter from the

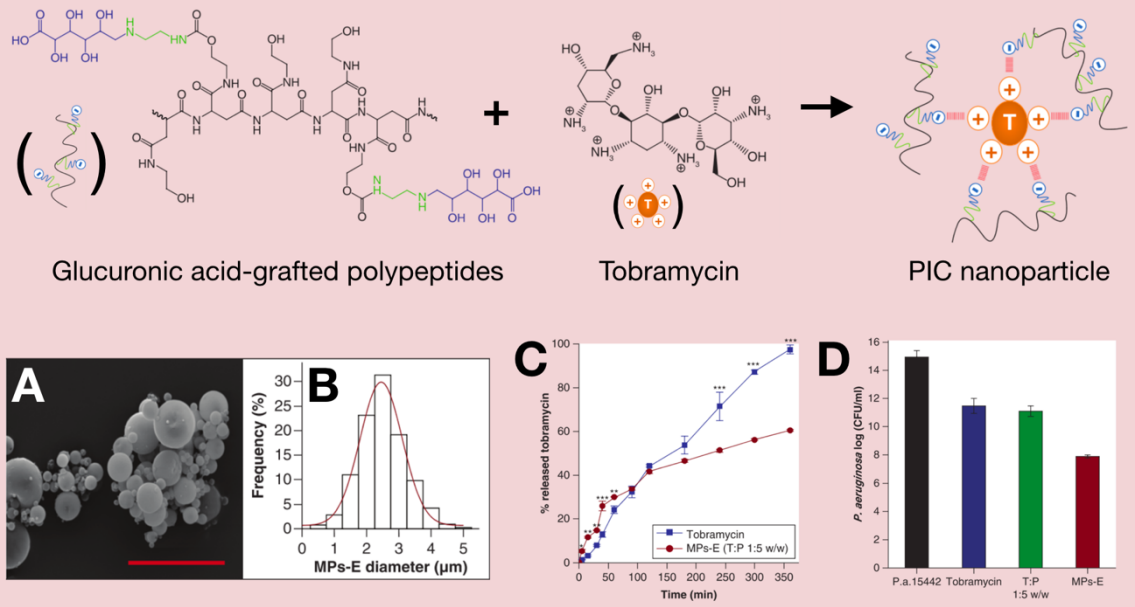

Figure 17 Top: Structures of polyelectrolytes assembled to form tobramycin-loaded PIC nanoparticles. Bottom: Scanning electron micrograph of the microparticles obtained after coating tobramycin-loaded PIC nanoparticles with mannitol (A, scale bar = 10 μm) and their size distribution (B); Release of tobramycin from mannitol-coated microparticles (MPs-E) across synthetic membranes mimicking lung mucus, compared to the diffusion of the free drug (C); Anti-biofilm action against *Pseudomonas aeruginosa* of mannitol-coated microparticles (MPs-E), PIC nanoparticles (T:P 1:5 w/w) and free drug (tobramycin), measured as living bacterial cells within the biofilms (CFU/mL) after treatment, compared to an untreated control (P.a. 15442) (D). Adapted from reference [30] with permission of Future Medicine Ltd.

original tobramycin/polypeptide complexes of *ca*. 90 nm. Mannitol was incorporated due to its capacity to overcome the mucus barrier of the lungs, known to cause an influx of water in the mucus that facilitates drug diffusion. Mannitol-coated PIC microparticles showed faster initial tobramycin release across synthetic membranes mimicking the lung mucus found in cystic fibrosis patients, and lower toxicity against human bronchial cells than the free drug. Furthermore, these microparticles displayed stronger antimicrobial activity and prevented the formation of bacterial biofilms more efficiently than the free drug and parent PIC nanoparticles *in vitro*. This novel 'nano-to-micro' approach to further re-formulate PIC nanoparticles arises as a powerful tool to develop new-generation antimicrobial therapies, capable of not only improving the activity and compatibility of traditional antibiotics, but also modify the properties of the biological environment to the advantage of the therapeutic action.

In conclusion, polymeric nanomaterials are versatile platforms to access new antimicrobial therapies from known drugs, allowing to control the distribution, action and stability of antibiotics in the body. Examples have been presented in this section to point out the application of different polymer-based antimicrobial delivery systems to direct the accumulation of drug to infected sites (*e.g*. inflamed tissue[16] and host macrophages[23]), protect antibiotics from inactivation by drug-resistant bacteria,[11,13,26] to sustain the release – and therefore the action – of drug from different nanomaterials,[17,18,26-29] and to reduce the toxicity of antimicrobial agents towards host cells.[14,16-18,23,27,30] As such, antimicrobial delivery through nanotechnology opens new avenues to 'recycle' traditional antibiotics into more powerful and efficient nanomedicines to fight the rise of antimicrobial resistance. From all the polymer-based nanomaterials presented in this section, **PIC nanoparticles offer important advantages** that make them particularly attractive for drug delivery:

- Accessibility – PIC nanoparticles can be assembled from affordable commercial polymers under mild conditions using very simple lab equipment.

- Scalability – From a production and commercialisation point of view, the assembly of PIC nanoparticles is a one-step process of easier scaling than more complex nanomaterials that require several formulation steps.
- Versatility – Not only PIC particles allow the formulation of virtually any charged small molecule and/or polymer into defined nanomaterials, but also their properties and structure can be adjusted in many different ways:
  - The size, charge, colloidal stability and drug loading of PIC nanoparticles can be varied by simply adjusting the mixing ratio of polyelectrolytes.[31]
  - Structural variations of the polymeric component(s) of PIC nanoparticles (*e.g*. Mw, pK_a and topology) can be exploited to access particles with different stabilities and drug release kinetics.[31]
  - Similarly, the addition of cross-linking agents to PIC nanoparticles offers another simple method to control particle stability and therapeutic action as a function of cross-linking degree.[31]
  - Being held together by (relatively) weak intermolecular forces, the structure of PIC particles changes with biological conditions that weaken/strengthen these interactions (*e.g*. pH[29] and osmotic pressure), which can translate into changes in drug release in response to different biological media.
  - PIC particles that disassemble in the presence of specific stimuli (*e.g*. reducing agents and enzymes) can be obtained by using sacrificial polyelectrolytes degradable by these stimuli.[31]
  - As discussed in this section, PIC particles also offer the possibility of tuning their structure and therapeutic action post-assembly, for example being applied as surface coatings[28] or undergoing a second complexation with additional polyelectrolytes to give PIC microparticles.[30]

Despite the recent advances in nanotechnology for antimicrobial delivery, important **challenges** remain to be addressed for the development of optimal antimicrobial nanotherapies. Firstly, bacteria-targeted nanomaterials capable of specifically directing antibiotics to the focus of infection would allow maximum drug efficiency with minimum toxicity to the host. To this end, nanomaterials capable of sensing and responding to bacteria – or their markers – with high specificity

are necessary, so bacteria can trigger the release of drug upon encounter with the nanoparticles. Secondly, nanomaterials capable of burst-releasing high doses of antibiotic would provide a powerful means to attack pathogens with high antimicrobial levels on a first exposure. As such, burst drug release can be applied as initial therapy to deliver a strong antimicrobial effect to the pathogens, to then apply sustained drug release to maintain therapeutic antimicrobial levels over long periods with low toxicity. Ideally, both bacteria-targeting and burst release should be combined for localised and potent antimicrobial nanotherapies. Finally, a third challenge is directly linked to PIC nanoparticles, and it is their exploration for biomedical applications beyond gene delivery. The literature outside this application is scarce – in particular for the delivery of traditional antibiotics, the developments over the last five years are limited to the paragraph dedicated to PIC nanoparticles in this section –, and gene delivery has clearly dominated the therapeutic research of PIC nanoparticles over the last decades.

It is the aim of this Thesis to address some of these challenges and explore PIC nanoparticles for antimicrobial drug delivery, studying their rational design, self-assembly, structural characterisation, stability, bacteria-triggered disassembly, and antimicrobial action. As such, this Thesis may not only contribute to the development of powerful tools to tackle the current threat of antimicrobial resistance, but it will also create valuable knowledge to understand the properties of PIC nanoparticles and expand their application to other areas at the biology/chemistry interface.

References and notes

1 K. Hede, *Nature*, 2014, **509**, S2–3.

2 M. N. Alekshun and S. B. Levy, *Cell*, 2007, **128**, 1037–1050.

3 World Health Organization, *Antimicrobial resistance: global report on surveillance*, 2014.

4 J. M. A. Blair, M. A. Webber, A. J. Baylay, D. O. Ogbolu, L. J. V. Piddock, *Nat. Rev. Microbiol.*, 2015, **13**, 42–51.

5 M. A. Cooper, D. Shlaes, *Nature*, 2011, **472**, 32–32.

6 L. Czaplewski, R. Bax, M. Clokie, M. Dawson, H. Fairhead, V. A. Fischetti, S. Foster, B. F. Gilmore, R. E. W. Hancock, D. Harper, I. R. Henderson, K. Hilpert, B. V. Jones, A. Kadioglu, D. Knowles, S. Ólafsdóttir, D. Payne, S. Projan, S. Shaunak, J. Silverman, C. M. Thomas, T. J. Trust, P. Warn and J. H. Rex, *Lancet Infect. Dis.*, 2016, **16**, 239–251.

7 W. Gao, Y. Chen, Y. Zhang, Q. Zhang and L. Zhang, *Adv. Drug Deliv. Rev.*, 2017, DOI: 10.1016/j.addr.2017.09.015.

8 H. Zazo, C. I. Colino, J. M. Lanao, *J. Control. Release*, 2016, **224**, 86–102.

9 R. S. Kalhapure, N. Suleman, C. Mocktar, N. Seedat and T. Govender, *J. Pharm. Sci.*, 2015, **104**, 872–905.

10 B. Devrim and A. Bozkır, in *Nanostructures for Antimicrobial Therapy*, Elsevier, 2017, pp. 169–202.

11 M. Schmidt, L. K. Bast, F. Lanfer, L. Richter, E. Hennes, R. Seymen, C. Krumm and J. C. Tiller, *Bioconjugate Chem.*, 2017, **28**, 2440–2451.

12 M. Schmidt, S. Harmuth, E. R. Barth, E. Wurm, R. Fobbe, A. Sickmann, C. Krumm and J. C. Tiller, *Bioconjugate Chem.*, 2015, **26**, 1950–1962.

13 J. Zhang, Y. P. Chen, K. P. Miller, M. S. Ganewatta, M. Bam, Y. Yan, M. Nagarkatti, A. W. Decho and C. Tang, *J. Am. Chem. Soc.*, 2014, **136**, 4873–4876.

14 P. Yang, M. Bam, P. Pageni, T. Zhu, Y. P. Chen, M. Nagarkatti, A. W. Decho and C. Tang, *ACS Infect. Dis.*, 2017, DOI: acsinfecdis.7b00132–9.

15 Y. Cai, W. Lee and A. L. Kwa, *Expert Rev. Anti Infect. Ther.*, 2015, **13**, 1481–1497.

16 E. L. Ferguson, E. Azzopardi, J. L. Roberts, T. R. Walsh and D. W. Thomas, *Mol. Pharm.*, 2014, **11**, 4437–4447.

17 T. Liu, H. Liu, Z. Wu, T. Chen, L. Zhou, Y. Liang, B. Ke, H. Huang, Z. Jiang, M. Xie and T. Wu, *Mater. Sci. Eng. C.*, 2014, **43**, 622–629.

18 T. Chen, Q. Li, L. Guo, L. Yu, Z. Li, H. Guo, H. Li, M. Zhao, L. Chen, X. Chen, Q. Zhong, L. Zhou and T. Wu, *Mater. Sci. Eng. C.*, 2016, **58**, 659–665.

19 M. J. Kettel, E. Heine, K. Schaefer and M. Moeller, *Macromol. Biosci.*, 2017, **17**, 1600230.

20 G. Hermanson, in *Bioconjugate Techniques*, Chapter 8: *Dendrimers and Dendrons*, 3rd Ed, Elsevier Inc., 2013.

21 K. Winnicka, M. Wroblewska, P. Wieczorek, P. T. Sacha and E. A. Tryniszewska, *Molecules*, 2013, **18**, 8607–8617.

22 M. U. Gurbuz, A. S. Erturk and M. Tulu, *Pharm. Dev. Technol.*, 2017, **22**, 678–689.

23 K. Jain, A. K. Verma, P. R. Mishra and N. K. Jain, *Nanomedicine*, 2015, **11**, 705–713.

24 R. Nordström and M. Malmsten, *Adv. Colloid Interface Sci.*, 2017, **242**, 17–34.

25 E. Briones, C. Isabel Colino and J. M. Lanao, *J. Control. Release*, 2008, **125**, 210–227.

26 M. I. Shaaban, M. A. Shaker and F. M. Mady, *J. Bionanotechnol.*, 2017, **15**.

27 A. H. A. Mohamed-Ahmed, K. A. Les, K. Seifert, S. L. Croft and S. Brocchini, *Mol. Pharm.*, 2013, **10**, 940–950.

28 D. Vehlow, R. Schmidt, A. Gebert, M. Siebert, K. S. Lips and M. Müller, *Nanomaterials*, 2016, **6**, 53.

29 T. Cerchiara, A. Abruzzo, C. Parolin, B. Vitali, F. Bigucci, M. C. Gallucci, F. P. Nicoletta and B. Luppi, *Carbohydr. Polym.*, 2016, **143**, 124–130.

30 E. F. Craparo, B. Porsio, D. Schillaci, M. G. Cusimano, D. Spigolon, G. Giammona and G. Cavallaro, *Nanomedicine*, 2017, **12**, 25–42.

31 I. Insua, A. Wilkinson and F. Fernández-Trillo, *Eur. Polym. J.*, 2016, **81**, 198–215.

CHAPTER 2

Enzyme-responsive polyion complex (PIC) nanoparticles for the targeted delivery of antimicrobial polymers

Format: Paper.

Information: I. Insua, E. Liamas, Z. Zhang, A. F. A. Peacock, A. M. Krachler and F. Fernandez-Trillo, *Polym. Chem.*, 2016, **7**, 2684-2690. – Published by the Royal Society of Chemistry.

Overview: In this Chapter, we present a novel PIC particle system for the targeted delivery of antimicrobial polymers in the presence of pathogenic *Pseudomonas aeruginosa*. These nanoparticles consist of a cationic antimicrobial polymer and an anionic peptide, which can be degraded by elastase B (LasB), a virulent factor released by *P. aeruginosa* during infection. Thus, the peptide component can be hydrolysed by LasB, triggering the disassembly of the nanoparticle and release of the antimicrobial on-demand.

The first milestone in this thesis was to develop these bacteria-targeted nanoparticles, as they would have the most useful properties for a potential clinical application: the localised delivery of antimicrobials in the presence of bacteria could not only improve the efficiency of the antimicrobials by accumulating them in bacterial niches, but also avoid any toxic effects derived from their unspecific interaction with healthy organs. Since, as explained in Chapter 1, large and highly multivalent polyelectrolytes can assemble PIC nanoparticles more easily, we decided to start our investigations exploring an antimicrobial polymer, poly(ethylene imine) (PEI), as an inexpensive model to develop these nanomaterials.

This paper covers the study of the antimicrobial properties of a number of PEIs, the optimisation of the peptide sequence, the distinct characteristics and physiological stability of different particle formulations, and the specific enzyme-responsive and antimicrobial properties of these PIC particles.
These nanoparticles displayed a remarkable enzyme specificity, being degraded by bacterial and not a human elastase used as control, and displayed strain-specific antimicrobial properties only towards a pathogenic strain of *P. aeruginosa* and not a non-virulent mutant (*i.e.* LasB-deficient). The capacity of these nanoparticles to vectorise the activity of antimicrobial polymers opens up a new opportunity to develop more efficient therapies and fight multidrug resistance.

Contributions: All authors contributed to the experimental set-up and discussed the results. II and FFT designed the nanoparticle synthesis and characterisation; and II, FFT and AMK designed the microbiological assays. EL and ZZ designed and performed the AFM experiments. II carried out all other experiments. II and FFT analysed the data and wrote the paper, with all other authors contributing to the final version of the manuscript.

Polymer Chemistry

PAPER

View Article Online
View Journal | View Issue

Cite this: *Polym. Chem.*, 2016, **7**, 2684

Enzyme-responsive polyion complex (PIC) nanoparticles for the targeted delivery of antimicrobial polymers†

Ignacio Insua,[a] Evangelos Liamas,[b] Zhenyu Zhang,[b] Anna F. A. Peacock,[a] Anne Marie Krachler[c,d] and Francisco Fernandez-Trillo*[a,d]

Received 26th January 2016,
Accepted 13th March 2016

DOI: 10.1039/c6py00146g

www.rsc.org/polymers

Here we present new enzyme-responsive polyion complex (PIC) nanoparticles prepared from antimicrobial poly(ethylene imine) and an anionic enzyme-responsive peptide targeting *Pseudomonas aeruginosa*'s elastase. The synthetic conditions used to prepare these nanomaterials allowed us to optimise particle size and charge, and their stability under physiological conditions. We demonstrate that these enzyme responsive PIC nanoparticles are selectively degraded in the presence of *P. aeruginosa* elastase without being affected by other endogenous elastases. This enzyme-responsive PIC particle can exert an elastase-specific antimicrobial effect against *P. aeruginosa* without affecting non-pathogenic strains of these bacteria. These targeted enzyme-responsive PIC nanoparticles constitute a novel platform for the delivery of antimicrobial peptides and polymers, and can be a powerful tool in the current race against antimicrobial resistance.

Introduction

There is an increasing concern with the emergence of microbial strains that can resist the action of current antimicrobials.[1–3] As evidenced over the last decades, the limited pipeline of new antibiotics cannot cope with this increasing number of resistant microbes,[4–6] and new antimicrobial strategies are needed that go beyond the development of new drugs.[7,8] One such strategy is the re-evaluation of drug candidates, which have been discarded due to toxicity and side effects. This is the case for antimicrobial peptides,[9–11] that are amongst the few last-resort treatments against multidrug resistant strains.[12,13]

Despite being powerful antimicrobial agents, the widespread use of antimicrobial peptides in the clinic is limited by their inactivation by serum proteases, toxicity to eukaryotic cells and high production cost.[9–11] The positively-charged amphiphilic structure of antimicrobial peptides is responsible for damaging bacterial membranes and cytosol components, resulting in a fast and multi-target antimicrobial action with broad spectra, but also in toxicity to the host.[9–11] Polymeric mimics of these peptides have been developed as an affordable alternative with increased protease stability and selectivity for prokaryotic cells. However, the clinical application of these polymer mimics is compromised by poor bioavailability, limited diffusion in tissues, polyelectrolyte complexation with negatively charged microbial peptidoglycans and extracellular polymers, and insufficient toxicological characterisation.[14,15] Further strategies to improve the therapeutic profile of antimicrobial peptides and mimics include masking of the positive charge.[16] However this often results in a reduced antimicrobial activity as a consequence of slow or incomplete cleavage of the masking group.

Less explored has been the use of controlled (and ideally targeted) delivery when optimising antimicrobial therapeutic profile.[17,18] However, this is a very attractive alternative to improve the medical profile of current antimicrobials: strategies that can deliver antimicrobials at the site of infection can minimise off-target effects such as toxicity or the emergence of reservoirs of microbial resistance genes in non-pathogenic strains such as commensal bacteria.[5]

Towards this end, here we present a new targeted enzyme-responsive nanoparticle that selectively delivers antimicrobial polymers in the presence of *Pseudomonas aeruginosa*, whose infections are very hard to treat.[19] In our system, the toxicity of cationic antimicrobial poly(ethylene imine) (PEI) was minimised through polyelectrolyte complexation with an anionic peptide, to form well-defined polyion complex (PIC) nanoparticles (Scheme 1). We demonstrate that our synthetic

[a]*School of Chemistry, University of Birmingham, B15 2TT Birmingham, UK*
[b]*School of Chemical Engineering, University of Birmingham, B15 2TT Birmingham, UK*
[c]*School of Biosciences, University of Birmingham, B15 2TT Birmingham, UK*
[d]*Institute of Microbiology and Infection, University of Birmingham, B15 2TT Birmingham, UK. E-mail: f.fernandez-trillo@bham.ac.uk*

†Electronic supplementary information (ESI) available: Peptide synthesis, further details of PIC nanoparticle characterisation and full data from microbiology assays. See DOI: 10.1039/c6py00146g

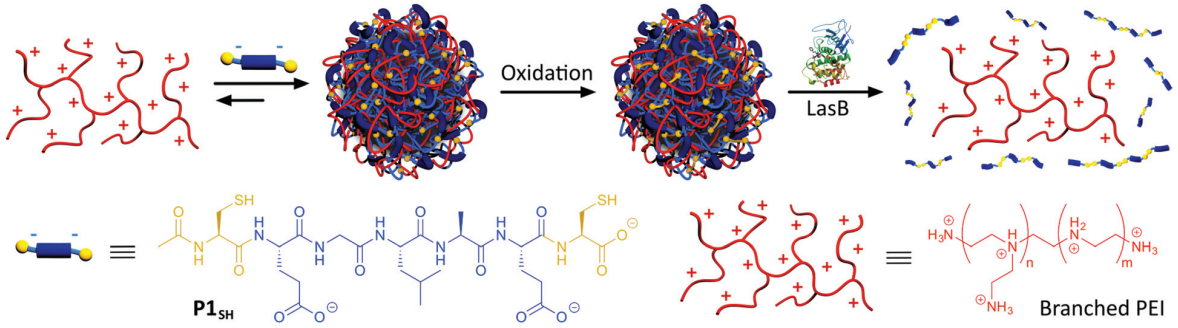

Scheme 1 Assembly and oxidative cross-linking of PIC nanoparticles from $\mathbf{P1_{SH}}$ (Ac-C-E-GLA-E-C-OH) and antimicrobial branched PEI. Degradation of PIC nanoparticles by LasB and subsequent PEI release.

approach is highly modular, letting us tune particle size and charge, and the stability of the PIC nanoparticles under physiological conditions. By introducing a *P. aeruginosa*'s elastase (LasB) cleavable sequence into our anionic peptide, PIC nanoparticles could be degraded in the presence of this *P. aeruginosa*'s virulence factor,[20,21] and more importantly, remained unchanged when treated with human leucocyte elastase (HLE), a human elastase secreted at the site of infection. Finally, we demonstrate that these enzyme-responsive PIC nanoparticles have a targeted antimicrobial effect against *P. aeruginosa* and that this antimicrobial effect is not observed for *P. aeruginosa* strains that do not produce the triggering LasB elastase.

Experimental

Materials

Enzymes (*Pseudomonas aeruginosa* Elastase (LasB): EC 3.4.24.26 and Human Leucocyte Elastase (HLE): EC 3.4.21.37) were purchased from Merck Millipore. Branched poly(ethylene imine) 25 kDa average molecular weight (B-PEI_{25}), 4-(2-hydroxyethyl)piperazine-1-ethanesulfonic acid (HEPES), Luria Bertani (LB) broth (Miller) and Dulbecco's modified eagle medium (DMEM) were bought from Sigma-Aldrich®. Fluorescamine and dimethylsulphoxide (DMSO) were purchased from Acros Organics™. Ethylenediaminetetraacetic acid (EDTA) was purchased from Alfa Aesar®. Nylon 0.45 μm syringe filters were purchased from Camlab. *P. aeruginosa* strains were kindly donated by Suzanne M. J. Fleiszig. We studied PAO1V as a pathogenic strain and a deletion strain of *lasA* and *lasB* genes of PAO1V was used as LasB-negative control (*ΔlasAB*).[22] Live/Dead® BacLight™ viability kit was purchased from Thermo Fisher Scientific Inc.

Instrumentation

Dynamic light scattering (DLS) and ζ-potential measurements were carried out in a Zetasizer Nano ZS (Malvern Instruments Ltd) stabilised at 37 °C. DLS was read at 173° (backscattering) for 60 seconds in triplicate and ζ-potentials were recorded 30 times at 140 V. A FLUOstar Omega (BMGLabtech Gmbh) microplate reader was used to measure fluorescamine reactions. Atomic force microscopy (AFM) measurements were carried out in 5 mM HEPES buffer at pH 7.4 with intermittent contact mode, using a NanoWizard® II (JPK Instruments Ltd) fitted with SiNi cantilevers (BudgetSensors®) with a spring constant of 0.27 N m^{-1}. PIC particle size was measured from AFM images with ImageJ software (version 1.48v). FACS was performed on an Attune® Acoustic Focusing Cytometer (Applied Biosystems™) measuring 10 000 events per sample. BacLight™ fluorescent dyes were excited at 488 nm and emission was read at 515–545 and 640 nm for green and red probes, respectively.

Enzymatic degradation – fluorescamine assay

Stock solutions of peptide (1 mM) or succinyl casein (0.5 mg mL^{-1}) were prepared in 2.5 mM $Na_2B_4O_7$ buffer at pH 8.0 with 10 mM $CaCl_2$ and 10% DMSO. 125 μL of these substrate solutions were added to a 96-well black-walled microplate and mixed with 125 μL of the same buffer without DMSO, containing 0.6 μg of enzyme (LasB or HLE). Solutions of enzymes and substrates alone were prepared as blanks. Every sample was prepared in triplicate. The microplate was incubated at 37 °C for 4 hours under orbital shaking. After 4 hours, 50 μL of 0.1 M ethylenediaminetetraacetic acid (EDTA) in water at pH 8.0 were added to each well to quench all enzymatic activity.[23] Then, each sample was mixed in a 1 : 1 volume with a 1 mM solution of fluorescamine[24] in methanol. The microplate was incubated at 37 °C under orbital shaking for 30 minutes. After this time, fluorescence was measured exciting at 355 nm and reading the emission at 460 ± 10 nm.

Preparation of PIC nanoparticles

For nanoparticles prepared at a 1 : 0.3 N : COOH ratio (defined as the ratio between amines in PEI and carboxylic acids in the peptides), stock solutions of B-PEI_{25} (2.5 mM in amines) and Ac-C-E-GLA-E-C-OH ($\mathbf{P1_{SH}}$) (0.25 mM) in 5 mM 4-(2-hydroxyethyl)piperazine-1-ethanesulfonic acid (HEPES) buffer at pH 7.4 were prepared. Then, both solutions were filtered and mixed drop-wise under stirring. The reaction mixture was stirred at room temperature for 24 hours open to air to allow

thiol oxidation with atmospheric oxygen. PIC nanoparticles prepared at different N : COOH ratios were obtained by changing the concentration of peptide stock solution and mixing with 2.5 mM B-PEI$_{25}$ following the same protocol (Table S2†). After 24 hours, samples were analysed directly by DLS and ζ-potential without prior filtration.

Enzymatic degradation of PIC nanoparticles

1 mL of PIC nanoparticles prepared at 1 : 0.3 N : COOH ratio was incubated at 37 °C with 50 μL (5 μg) of LasB in 2.5 mM $Na_2B_4O_7$ buffer at pH 8.0. As controls, PIC nanoparticles were incubated under the same conditions with HLE (5 μg) or $Na_2B_4O_7$ buffer to assess the enzymatic specificity and effect of salts in the buffer, respectively. Each sample was prepared in triplicate from three different batches of PIC nanoparticles. DLS data was acquired over time (1–4 hours). The number of amines was monitored after 4 hours of incubation as described before (fluorescamine assay).

Antimicrobial activity of PIC nanoparticles

1 mL aliquots of *P. aeruginosa* PAO1V and *ΔlasAB* cultures in LB broth (OD_{600} = 1.0) were centrifuged and resuspended in 1 mL of DMEM. These samples were incubated at 37 °C for 6 hours under orbital shaking to allow LasB production. After this time, samples were centrifuged and half of the supernatant replaced with the same volume of 5 mM HEPES buffer at pH 7.4 (live control), PIC nanoparticles (prepared at a 1 : 0.3 N : COOH ratio as described above) and 1.25 mM B-PEI$_{25}$ in 5 mM HEPES buffer at pH 7.4. A dead control was also prepared by replacing all the supernatant after centrifugation with 70% v/v aqueous 2-propanol. Samples were resuspended and incubated at 37 °C under orbital shaking. Each sample was prepared in triplicate. Every hour, 200 μL of each sample were taken and the rest was kept shaking at 37 °C. These 200 μL aliquots were incubated in the dark for 10 minutes with 1 μL of a 10-fold diluted 1 : 1 mixture of BacLight™ probes in DMEM. Dead control samples had to be centrifuged and resuspended in assay buffer before staining with fluorescent dyes. Then, samples were analysed by FACS setting gates for dead bacteria in green *versus* red emission dot plots from the live and dead controls.

Results and discussion

Peptide synthesis and enzymatic degradation

Our goal was to develop a delivery method that did not require chemical modification of the antimicrobial. PIC particles[25] are ideal for this purpose because the cationic antimicrobial peptides or mimics thereof can be encapsulated within a particle formed upon polyelectrolyte complexation with negatively charged materials. This strategy of complexing oppositely charged materials has been extensively used to deliver other "precious" therapeutics, in particular nucleic acids.[26]

In our case, PIC nanoparticles would be prepared by the combination of a tailor-made anionic peptide and the positively charged backbone of the antimicrobial (Scheme 1). In addition, we wanted our system to be selectively degraded in the presence of pathogenic bacteria, but not in their absence: for example, in the presence of commensal bacteria or non-pathogenic strains, unable to produce virulence factors. As such, our system would be pathogen specific and enable a targeted delivery of the antimicrobial. Here we chose *P. aeruginosa* as a model pathogen: *P. aeruginosa* is an opportunistic pathogen commonly associated with hospital-acquired infections, often colonising wounds and immunocompromised patients.[19] Interestingly, amongst the virulence factors that *P. aeruginosa* secretes to mediate infection, LasB,[20,21] a zinc-metalloprotease, constituted an excellent target to develop our system. LasB has elastolytic activity and a preference to cleave sites with small hydrophobic residues.[27,28] Thus, we designed our anionic peptides to contain a short LasB-cleavable sequence (*e.g.* GLA,[27] Scheme 1) flanked by two glutamic acids, responsible for providing overall negative charge to our peptide. We postulated that multivalency would be lost upon LasB mediated cleavage of the peptide, resulting in degradation of the particle and delivery of the antimicrobial (Scheme 1).

Two peptides were prepared at this stage: **P1**, containing the Gly-Leu-Ala sequence[27] and **P2**, containing a tetraalanine site,[28] both sequences having been reported to be cleaved by LasB. The N-terminus of both peptides was capped as a neutral acetamide to mask the cationic amine functionality. All peptides were prepared by solid-phase synthesis in good to excellent yields and high purity without any chromatographic purification (see ESI: section 3, Fig. S1–S6† for experimental details and characterisation).

A fluorogenic assay was then used to evaluate enzymatic degradation of these peptides.[24] Peptides were incubated with LasB, treated with fluorescamine and the increase in emission at 460 nm correlated with the amount of amines produced upon enzymatic hydrolysis of the peptides. In each assay, degradation of succinyl casein by the evaluated elastases was monitored, to confirm that the enzymes had not lost their activity upon storage.[29] Additionally, the values obtained from fluorescence measurements were normalised to that produced by a model peptide (H_2N-LA-E-OH (**P3**), Fig. S7†), which should be produced upon enzymatic hydrolysis of **P1**.[27] In our hands, the GLA sequence in **P1** was degraded to a higher extent than the tetraalanine in **P2**, showing an increase in amine content of 60% after four hours (Fig. 1). More importantly, when these peptides were incubated with HLE, a human elastase secreted by the immune system during inflammation, little to no degradation was observed for both peptides. This demonstrated that both of these peptides were excellent candidates to develop LasB-responsive nanoparticles, which would only be degraded by LasB, even if endogenous elastases were present in the media. All subsequent experiments were performed with **P1** because it is degraded to a greater extent by LasB.

PEI as a model antimicrobial polymer against *P. aeruginosa*

Having established the peptide sequence to be employed in the synthesis of our enzyme-responsive PIC nanoparticles, we

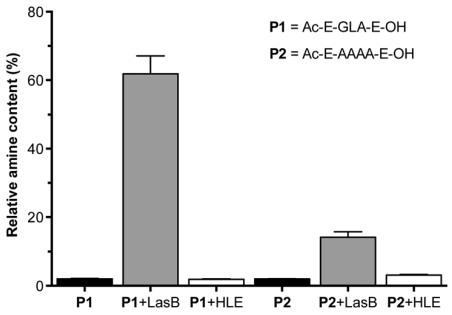

Fig. 1 Relative amine content in samples of LasB responsive anionic peptides evaluated in this work. Relative amine content was calculated from fluorescamine conjugates formed following incubation with enzymes for 4 hours and normalised to the fluorescence observed with a model degradation peptide (**P3**, H_2N-LA-E-OH) (Fig. S7†). Peptide blanks (*i.e.* without enzyme) in black. $n = 3$.

then turned our attention to the choice of antimicrobial. PEI has been reported as an efficient antimicrobial against both Gram positive and Gram negative bacteria.[30,31] Its antimicrobial activity can be tuned as a function of its degree of branching and molecular weight. Moreover, PEI has been extensively applied as a starting material for the preparation of polyelectrolyte complexes.[25] These features, and its commercial availability, made it an ideal candidate with which we could optimise the preparation of our PIC nanoparticles.

However, the antimicrobial activity of PEI towards *P. aeruginosa* had not been reported. Thus, five commercial PEIs of various molecular weights and branching were evaluated for their antimicrobial activity against *P. aeruginosa*. A pathogenic *P. aeruginosa* strain (PAO1V) was cultured overnight in the absence or presence of different concentrations of PEI and viability checked using a LIVE/DEAD® staining assay (Fig. S8†). This assay reports on membrane integrity and thus is especially suited to evaluate the activity of antimicrobial peptides and mimics. As expected, activity depended on the amount of PEI used. Aggregates could be visibly observed on the sides of the cuvettes for the larger polymers at the highest concentration tested (0.1 mg mL^{-1}), compromising the characterisation of the system. These aggregates may form as a result of the clustering of bacteria by the cationic polymers,[32,33] or these polymers being trapped by debris from dead bacteria. Increasing the molecular weight resulted in an increase in the percentage of dead cells. Moreover, the results at 0.01 mg mL^{-1} suggested that branching had a beneficial effect on antimicrobial activity. Therefore, B-PEI_{25} was selected as the candidate PEI to prepare our enzyme-responsive PIC nanoparticles.

PIC nanoparticle synthesis

Enzyme-responsive PIC nanoparticles were prepared by mixing stock solutions of the peptide (in 5 mM HEPES buffer at pH 7.4) with a 2.5 mM stock solution of B-PEI_{25} prepared in the same buffer. Initial attempts to make PIC nanoparticles with **P1** did not result in the formation of stable aggregates. Thus, we decided to introduce two cysteine residues in our peptides, to allow for chemical oxidation during the nanoparticle formation and cross-linking of the peptides. This strategy has been employed in the synthesis of other PIC complexes, such as nucleic acid polyplexes.[34–36] PIC nanoparticles were successfully made with this modified peptide ($\mathbf{P1_{SH}}$), by mixing peptide and B-PEI_{25} stock solutions and allowing the nanoparticles to oxidise overnight under stirring and open to air (Scheme 1). The kinetics of thiol cross-linking was studied by monitoring the decrease of accessible free thiols during nanoparticle formation using Ellman's reagent.[37] Complete depletion of thiols was observed after nine hours for $\mathbf{P1_{SH}}$ in the presence of B-PEI_{25}, whereas only 13% of initial thiols contained in $\mathbf{P1_{SH}}$ had oxidised after ten hours in its absence (Fig. S9†). This result is in agreement with the literature, where it is proposed that electrostatic complexation of polyions increases the local concentration of thiols and thus increases oxidation rates.[38]

Different mixtures of B-PEI_{25} to $\mathbf{P1_{SH}}$ (expressed as N : COOH ratio) were evaluated to determine the optimal ratio to prepare PIC nanoparticles (Fig. 2, Table S2†). Of all the N : COOH ratios tested, only those between 1 : 0.8 and 1 : 0.3 formed stable PIC nanoparticles. This phenomenon could be due to the lack of enough peptide below 1 : 0.3 to condense B-PEI_{25} into particles, and the generation of neutral and unstable coacervates at equimolar mixtures of positive and negative charge, in agreement with the decrease in ζ-potential observed with increasing peptide content (Fig. 2b). Interestingly, we were not able to form PIC nanoparticles in the presence of an excess of COOH groups (*i.e.* peptide). We believe the nucleation of these PIC nanoparticles is driven by complexation of the anionic peptides onto the B-PEI_{25} backbone. Once the positive charges on the surface of the growing nanoparticles are

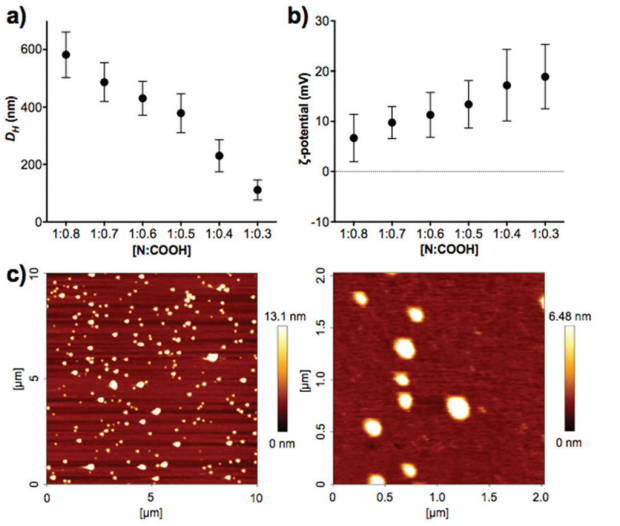

Fig. 2 (a) Hydrodynamic diameter (D_H) and (b) ζ-potential of $\mathbf{P1_{SH}}$ PIC nanoparticles prepared at different N : COOH ratios. (c) AFM characterisation of PIC nanoparticles prepared at a 1 : 0.3 N : COOH ratio. D = 127 ± 42 nm, $n = 48$.

neutralised, complexation of further peptide is hindered and thus prevents the formation of negatively charged particles.

A clear trend was found in particle size, with smaller particles being formed with decreasing amounts of peptide (Fig. 2a). AFM measurements were carried out to confirm the size and shape of these nanomaterials. PIC nanoparticles prepared at a 1 : 0.3 N : COOH ratio were selected for AFM analysis due to their narrow size distribution in DLS characterisation. AFM images showed the presence of spherical nanoparticles of 127 ± 42 nm in diameter (Fig. 2c), in agreement with the 111 ± 35 nm hydrodynamic diameter measured by DLS.

Physiological stability of PIC nanoparticles

PIC aggregates are disrupted in the presence of other electrolytes, which can shield and weaken the electrostatic forces holding the aggregates together, and potentially lead to the rupture of the particles.[25] In this regard, the high contents of salts in the body could compromise the efficacy of PIC nanoparticles in biological settings. With this in mind, the stability of PIC nanoparticles under physiological conditions was assessed by diluting them into a final concentration of 154 mM NaCl and incubating them at 37 °C.[39] The size of PIC nanoparticles incubated under these conditions was monitored by DLS over four hours (Fig. 3). All PIC nanoparticles tested swelled under experimental conditions, as expected from the addition of small Na^+ and Cl^- ions that can permeate these soft nanoparticles and shield the interactions between the polyions. A trend in the extent of this swelling was observed and, in general, decreasing the amount of $\mathbf{P1_{SH}}$ (*i.e.* COOH component) resulted in nanoparticles with increasing swelling. Interestingly, only the nanoparticles prepared at a 1 : 0.3 N : COOH ratio remained stable in size after the initial swelling for the whole duration of the experiment, with all of the other nanoparticles eventually reducing their size after two hours of incubation. PIC nanoparticles prepared at high N : COOH ratios were the most unstable and no aggregates could be detected for most of these systems following incubation for at least two hours (Fig. 3, hollow symbols).

DLS autocorrelation function curves (Fig. S10†), size distributions (Fig. S11†) and count plots (Fig. S12†) strongly support these observations: while PIC nanoparticles prepared with higher concentrations of peptide (N : COOH ratios 1 : 0.8–1 : 0.6) were unable to scatter light following incubation with NaCl, in some cases for as little as two hours, those prepared with a lower proportion of peptide (N : COOH ratios 1 : 0.5–1 : 0.3) did produce autocorrelation curves that could be fitted by the DLS software. However, only those prepared at a 1 : 0.3 N : COOH ratio were stable enough to scatter light over a prolonged period of time, as observed in the detection counts. Consequently, PIC nanoparticles prepared at this N : COOH ratio of 1 : 0.3 were selected for biological studies due to their higher stability.

A similar effect was observed when particles were incubated with other biologically relevant cations, such as Ca^{2+} (Fig. S13†). Multivalent cations have a high affinity for polyanionic peptides and thus our PIC particles swelled when exposed to $CaCl_2$, as evidenced by the shift in their DLS autocorrelation curves towards longer relaxation times. This swelling was bigger with bigger amounts of $CaCl_2$ added and resulted in uneven light scattering profiles and multimodal size distributions at the highest concentrations tested.

Enzymatic degradation of PIC nanoparticles

The enzyme-triggered disassembly of these (1 : 0.3)-PIC nanoparticles was evaluated first by DLS, monitoring the amount of light scattered by three different batches of these nanomaterials when exposed to LasB at 37 °C (Fig. 4, hollow circles). Even after only one hour of incubation, PIC nanoparticles treated with LasB scattered 25% less light, and this scattering kept decreasing for the duration of the experiment, reaching 40% of the initial scattering intensity after four hours.

As a comparison, incubation with HLE caused nanoparticles to scatter 15% more light after one hour incubation and remained close to 100% of the initial scattering for the duration of the experiment (Fig. 4, hollow squares). This initial increase in scattering intensity may be due to the swelling of the PIC nanoparticles after addition of the enzyme

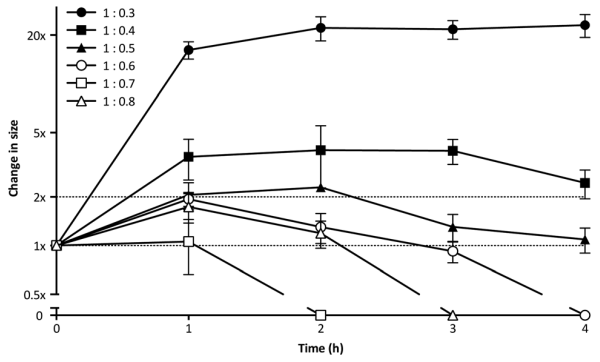

Fig. 3 Relative change in size for $\mathbf{P1_{SH}}$ PIC nanoparticles prepared at different N : COOH ratios and incubated under simulated physiological conditions (154 mM NaCl, pH 7.4, 37 °C). Particle size was normalised to that of a control in the absence of NaCl (1×). n = 3.

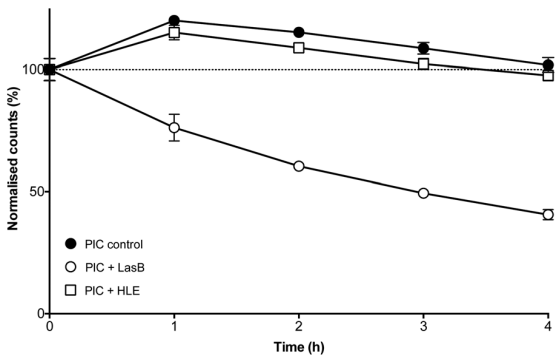

Fig. 4 Normalised detection counts (%) for $\mathbf{P1_{SH}}$ PIC nanoparticles prepared at a 1 : 0.3 N : COOH ratio in the absence (●) and presence of LasB (○) and HLE (□). Data normalised to the initial counts for each of the individual experiments. n = 3.

buffer (2.5 mM $Na_2B_4O_7$, pH 8.0), in a similar fashion to the swelling observed under physiological conditions (Fig. 3). A similar swelling was observed when PIC nanoparticles were incubated with this buffer in the absence of any of the enzymes (Fig. 4, dark circles). No significant difference was observed when this scattering was compared to that of HLE, proving that the human enzyme was not having an effect on the stability of these PIC nanoparticles. A similar effect could be observed in the DLS size distributions (Fig. S14†) with broader distributions and smaller sizes being observed upon treatment with LasB, as opposed to the almost invariable profile for HLE and the buffer controls.

The ability of LasB to degrade these PIC nanoparticles was also assessed, as before, monitoring the formation of amines upon enzymatic treatment. When PIC nanoparticles were reacted with fluorescamine after four hours of incubation with LasB or HLE, no significant difference in amine content was observed for those treated with HLE when compared to PIC nanoparticles incubated in the absence of any enzyme (Fig. S15†). However, an increase in fluorescence emission (up to 30%) was observed for the samples incubated with LasB. This increase in the amount of amines, together with the DLS data, confirms the selective cleavage of **$P1_{SH}$** within the nanoparticle and consequent disassembly of these PIC nanoparticles when exposed to the bacterial elastase.

Antimicrobial activity of PIC nanoparticles

Having established the selectivity of the degradation of these PIC nanoparticles in the presence of *P. aeruginosa* LasB, the antimicrobial activity of these enzyme-responsive nanoparticles was assessed. *P. aeruginosa* PAO1V, a pathogenic strain that secretes LasB, was incubated with PIC nanoparticles (1 : 0.3 N : COOH ratio) or B-PEI_{25}, aliquots were taken every hour for four hours, and stained using the LIVE/DEAD® viability kit. As expected, the antimicrobial activity for the PIC nanoparticles was significantly reduced when compared to B-PEI_{25}, with the nanoparticles exhibiting, after two hour incubation, less than 10% of the activity of B-PEI_{25} (Fig. 5), thus confirming the potential of these PIC nanoparticles to reduce the toxicity of antimicrobial polymers. This antimicrobial activity was slowly recovered upon incubation with the bacteria, and up to 25% of the antimicrobial activity of B-PEI_{25} could be observed for PIC nanoparticles after four hours of incubation, before the assay conditions become too harsh to have viable controls of *P. aeruginosa*. When the same experiment was performed with a LasB-deletion strain (*ΔlasAB*), which does not produce this elastase, a similar reduction in toxicity could be observed with the PIC nanoparticles (Fig. 5, white bars), despite the slightly higher susceptibility of this strain towards the antimicrobial polymer (Fig. S16 and S17†). More importantly, the antimicrobial activity for the PIC nanoparticles against this *ΔlasAB* mutant remained constantly low over the duration of the experiment, demonstrating that this strain was unable to degrade the nanoparticle and thus release the antimicrobial polymer.

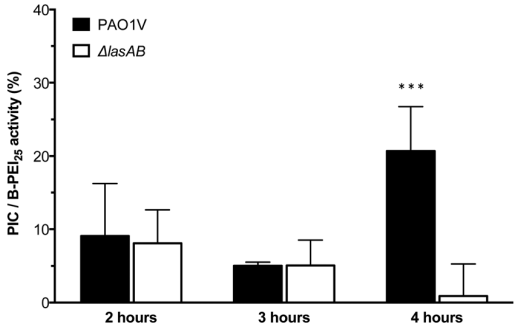

Fig. 5 Normalised antimicrobial activity over time of **$P1_{SH}$** PIC nanoparticles prepared at a 1 : 0.3 N : COOH ratio. Activity has been normalised by dividing the relative antimicrobial activity (Fig. S17†) from PIC nanoparticles by that of B-PEI_{25}. *** $p < 0.001$ between PAO1V and *ΔlasAB* (CI = 99.9%) after 4 hours. $n = 3$.

Conclusions

Here, we have developed an easy methodology for the preparation, under aqueous conditions, of PIC nanoparticles from an enzyme-responsive anionic peptide and a cationic antimicrobial polymer. The size of these nanoparticles could be tuned between 100 and 600 nm by simply adjusting the N : COOH ratio. We have demonstrated that disulfide mediated cross-linking and N : COOH ratios were fundamental to impart these PIC nanoparticles with stability under physiological conditions. Furthermore, we have shown that both the starting peptide and the formed PIC nanoparticles can be selectively degraded in the presence of LasB elastase, a virulence factor secreted by the opportunistic pathogen *P. aeruginosa*, while no degradation was observed in the presence of HLE, an elastase secreted by human leucocytes. Finally, we demonstrate that the toxicity of B-PEI_{25} was significantly reduced within these nanoparticles. Antimicrobial activity was slowly recovered when these PIC nanoparticles were incubated with a pathogenic *P. aeruginosa* strain, while remaining non-toxic in the presence of a strain that cannot produce the elastase.

We believe these enzyme-responsive PIC nanoparticles have a great versatility and potential in the current fight against antimicrobial resistance, and our efforts to optimise antimicrobial activity, while maintaining the low toxicity against non-targeted cells we observe here, will be reported in due course.

Author contributions

All authors contributed to the experimental set-up and discussed the results. II and FFT designed the nanoparticle synthesis and characterisation; and II, FFT and AMK designed the microbiological assays. EL and ZZ designed and performed the AFM experiments. II carried out all other experiments. FFT and AMK secured funding. II and FFT analysed the data and wrote the paper, with all other authors contributing to the final version of the manuscript.

Acknowledgements

FFT thanks the University of Birmingham for the John Evans Fellowship. AMK thanks the University of Birmingham for a Birmingham Fellowship. FFT and AMK thank the Wellcome Trust (177ISSFPP) for funding. II thanks the University of Birmingham for a PhD studentship. Some equipment used was obtained through Birmingham Science City: Innovative Uses for Advanced Materials in the Modern World (West Midlands Centre for Advanced Materials Project 2) and Birmingham Science City Translational Medicine: Experimental Medicine Network of Excellence project, with support from Advantage West Midlands (AWM) and part funded by European Regional Development fund (ERDF). The authors thank Dr Marie-Christine Jones and Dr Hannene Ali-Boucetta (School of Pharmacy, UoB) for the access to the DLS, and Nicolas Perez for useful discussions and help with the microbiology assays. The authors thank Prof. Suzanne M. J. Fleiszig for the kind donation of *P. aeruginosa* strains.

Notes and references

1 European Antimicrobial Resistance Surveillance Network, *Antimicrobial resistance surveillance in Europe*, European Centre for Disease Prevention and Control, 2013.
2 World Health Organization, *Antimicrobial resistance: global report on surveillance*, World Health Organization, 2014.
3 K. Hede, *Nature*, 2014, **509**, S2–S3.
4 M. A. Cooper and D. Shlaes, *Nature*, 2011, **472**, 32.
5 K. Bush, P. Courvalin, G. Dantas, J. Davies, B. Eisenstein, P. Huovinen, G. A. Jacoby, R. Kishony, B. N. Kreiswirth, E. Kutter, S. A. Lerner, S. Levy, K. Lewis, O. Lomovskaya, J. H. Miller, S. Mobashery, L. J. V. Piddock, S. Projan, C. M. Thomas, A. Tomasz, P. M. Tulkens, T. R. Walsh, J. D. Watson, J. Witkowski, W. Witte, G. Wright, P. Yeh and H. I. Zgurskaya, *Nat. Rev. Microbiol.*, 2011, **9**, 894–896.
6 J. O'Neill, *The Wellcome Trust, HM Government*, 2015.
7 C. Nathan, *Sci. Transl. Med.*, 2012, **4**, 140sr2.
8 B. Spellberg, J. G. Bartlett and D. N. Gilbert, *N. Engl. J. Med.*, 2013, **368**, 299–302.
9 R. E. W. Hancock and H.-G. Sahl, *Nat. Biotechnol.*, 2006, **24**, 1551–1557.
10 C. D. Fjell, J. A. Hiss, R. E. W. Hancock and G. Schneider, *Nat. Rev. Drug Discovery*, 2012, **11**, 37–51.
11 J. L. Fox, *Nat. Biotechnol.*, 2013, **31**, 379–382.
12 M. E. Evans, D. J. Feola and R. P. Rapp, *Ann. Pharmacother.*, 1999, **33**, 960–967.
13 E. A. Azzopardi, E. L. Ferguson and D. W. Thomas, *J. Crit. Care*, 2013, **28**, 219.
14 K. Kuroda and G. A. Caputo, *Wiley Interdiscip. Rev.: Nanomed. Nanobiotechnol.*, 2013, **5**, 49–66.
15 A. Jain, L. S. Duvvuri, S. Farah, N. Beyth, A. J. Domb and W. Khan, *Adv. Healthcare Mater.*, 2014, **3**, 1969–1985.
16 J. Bergen, J. Li, C. R. Rayner and R. L. Nation, *Antimicrob. Agents Chemother.*, 2006, **50**, 1953–1958.
17 M.-H. Xiong, Y. Bao, X.-Z. Yang, Y.-H. Zhu and J. Wang, *Adv. Drug Delivery Rev.*, 2014, **78**, 63–76.
18 V. W. L. Ng, J. M. W. Chan, H. Sardon, R. J. Ono, J. M. García, Y. Y. Yang and J. L. Hedrick, *Adv. Drug Delivery Rev.*, 2014, **78**, 46–62.
19 E. B. M. Breidenstein, C. de la Fuente-Núñez and R. E. W. Hancock, *Trends Microbiol.*, 2011, **19**, 419–426.
20 B. Wretlind and O. R. Pavlovskis, *Rev. Infect. Dis.*, 1983, **5**, S998–S1004.
21 E. Kessler and D. E. Ohman, in *Handbook of Proteolytic Enzymes - (Third Edition) - ScienceDirect*, ed. N. D. Rawlings and G. Salvesen, Academic Press, London, 3rd edn, 2013, vol. 1, pp. 582–592.
22 B. A. Cowell, S. S. Twining, J. A. Hobden, M. S. F. Kwong and S. M. J. Fleiszig, *Microbiology*, 2003, **149**, 2291–2299.
23 C. T. Supuran and A. Mastrolorenzo, *Curr. Enzyme Inhib.*, 2011, **7**, 2–23.
24 S. Udenfriend, S. Stein, P. Böhlen, W. Dairman, W. Leimgruber and M. Weigele, *Science*, 1972, **178**, 871–872.
25 H. Yoon, E. J. Dell, J. L. Freyer, L. M. Campos and W.-D. Jang, *Polymer*, 2014, **55**, 453–464.
26 U. Lächelt and E. Wagner, *Chem. Rev.*, 2015, **115**, 11043–11078.
27 K. Morihara and H. Tsuzuki, *Arch. Biochem. Biophys.*, 1971, **146**, 291–296.
28 J. M. Saulnier, A. M. Rayssiguie, M. C. Duclos and J. M. Wallach, *Biochem. Soc. Trans.*, 1990, **18**, 900–901.
29 T. Hatakeyama, H. Kohzaki and N. Yamasaki, *Anal. Biochem.*, 1992, **204**, 181–184.
30 K. A. Gibney, I. Sovadinova, A. I. Lopez, M. Urban, Z. Ridgway, G. A. Caputo and K. Kuroda, *Macromol. Biosci.*, 2012, **12**, 1279–1289.
31 T. He and V. Chan, *J. Biomed. Mater. Res., Part A*, 2010, **95A**, 454–464.
32 L. T. Lui, X. Xue, C. Sui, A. Brown, D. I. Pritchard, N. Halliday, K. Winzer, S. M. Howdle, F. Fernandez-Trillo, N. Krasnogor and C. Alexander, *Nat. Chem.*, 2013, **5**, 1058–1065.
33 I. Louzao, C. Sui, K. Winzer, F. Fernandez-Trillo and C. Alexander, *Eur. J. Pharm. Biopharm.*, 2015, **95**, 47–62.
34 D. L. MacKenzie, K. Y. Kwok and K. G. Rice, *J. Biol. Chem.*, 2000, **275**, 9970–9977.
35 R. Nasanit, P. Iqbal, M. Soliman, N. Spencer, S. Allen, M. C. Davies, S. S. Briggs, L. W. Seymour, J. A. Preece and C. Alexander, *Mol. BioSyst.*, 2008, **4**, 741–745.
36 M. Soliman, S. Allen, M. C. Davies and C. Alexander, *Chem. Commun.*, 2010, **46**, 5421–5433.
37 P. W. Riddles, R. L. Blakeley and B. Zerner, *Anal. Biochem.*, 1979, **94**, 75–81.
38 T. Blessing, J. S. Remy and J. P. Behr, *Proc. Natl. Acad. Sci. U. S. A.*, 1998, **95**, 1427–1431.
39 B. M. Koeppen and B. A. Stanton, in *Renal Physiology*, Elsevier, 2013, pp. 1–14.

Enzyme-responsive polyion complex (PIC) nanoparticles for the targeted delivery of antimicrobial polymers

Ignacio Insua,[a] Evangelos Liamas,[b] Zhenyu Zhang,[b] Anna F. A. Peacock,[a] Anne Marie Krachler[c,d] and Francisco Fernandez-Trillo[a,d]*

[a] *School of Chemistry,* [b] *School of Chemical Engineering,* [c] *School of Biosciences and* [d] *Institute of Microbiology and Infection, University of Birmingham, Edgbaston, B15 2TT Birmingham, United Kingdom. E-mail: f.fernandez-trillo@bham.ac.uk*

1. Materials

Fmoc-protected-L-amino acids were purchased from Merck Millipore. Dimethylformamide (DMF), piperidine 20% v/v in DMF, 5,5'-dithiobis(2-nitrobenzoic acid) (DTNB) and linear poly(ethylene imine) 2.5 KDa average molecular weight (L-$PEI_{2.5}$) were purchased from Sigma-Aldrich®. H_2N-L-Glu(O^tBu)-2-chlorotrityl resin (0.58 mmol/g) was bought from AGTC Bio Products Ltd. 2-chlorotrityl chloride resin (1.49 mmol/g) was obtained from Iris Biotech Gmbh. Linear poly(ethylene imine) 25 KDa average molecular weight (L-PEI_{25}), branched poly(ethylene imine) 1.2 KDa average molecular weight (B-$PEI_{1.2}$), *N,N*-diisopropylethylamine (DIPEA), triisopropylsilane (TIPS), 1,2-ethanedithiol (EDT), trifluoroacetic acid (TFA), casein from bovine milk (technical grade) and succinic anhydride were bought from Alfa Aesar®. *N*,*N*,*N*',*N*'-tetramethyl-*O*-(1*H*-benzotriazol-1-yl)uronium hexafluorophosphate

(HBTU) was purchased from Carbosynth Ltd. Spectra/Por® 6 dialysis membranes (molecular weight cut off 1 KDa) were purchased from Spectrum® Laboratories. Penta(ethylene imine) (L-PEI_{5n}) was purchased from Acros Organics™. All other chemicals were purchased from Fisher Scientific UK Ltd. and were used without further purification.

2. Instrumentation

NMR data was acquired on a Bruker Avance III operating at 400 MHz and fitted with a 5 mm DUL probe ($^{1}H/^{13}C$). MS spectra were obtained on a Xevo® G2-XS ToF (Waters) from electrospray ionisation (ESI) and time-of-flight (TOF) measurement in positive ion mode. High-resolution MS data was calculated by comparison with leucine-enkephalin as internal standard. Reverse phase (RP) HPLC analysis was run through a Kinetex® C18-EVO column (Phenomenex®): 5 µm, 100 Å, 250 x 4.60 mm. A gradient from 3 to 20% of (CH_3CN + 0.05% TFA) in (H_2O + 0.05% TFA) was used at 1 mL/min. The column was maintained at 35°C and UV-VIS detection was set at 210 nm. UV-VIS spectra were acquired on a Cary 5000 NIR (Agilent) in polystyrene cuvettes of 1 mm light paths. Dynamic light scattering (DLS) and ζ-potential measurements were carried out in a Zetasizer Nano ZS (Malvern Instruments Ltd) stabilised at 37°C. DLS was read at 173° (backscattering) for 60 seconds in triplicate and ζ-potentials were recorded 30 times at 140 V.

3. Synthesis and characterisation of peptides

3.1. Loading of Fmoc-L-Cys(Trt)-OH on 2-chlorotrityl chloride resin

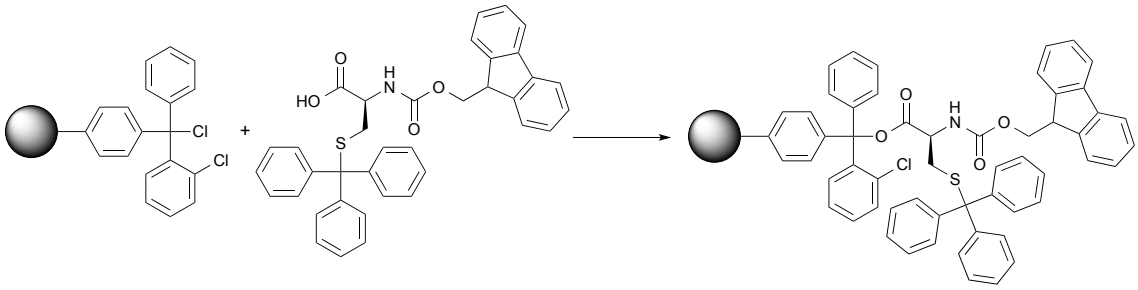

A solution of Fmoc-L-Cys(Trt)-OH (1.10 g, 1.9 mmol) in 10 mL of DCM:anhydrous DMF (9:1) was purged with argon for 10 min. Then, the solution was added under inert conditions into a sealed flask with commercial preswollen 2-chlorotrityl chloride resin (1.00 g, 1.5 mmol), and DIPEA (1.3 mL, 7.5 mmol) was added to the mixture. The reaction was left under stirring at room temperature for 2 hours. After this time, the resin was filtered and washed with 10 mL of DCM:MeOH:DIPEA (17:2:1) 3 times. Finally, the resin was washed with 10 mL of DCM (x3) and 10 mL of Et_2O (x3) and dried under vacuum. Amino acid loading was calculated following the protocol described by Kay et al.,[1] giving a final value of 0.44 mmol/g of resin.

3.2. Solid-phase synthesis of peptides

For peptides without cysteine (**P1**, **P2** and **P3**), commercial H_2N-L-Glu(O^tBu)-2-chlorotrityl resin (250-400 mg, 0.14-0.23 mmol) was swollen in 4 mL of DMF for 30 minutes. Then, solutions of Fmoc-L-amino acid (3 eq), *N*,*N*,*N*',*N*'-tetramethyl-*O*-(1*H*-benzotriazol-1-yl)uronium hexafluorophosphate (HBTU) (2.8 eq) and DIPEA (2.8 eq) in DMF were added to a final volume of 4 mL. The reaction mixture was shaken for 1 hour at room temperature, after which a negative chloranil test[2] indicated the reaction had gone to completion. *N*-terminal Fmoc protecting group was removed with 4 mL of piperidine in DMF 20% v/v during 10 minutes. A positive chloranil test confirmed the removal of the Fmoc group, and the previous steps were repeated to couple all amino acids in the sequence. Following coupling of the last amino acid, the Fmoc group was removed and, if necessary, the terminal amine in the peptide was capped with 4 mL of Ac_2O:DIPEA:DMF (1:1:3) for 1 hour at room temperature. Then, the resin was thoroughly

washed with Et_2O and the peptide was cleaved from the resin with 4 mL of aqueous TFA (95%) for 1 hour. The solution obtained was concentrated under argon and precipitated in chilled Et_2O. Finally, this suspension was centrifuged and the pellets were freeze-dried from acidic water.

For peptide **$P1_{SH}$** (containing cysteine), Fmoc-L-Cys(Trt)-OH loaded 2-chlorotrityl chloride resin (1.00 g, 0.44 mmol), prepared as indicated in 3.1., was deprotected twice with 10 mL of piperidine in DMF 20% v/v before coupling subsequent amino acids. The elongation and capping of the peptide was performed as indicated above for **P1**-**P3**, and the peptide was cleaved from the resin with 10 mL of TFA (80%), TIPS (8%) and EDT (12%) for 2 hours to protect thiols from side reactions. This solution was concentrated under argon and precipitated in chilled Et_2O:hexane (1:4). Finally, this suspension was centrifuged and the pellets were freeze-dried from acidic water. All peptides were isolated as white solids, regardless of the synthetic method. Purity was determined by HPLC.

Table S1 Sequences and structures of the peptides prepared in this work.

Peptide	Sequence	Structure
P1	Ac-EGLAE-OH	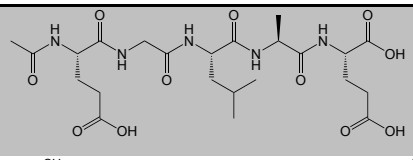
$P1_{SH}$	Ac-CEGLAEC-OH	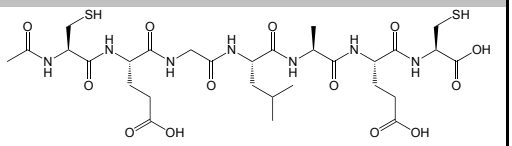
P2	Ac-EAAAAE-OH	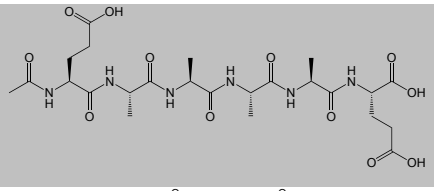
P3	H_2N-LAE-OH	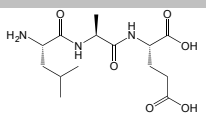

3.3. Characterisation of peptides

P1, Ac-E-GLA-E-OH (83.8 mg, 96% yield) **^{1}H-NMR** (400 MHz, DMSO-d_6): δ 0.84(dd, *J*=15.1, 6.5 Hz, 6H, H^{δ}-Leu); 1.21(d, *J*=7.0 Hz, 3H, H^{β}-Ala); 1.36-1.49(m, 2H, H^{β}-Leu); 1.51-1.61(m, 1H, H^{γ}-Leu); 1.67-2.00(m, 4H, H^{β}-Glu); 1.85(s, 3H, Ac); 2.20-2.33(m, 4H, H^{γ}-Glu); 3.68(d, *J*=5.8 Hz, 2H, H^{α}-Gly); 4.15-4.34(m, 4H, H^{α}); 7.83(d, *J*=8.2 Hz, 1H, NHCO); 7.96(d, *J*=7.8 Hz, 1H, NHCO); 8.04(d, *J*=7.4 Hz, 1H, NHCO); 8.11(d, *J*=7.4 Hz, 1H, NHCO); 8.21(t, *J*=5.8 Hz, 1H, NHCO) ppm. **^{13}C-NMR** (400 MHz, DMSO-d_6): δ 17.9(C^{β}-Ala); 21.6(C^{δ}-Leu); 22.5(Ac); 23.2(C^{δ}-Leu); 24.1(C^{γ}-Leu); 26.4(C^{β}-Glu); 27.1(C^{β}-Glu); 30.0(C^{γ}-Glu); 30.2(C^{γ}-Glu); 40.8(C^{β}-Leu); 42.0(C^{α}-Gly); 48.0(C^{α}); 50.8(C^{α}); 51.1(C^{α}); 52.3(C^{α}); 168.6(NHCO); 169.8(Ac); 171.6(NHCO); 171.8(NHCO); 172.2(NHCO); 173.1(*C*-term); 173.8(C^{δ}-Glu); 174.0(C^{δ}-Glu) ppm. **MS** (ESI-TOF, +eV): m/z 614.2 $[M+Na+CH_3OH]^+$; 604.2 $[M-H+2Na]^+$; 582.2 $[M+Na]^+$. **HR-MS** (ESI-TOF, +eV): m/z 582.2387 (calculated for $[M+Na]^+$) 582.2385 (found). Purity by **HPLC** = 88%.

$P1_{SH}$, Ac-C-E-GLA-E-C-OH (214.3 mg, 64% yield). **^{1}H-NMR** (400 MHz, DMSO-d_6): δ 0.84(dd, *J*=14.8, 6.5 Hz, 6H, H^{δ}-Leu); 1.20(d, *J*=7.1 Hz, 3H, H^{β}-Ala); 1.43(t, *J*=7.0 Hz, 2H, H^{β}-Leu); 1.50-1.63(m, 1H, H^{γ}-Leu); 1.67-1.83(m, 2H, H^{β}-Glu); 1.84-1.98(m, 2H, H^{β}-Glu); 1.87(s, 3H, Ac); 2.18-2.29(m, 4H, H^{γ}-Glu); 2.34(t, *J*=8.5 Hz, 1H, SH); 2.44(t, *J*=8.5 Hz, 1H, SH); 2.62-2.90(m, 4H, H^{β}-Cys); 3.70(dd, *J*=11.2, 5.7 Hz, 2H, H^{α}-Gly); 4.19-4.41(m, 6H, H^{α}); 7.87-7.92(m, 2H, NHCO); 8.07-8.19(m, 5H, NHCO) ppm. **^{13}C-NMR** (400 MHz, DMSO-d_6): δ 17.7(C^{β}-Ala); 21.6(H^{δ}-Leu); 22.6(Ac); 23.1(H^{δ}-Leu);

24.1(H^{γ}-Leu); 25.4(C^{β}-Cys); 26.0(C^{β}-Cys); 27.1(C^{β}-Glu); 27.5(C^{β}-Glu); 29.9(C^{γ}-Glu); 30.0(C^{γ}-Glu); 41.0(C^{β}-Leu); 41.9(C^{α}-Gly); 48.2(C^{α}); 50.8(C^{α}); 51.6(C^{α}); 52.2(C^{α}); 54.3(C^{α}); 55.1(C^{α}); 168.4(NHCO); 169.7(Ac); 170.2(NHCO); 171.1(NHCO); 171.3(NHCO); 171.4(NHCO); 171.8(NHCO); 172.0(*C*-term); 174.0(C^{δ}-Glu) ppm. **MS** (ESI-TOF, +eV): m/z 810.2 $[M-H+2Na]^+$, 788.3 $[M+Na]^+$. **HR-MS** (ESI-TOF, +eV): m/z 788.2571 (calculated for $[M+Na]^+$) 788.2568 (found). Purity by **HPLC** = 92%.

P2, Ac-E-AAAA-E-OH (118.8 mg, 97% yield) **^{1}H-NMR** (400 MHz, DMSO-d_6): δ 1.18-1.21(m, 12H, H^{β}-Ala); 1.64-2.00(m, 4H, H^{β}-Glu); 1.84(s, 3H, Ac); 2.17-2.33(m, 4H, H^{γ}-Glu); 4.16-4.30(m, 6H, Hα); 7.91(d, J=7.4 Hz, 2H, NHCO); 7.99(d, *J*=7.3 Hz, 1H, NHCO); 8.03(d, *J*=8.1 Hz, 1H, NHCO); 8.05(d, *J*=7.7 Hz, 2H, NHCO) ppm. **^{13}C-NMR** (400 MHz, DMSO-d_6): δ 17.9(C^{β}-Ala); 18.1(C^{β}-Ala); 18.1(C^{β}-Ala); 22.5(Ac); 26.4(C^{β}-Glu); 27.4(C^{β}-Glu); 30.0(C^{γ}-Glu); 30.2(C^{γ}-Glu); 47.8(C^{α}); 48.0(C^{α}); 48.1(C^{α}); 48.1(C^{α}); 51.1(C^{α}); 51.8(C^{α}); 169.4(Ac); 171.1(NHCO); 171.6(NHCO); 171.8(NHCO); 171.9(NHCO); 172.2(*C*-term); 173.1(NHCO); 173.7(C^{δ}-Glu); 174.0(C^{δ}-Glu) ppm. **MS** (ESI-TOF, +eV): m/z 647.2 $[M-H+2Na]^+$; 625.3 $[M+Na]^+$. **HR-MS** (ESI-TOF, +eV): m/z 625.2445 (calculated for $[M+Na]^+$) 625.2444 (found). Purity by **HPLC** = 98%.

P3, H_2N-LA-E-OH (50.4 mg, 66% yield) **^{1}H-NMR** (400 MHz, DMSO-d_6): δ 0.88(dd, *J*=8.8, 6.4 Hz, 6H, H^{δ}-Leu); 1.24(d, *J*=7.0 Hz, 3H, H^{β}-Ala); 1.45-1.59(m, 2H, H^{β}-Leu); 1.61-1.69(m, 1H, H^{γ}-Leu); 1.71-1.81(m, 1H, H^{β}-Glu); 1.91-2.00(m, 1H, H^{β}-Glu); 2.19-2.32(m, 2H, H^{γ}-Glu); 3.77(t, *J*=6.6 Hz, 1H, H^{α}-Leu); 4.16-4.21(m, 1H, H^{α}-Glu); 4.38(p, *J*=7.1 Hz, 1H, H^{α}-Ala); 8.21(d, *J*=7.8 Hz, 1H, NHCO); 8.69(d, *J*=7.4 Hz, 1H, NHCO) ppm. **^{13}C-NMR** (400 MHz, DMSO-d_6): δ 18.1(C^{β}-Ala); 22.0(H^{δ}-Leu); 22.7(H^{δ}-Leu); 23.6(C^{γ}-Leu); 26.5(C^{β}-Glu); 30.1(C^{γ}-Glu); 40.3(C^{β}-Leu); 48.2(C^{α}-Ala); 50.8(C^{α}-Leu); 51.3(C^{α}-Glu); 168.3(NHCO); 171.7(NHCO); 173.1(*C*-term); 173.9(C^{δ}-Glu) ppm. **MS** (ESI-TOF, +eV): m/z 332.2 $[M+H]^+$. **HR-MS** (ESI-TOF, +eV): m/z 332.1822 (calculated for $[M+H]^+$) 332.1824 (found). Purity by **HPLC** = 99%.

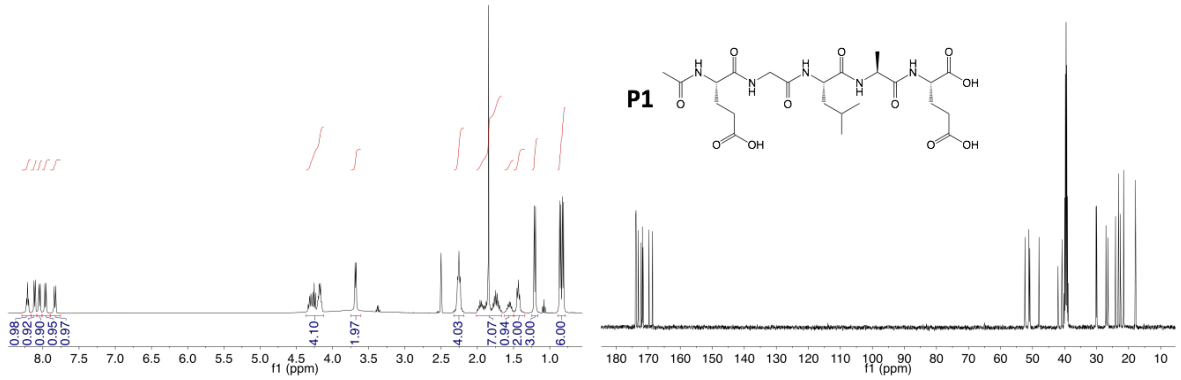

Fig. S1 ^{1}H (left) and ^{13}C (right) NMR (400 MHz, DMSO-*d6*) spectra of **P1** (Ac-E-GLA-E-OH).

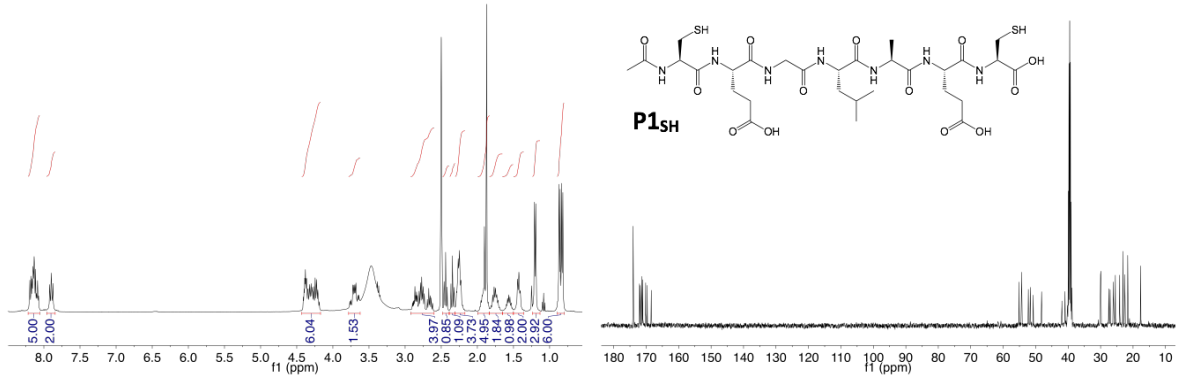

Fig. S2 ^{1}H (left) and ^{13}C (right) NMR (400 MHz, DMSO-*d6*) spectra of **P1$_{SH}$** (Ac-C-E-GLA-E-C-OH).

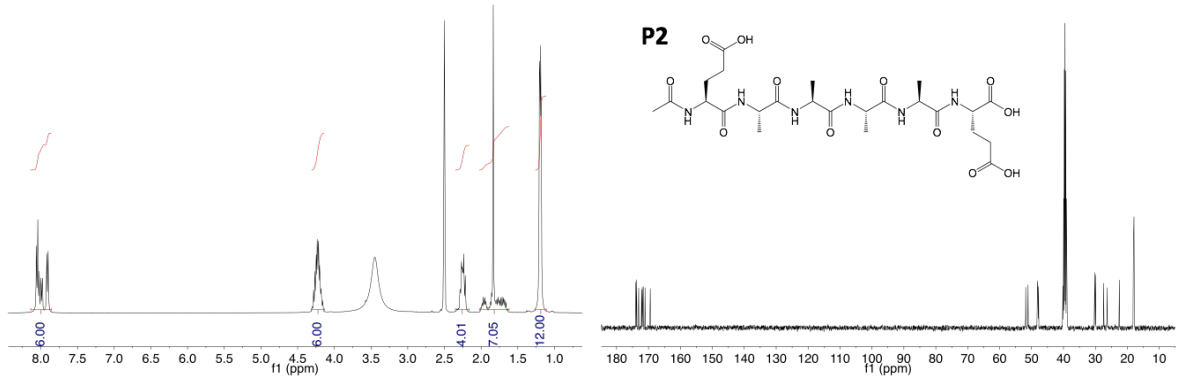

Fig. S3 ^{1}H (left) and ^{13}C (right) NMR (400 MHz, DMSO-*d6*) spectra of **P2** (Ac-E-AAAA-E-OH).

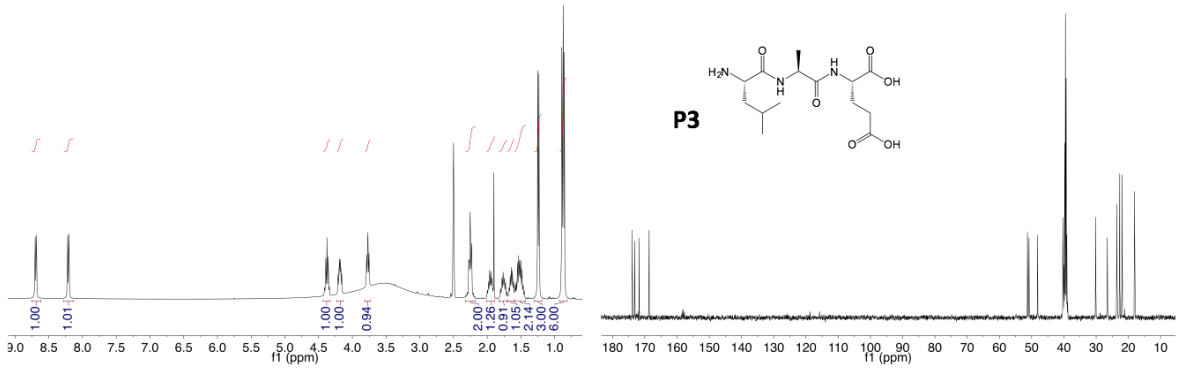

Fig. S4 ^{1}H (left) and ^{13}C (right) NMR (400 MHz, DMSO-*d6*) spectra of **P3** (H_2N-LA-E-OH).

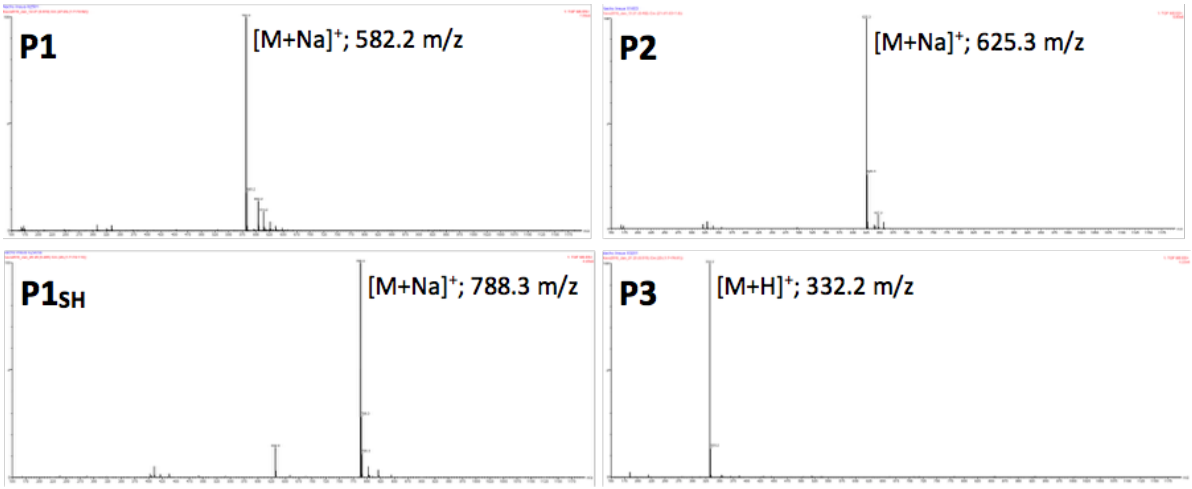

Fig. S5 ESI-TOF mass spectra of **P1**(Ac-E-GLA-E-OH), **P1$_{SH}$**(Ac-C-E-GLA-E-C-OH), **P2**(Ac-E-AAAA-E-OH) and **P3**(H_2N-LA-E-OH).

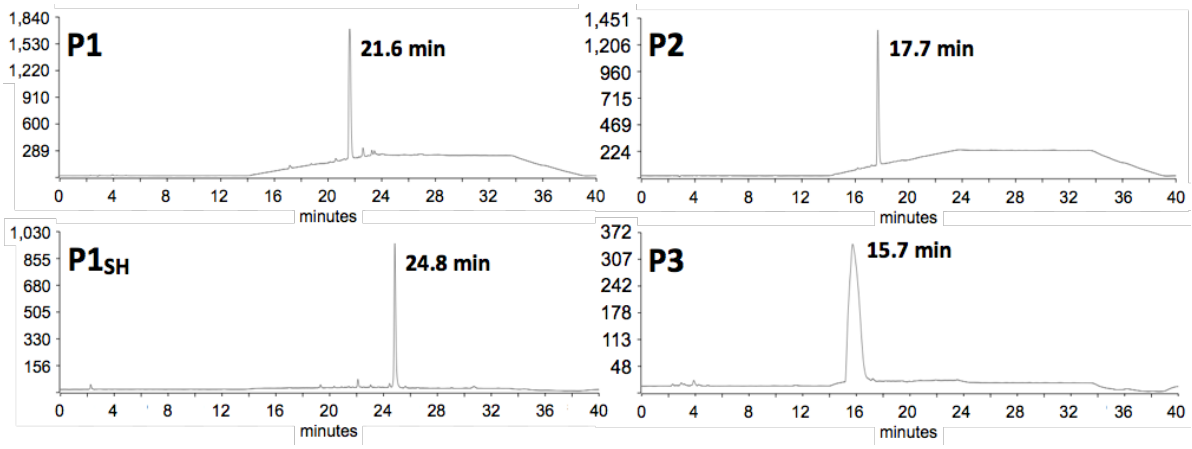

Fig. S6 RP-HPLC chromatograms of **P1**(Ac-E-GLA-E-OH), **P1$_{SH}$**(Ac-C-E-GLA-E-C-OH), **P2**(Ac-E-AAAA-E-OH) and **P3**(H_2N-LA-E-OH).

4. Enzymatic degradation of peptides

4.1. Synthesis of succinyl casein (SC)

A modified procedure from the literature was used for the preparation of SC:[3] commercial casein (500 mg, 0.02 mmol) was heated at 60°C with succinic anhydride (400 mg, 4.00 mmol) in 100 mL of $NaHCO_3$ buffer at pH 8.0. The pH of the reaction was maintained at 8.0 by addition of NaOH 1M. After 1 hour, the reaction mixture was left to reach room temperature and dialysed against deionised water for 2 days. Then, the suspension was freeze-dried to give a white solid (481.8 mg).

SC was used as a control to monitor enzymatic activity because SC is degraded by both proteases. For each experiment, degradation of SC was monitored to ensure that enzymatic activity for LasB and HLE was not lost upon storage. In general, we observed a higher degradation of SC in the presence of HLE (**Fig. S7**). This increase in enzymatic degradation by HLE can be due to a higher content of HLE cleavable sites in SC. Thus, we prepared a model degradation peptide (H_2N-LA-E-OH, **P3**) that corresponds to the product obtained upon enzymatic hydrolysis of **P1**.[4] This peptide has a terminal amine and is not cleaved by any of the elastases. Thus, fluorescence intensity can be normalised to that observed in the presence of this peptide, which corresponds to 100% degradation.

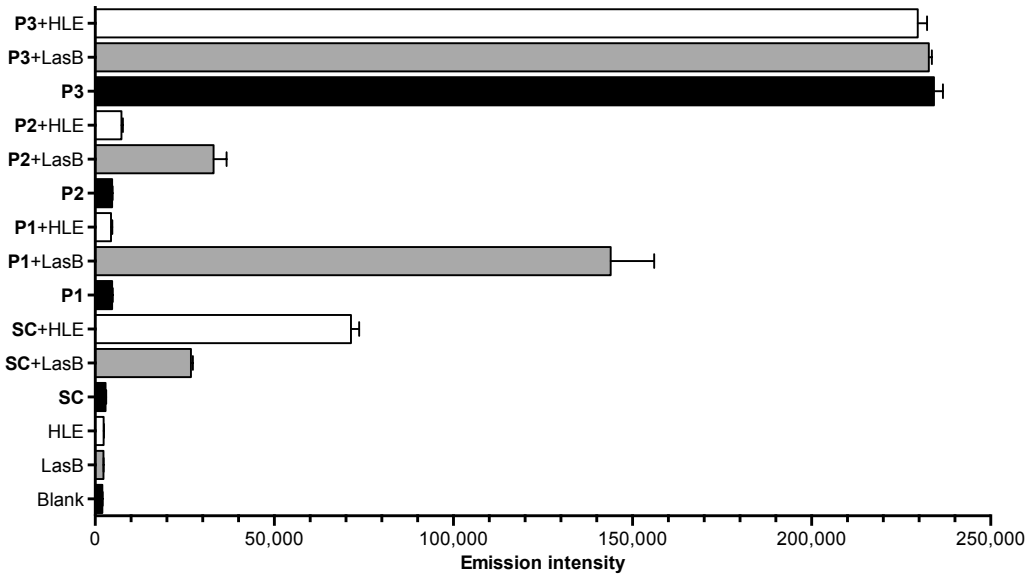

Fig. S7 Emission intensity (λ_{exc} 355 nm, λ_{em} 460 nm) of fluorescamine conjugates for $Na_2B_4O_7$ buffer (blank), succinyl casein (SC) as a control for enzymatic activity, LasB responsive anionic peptides (Ac-E-GLA-E-OH, **P1**; Ac-E-AAAA-E-OH, **P2**) and degradation peptide (H_2N-LA-E-OH, **P3**) as a control to normalise fluorescence intensity. All substrates were evaluated in the absence and presence of LasB or HLE. Incubation time: 4 hours. n=3.

5. Antimicrobial activity of commercial PEIs

1 mL aliquots of a *P. aeruginosa* PAO1V culture in LB broth (OD_{600} = 1.0) were centrifuged and resuspended in the same volume of a PEI solution prepared in DMEM. 5 different PEIs were tested: 3 linear (25 KDa, 2.5 KDa and pentamer) and 2 branched (25 and 1.2 KDa) at 3 different concentrations. Bacteria were also resuspended in pure DMEM and 70% v/v aqueous 2-propanol as live and dead controls, respectively. All samples were incubated at room temperature for twenty hours. After this time, 300 µL of each sample were reacted in the dark with 1 µL of a 1:1 mixture of BacLight™ probes for 10 minutes. Then, samples were analysed by FACS setting gates in green *versus* red emission dot plots from the live and dead controls. For some of the higher concentrations, aggregation, biofilms or bacterial debris were observed in the culture well before FACS analysis.

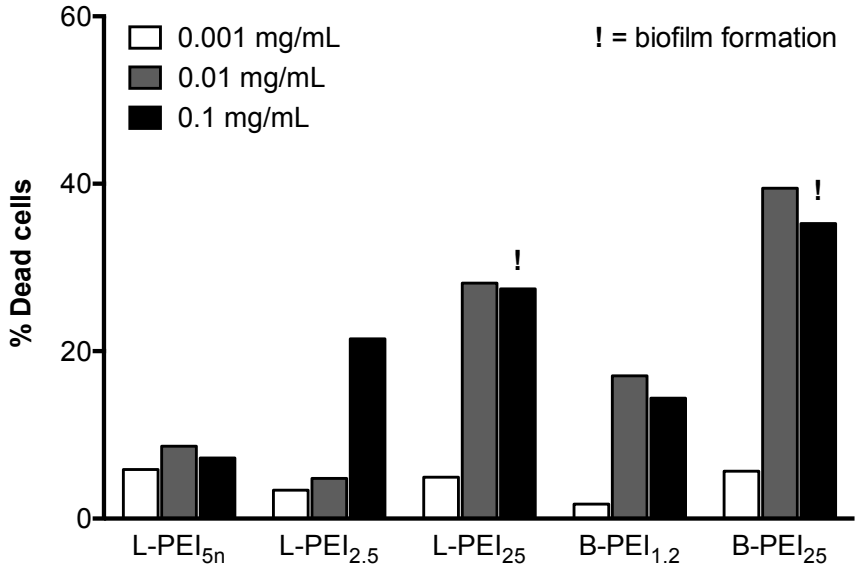

Fig. S8 Normalised population of *P. aeruginosa* PAO1V presented as the percentage of red (dead) cells. n=1.

6. Characterisation of PIC nanoparticles

Table S2 Hydrodynamic diameter (D_H) and ζ-potential of PIC nanoparticles prepared at different N:COOH ratios. SD indicates the dispersion in D_H or ζ of the only size or charge population fitted by the software.

N:COOH RATIO	D_H ± SD (nm)	ζ ± SD (mV)	Notes
1:2.0	-	-	No PIC particles formed
1:1.5	-	-	No PIC particles formed
1:1.0	-	-	No PIC particles formed
1:0.8	582 ± 79	6.7 ± 4.7	-
1:0.7	487 ± 67	9.8 ± 3.2	-
1:0.6	431 ± 59	11.3 ± 4.5	-
1:0.5	379 ± 68	13.4 ± 4.7	-
1:0.4	230 ± 56	17.2 ± 7.1	-
1:0.3	111 ± 35	18.9 ± 6.4	-
1:0.2	-	-	No PIC particles formed

6.1. Cross-linking kinetics of PIC nanoparticles

Ellman's assay was used to quantify by UV-VIS spectroscopy the amount of accessible sulfhydryl groups present in the sample. PIC nanoparticles were prepared at a 1:0.3 N:COOH ratio as described in the main text. 300 µL of sample were taken at different time points and mixed with 300 µL of 1 mM 5,5'-dithiobis(2-nitrobenzoic acid) (DTNB) solution in degassed 100 mM phosphate buffer at pH 7.27 containing with 1 mM EDTA. Absorbance was measured at 412 nm. Thiol concentration in a solution of **P1$_{SH}$** at the same concentration was used as a control.

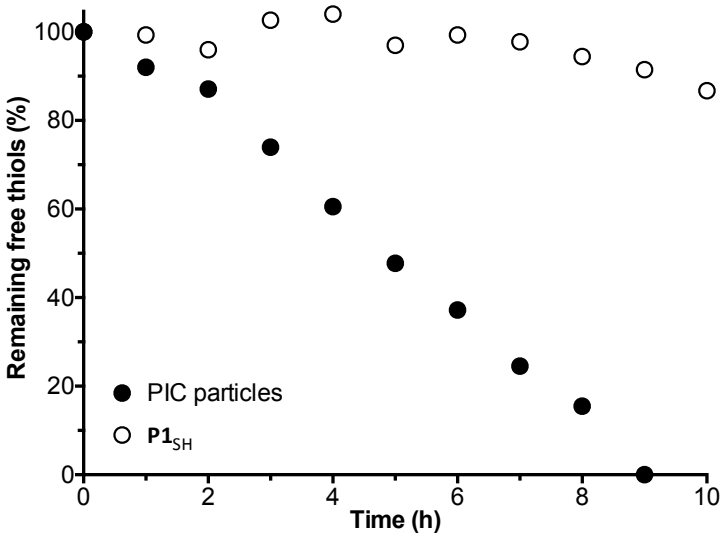

Fig. S9 Amount of accessible thiols, as monitored using Ellman's assay, following incubation of $\mathbf{P1_{SH}}$ (○) or PIC nanoparticles (●) prepared at a 1:0.3 N:COOH ratio in phosphate/EDTA buffer (pH 7.27) under stirring and open to air. n=1.

7. Physiological stability of PIC nanoparticles

1 mL of a PIC nanoparticles (**Table S2**), prepared as described in the main text, was diluted with 182 µL of a 1 M NaCl solution in water to give a final NaCl concentration of 154 mM (physiological osmolarity).[5] All samples were incubated at 37°C and analysed by DLS over time for up to 4 hours. Autocorrelation function (ACF), intensity distributions and detection counts for these samples were compared to that of a control in the absence of NaCl (**Fig. S10**-**Fig. S12**).

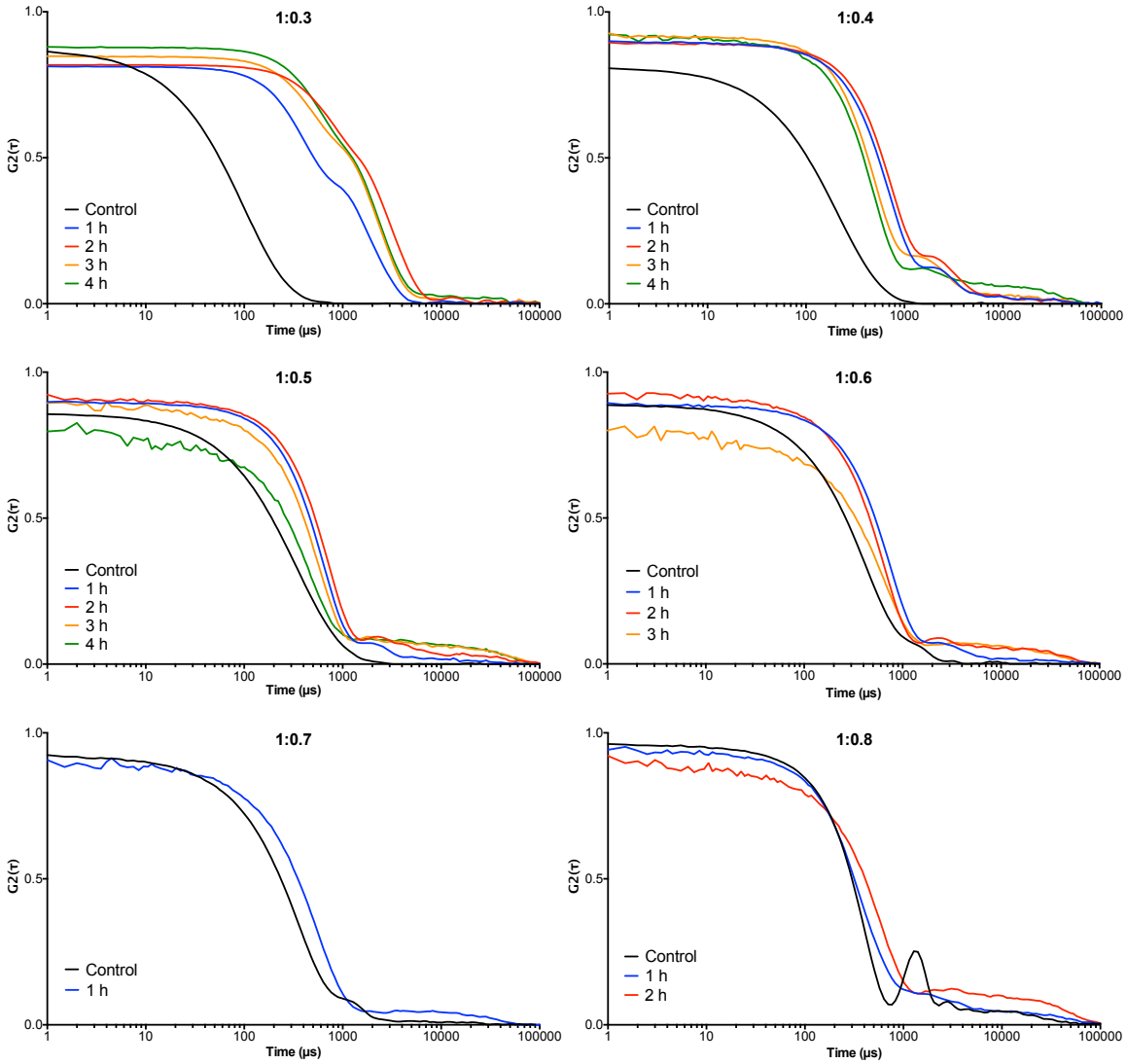

Fig. S10 Representative autocorrelation function[†] (ACF) curves for **P1$_{SH}$** PIC nanoparticles prepared using six different N:COOH ratios (**Table S2**) in the absence (control) and presence of 154 mM NaCl at 37°C over time (1-4 hours).

[†] Because of the dispersion in DLS measurements observed for unstable particles (e.g. 1:0.6 N:COOH ratio at 3 hours) only representative plots are shown. 3 technical replicates were recorded for each sample.

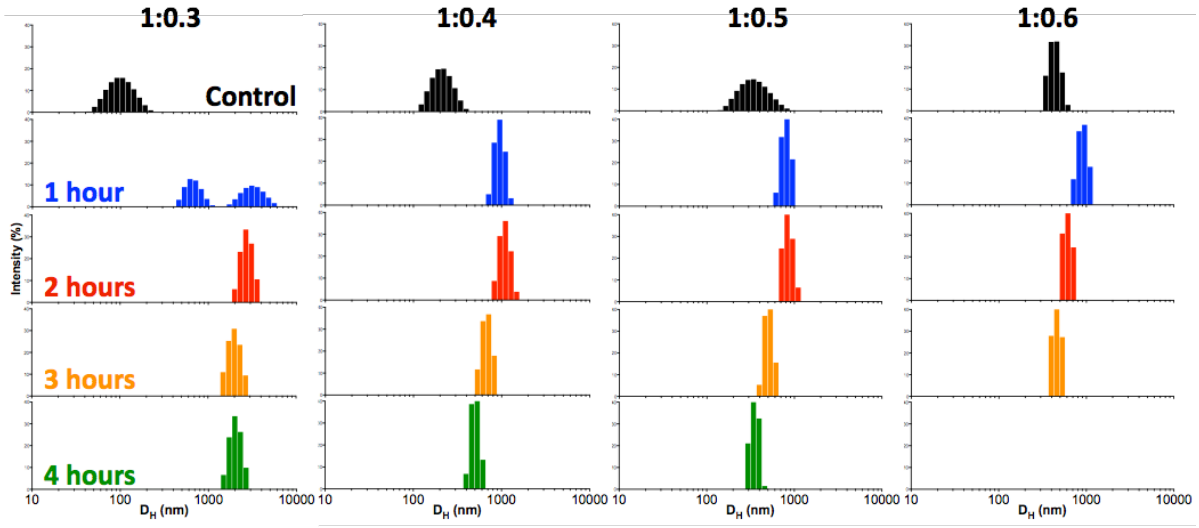

Fig. S11 Representative intensity distributions[†] of sizes for the four most stable **P1$_{SH}$** PIC nanoparticles analysed (**Table S2** and **Fig. S10**) in the absence (control) and presence of 154 mM NaCl at 37°C over time (1-4 hours).

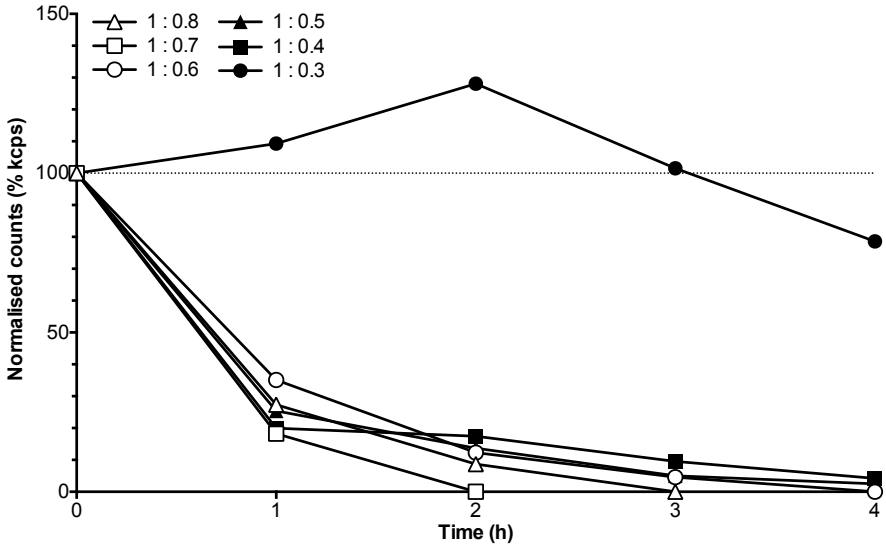

Fig. S12 Normalised detection counts for **P1$_{SH}$** PIC nanoparticles prepared using six different N:COOH ratios (**Table S2**) in the absence (0 h) and presence of 154 mM NaCl at 37°C over time (1-4 hours). Data was normalised to the size of the particles in the absence of NaCl (100%). Values plotted are the average of 3 technical replicates.

8. Stability in the presence of divalent cations – Treatment with CaCl2

To 500 µL of PIC particles (1:0.6 in N:COOH), prepared as described in the main text, a 1 M solution of $CaCl_2$ in water was added to give a final concentration of 10, 50 and 100 mM in Ca^{2+}. The samples were analysed by DLS immediately after addition of $CaCl_2$.

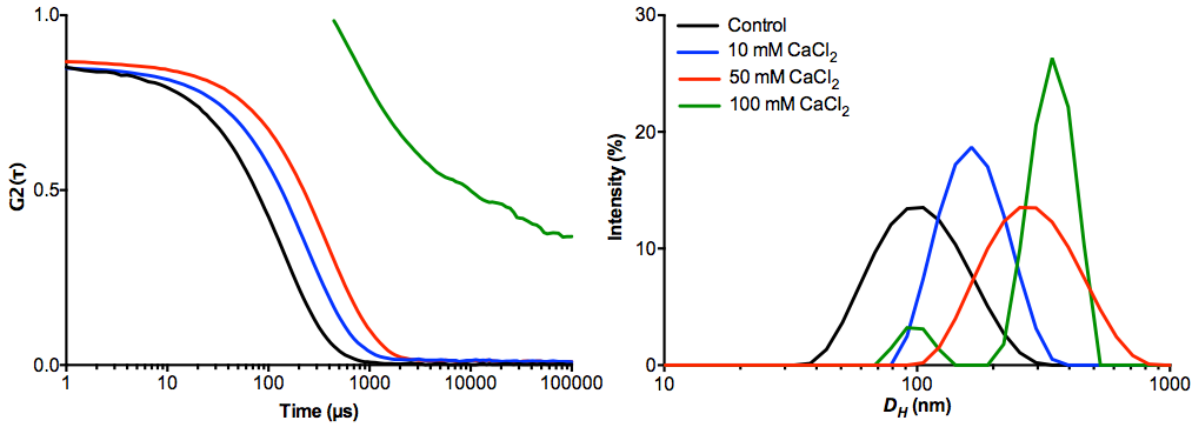

Fig. S13 Representative DLS autocorrelation function (ACF) curves (left) and intensity distributions of sizes (right) of PIC particles (1:0.6 in N:COOH) in the absence (control) and presence of increasing concentrations of $CaCl_2$.

9. Enzymatic degradation of PIC nanoparticles

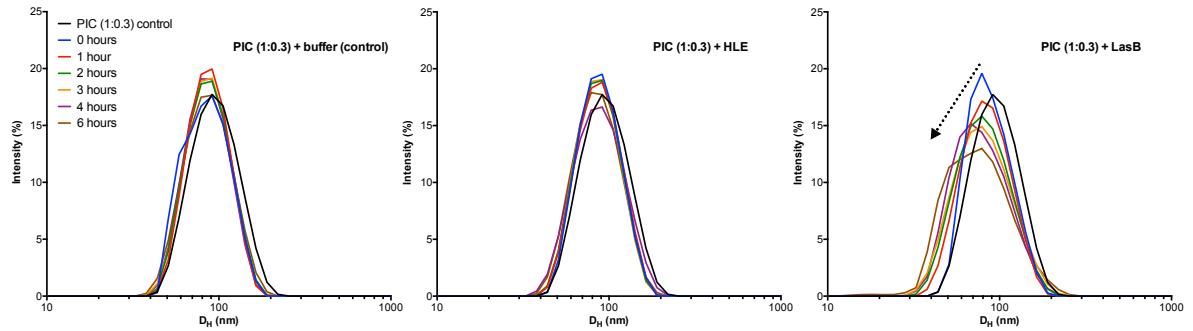

Fig. S14 Representative intensity distributions of sizes for $\mathbf{P1_{SH}}$ PIC nanoparticles prepared at a 1:0.3 N:COOH ratio incubated with $Na_2B_4O_7$ buffer (left), HLE (middle) and LasB (right) over time. Distribution for LasB broadens upon increasing incubation time (arrow). Values plotted are the average of 3 sample replicates, each measured 3 times. n=9.

DLS correlograms for this dataset can be found in **Fig. S18**.

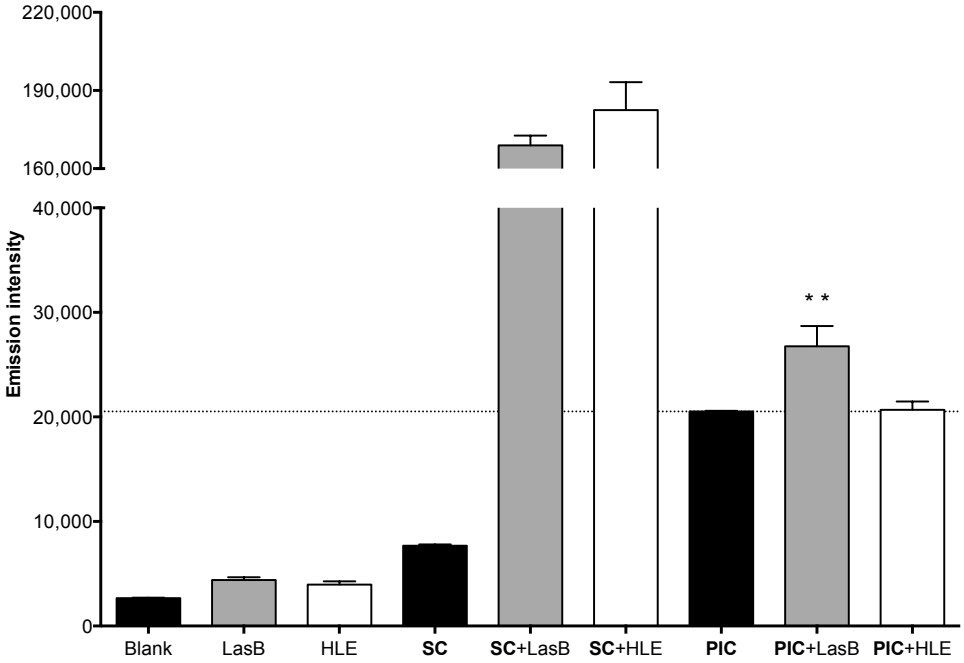

Fig. S15 Emission intensity (λ_{exc} 355 nm, λ_{em} 460 nm) of fluorescamine conjugates for enzymes, succinyl casein (SC) as a control for enzymatic activity and **P1$_{SH}$** PIC nanoparticles prepared at a 1:0.3 N:COOH ratio. All substrates were evaluated in the absence and presence of LasB or HLE and incubated for 4 hours. ** $p < 0.01$ between PIC and PIC + LasB. n=3.

10. Antimicrobial activity of PIC nanoparticles

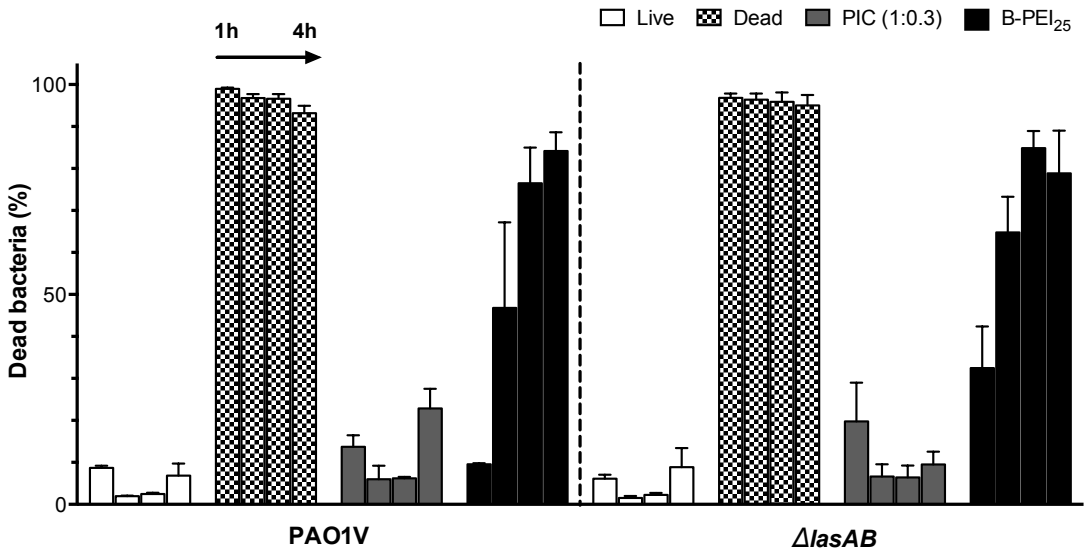

Fig. S16 Raw FACS data for *P. aeruginosa* wild type (PAO1V) and *ΔlasAB* mutant in the absence (live control, white bars) and presence of **P1$_{SH}$** PIC nanoparticles (1:0.3 N:COOH ratio, grey bars), B-PEI$_{25}$ (black bars) and 70% v/v aqueous 2-propanol (dead control, dotted bars). Population presented as the percentage of red (dead) cells. In each group of four, each bar represents a time point (1, 2, 3 and 4 hours from left to right). Toxicity of B-PEI$_{25}$ after one hour was not statistically different from the live control and thus that time point has not been included in **Fig. 5**. n=3.

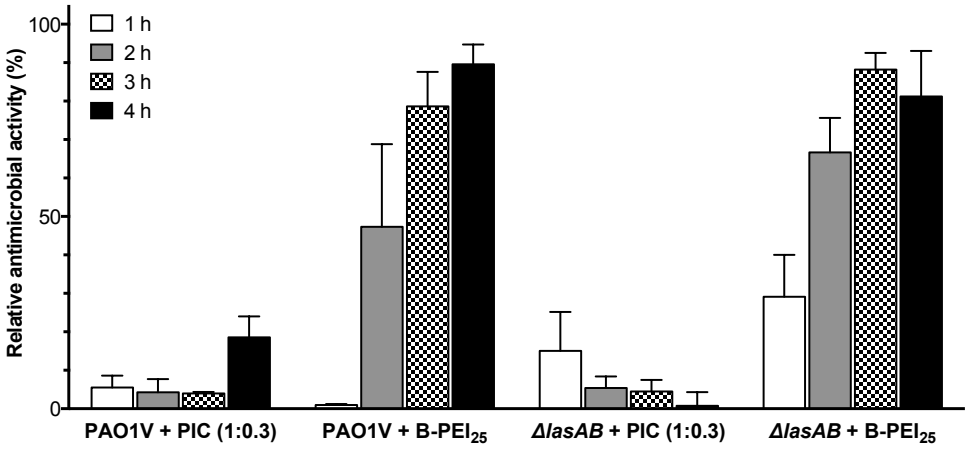

Fig. S17 Relative antimicrobial activity for *P. aeruginosa* wild type (PAO1V) and *ΔlasAB* in the presence of $\mathbf{P1_{SH}}$ PIC nanoparticles (1:0.3 N:COOH ratio, grey bars) and B-PEI_{25} (black bars). Relative antimicrobial activity was calculated normalising data from **Fig. S16** to live control (0% of antimicrobial activity) and dead control (100% of antimicrobial activity) at each time point. n=3.

11. Supplementary references

[1] C. Kay, O. E. Lorthioir, N. J. Parr, M. Congreve, S. C. McKeown, J. J. Scicinski and S. V. Ley, *Biotechnol. Bioeng.*, 2001, **71**, 110.
[2] T. Vojkovsky, *Pept. Res.*, 1995, **8**, 236.
[3] T. Hatakeyama, H. Kohzaki and N. Yamasaki, *Anal. Biochem.*, 1992, **204**, 181.
[4] K. Morihara and H. Tsuzuki, *Arch. Biochem. Biophys.*, 1971, **146**, 291–296.
[5] E. Kessler and D. E. Ohman, in *Handbook of Proteolytic Enzymes - (Third Edition) - ScienceDirect*, eds. N. D. Rawlings and G. Salvesen, Academic Press, London, 3rd edn. 2013, vol. 1, pp. 582–592.

2.3. Additional figures

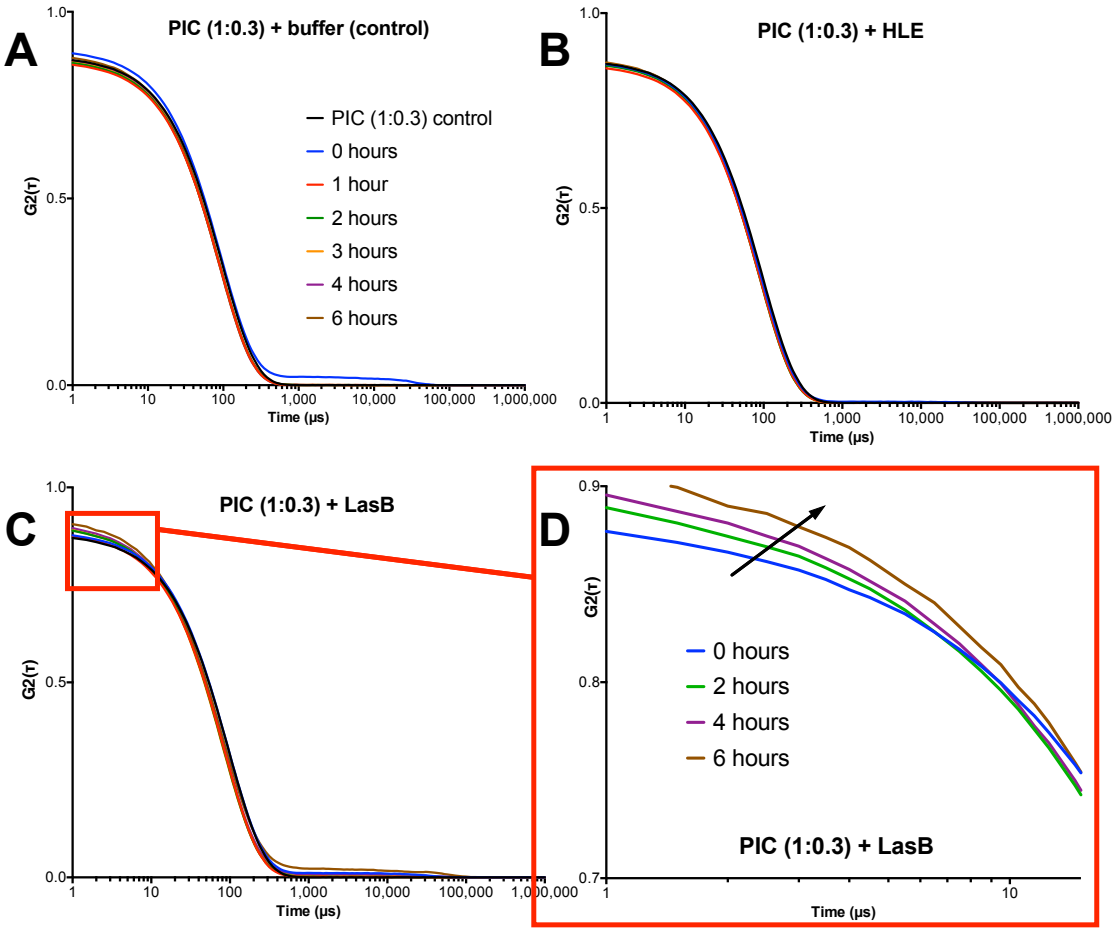

Figure S18 DLS correlograms for **P1$_{SH}$** PIC nanoparticles prepared at a 1:0.3 N:COOH ratio incubated with $Na_2B_4O_7$ buffer (A), HLE (B) and LasB (C) over time. Graph D shows a closer look at the framed section of plot C, where the arrow indicates increasing incubation times. DLS Size-Intensity plots for this dataset can be found in **Fig. S14**.

CHAPTER 3

Elastase-sensitive peptides with higher multivalency form more stable polyion complex (PIC) nanoparticles with compromised susceptibility to enzymatic degradation

Format: Paper draft (unpublished).

Authors: I. Insua, M. Petit, L. D. Blackman, R. Keogh, A. Pitto-Barry, R. K. O'Reilly, A. F. A. Peacock, A. M. Krachler and F. Fernandez-Trillo.

Overview: In this Chapter, we attempt to optimise the saline stability and activity of the enzyme-responsive PIC particles described in Chapter 2. Our motivation was double: Firstly, the swelling and even breakdown experienced by these nanoparticles in the presence of salt can compromise their targeted properties by triggering the release of antibiotic in virtually any biological (*i.e*. saline) fluid. Hence the specificity of their antimicrobial action could be improved by developing more salt-tolerant nanomaterials, which only release the loaded antibiotic in the presence of the target pathogen. Secondly, only the antimicrobial properties of one PIC particle formulation were evaluated in the Chapter 2, as the nanoparticles prepared at other charge ratios were not stable enough to be tested. Improving the stability of PIC particles could allow the exploration of other formulations, or charge ratios, which may display higher and/or faster antimicrobial activities due to the distinct exposure of the peptides in the nanoparticle: for example, charge ratios with an excess of negative component, which could not be prepared in Chapter 2, would lead to an accumulation of peptide on the surface of

the nanoparticle, thus increasing its exposure to LasB and potentially trigger the release the antibiotic more rapidly.

Here, based on the direct relationship between the polyelectrolytes' net charge (*i.e*. multivalency) and their binding affinity described in Chapter 1, we present a collection of new LasB-responsive peptides with increased multivalency and cross-linking units, aiming to strengthen the attraction between the polyelectrolytes and the mechanical resistance of the resulting nanoparticles, respectively. As such, these modifications contribute to form more tightly bound and stable PIC particles, and hence could allow the preparation of new charge ratios.

The nanoparticles obtained from these new peptides were characterised by a range of light scattering techniques and ζ-potential, and their stability under simulated physiological conditions and antimicrobial properties were evaluated. We found that peptides with higher multivalencies and cross-linking degree allowed the formulation of new charge ratios, and improved the saline stability of PIC particles. However, none of the resulting PIC particles tested were hydrolysed by LasB, hence no antimicrobial activity was displayed by these new PIC particles in the presence of pathogenic *Pseudomonas aeruginosa*. It was therefore concluded that the activity of the PIC particles introduced in Chapter 2 could not be optimised by increasing the peptides' multivalency and cross-linking degree.

The observations described in this Chapter contribute to gain further insight into developing new PIC particle formulations, and how the polyelectrolyte's multivalency and cross-linking degree can impact the stability and enzymatic susceptibility of PIC particles. An important contribution to this thesis is the structural analysis of PIC particles by SLS and SAXS presented exclusively in this Chapter, which provides further insight into the characteristics of these nanomaterials.

Contributions: All authors contributed to the experimental set-up and discussed the results. II and FFT designed the peptides and nanoparticle preparation; and II, FFT and AMK designed the microbiological assays. MP synthesised and characterised the peptides. LDB, RK and RKOR designed and performed the SLS experiments. APB interpreted the SAXS data. II carried out all other experiments. II wrote the manuscript.

Elastase-sensitive peptides with higher multivalency form more stable polyion complex (PIC) nanoparticles with compromised susceptibility to enzymatic degradation

Ignacio Insua,[a,b] Marion Petit,[a] Lewis D. Blackman,[c] Robert Keogh,[c] Anaïs Pitto-Barry,[c] Rachel K. O'Reilly,[c] Anna F. A. Peacock,[a] Anne Marie Krachler[b,d] and Francisco Fernandez-Trillo[a,b,*]

[a]*School of Chemistry, University of Birmingham, B15 2TT Birmingham, UK.*
[b]*Institute of Microbiology and Infection, School of Biosciences, University of Birmingham, B15 2TT Birmingham, UK.*
[c]*Department of Chemistry, University of Warwick, CV4 7AL Coventry, UK.*
[d]*Department of Microbiology and Molecular Genetics, University of Texas, 6431 Fannin. Houston (TX), USA.*
**Email: f.fernandez-trillo@bham.ac.uk*

Electronic Supplementary Information (ESI) available at the end of this article: Peptide synthesis and characterisation, further details of PIC particle characterisation and stability and full data from biological experiments.

A comparative study was conducted between four anionic peptides that can be degraded by *P. aeruginosa*'s elastase LasB, to evaluate the influence of their net charge and cross-linking degree on the properties of polyion complex (PIC) nanoparticles prepared from these peptides and the antimicrobial poly(ethylene imine). Peptides with higher net charges and cross-linking units led to PIC particles with superior stability to saline buffer and displayed a remarkable reduction in the toxicity of poly(ethylene imine). However, LasB was not capable to trigger the disassembly and antimicrobial activity of these more stable nanoparticles.

Introduction

Polyion complex (PIC) nanoparticles are soft colloids made from oppositely charged polyelectrolytes that self-assemble in solution.[1] These nanomaterials have drawn a lot of attention for being remarkably versatile vehicles for drug delivery applications.[2] Such nanomaterials can be easily prepared from charged therapeutics in combination with an oppositely charged polymer. As such, PIC particles are modular systems that allow the control of the therapeutic properties of pre-loaded drugs by simple formulation modifications. The size, charge, colloidal stability and biological activity of PIC particles can be tuned by simply adjusting the relative content of polyelectrolytes. The assembly of these nanomaterials occurs spontaneously in water, does not require the chemical modification of charged therapeutics, and the 'excipient' polyelectrolyte (*i.e.* pharmacologically inactive) can be adjusted in size and structure to tune the properties of the resulting nanoparticles.[3,4]

PIC particles have reduced the toxicity and improved the performance of charged antineoplastics,[5] antimicrobials,[6-8] and allowed the delivery of nucleic acids to the inside of cells.[2] The release of drugs from these materials occurs when the attractive forces between polyelectrolytes are weakened, leading to the dissolution of their components and breakdown of the nanoparticles. As such, polyelectrolytes that can degrade in the presence of certain stimuli can allow the assembly of responsive PIC particles that dissociate when exposed to a particular degrading agent or trigger. Particle dissociation occurs because a longer polyelectrolyte is broken down into smaller fragments by the trigger, thus causing a sudden loss of net charge (*i.e.* multivalency) in this component that weakens the electrostatic forces involved.

Given the key role of enzymes in many pathologies and their remarkable specificity, PIC particles prepared from polyelectrolytes that degrade in the presence of certain enzymes are particularly interesting for biomedical applications.[9] Enzyme-responsive PIC particles can establish a communication between the host (or pathogen) and the nanoparticle, allowing to tune the therapeutic effect in response to disease markers.

We recently reported enzyme-responsive PIC particles for the delivery of the antimicrobial polymer poly(ethylene imine) (B-PEI) in the presence of *Pseudomonas aeruginosa*'s elastase LasB.[10] These nanoparticles consist of cationic B-PEI complexed with an anionic peptide (**P1$_{SH}$**) that is hydrolysed by LasB, so the latter component can be degraded from the PIC particle by the elastase, thus releasing the antimicrobial from the colloid when exposed to a pathogenic strain of *P. aeruginosa* that produces LasB. However, these PIC particles suffered from poor stability to physiological salt concentrations, swelling up to twenty times their original size or even breaking down under simulated physiological conditions. In order to fully exploit the therapeutic potential of this system, the salt stability of these nanoparticles must be improved to ensure their integrity in biological settings and control over the release of the antimicrobial.

Here we present a collection of new LasB-responsive peptides prepared across a range of multivalencies and cross-linking units, which were used in combination with B-PEI to assemble PIC particles. The characterisation of the resulting nanoparticles and their salt tolerance was evaluated as a function of the multivalency and cross-linking units present in these peptides. PIC particles were characterised by a range of light scattering techniques to identify any structural differences caused in these nanomaterials by particular peptides. Finally, the antimicrobial activity of these PIC nanoparticles was assessed against *P. aeruginosa*, and the results were compared to the distinct susceptibility of peptides and PIC particles to LasB's action.

Experimental

Materials

Enzymes (*Pseudomonas aeruginosa* Elastase (LasB): EC 3.4.24.26 and Human Leucocyte Elastase (HLE): EC 3.4.21.37) were purchased from Merck Millipore. Branched poly(ethylene imine) 25 kDa average molecular weight (B-PEI), 4-(2-hydroxyethyl)piperazine-1-ethanesulfonic acid (HEPES), Luria Bertani (LB) broth (Miller) and Dulbecco's modified eagle medium (DMEM) were bought from Sigma-Aldrich®. Fluorescamine and dimethylsulphoxide (DMSO) were purchased from Acros Organics™. Ethylenediaminetetraacetic acid (EDTA) was purchased from Alfa Aesar®. Nylon 0.45 µm syringe filters were purchased from Camlab. *P. aeruginosa* strains were kindly donated by Suzanne M. J. Fleiszig. We studied PAO1V as a pathogenic strain (wild type) and a deletion strain of *lasA* and *lasB* genes of PAO1V was used as LasB-negative control (*ΔlasAB*). Live/Dead® BacLight™ viability kit was purchased from Thermo Fisher Scientific Inc.

Instrumentation

Dynamic Light Scattering (DLS) and ζ-potential measurements were carried out in a Zetasizer Nano ZSP (Malvern Instruments Ltd.) stabilised at 37 °C. DLS was read at 173 ° (backscattering) for 60 seconds in triplicate and ζ-potentials were recorded 30 times at 140 V. A FLUOstar Omega (BMGLabtech Gmbh) microplate reader was used to measure fluorescamine reactions. Static Light Scattering (SLS) and simultaneous DLS data was collected using an ALV/CGS-3 Compact Goniometer System operating at a wavelength of 633 nm. Small Angle X-ray Scattering (SAXS) measurements were performed at Diamond Light Source on beamline B21, at a photon energy of 12.4 keV and 1 Å wavelength (monochromatic beam), from samples prepared in 5 mM HEPES buffer pH 7.4, stabilised at 15.0 °C and analysed from quartz capillary tubes with a diameter of 1.6 mm. SAXS spectra were recorded using a Pilatus 2M detector (DECTRIS®) situated at 4.04 m from the sample, and the fitting of SAXS spectra to structural models was performed using IGOR Pro (version 6.37) by WaveMetrics. Fluorescence-Activated Cell Sorting (FACS) was performed on an Attune® Acoustic Focusing Cytometer (Applied Biosystems™) measuring 10,000 events per sample using BacLight™ fluorescent dyes, which were excited at 488 nm and emission was read at 515–545 and 640 nm for green and red probes, respectively.

Preparation of PIC nanoparticles

For nanoparticles prepared at a 1:0.3 [N:COOH] ratio (defined as the ratio between amines in B-PEI and carboxylic acids in the peptides), stock solutions of B-PEI (2.5 mM in amines) and peptide (**P2-4$_{SH}$**) (0.75 mM in carboxylate groups) in 5 mM HEPES buffer at pH 7.4 were prepared. Then, both solutions were filtered and mixed in equal volumes drop-wise under stirring. The reaction mixture was stirred at room temperature for 24 hours open to air to allow thiol oxidation. PIC nanoparticles prepared at different [N:COOH] ratios were obtained by changing the concentration of peptide stock solution and mixing with the 2.5 mM B-PEI stock following the same protocol (**Table S1**). After 24 hours, samples were analysed directly by DLS and ζ-potential without prior filtration.

Antimicrobial activity of PIC nanoparticles

1 mL aliquots of *P. aeruginosa* PAO1V and *ΔlasAB* cultures in LB broth (OD_{600} = 1.0) were centrifuged and resuspended in 1 mL of DMEM. These samples were incubated at 37 °C for 6 hours under orbital shaking to allow LasB production. After this time, samples were centrifuged and half of the super- natant replaced with the same volume of 5 mM HEPES buffer at pH 7.4 (live control), PIC nanoparticles or 1.25 mM B-PEI in 5 mM HEPES buffer at pH 7.4. A dead control was also prepared by replacing all the supernatant after centrifugation with 70% v/v aqueous 2-propanol. Samples were resuspended and incubated at 37 °C under orbital shaking. Each sample was prepared in triplicate. Every hour during a total of 4 hours, 200 µL of each sample were taken and the rest was kept shaking at 37 °C. These 200 µL aliquots were incubated in the dark for 10 minutes with 1 µL of a 10-fold diluted 1:1 mixture of BacLight™ probes in DMEM. Dead control samples had to be centrifuged and resuspended in assay buffer before staining with fluorescent dyes. Then, samples were analysed by FACS setting gates for dead bacteria in green *versus* red emission dot plots from the live and dead controls.

Enzymatic degradation of peptides – Fluorescamine assay

Stock solutions of peptide (1 mM) or succinyl casein (0.5 mg/mL) were prepared in 25 mM $Na_2B_4O_7$ buffer at pH 8.0 with 10 mM $CaCl_2$ and 10% v/v DMSO. 125 µL of these substrate solutions were added to a 96-well black-walled microplate and mixed with 125 µL of the same buffer without DMSO, containing 15 µg of enzyme (LasB or HLE). Solutions of enzymes and substrates alone were prepared as blanks. Every sample was prepared in triplicate. The microplate was incubated at 37 °C for 4 hours under orbital shaking. After 4 hours, 50 µL of 0.1 M EDTA in water at pH 8.0 were added to each well to quench all enzymatic activity. Then, each sample was mixed in a 1:1 volume ratio with a 1 mM solution of fluorescamine in methanol. The microplate was incubated at 37 °C under orbital shaking for 30 minutes. After this time, fluorescence was measured exciting at 355 nm and reading the emission at 460 ± 10 nm.

Enzymatic degradation of PIC nanoparticles

1 mL of PIC nanoparticles prepared at 1:0.3 [N:COOH] ratio was incubated at 37 °C with 50 µL (5 µg) of LasB in 2.5 mM $Na_2B_4O_7$ buffer at pH 8.0. As control experiments, PIC nanoparticles were incubated under the same conditions with enzyme (LasB or HLE, 5 µg) or $Na_2B_4O_7$ buffer to assess the enzymatic specificity and effect of salts in the buffer, respectively. Each sample was prepared in triplicate from three different batches of PIC nanoparticles. DLS data was acquired over time (1–4

hours). The number of amines was monitored after 4 hours of incubation as described before (fluorescamine assay).

Results and discussion

Peptide design and synthesis

Based on the structure of the LasB-responsive peptide **P1$_{SH}$** (Ac-C-E-GLA-E-C-OH) previously reported by our group,[10] two modifications were proposed to enhance the salt stability of the resulting PIC particles: i) Additional glutamic acids were included to increase the multivalency (*i.e.* net charge) of this anionic peptide, potentially leading to a stronger affinity for antimicrobial B-PEI. ii) The incorporation of a third cysteine would allow these peptides to oxidise forming branched chains, which is expected to provide a more densely cross-linked network and higher mechanical resistance to the nanoparticles.[2]

Peptides **P2$_{SH}$**, **P3$_{SH}$** and **P4$_{SH}$** were thus prepared by conventional solid-phase peptide synthesis, and included the amino acid sequence –GLA–, which is degradable by the pathogenic enzyme LasB. These peptides included two additional glutamic acids (**P2$_{SH}$**), four additional glutamic acids (**P3$_{SH}$**), and four extra glutamic acids and one additional cysteine (**P4$_{SH}$**) compared to **P1$_{SH}$**. Therefore, peptides **P2$_{SH}$** and **P3$_{SH}$** were designed to study the effect of multivalency, whereas the influence of the branched cross-linking was studied with peptides **P3$_{SH}$** and **P4$_{SH}$** (**Figure 1**).

Self-assembly and characterisation of PIC particles

PIC particles were prepared by mixing peptides **P2-4$_{SH}$** with B-PEI in aqueous medium at physiological pH as previously reported.[10] Given the implication of the charge ratio of PIC particles –this is the relative number of positive and negative charges mixed in the formulation– in their colloidal stability, a range of formulations was tested with each peptide. Denoted as [N:COOH], charge ratios from 1:2.0 to 1:0.2 were prepared, indicating the relative number of cationic amines in B-PEI versus anionic carboxylic acids in peptides **P2-4$_{SH}$** respectively, and the resulting complexes were characterised by DLS and ζ-potential.

Based on their ζ-potentials, three regions were found for all LasB-responsive peptides: one towards higher peptide contents that gave negatively charged complexes; another at lower peptide ratios giving cationic PIC particles; and one in between where no PIC particles formed (**Figure 2**, **Table S1**). These results can be explained from the proposed structure of PIC particles,[1,2] which consist of a neutral core made of a stoichiometric mixture of oppositely charged polyelectrolytes, surrounded by a corona of the polyion in excess. Therefore,

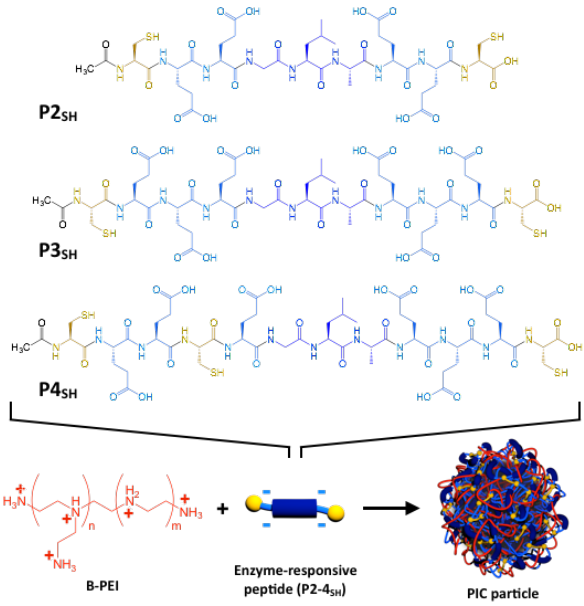

Figure 1 Structures of LasB-responsive peptides **P2$_{SH}$** (Ac-C-EE-GLA-EE-C-OH), **P3$_{SH}$** (Ac-C-EEE-GLA-EEE-C-OH), **P4$_{SH}$** (Ac-C-EE-C-E-GLA-EEE-C-OH) and branched poly(ethylene imine) (B-PEI) and their self-assembly into PIC particles.

the ζ-potential of PIC particles will have the sign of the polyion in excess (*i.e.* in the corona), whereas neutral complexes form at 1:1 charge ratios leading to the aggregation and sedimentation of particles without a stabilising corona. This neutralisation point was found between the [N:COOH] ratios of 1:0.8 and 1:0.5 for **P2$_{SH}$**, whereas peptides **P3$_{SH}$** and **P4$_{SH}$** only formed neutral complexes at a [N:COOH] ratio of 1:0.5. The deviation from the theoretical neutral point at [N:COOH] = 1:1 towards more B-PEI-rich mixtures had been previously described for a different PIC particle system containing B-PEI,[3] and it is likely due to the incomplete protonation of all amines in B-PEI due to Coulombic interactions between neighbouring ammonium groups.[11] Similarly, since more multivalent peptides should have stronger affinities for B-PEI, the exchange of peptides **P3$_{SH}$** and **P4$_{SH}$** between PIC particles and the solution should be slower than for **P2$_{SH}$**, ultimately leading to more defined neutral regions in the former case. Additionally, **P3$_{SH}$** and **P4$_{SH}$** showed no significant difference in the size or charge of any of the resulting PIC particles (**Figure 2**B-C), suggesting that multivalency is the predominant factor that governs the self-assembly of this collection of peptides. Regardless of the peptide used, the [N:COOH] ratio 1:0.2 did

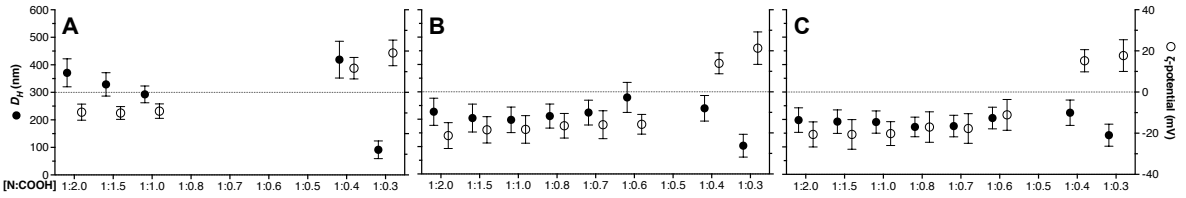

Figure 2 Hydrodynamic diameter (D_H, ●) and ζ-potential (○) of PIC particles prepared from peptides **P2$_{SH}$** (A), **P3$_{SH}$** (B) and **P4$_{SH}$** (C) at different [N:COOH] ratios. Each value represents the mean size and charge of the only population fitted by the software for each sample ± its standard deviation. Empty spaces indicate formulations that did not form PIC particles. The [N:COOH] ratio 1:0.2 is not presented here as none of these peptides formed PIC particles at that particular mixture. Further details can be found in **Table S1**.

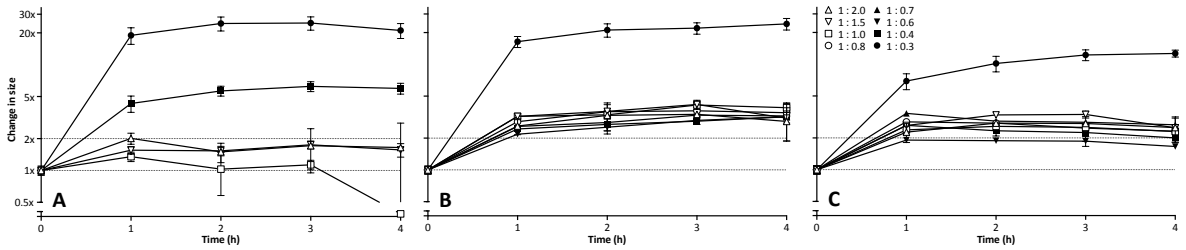

Figure 3 Size evolution of PIC particles prepared from peptides **P2$_{SH}$** (**A**), **P3$_{SH}$** (**B**) and **P4$_{SH}$** (**C**) at different [N:COOH] ratios (symbols) under simulated physiological conditions (37 °C, 154 mM NaCl, pH 7.4) over 4 hours. The D_H values measured at each time point were normalised to that of those PIC particles in the absence of salt (0 hours, 1x). n = 3, mean values ± SD.

not form PIC particles, probably due to the lack of enough peptide in these formulations to condense B-PEI.

Size-wise, particles with hydrodynamic diameters (D_H) were obtained for **P2$_{SH}$** (*ca*. 300-400 nm) than for **P3$_{SH}$** and **P4$_{SH}$** (*ca*. 100-300 nm), regardless of the [N:COOH] ratio tested (**Figure 2**). The smaller size of the latter PIC particles is expected as a result of the higher multivalency of their consisting peptides (-7 for **P3$_{SH}$** and **P4$_{SH}$** *versus* -5 for **P2$_{SH}$**), which should form more strongly and tightly bound polyelectrolyte networks within these nanoparticles. For all peptides, formulations prepared at a [N:COOH] ratio of 1:0.3 gave the smallest PIC particles, with an average D_H of *ca*. 110 nm and ζ-potential of +19 mV – in close agreement with the values previously found for this [N:COOH] ratio with **P1$_{SH}$**.[10]

Physiological stability of PIC particles

The electrostatic forces that keep PIC particles together can be shielded by small electrolytes, which can result in the swelling and ultimately breakdown of these nanoparticles. Hence, the integrity of PIC particles may be compromised by the high concentrations of salts present in biological fluids. In order to assess their tolerance to physiological salinity, PIC particles were incubated in the presence of 154 mM NaCl at 37 °C, and their D_H was monitored over four hours (**Figure 3**). It was observed that all PIC particles swelled when exposed to NaCl, and this response was proportional to the peptides' multivalency and cross-linking degree. Particles prepared from the least multivalent peptide **P2$_{SH}$** showed more polydisperse aggregates after 2 and 3 hours, and even broke down after 4 hours at a [N:COOH] ratio of 1:1 (**Figure 3A**). Nevertheless, **P2$_{SH}$** complexes showed better physiological stabilities than those made from the less multivalent **P1$_{SH}$**,[10] reinforcing the direct correlation between peptide multivalency and PIC particle stability. For all peptides, PIC particles made at a [N:COOH] of 1:0.3 swelled the most, reaching 26 and 28 times their original size after 4 hours with peptides **P2$_{SH}$** and **P3$_{SH}$**, respectively. However, PIC particles prepared from **P4$_{SH}$** (with one extra cross-linking cysteine residue) at the same [N:COOH] ratio were less affected by this saline medium, displaying 14 times their original size after 4 hours (**Figure 3C**). These results highlight the critical effect multivalency and cross-linking degree have on the salt tolerance of PIC particles, as evidenced by their physiological stability: **P1$_{SH}$**<**P2$_{SH}$**<**P3$_{SH}$**<**P4$_{SH}$**.

Structural characterisation of PIC particles

In order to further understand the impact peptides **P1**-**4$_{SH}$** have on the structure of PIC particles, these nanomaterials were characterised by Static Light Scattering (SLS) and Small Angle X-ray Scattering (SAXS). PIC particles prepared from all four peptides at a [N:COOH] ratio of 1:0.3 were selected for the analysis, being the most stable and consistent formulation throughout the collection of peptides studied.

For the SLS analysis, the scattering intensity from a suspension of PIC particles was measured at different angles ranging from 20 to 100°, and their DLS profiles were simultaneously recorded. Due to the intense scattering observed for these samples at low angles (below 40°), all PIC particle suspensions had to be filtered through 0.45 µm nylon filters to remove any larger scatterers than the expected nanoparticles – which were all smaller than the filter's cut-off size according to our previous DLS characterisation (**Figure 2**). Thus, the angle dependency observed for the unfiltered samples in their Zimm plots could be corrected (**Figure S13**), allowing the linear regression of $K{\cdot}c/R_\theta$ versus q^2 for filtered PIC particles; where K is a constant containing the optical parameters, c is the concentration of the sample and R_θ the Rayleigh ratio of the particles at a given scattering angle (θ), and q is the scattering wave vector.[8] As such, linear Zimm plots allowed the calculation of the radius of gyration (R_g) of the nanoparticles by SLS analysis (**Figure 4**), which was compared to the R_H obtained by DLS under the same conditions. The ratio between the R_g and R_H of nanomaterials provides information about the internal structure and shape of a particular colloid.[12] On this basis, PIC particles prepared from peptides **P2**-**P4$_{SH}$** showed R_g/R_H values of 1.0, which are considerably higher than the theoretical maximum of 0.775 expected for the core-shell structure of PIC particles. Moreover, nanoparticles prepared from peptide **P1$_{SH}$** showed a slight deviation towards R_g/R_H > 1, characteristic of anisotropic colloids. This distinct result for **P1$_{SH}$** could be explained from the tendency of these colloids to aggregate, as observed when their D_H was monitored over time under shelf storage conditions (**Figure S14**): Whereas PIC particles prepared from peptides **P2**-**4$_{SH}$** displayed the same size throughout the experiment, the D_H of the nanoparticles made from **P1$_{SH}$** increased by 50% after 10 days – the time that passed since the preparation of these PIC particles until their SLS analysis.

The SLS characterisation of these nanoparticles was in agreement with the R_g/R_H values previously reported for other PIC particle systems, ranging between 1 and 2.[13,14] The deviation above the theoretical R_g/R_H value for a solid sphere (0.775) has been explained from the intrinsic high polydispersity of PIC particles.[13,15]

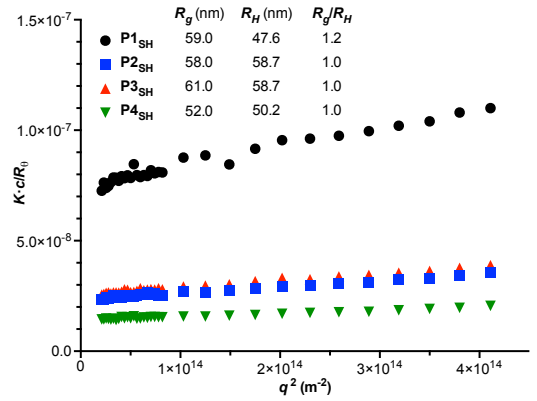

Figure 4 Zimm plots obtained by SLS of filtered PIC particles prepared from peptides **P1-4$_{SH}$** at a [N:COOH] ratio of 1:0.3. The inset indicates the gyration (R_g) and hydrodynamic (R_H) radii simultaneously calculated by SLS and DLS, respectively.

Additionally, the structural features of PIC particles were studied by SAXS at the Diamond Light Source synchrotron. Nanoparticle samples at a [N:COOH] ratio of 1:0.3 were chosen for the analysis to be compared with the previous SLS results. All four samples showed almost identical SAXS profiles regardless of the peptide used (**Figure 5**). It must be noted that the interpretation of these SAXS spectra was difficult due to lack of a Guinier region and very noisy results at high q values. Firstly, the data was fitted to a Guinier-Porod (GP) model to obtain an indication of the shape of these nanomaterials, taking into consideration our previous DLS and SLS results to assess the goodness of the Guinier region produced by the fit. For this GP fit, only the experimental points within the Porod region (*i.e.* q values between 0.004 and 0.02) were considered, and gave excellent fitting scores (χ^2) with values of 0.71 and below.[16] The R_g of these PIC particles obtained from the GP fit gave very similar results for all samples, with values between 73.0 and 77.3 nm. Although these R_g values should not be taken as accurate due to lack of experimental data in the Guinier region to validate the GP fit, they are in agreement with the R_g obtained by SLS – considering that SAXS samples were not filtered, unlike for SLS analysis, and therefore a higher R_g is expected in the samples analysed by SAXS from the contribution of additional large scatterers. Having thus accepted this GP fit based on the χ^2 and R_g obtained, this model allowed the calculation of the shape parameter 'S', which displayed values between 0.11 and 0.15 for all PIC particles, characteristic of spherical materials.

After establishing a spherical shape for these nanomaterials inferred from the GP fit, models of hard spherical objects were applied to the experimental data to characterise the internal structure of PIC nanoparticles, but these fits gave very poor χ^2 scores. 'Not hard' spherical models were explored instead, taking into consideration all experimental points between the q values of 0.004 and 0.3, and the only good fit identified was that of fractal polydisperse spheres (FPS, **Figure 5**). PIC particles of cationic hyperbranched polymers and DNA have been reported to self-assemble into spherical sponges or fractals.[17] These electrostatic interactions do not allow the formation of hard sphere objects, but give porous particles with some short repeat units that can be associated to fractal dimensions. Hence, analysis of such objects by SAXS often involves the use of fractal models. Also, the weakening and eventually disappearance of oscillations in the Porod region is known to be directly proportional to the sample's polydispersity,[18] which is consistent with the straight Porod region shown by these samples (**Figure 5**), and confirms the high polydispersity of PIC nanoparticles observed by DLS (**Table S1**), also inferred from the high R_g/R_H values obtained by SLS analysis (**Figure 4**). Therefore, it was concluded from SAXS analysis that these PIC particles are highly hydrated and polydisperse fractal materials, which present smooth surfaces, as indicated by the -4 slope of their Porod regions. Assuming the GP fit obtained is accurate, SAXS analysis confirms the R_g values determined by SLS (**Figure 4**) and the spherical shape previously observed for some of these PIC nanoparticles by imaging techniques.[10] However, in the absence of experimental data points in the Guinier region to verify the goodness of the GP fit, the size and shape of these samples inferred from SAXS are merely indicative.

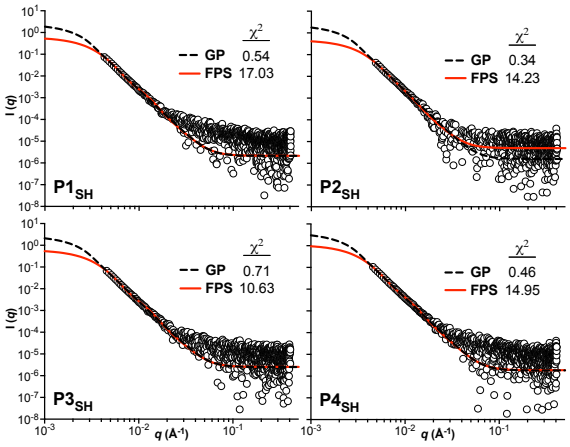

Figure 5 SAXS profiles of unfiltered PIC particles prepared from peptides **P1-P4$_{SH}$** at a [N:COOH] ratio of 1:0.3 (○) and fittings to structural models: Guinier-Porod (GP) and fractal polydisperse spheres (FPS). The inset indicates the fitting score (χ^2).

In summary, both SLS and SAXS consistently indicate that all PIC particles have the same internal structure, size and morphology regardless of the peptide used, as evidenced by their very similar profiles and structural parameters obtained from these two light scattering techniques.

Enzymatic degradation of peptides

The degradation of peptides **P1-4$_{SH}$** by *P. aeruginosa*'s elastase (LasB) was then evaluated. This experiment involved the fluorogenic quantification of the primary amines formed as a result of peptide hydrolysis using fluorescamine.[19] It is worth noting that LasB has an affinity to bind the –GLA– tripeptide, and can hydrolyse this sequence between the Gly and Leu residues.[20] Additionally, in order to assess their degradation by host enzymes, the peptides were also evaluated against Human Leukocyte Elastase (HLE), an elastase released by white

blood cells that shows enhanced activity during infections by *P. aeruginosa*.[21] The results of the fluorescamine assay were normalised to the fluorescence emission of the peptide fragment that would form upon enzymatic cleavage (**P5**, H_2N-LA-E-OH) at the same concentration, accounting for 100% hydrolysis.

Peptide **$P3_{SH}$** displayed the highest susceptibility to be hydrolysed by LasB, followed closely by **$P4_{SH}$** and **$P1_{SH}$** in that order (**Figure 6**, **Figure S15**). The fact that **$P2_{SH}$** was the least active of the four peptides led us to consider an effect of the secondary structure of the peptides on the activity, rather than simply an effect of their multivalency. However, circular dichroism analysis suggested all peptides had a random conformation (**Figure S16**), without any structural difference between them. Interestingly, while peptide **$P3_{SH}$** showed a complete specificity as substrate for LasB over HLE, the addition of an extra Cys residue in peptide **$P4_{SH}$** caused a severe loss in selectivity, which was degraded *ca*. 50% as much by HLE as by LasB. Hence, peptide **$P3_{SH}$** was selected for the preparation of PIC particles for biological evaluation for its superior activity and specificity.

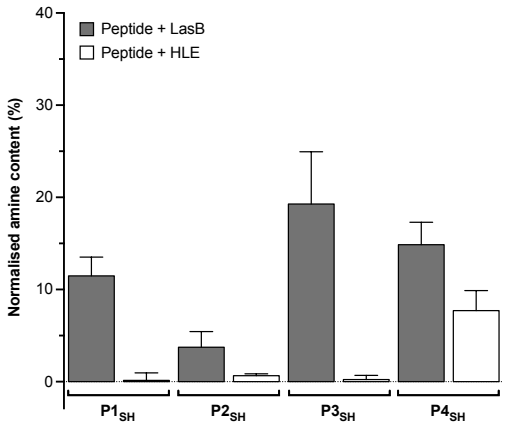

Figure 6 Normalised peptide hydrolysis quantified with fluorescamine after 4 hours of incubation of the peptides with bacterial (LasB) or human (HLE) elastase. *n* = 3, mean values ± SD.

Antimicrobial activity of PIC particles

The antimicrobial properties of PIC particles prepared from the most LasB-active peptide **$P3_{SH}$** (**Figure 6**) were assessed against *P. aeruginosa*. A pathogenic strain of this bacterium (wild type or WT) that produces LasB was incubated with PIC particles prepared at [N:COOH] ratios of 1:0.3 and 1:1.0. These two formulations were selected to test both positively and negatively charged nanoparticles, respectively (**Figure 2**). In this experiment, the antimicrobial activity of PIC particles was correlated to the number of cells stained in red with propidium iodide, a fluorescent probe that only stains bacteria with damaged membranes. The antimicrobial activity of PIC particles was measured every hour over four hours, and the red stained (*i.e.* dead) population of bacteria was normalised to that found in a positive (100% alive) and negative (100% dead) controls (**Figure S17**).

PIC particles displayed very weak antimicrobial activities, below 13%, regardless of the bacterial strain or incubation time (**Figure 7**). Unexpectedly, no distinct activities were found for any of the PIC particle formulations tested between strains. A LasB-specific activity was expected as only those nanoparticles exposed to the wild type, which secretes LasB, should trigger the antimicrobial effect of complexed B-PEI – as previously observed with PIC particles prepared from **$P1_{SH}$**.[10] Nevertheless, compared to the *ca*. 90% antimicrobial activity of B-PEI after 3 hours (**Figure S18**), PIC particles were dramatically less toxic than the uncomplexed antimicrobial polymer B-PEI. These results highlight the capacity of these nanomaterials to improve the therapeutic profile of certain drugs, allowing in this case an excellent reduction in the toxicity of the antimicrobial B-PEI.

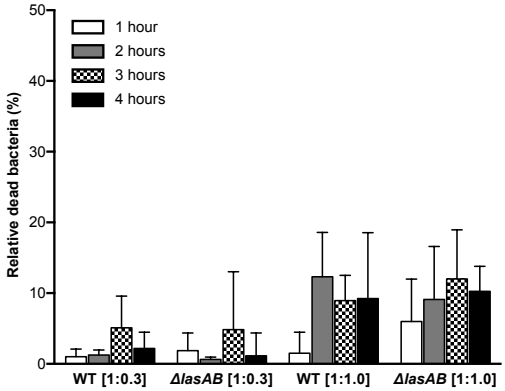

Figure 7 Normalised antimicrobial activity over time of **$P3_{SH}$** PIC nanoparticles prepared at [N:COOH] ratios of 1:0.3 and 1:1.0 (in brakets) against *P. aeruginosa* wild type (WT) and LasB-knockdown (*ΔlasAB*) strains. Activity normalised to that of the positive (0%) and negative (100%) controls for each time point (**Figure S17**). *n* = 3, mean values ± SD.

Enzymatic degradation of PIC particles

To understand the lack of enzyme-specific antimicrobial activity in these nanomaterials, we took one step back and evaluated their enzymatic degradation by the target enzyme LasB. PIC particles prepared from peptide **$P3_{SH}$** at a [N:COOH] ratio of 1:0.3 were incubated with LasB and HLE at 37 °C and their light scattering intensity was monitored over time. This experiment correlates the breakdown of particles with the decrease in the amount of scattered light (*i.e.* counts) detected by DLS over time. Surprisingly, such nanoparticles did not show any decrease in counts after 4 hours of incubation with LasB, suggesting that these colloids were not breaking down in the presence of LasB (**Figure S19B**). The observation by DLS that these PIC particles remained unaffected by LasB was confirmed by the fluorescence quantification of amines with fluorescamine: no increase in amine content –indicative of peptide hydrolysis– was found for PIC particles incubated with LasB after 4 hours (**Figure S20B**).

To further investigate this behaviour, PIC particles made from peptides **$P2_{SH}$** and **$P4_{SH}$** made at a [N:COOH] ratio of 1:0.3 were studied likewise. No enzymatic degradation was found for any of these other nanoparticles either (**Figure S19**). Finally, PIC particles prepared at a [N:COOH] ratio of 1:1.0 from the most

active peptide **P3$_{SH}$** were assessed. These nanoparticles, for having a negative ζ-potential (**Figure 2**), should have their surface coated with anionic peptide, thus exposing the enzyme-responsive component more than positively charged nanoparticles prepared at a [N:COOH] ratio of 1:0.3. Surprisingly, these PIC particles did not show any susceptibility to LasB's action either, as observed by DLS and fluorescamine assay (**Figure S19**-**S20**).

These results indicate that, although peptides **P2**-**4$_{SH}$** degrade in the presence of LasB when they are free in solution (**Figure 6**), their complexation with B-PEI inhibits the activity of this enzyme – an effect not found previously for peptide **P1$_{SH}$**.[10] This behaviour could be due to the stronger affinity of more multivalent peptides like **P2**-**P4$_{SH}$** for B-PEI than **P1$_{SH}$**, leading to more tightly bound and less accessible peptide chains within PIC particles. The selective enzymatic degradation of PIC particles based on the multivalency of their components has been previously observed in other polyelectrolyte systems. Leclercq *et al*. reported faster degradation rates by proteases when PIC particles were prepared from poly(L-lysine) with shorter poly(L-lysine citramide) chains.[22] Fischer *et al.* found that the degradation of DNA by nucleases was prevented when this plasmid was complexed with poly(diallyldimethyl-ammonium chloride) of an average Mw of 45 kDa or above, but not when a shorter analogue of 5 kDa was used.[14] Hence, it has been proposed that polyelectrolytes with high multivalencies can inhibit the enzymatic degradation of oppositely charged materials by acting as a physical and electrostatic barriers against enzymes.[23] However, this explanation does not justify why negatively charged particles (*i.e.* [N:COOH] = 1:1), with loose peptide chains on their surface, did not show any reactivity towards LasB. We think the polycarboxylate corona of these PIC particles can chelate divalent metals such as Ca^{2+} and Zn^{2+}, which are cofactors of LasB,[24] or displace these ions by the high concentration of cations located at the corona as counterions, which has shown to inhibit other metalloenzymes such as nucleases towards the degradation of anionic DNA-decorated nanoparticles.[25]

Conclusions

We have successfully synthesised and characterised a collection of three LasB-responsive peptides with increasing multivalencies and cross-linking units (**P2**-**4$_{SH}$**). PIC particles were assembled from these peptides in combination with B-PEI, and displayed tunable sizes and charges depending on their [N:COOH] ratio. It was also found that the stability under simulated physiological conditions of PIC particles improves with the multivalency and cross-linking degree of the peptides (**P1$_{SH}$**<**P2$_{SH}$**<**P3$_{SH}$**<**P4$_{SH}$**). The internal structure of these complexes was evaluated by SLS, DLS and SAXS, and suggested that these samples are highly polydisperse spheres, with no distinct structural features between them. The enzymatic degradation of these peptides was assessed against bacterial (LasB) and human (HLE) elastase, and it was found that additional Cys and Glu residues have an effect on their enzymatic susceptibility. Finally, it was observed that these PIC particles dramatically reduced the toxicity of B-PEI, however no LasB-specific antimicrobial activity was triggered in the presence of a pathogenic strain of *P. aeruginosa*. The observation that PIC particles did not degrade in the presence of LasB, whereas the uncomplexed peptides were hydrolysed by this enzyme, suggested that the peptide molecules are no longer accessible to LasB when complexed into PIC particles. This effect was not found previously for a less multivalent peptide (**P1$_{SH}$**), and suggests that more multivalent peptides (**P2**-**4$_{SH}$**) lead to more tightly bound polyelectrolytes within the PIC particles, thus compromising their enzymatic susceptibility. Alternatively, anionic PIC particles may inhibit LasB's activity by chelating and/or displacing its metal cofactors. Future work will encompass the deeper understanding and optimisation of more salt tolerant enzyme-responsive PIC particles and will be reported in due course.

Author contributions

All authors contributed to the experimental set-up and discussed the results. II and FFT designed the peptides and nanoparticle preparation; and II, FFT and AMK designed the microbiological assays. MP synthesised and characterised the peptides. LDB, RK and RKOR designed and performed the SLS experiments. APB interpreted the SAXS data. II carried out all other experiments. II wrote the manuscript.

Acknowledgements

The authors thank Prof. Suzanne M. J. Fleiszig for the kind donation of *P. aeruginosa* strains.[26]

Notes and references

1 D. V. Pergushov, A. H. E. Müller and F. H. Schacher, *Chem. Soc. Rev.*, 2012, **41**, 6888–6901.
2 I. Insua, A. Wilkinson and F. Fernández-Trillo, *Eur. Polym. J.*, 2016.
3 H. Sato and A. Nakajima, *Polym. J.*, 1975, **7**, 241–247.
4 M. Müller, *Polyelectrolyte Complexes in the Dispersed and Solid State II*, Springer, Berlin, 2013, vol. 256.
5 Y.-H. Hsieh, Y.-T. Hsiao and J.-S. Jan, *Soft Matter*, 2014, **10**, 9568–9576.
6 I. Insua, S. Majok, A. F. A. Peacock, A. M. Krachler and F. Fernández-Trillo, *Eur. Polym. J.*, 2017, **87**, 478–486.
7 A. H. A. Mohamed-Ahmed, K. A. Les, K. Seifert, S. L. Croft, S. J. Brocchini and S. Brocchini, *Mol. Pharm.*, 2013, **10**, 940–950.
8 K. L. Niece, A. D. Vaughan and D. I. Devore, *J. Biomed. Mater. Res. A*, 2013, **101**, 2548–2558.
9 R. V. Ulijn, *J. Mater. Chem.*, 2006, **16**, 2217–2225.
10 10 I. Insua, E. Liamas, Z. Zhang, A. F. A. Peacock, A. M. Krachler and F. Fernández-Trillo, *Polym. Chem.*, 2016, **7**, 2684–2690.
11 M. Borkovec and G. Koper, *Macromolecules*, 1997, **30**, 2151–2158.
12 J. P. Patterson, M. P. Robin, C. Chassenieux, O. Colombani and R. K. O'Reilly, *Chem. Soc. Rev.*, 2014, **43**, 2412–2425.
13 K. Ueno, H. Ueno and T. Sato, *Polym. J.*, 2011, **44**, 59–64.
14 D. Fischer, H. Dautzenberg, K. Kunath and T. Kissel, *Int. J. Pharm.*, 2004, **280**, 253–269.
15 H. Dautzenberg and J. Kriz, *Langmuir*, 2003, **19**, 5204–5211.
16 S. R. Kline, *J. Appl. Cryst.*, 2006, **39**, 895–900.
17 S. Prévost, S. Riemer, W. Fischer, R. Haag, C. Böttcher, J. Gummel, I. Grillo, M. S. Appavou and M. Gradzielski, *Biomacromolecules*, 2011, **12**, 4272–4282.
18 T. Rieker, A. Hanprasopwattana, A. Datye and P. Hubbard, *Langmuir*, 1999, **15**, 638–641.

19 S. Udenfriend, S. Stein, P. Böhlen, W. Dairman, W. Leimgruber and M. Weigele, *Science*, 1972, **178**, 871–872.
20 K. Morihara and H. Tsuzuki, *Arch. Biochem. Biophys.*, 1971, **146**, 291–296.
21 S. Suter, U. B. Schaad, L. Roux, U. E. Nydegger and F. A. Waldvogel, *J. Infect. Dis.*, 1984, **149**, 523–531.
22 L. Leclercq, M. Boustta, J. Rixte and M. Vert, *J. Colloid Interf. Sci.*, 2010, **350**, 459–464.
23 W. T. Godbey, M. A. Barry, P. Saggau, K. K. Wu and A. G. Mikos, *J. Biomed. Mater. Res.*, 2000, **51**, 321–328.
24 C. T. Supuran and A. Mastrolorenzo, *Curr. Enzym. Inhib.*, 2011, **7**, 2–23.
25 D. S. Seferos, A. E. Prigodich, D. A. Giljohann, P. C. Patel and C. A. Mirkin, *Nano Lett.*, 2009, **9**, 308–311.
26 B. Cowell, S. S. Twining, J. A. Hobden, M. S. F. Kwong and S. M. J. Fleiszig, *Microbiology*, 2003, **149**, 2291–2299.

Elastase-sensitive peptides with higher multivalency form more stable polyion complex (PIC) nanoparticles with compromised susceptibility to enzymatic degradation

Ignacio Insua,[a,b] Marion Petit,[a] Lewis D. Blackman,[c] Robert Keogh,[c] Anaïs Pitto-Barry,[c] Rachel K. O'Reilly,[c] Anna F. A. Peacock,[a] Anne Marie Krachler[b,d] and Francisco Fernandez-Trillo[a,b,*]

[a]School of Chemistry, University of Birmingham, B15 2TT Birmingham, UK. [b]Institute of Microbiology and Infection, School of Biosciences, University of Birmingham, B15 2TT Birmingham, UK. [c]Department of Chemistry, University of Warwick, CV4 7AL Coventry, UK. [d]Department of Microbiology and Molecular Genetics, University of Texas, 6431 Fannin. Houston (TX), USA. Email: f.fernandez-trillo@bham.ac.uk

Electronic Supplementary Information

Materials

N-Fmoc-protected L-amino acids were purchased from Merck Millipore. Dimethylformamide (DMF), piperidine 20% v/v in DMF and acetic anhydride were purchased from Sigma-Aldrich®. H-L-Cys(Trt)-2-chlorotrityl resin (0.49 mmol/g) was bought from AGTC Bio Products Ltd. *N,N*-diisopropylethylamine (DIPEA), triisopropylsilane (TIPS), 1,2-ethanedithiol (EDT) and trifluoroacetic acid (TFA) were bought from Alfa Aesar®. *N*,*N*,*N*',*N*'-tetramethyl-*O*-(1*H*-benzotriazol-1-yl)uronium hexafluorophosphate (HBTU) was purchased from Carbosynth Ltd. All other chemicals were purchased from Fisher Scientific UK Ltd and were used without further purification.

Instrumentation

NMR data was acquired on a Bruker Avance III operating at 400 MHz and fitted with a 5 mm DUL probe ($^{1}H/^{13}C$). MS spectra were obtained on a Xevo® G2-XS ToF (Waters) from electrospray ionisation (ESI) and time-of-flight (TOF) measurement in positive ion mode. High-resolution MS data was calculated by comparison with leucine-enkephalin as internal standard. Reverse phase (RP) HPLC analysis was run through a Kinetex® C18-EVO column (Phenomenex®): 5 µm, 100 Å, 250 x 4.60 mm. A gradient from 3 to 20% of (CH_3CN + 0.05% TFA) in (H_2O + 0.05% TFA) was used at 1 mL/min. The column was maintained at 35°C and UV-VIS detection was set at 210 nm. UV-VIS spectra were acquired on a Cary 5000 NIR (Agilent) 1 cm pathlength quartz cuvettes. Circular dichroism spectra were recorded in 1 mm pathlength quartz cuvettes on a Jasco J-715 spectropolarimeter. The observed ellipticity in millidegrees was converted into mean residue ellipticity, and is reported in units of $deg \cdot dmol^{-1} \cdot cm^{2} \cdot res^{-1}$.

Peptide synthesis

500 mg of cysteine-preloaded resin (0.245 mmol) were swollen in 5 mL of *N*,*N*-dimethylformamide (DMF) for 30 minutes. Then, solutions of Fmoc-L-amino acid (3 eq), *N*,*N*,*N*',*N*'-tetramethyl-*O*-(1*H*-benzotriazol-1-yl)uronium hexafluorophosphate (HBTU) (2.8 eq) and *N*,*N*-diisopropylethylamine (DIPEA) (2.8 eq) in DMF were added to a final volume of 5 mL. The reaction mixture was rolled for 1 h at room temperature, after which a negative chloranil test[1] indicated the reaction had gone to completion. The *N*-terminal Fmoc protecting group was removed by washing the resin with 5 mL of piperidine 20% v/v in DMF during 10 minutes. A positive chloranil test confirmed the removal of the Fmoc group, and the previous steps were repeated to couple all amino acids in the sequence. Following the coupling of the last amino acid, the Fmoc group was removed and the terminal amine of the peptide was capped by reacting with 5 mL of acetic anhydride:DIPEA:DMF (1:1:3) for 1 h at room temperature. Then, the resin was thoroughly washed with DMF and diethyl ether, and the peptide was cleaved from the resin with 5 mL of a mixture containing TFA (80%), TIPS (8%) and EDT (12%) for 2 h. After this time, the solution was concentrated under argon and precipitated in chilled diethyl ether:hexane (1:4). Finally, the suspension was centrifuged and the pellets were washed twice with diethyl ether:hexane (1:4), dissolved in water and freeze-dried. Peptides that showed impurities by ^{1}H-NMR (*e.g.* trityl protecting groups) were further purified by dissolving the material in 2 mL of a 10% TIPS solution in TFA and precipitating in chilled diethyl ether:hexane (1:4), to be then centrifuged and freeze-dried as explained above. Peptide purity was determined by HPLC.

Peptide characterisation

The synthesis and characterisation of peptides **P1$_{SH}$** (**Ac-CEGLAEC-OH**) and **P5** (**H$_2$N-LA-E-OH**) was previously reported.[2]

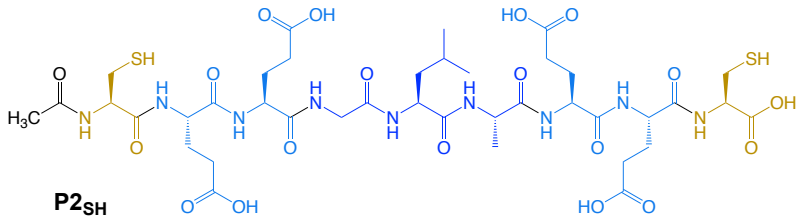

P2$_{SH}$, Ac-CEEGLAEEC-OH (154.8 mg, 62% yield) **^{1}H-NMR** (400 MHz, DMSO-*d6*): δ 0.84(dd, *J*=15.0, 6.5 Hz, 6H, H$^{\delta}$-Leu); 1.20(d, *J*=7.1 Hz, 3H, H$^{\beta}$-Ala 1.35-1.47(m, 2H, H$^{\beta}$-Leu); 1.50-1.63(m, 1H, H$^{\gamma}$-Leu); 1.66-1.80(m, 4H, H$^{\beta}$-Glu); 1.84-1.96(m, 4H, H$^{\beta}$-Glu); 1.87(s, 3H, Ac); 2.16-2.31(m, 8H, H$^{\gamma}$-Glu); 2.36(t, *J*=8.5 Hz, 1H, SH); 2.45(t, *J*=8.6 Hz, 1H, SH); 2.62-2.89(m, 4H, H$^{\beta}$-Cys); 3.70(ddd, *J*=56.8, 16.7, 5.7 Hz, 2H, H$^{\alpha}$-Gly); 4.20-4.41(m, 8H, H$^{\alpha}$); 7.89(d, *J*=8.1 Hz, 1H, NHCO); 7.92(d, *J*=8.5 Hz, 1H, NHCO); 7.95(d, *J*=7.7 Hz, 1H, NHCO); 7.98(d, *J*=7.7 Hz, 1H, NHCO); 8.11-8.22(m, 5H, NHCO); 12.20(br.s, 4H, COOH) ppm. **^{13}C-NMR** (400 MHz, DMSO-*d6*): δ 17.4(C$^{\beta}$-Ala); 21.4(H$^{\delta}$-Leu); 22.3(Ac); 22.9(H$^{\delta}$-Leu); 23.9(H$^{\gamma}$-Leu); 25.2(C$^{\beta}$-Cys); 25.9(C$^{\beta}$-Cys); 26.7(C$^{\beta}$-Cys); 27.2(C$^{\beta}$-Glu); 29.7(C$^{\gamma}$-Glu); 29.8(C$^{\gamma}$-Glu); 29.8(C$^{\gamma}$-Glu); 29.9(C$^{\gamma}$-Glu); 40.7(C$^{\beta}$-Leu); 41.6(C$^{\alpha}$-Gly); 48.0(C$^{\alpha}$); 50.6(C$^{\alpha}$); 51.4(C$^{\alpha}$); 51.5(C$^{\alpha}$); 51.8(C$^{\alpha}$); 52.0(C$^{\alpha}$); 54.2(C$^{\alpha}$); 55.0(C$^{\alpha}$); 168.5(NHCO); 169.8(Ac); 170.2(NHCO); 170.9(NHCO); 171.0(NHCO); 171.1(NHCO); 171.3(NHCO); 171.4(NHCO); 171.9(NHCO); 172.2(NHCO); 174.0(COOH) ppm. **MS** (ESI-TOF, +eV): m/z 1024.4 $[M+H]^+$; 531.7 $[M+Ca]^{2+}$. **HR-MS** (ESI-TOF, +eV): m/z 1024.3603 (calculated for $[M+H]^+$); 1024.3605 (found). Purity by **HPLC** = 92% (Rt = 24.2 min).

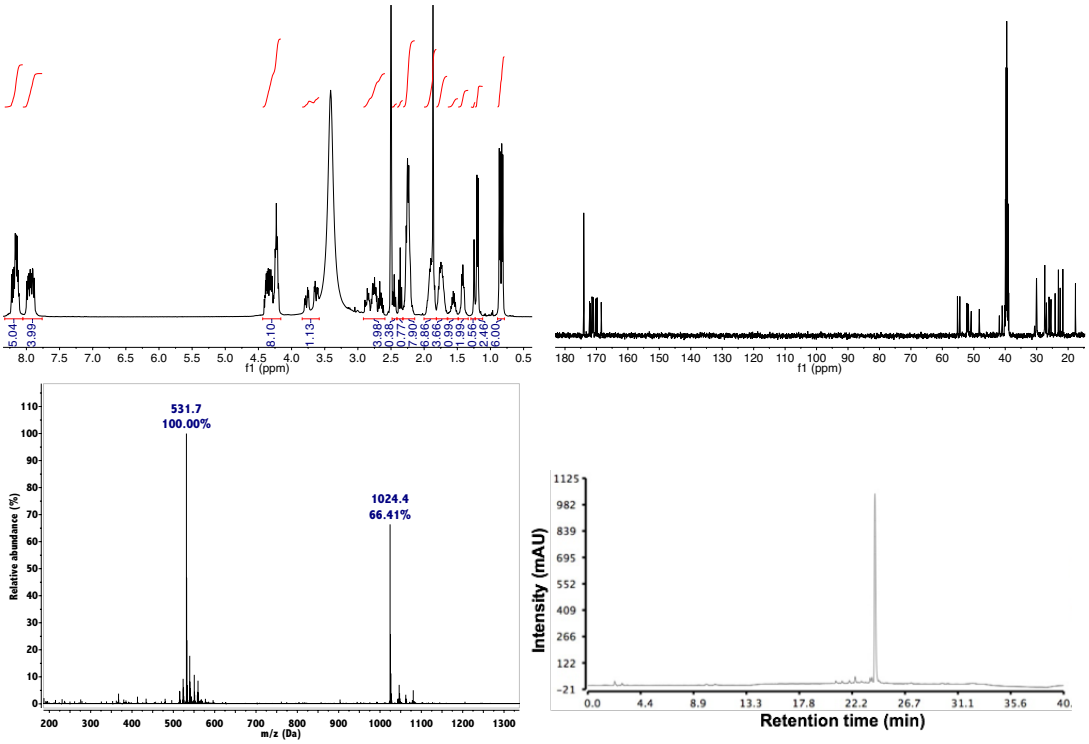

Figure S1 Characterisation of peptide **P2$_{SH}$** (Ac-C-EE-GLA-EE-C-OH). Top: ^{1}H (left) and ^{13}C (right) NMR spectra (400 MHz, DMSO-d_6). Bottom: Mass spectrum (left) and RP-HPLC chromatogram (right).

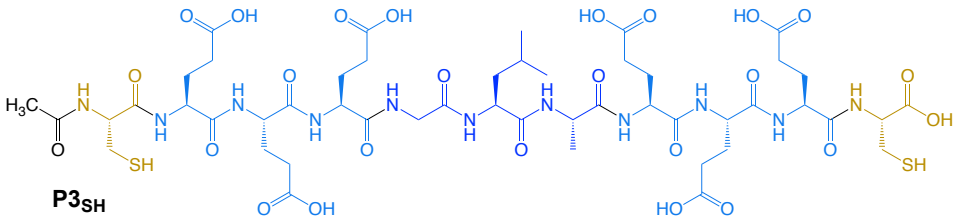

$P3_{SH}$, Ac-CEEEGLAEEEC-OH (152.5 mg, 72% yield) **^{1}H-NMR** (400 MHz, DMSO-*d6*): δ 0.84(dd, *J*=14.8, 6.4 Hz, 6H, H^{δ}-Leu); 1.19(d, *J*=7.0 Hz, 3H, H^{β}-Ala); 1.36-1.47(m, 2H, H^{β}-Leu); 1.50-1.63(m, 1H, H^{γ}-Leu); 1.67-1.81(m, 6H, H^{β}-Glu); 1.84-1.95(m, 6H, H^{β}-Glu); 1.87(s, 3H, Ac); 2.17-2.29(m, 12H, H^{γ}-Glu); 2.34(t, *J*=8.5 Hz, 1H, SH); 2.44(t, *J*=8.6 Hz, 1H, SH); 2.62-2.89(m, 4H, H^{β}-Cys); 3.70(ddd, *J*=75.2, 16.7, 5.7 Hz, 2H, H^{α}-Gly); 4.19-4.42(m, 10H, H^{α}); 7.89-7.94(m, 4H, NHCO); 8.04(d, *J*=7.4 Hz, 1H, NHCO); 8.08(d, *J*=7.6 Hz, 1H, NHCO); 8.11-8.20(m, 5H, NHCO); 12.17(br.s, 5H, COOH) ppm. **^{13}C-NMR** (400 MHz, DMSO-*d6*): δ 17.4(C^{β}-Ala); 21.4(H^{δ}-Leu); 22.3(Ac); 22.8(H^{δ}-Leu); 23.9(H^{γ}-Leu); 25.2(C^{β}-Cys); 25.9(C^{β}-Cys); 26.7(C^{β}-Cys); 27.0(C^{β}-Glu); 27.1(C^{β}-Glu); 27.2(C^{β}-Glu); 29.9 (C^{γ}-Glu); 40.8(C^{β}-Leu); 41.6(C^{α}-Gly); 48.0(C^{α}); 50.6(C^{α}); 51.5(C^{α}); 51.6(C^{α}); 51.7(C^{α}); 51.8(C^{α}); 51.9(C^{α}); 54.2(C^{α}); 54.9(C^{α}); 168.5(NHCO); 169.7(Ac); 170.1(NHCO); 171.0(NHCO); 171.0(NHCO); 171.2(NHCO); 171.4(NHCO); 171.4(NHCO); 171.9(NHCO); 172.3(NHCO); 174.0(COOH) ppm. **MS** (ESI-TOF, +eV): m/z 1282.4 $[M+H]^{+}$; 668.7 $[M+H+Na+CH_3OH]^{2+}$; 660.7 $[M+Ca]^{2+}$; 641.7 $[M+2H]^{2+}$. **HR-MS** (ESI-TOF, +eV): m/z 1282.4455 (calculated for $[M+H]^{+}$); 1282.4452 (found). Purity by **HPLC** = 90% (Rt = 23.8 min).

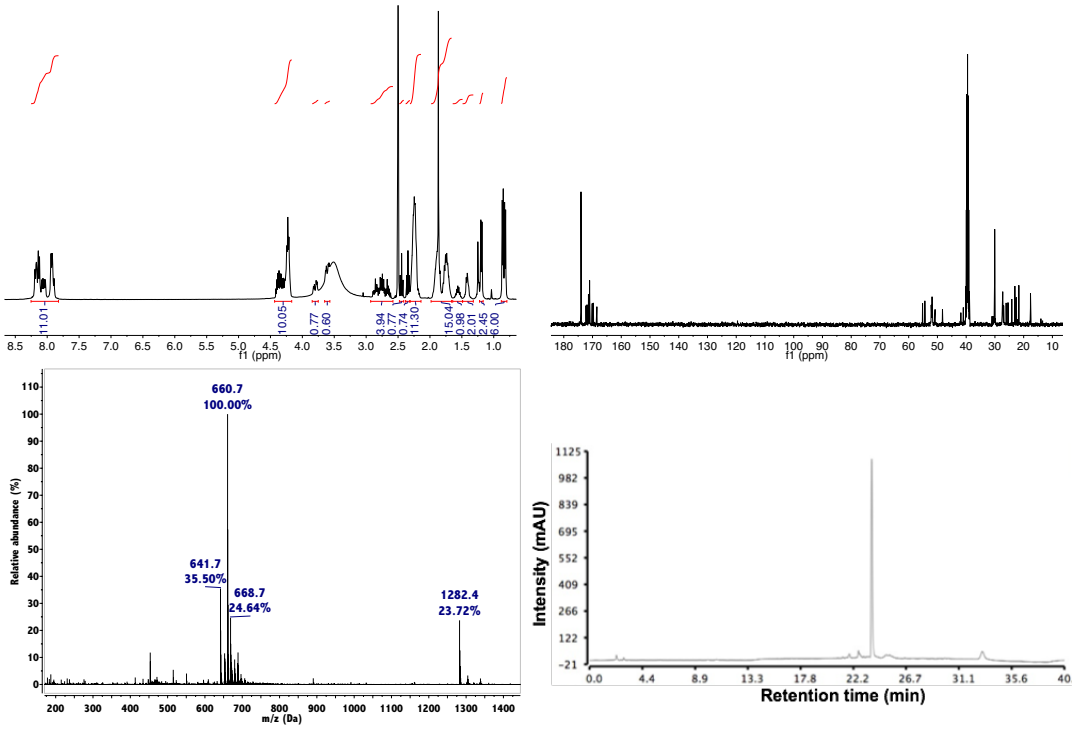

Figure S2 Characterisation of peptide **$P3_{SH}$** (Ac-C-EEE-GLA-EEE-C-OH). Top: ^{1}H (left) and ^{13}C (right) NMR spectra (400 MHz, DMSO-d_6). Bottom: Mass spectrum (left) and RP-HPLC chromatogram (right).

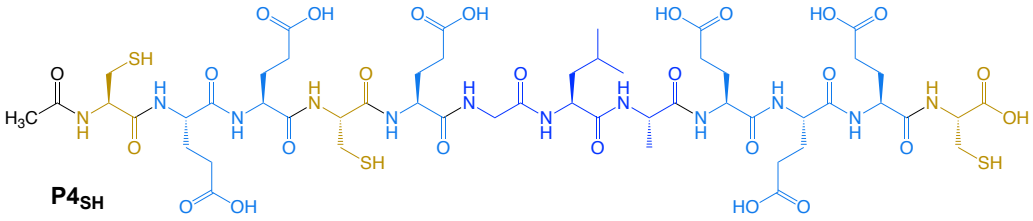

$P4_{SH}$, Ac-CEECEGLAEEEC-OH (208.0 mg, 98% yield) **^{1}H-NMR** (400 MHz, DMSO-*d6*): δ 0.84(dd, *J*=14.5, 6.6 Hz, 6H, H^{δ}-Leu); 1.19(d, *J*=7.0 Hz, 3H, H^{β}-Ala); 1.36-1.46(m, 2H, H^{β}-Leu); 1.51-1.61(m, 1H, H^{γ}-Leu); 1.67-1.81(m, 6H, H^{β}-Glu); 1.83-1.95(m, 6H, H^{β}-Glu); 1.87(s, 3H, Ac); 2.17-2.31(m, 12H, H^{γ}-Glu); 2.36(dt, *J*=8.5, 2.8 Hz, 2H, SH); 2.44(t, *J*=8.5 Hz, 1H, SH); 2.62-2.89(m, 6H, H^{β}-Cys); 3.70(ddd, *J*=54.5, 16.7, 5.8 Hz, 2H, H^{α}-Gly); 4.19-4.42(m, 11H, H^{α}); 7.90-8.20(m, 12H, NHCO); 12.16(br.s, 5H, COOH) ppm. **^{13}C-NMR** (400 MHz, DMSO-*d6*): δ 17.4(C^{β}-Ala); 21.4(H^{δ}-Leu); 22.3(Ac); 22.9(H^{δ}-Leu); 23.9(H^{γ}-Leu); 25.2(C^{β}-Cys); 25.9(C^{β}-Cys); 26.8(C^{β}-Cys); 27.0(C^{β}-Glu); 27.1(C^{β}-Glu); 27.1(C^{β}-Glu); 27.2(C^{β}-Glu); 40.8(C^{β}-Leu); 41.6(C^{α}-Gly); 48.0(C^{α}); 50.5(C^{α}); 51.5(C^{α}); 51.6(C^{α}); 51.7(C^{α}); 51.9(C^{α}); 52.1(C^{α}); 54.2(C^{α}); 54.8(C^{α}); 54.9(C^{α}); 168.4(NHCO); 169.7(Ac); 170.1(NHCO); 171.0(NHCO); 171.0(NHCO); 171.1(NHCO); 171.1(NHCO); 171.2(NHCO); 171.3(NHCO); 171.4(NHCO); 171.9(NHCO); 172.2(NHCO); 174.0(COOH) ppm. **MS** (ESI-TOF, +eV): m/z 1407.4 $[M+Na]^{+}$; 1385.5 $[M+H]^{+}$; 712.2 $[M+Ca]^{2+}$; 704.2 $[M+H+Na]^{2+}$; 693.2 $[M+2H]^{2+}$. **HR-MS** (ESI-TOF, +eV): m/z 1385.4547 (calculated for $[M+H]^{+}$); 1385.4545 (found). Purity by **HPLC** = 91% (Rt = 26.6 min).

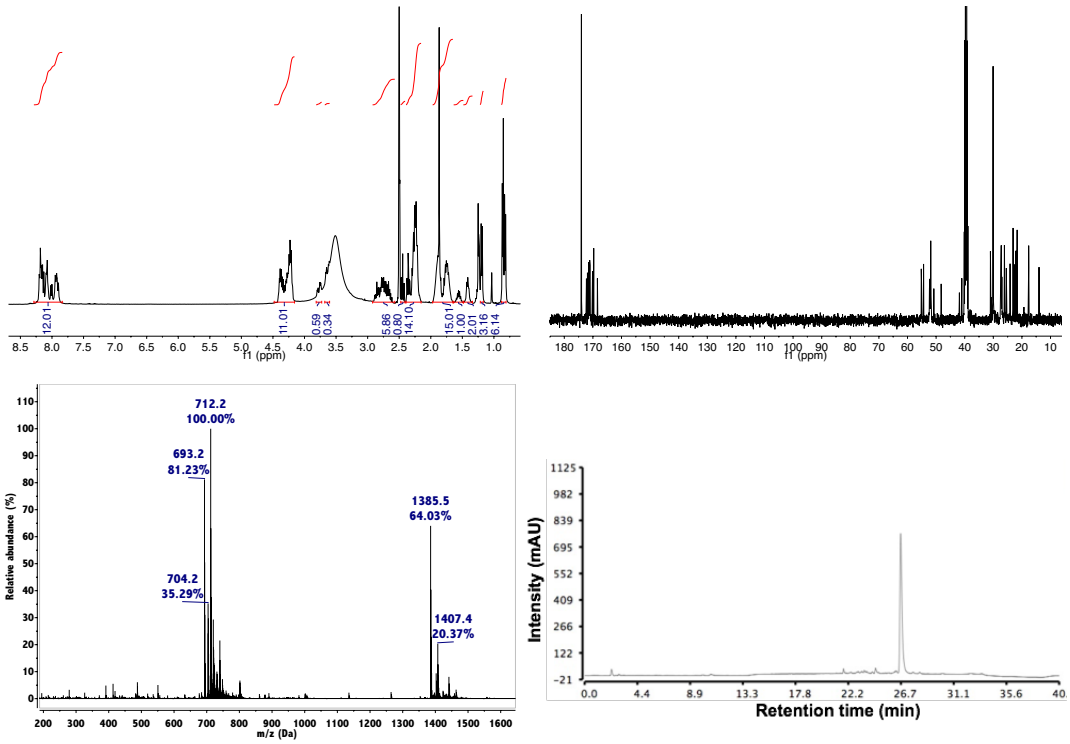

Figure S3 Characterisation of peptide **$P4_{SH}$** (Ac-C-EE-C-E-GLA-EEE-C-OH). Top: ^{1}H (left) and ^{13}C (right) NMR spectra (400 MHz, DMSO-d_6). Bottom: Mass spectrum (left) and RP-HPLC chromatogram (right).

PIC particle characterisation

Table S1 Hydrodynamic diameter (D_H) and ζ-potential of PIC particles prepared from peptides **P2**-**4**$_{SH}$ and B-PEI at different [N:COOH] ratios. SD indicates the standard deviation found for the only size or charge population fitted by the software.

Peptide	[N:COOH] ratio	D_H ± SD (nm)	ζ-potential ± SD (mV)	Notes
P2$_{SH}$	1 : 2.0	371 ± 51	-9.6 ± 3.9	-
	1 : 1.5	329 ± 42	-10.0 ± 3.1	-
	1 : 1.0	293 ± 30	-9.1 ± 3.5	-
	1 : 0.8	-	-	No particles found
	1 : 0.7	-	-	No particles found
	1 : 0.6	-	-	No particles found
	1 : 0.5	-	-	No particles found
	1 : 0.4	419 ± 67	+11.7 ± 5.2	-
	1 : 0.3	91 ± 32	+19.1 ± 6.2	-
	1 : 0.2	-	-	No particles found
P3$_{SH}$	1 : 2.0	227 ± 50	-21.3 ± 6.3	-
	1 : 1.5	204 ± 51	-18.5 ± 6.4	-
	1 : 1.0	198 ± 47	-18.3 ± 6.7	-
	1 : 0.8	212 ± 44	-16.5 ± 6.0	-
	1 : 0.7	224 ± 45	-16.0 ± 6.8	-
	1 : 0.6	280 ± 55	-15.8 ± 4.8	-
	1 : 0.5	-	-	No particles found
	1 : 0.4	240 ± 47	+13.9 ± 5.1	-
	1 : 0.3	103 ± 42	+21.3 ± 7.9	-
	1 : 0.2	-	-	No particles found
P4$_{SH}$	1 : 2.0	198 ± 45	-20.6 ± 6.1	-
	1 : 1.5	192 ± 43	-20.6 ± 7.2	-
	1 : 1.0	191 ± 41	-20.2 ± 5.8	-
	1 : 0.8	173 ± 36	-17.0 ± 7.4	-
	1 : 0.7	176 ± 39	-17.7 ± 7.2	-
	1 : 0.6	205 ± 39	-11.1 ± 7.5	-
	1 : 0.5	-	-	No particles found
	1 : 0.4	225 ± 46	+15.2 ± 5.4	-
	1 : 0.3	143 ± 40	+17.7 ± 7.7	-
	1 : 0.2	-	-	No particles found

DLS data for simulated physiological stability assay

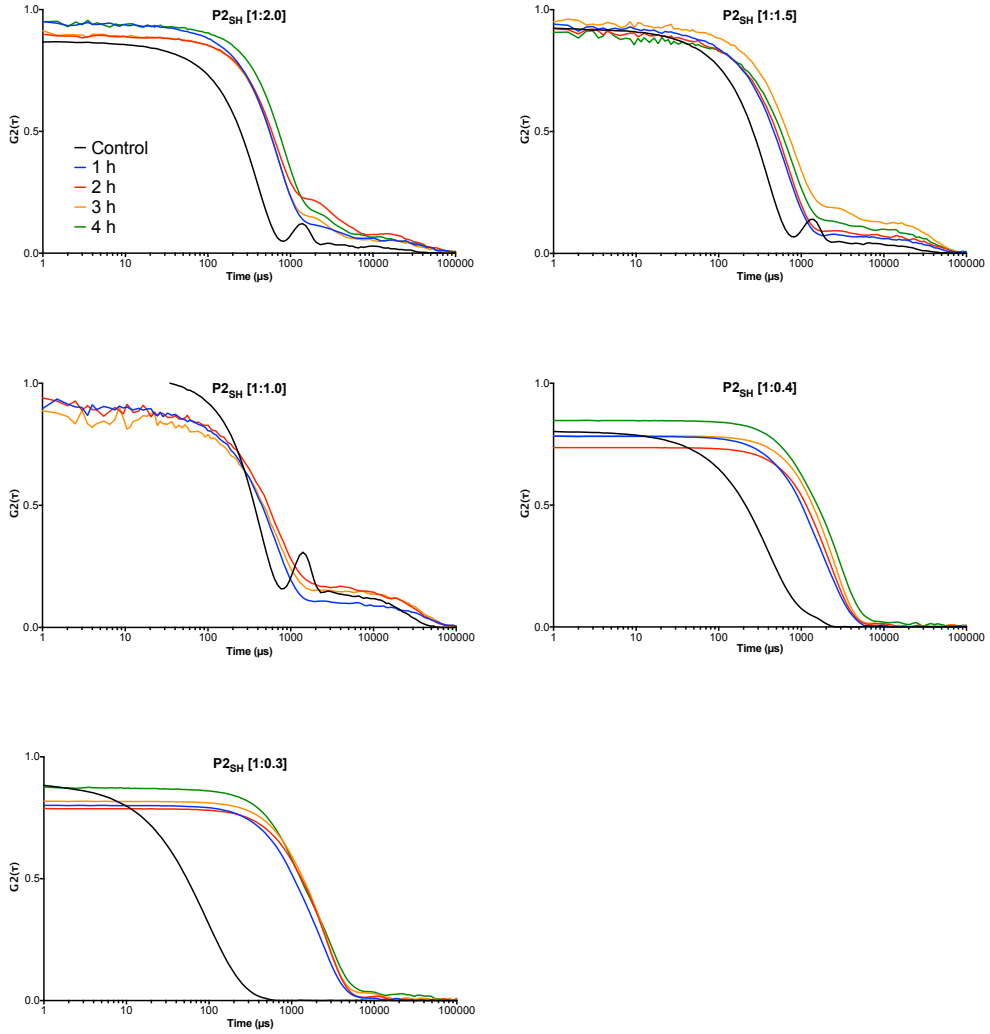

Figure S4 DLS correlograms of PIC particles prepared from peptide **P2$_{SH}$** at the [N:COOH] ratios indicated in brackets in the absence (control) and presence of 154 mM NaCl at 37 °C over time (1-4 hours).

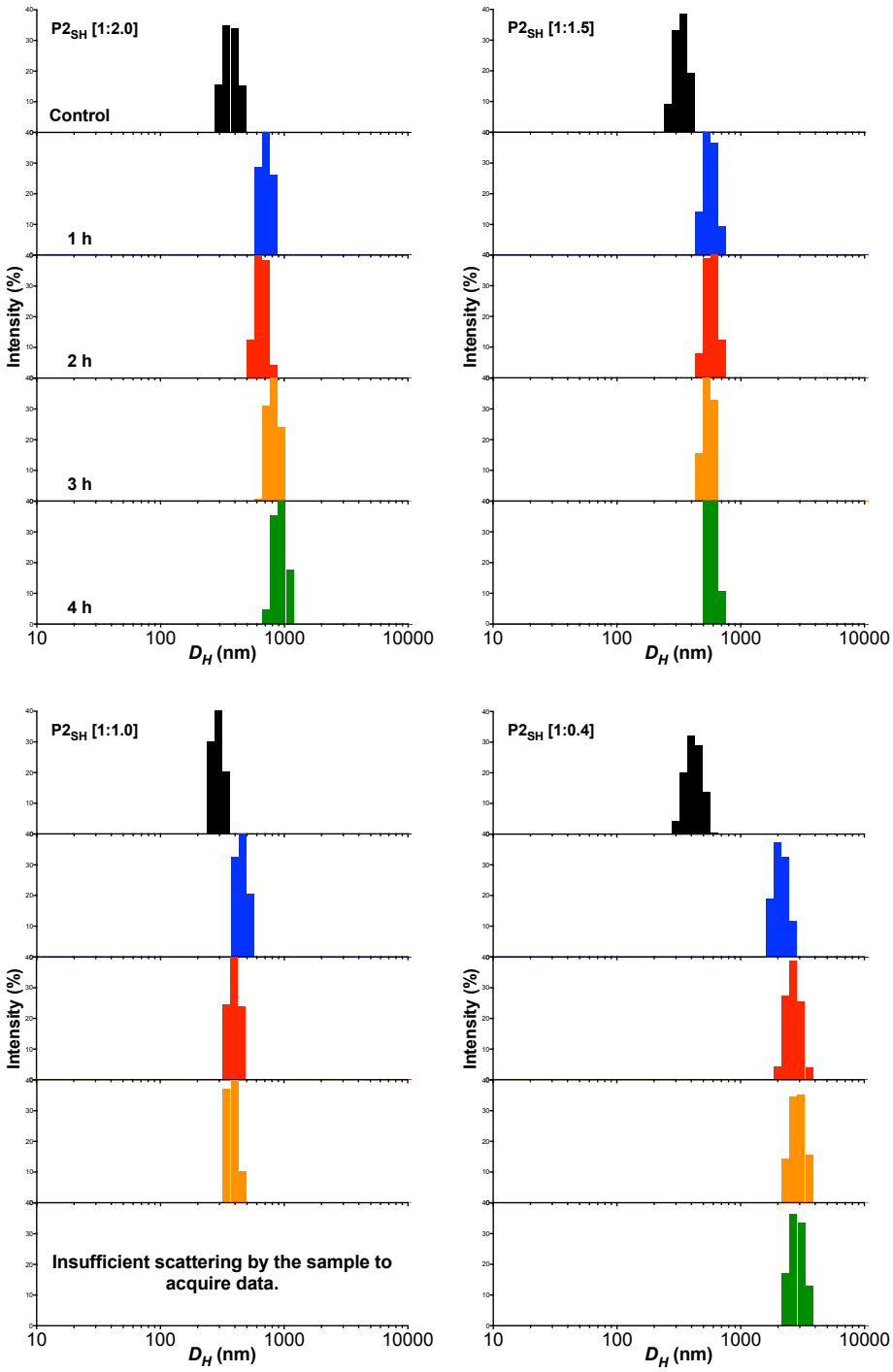

Figure S5 DLS Size-Intensity distributions of PIC particles prepared from peptide **P2$_{SH}$** at the [N:COOH] ratios indicated in brackets in the absence (control) and presence of 154 mM NaCl at 37 °C over time (1-4 hours).

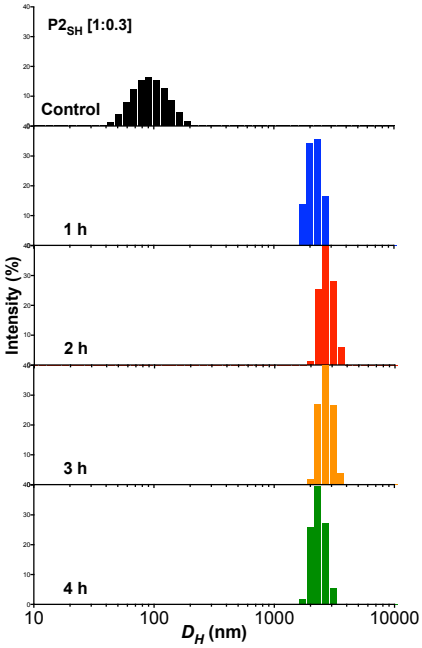

Figure S6 DLS Size-Intensity distributions of PIC particles prepared from peptide **P2$_{SH}$** at the [N:COOH] ratios indicated in brackets in the absence (control) and presence of 154 mM NaCl at 37 °C over time (1-4 hours).

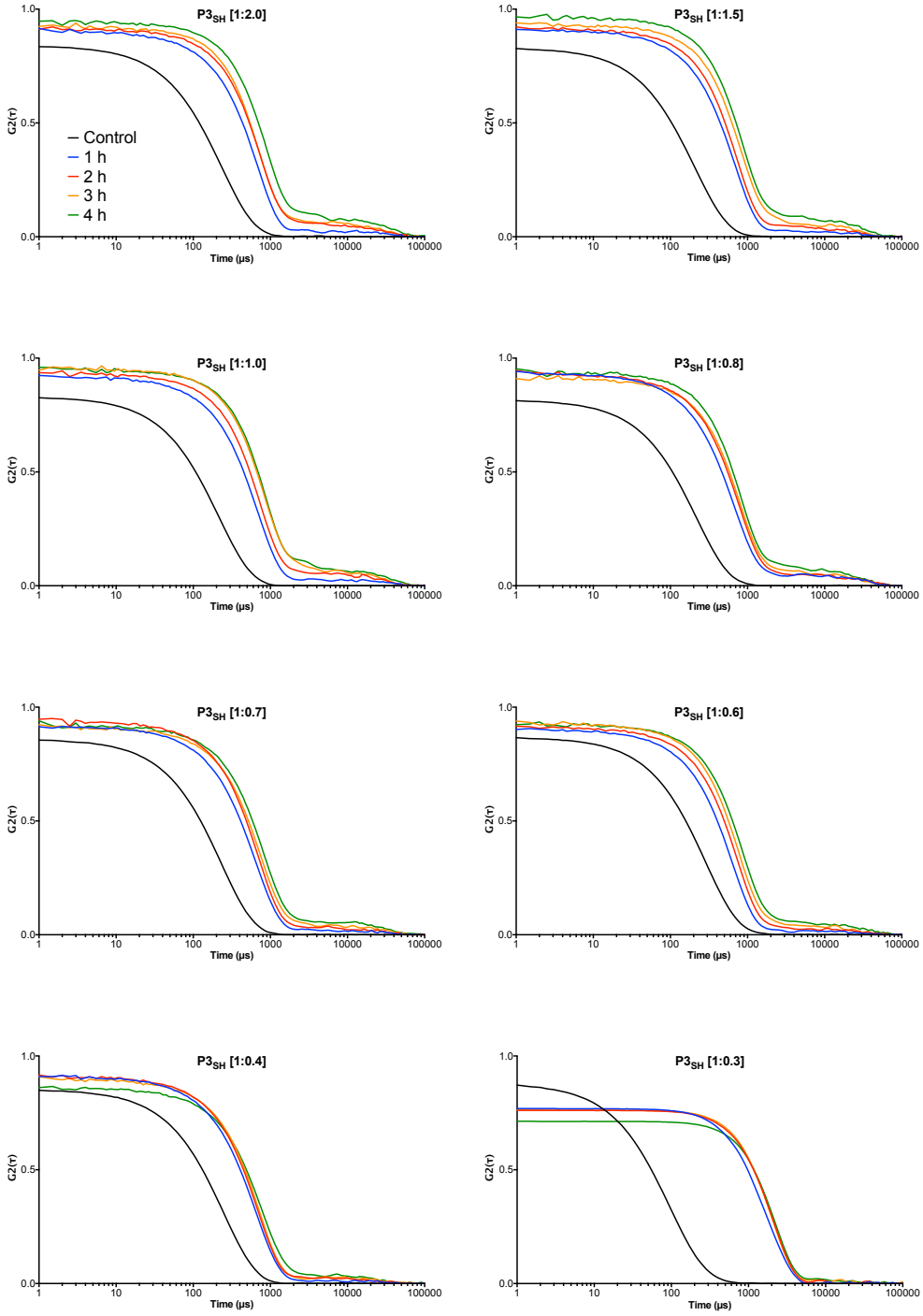

Figure S7 DLS correlograms of PIC particles prepared from peptide **P3$_{SH}$** at the [N:COOH] ratios indicated in brackets in the absence (control) and presence of 154 mM NaCl at 37 °C over time (1-4 hours).

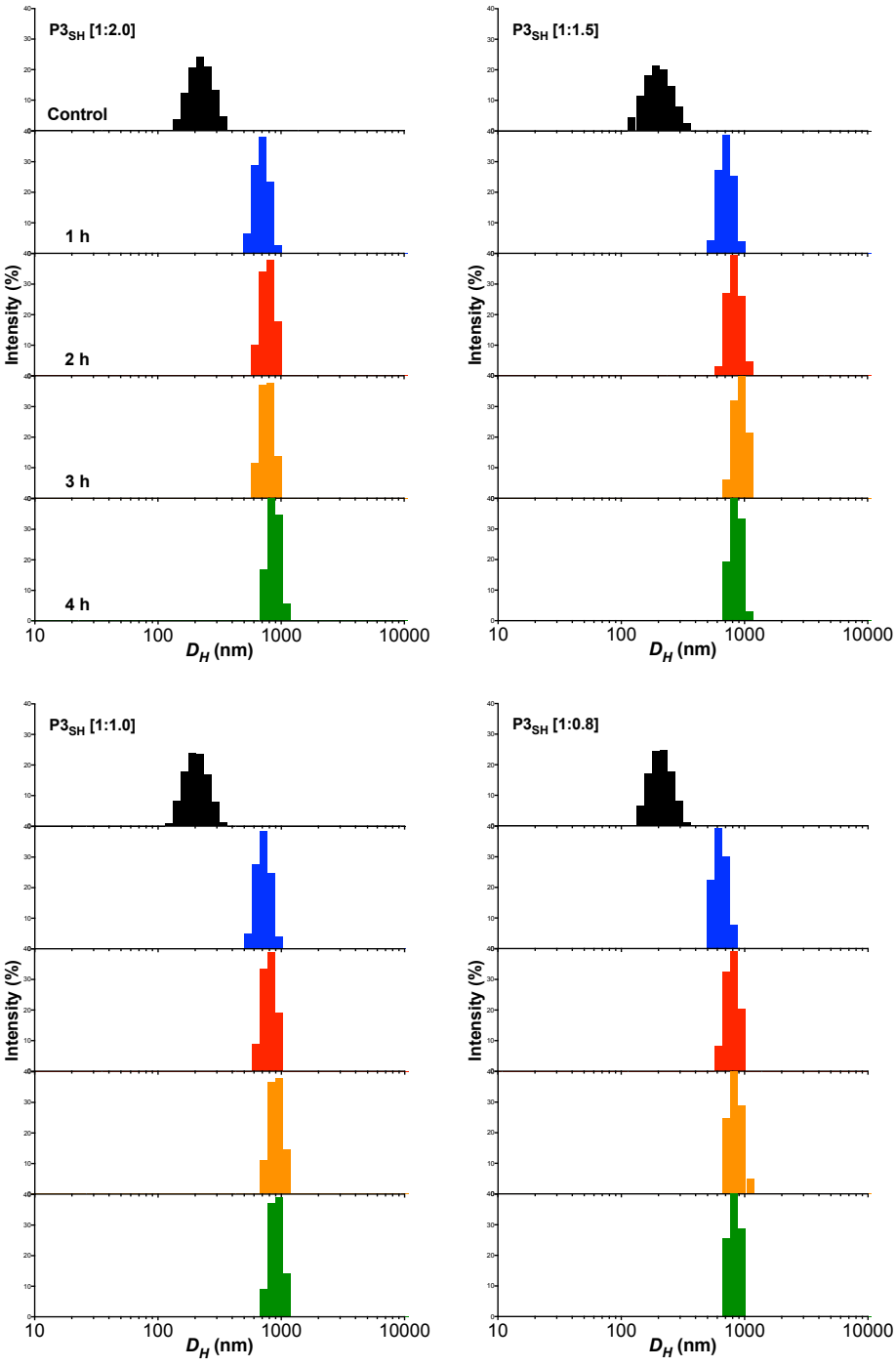

Figure S8 DLS Size-Intensity distributions of PIC particles prepared from peptide **P3$_{SH}$** at the [N:COOH] ratios indicated in brackets in the absence (control) and presence of 154 mM NaCl at 37 °C over time (1-4 hours).

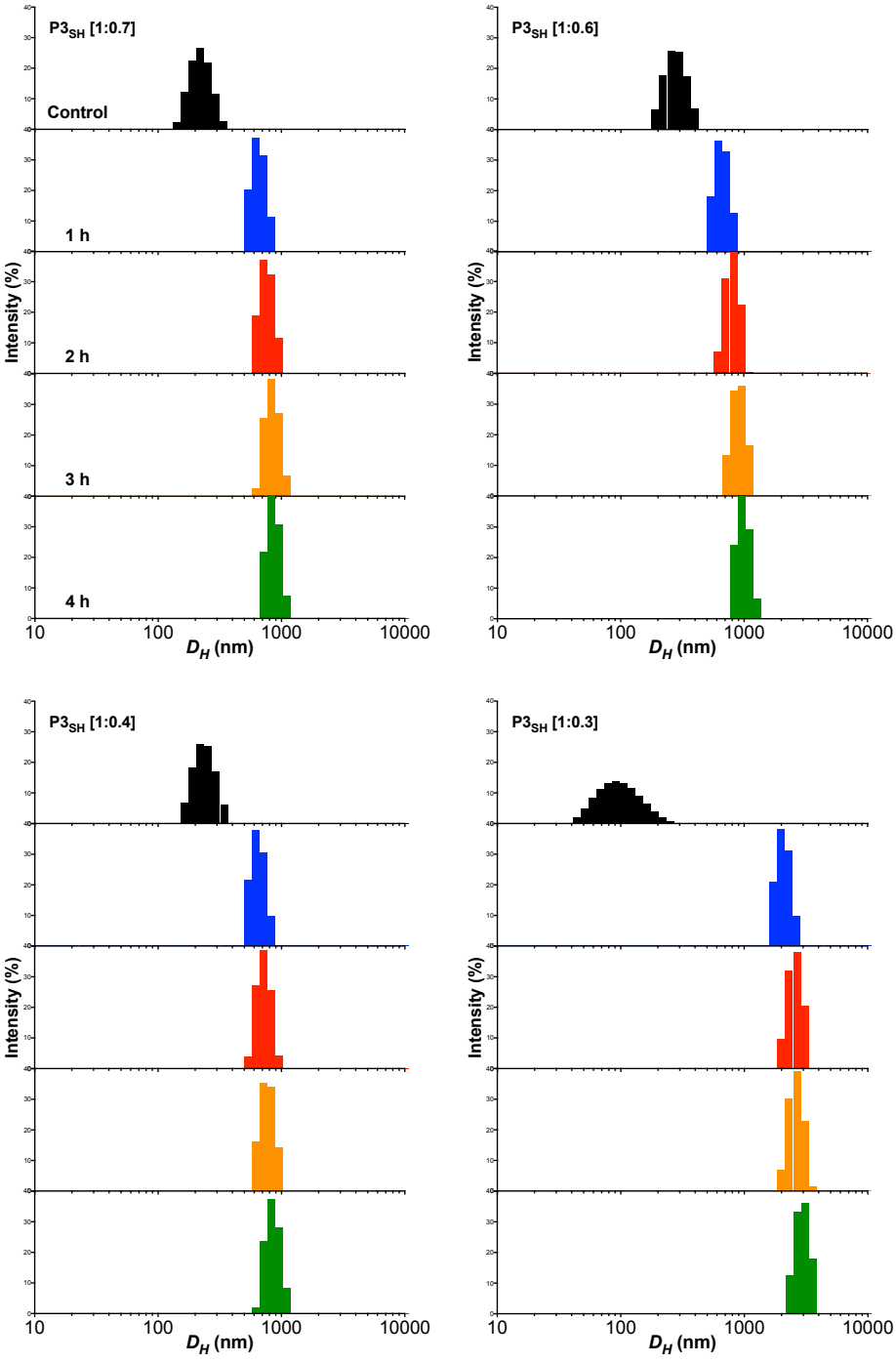

Figure S9 DLS Size-Intensity distributions of PIC particles prepared from peptide **P2$_{SH}$** at the [N:COOH] ratios indicated in brackets in the absence (control) and presence of 154 mM NaCl at 37 °C over time (1-4 hours).

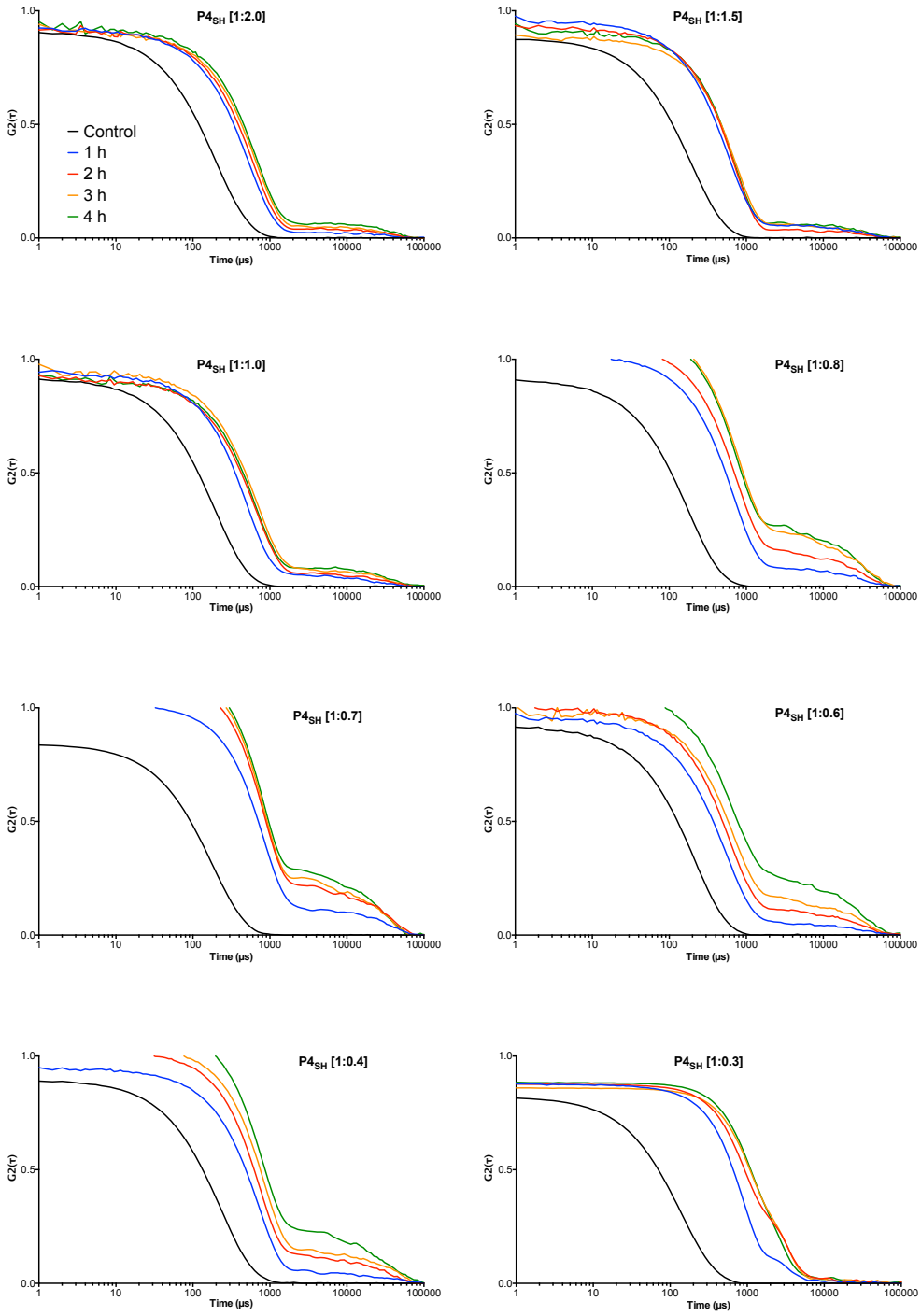

Figure S10 DLS Size-Intensity distributions of PIC particles prepared from peptide **P4$_{SH}$** at the [N:COOH] ratios indicated in brackets in the absence (control) and presence of 154 mM NaCl at 37 °C over time (1-4 hours).

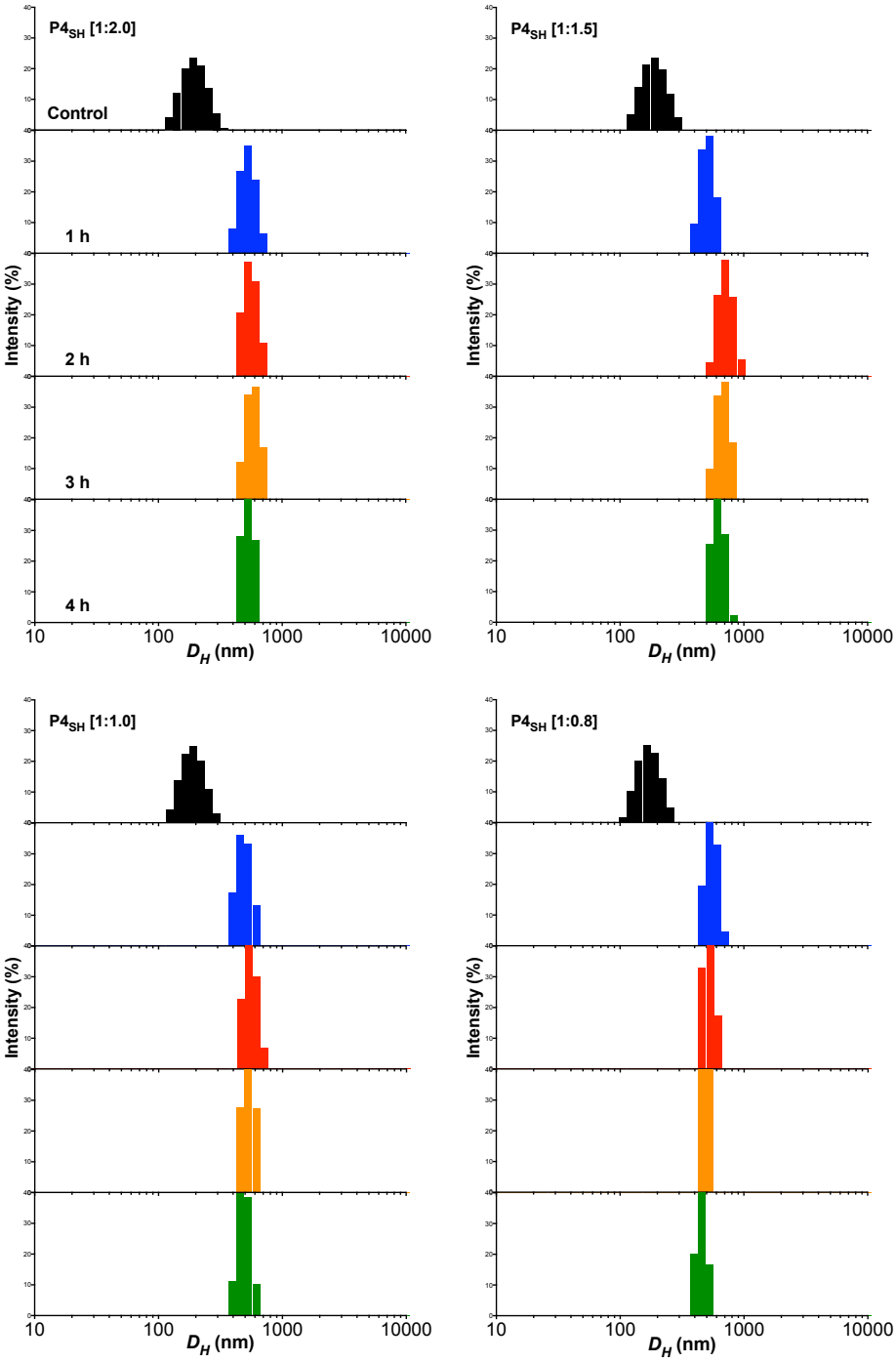

Figure S11 DLS Size-Intensity distributions of PIC particles prepared from peptide **P4$_{SH}$** at the [N:COOH] ratios indicated in brackets in the absence (control) and presence of 154 mM NaCl at 37 °C over time (1-4 hours).

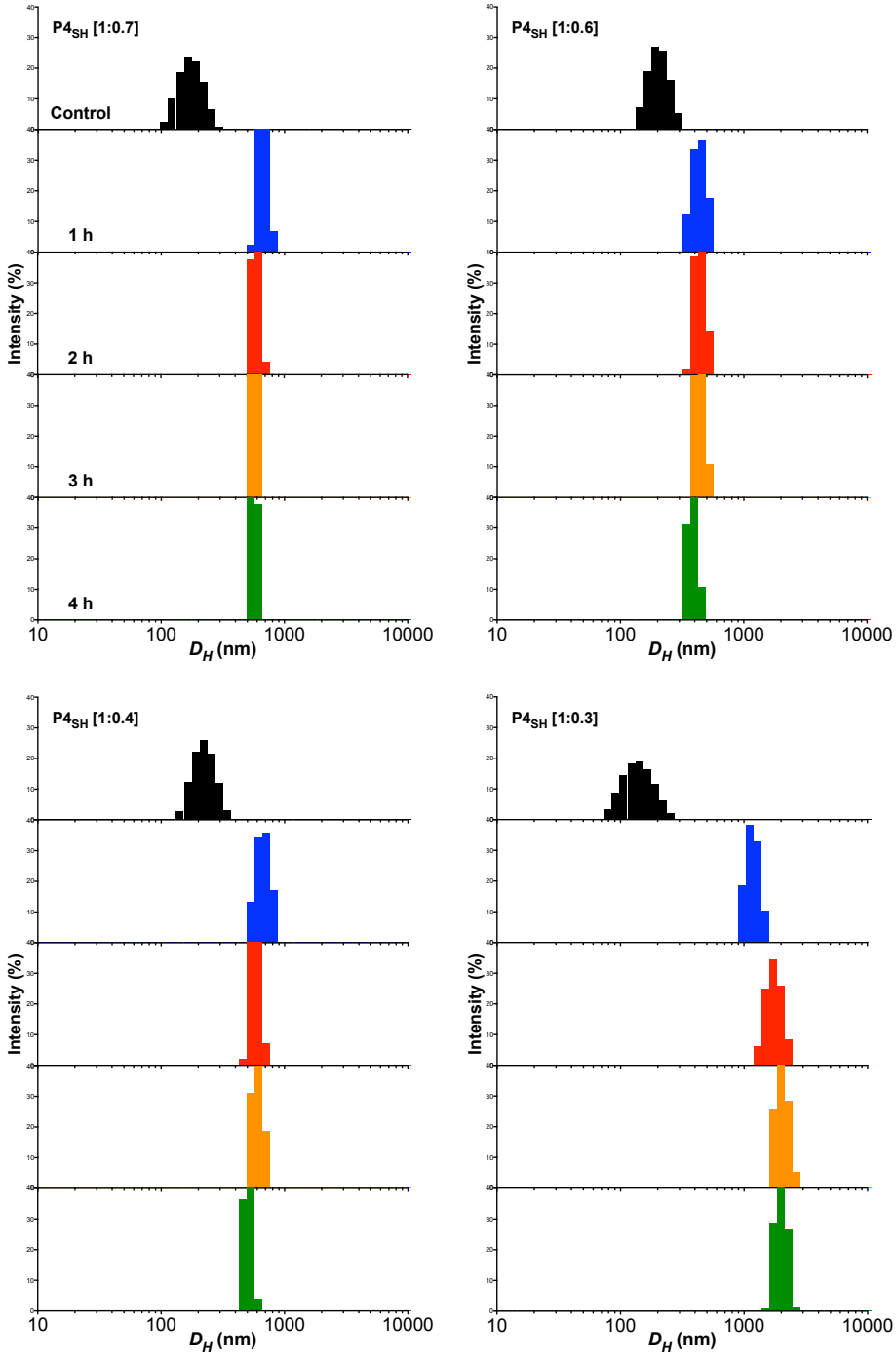

Figure S12 DLS Size-Intensity distributions of PIC particles prepared from peptide **P4$_{SH}$** at the [N:COOH] ratios indicated in brackets in the absence (control) and presence of 154 mM NaCl at 37 °C over time (1-4 hours).

SLS characterisation of unfiltered PIC particles

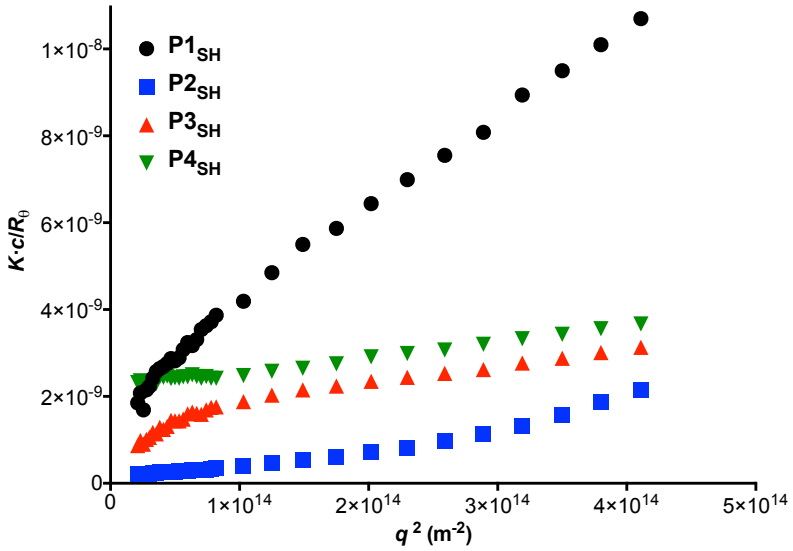

Figure S13 Zimm plots obtained by SLS of unfiltered PIC particles prepared from peptides **P1**-$\mathbf{4_{SH}}$ at a [N:COOH] ratio of 1:0.3.

Shelf stability of PIC particles

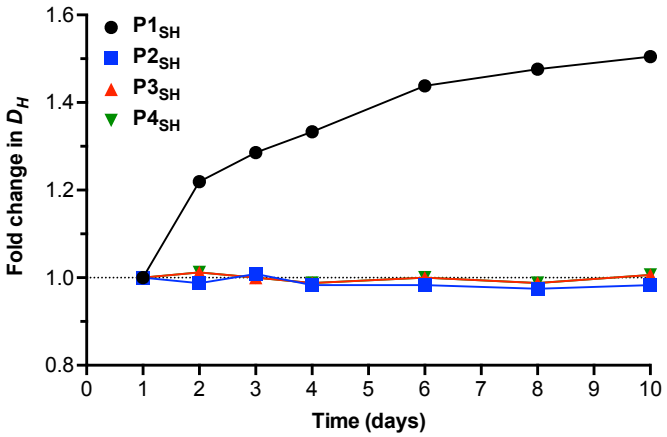

Figure S14 Hydrodynamic diameter (D_H) of PIC particles prepared at a [N:COOH] ratio of 1:0.3 over time, stored in a dark, cool and dry place. The D_H values calculated by DLS were normalised to that of freshly made PIC particles (day 1).

Enzymatic degradation of peptides

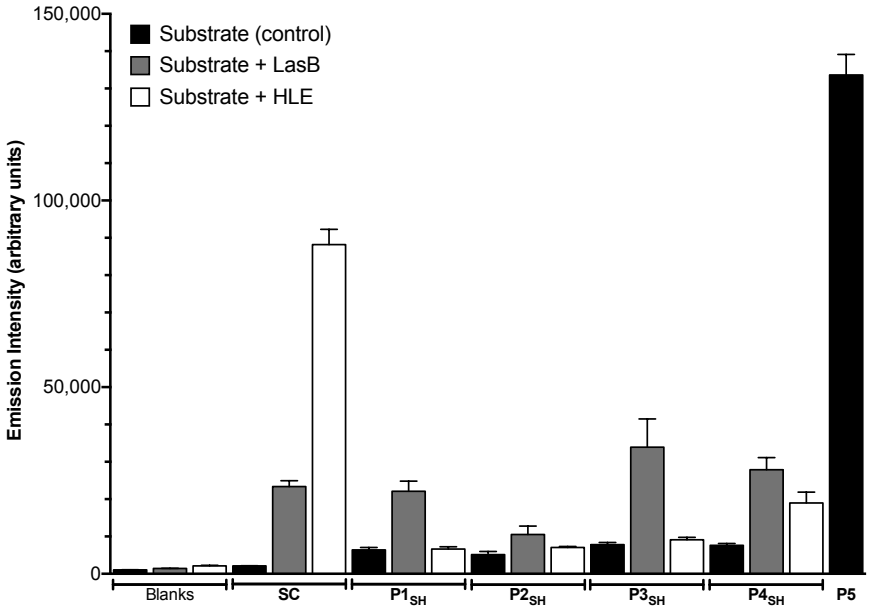

Figure S15 Amine quantification assay using fluorescamine after 4 hours of incubation of peptides **P1**-**4**$_{SH}$ or succinyl casein (SC) with bacterial (LasB) or human (HLE) elastase, and control peptide **P5** (100% hydrolysis). *n* = 3, mean ± SD.

Circular dichroism characterisation of peptides

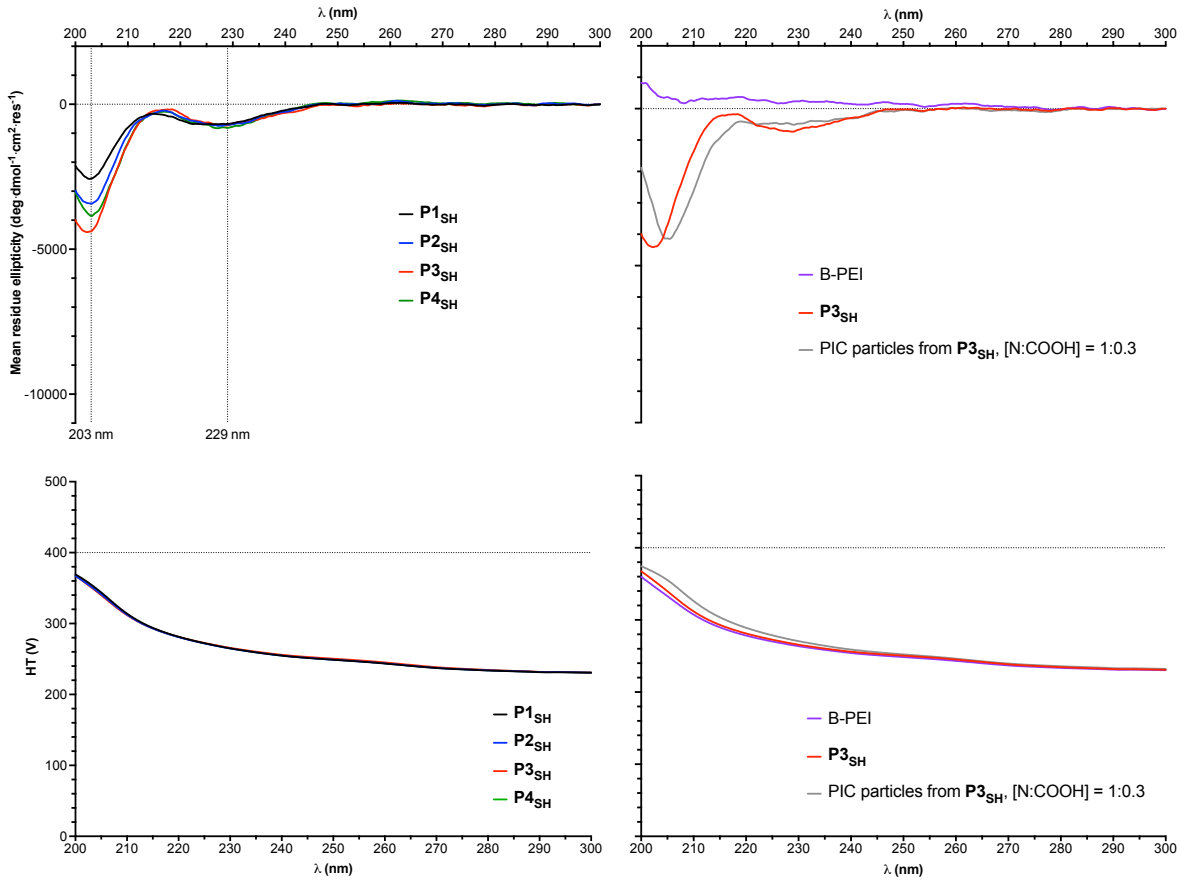

Figure S16 Top: Circular dichroism absorption spectra of peptides **P1**-**P4$_{SH}$** (left), and comparison between the spectra of **P3$_{SH}$**, B-PEI and PIC particles prepared from these two materials at a [N:COOH] ratio of 1:0.3 (right). Bottom: Dynode (HT) voltages recorded for the spectra above.

Antimicrobial activity of PIC particles

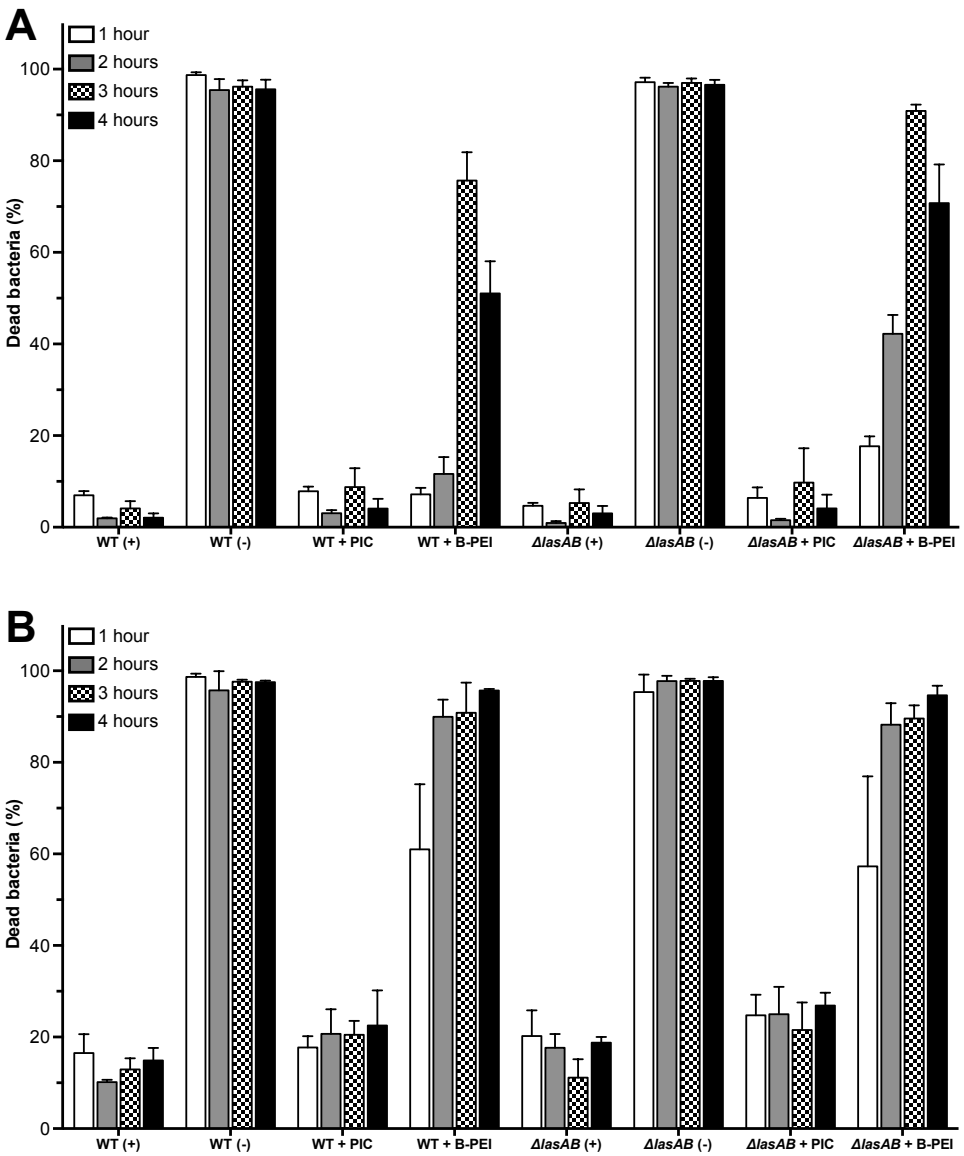

Figure S17 Raw FACS data for *P. aeruginosa* wild type (WT) and *ΔlasAB* mutant incubated in the absence (+) and presence of $\mathbf{P3_{SH}}$ PIC nanoparticles (PIC), B-PEI and 70% v/v aqueous 2-propanol (-) over time. Formulations prepared at a [N:COOH] ratio of 1:0.3 (A) and 1:1.0 (B) tested. Populations represent the percentage of red (dead) cells over the total. *n* = 3, mean ± SD.

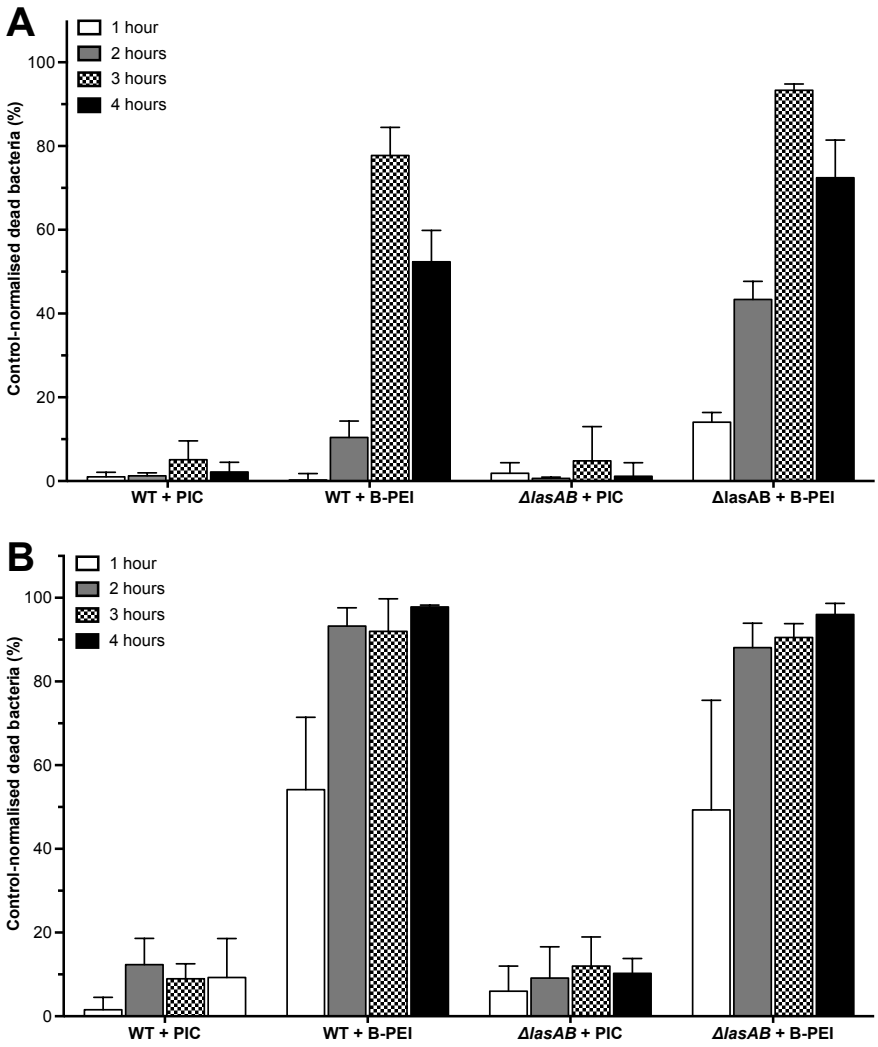

Figure S18 Normalised antimicrobial activity over time of **P3$_{SH}$** PIC nanoparticles prepared at [N:COOH] ratios of 1:0.3 (A) and 1:1.0 (B) and B-PEI against *P. aeruginosa* wild type (WT) and LasB-knockdown (*ΔlasAB*) strains. Activity normalised to that of the positive (0%) and negative (100%) controls for each time point (**Figure S17**). *n* = 3, mean values ± SD.

Enzymatic degradation of PIC particles – DLS analysis

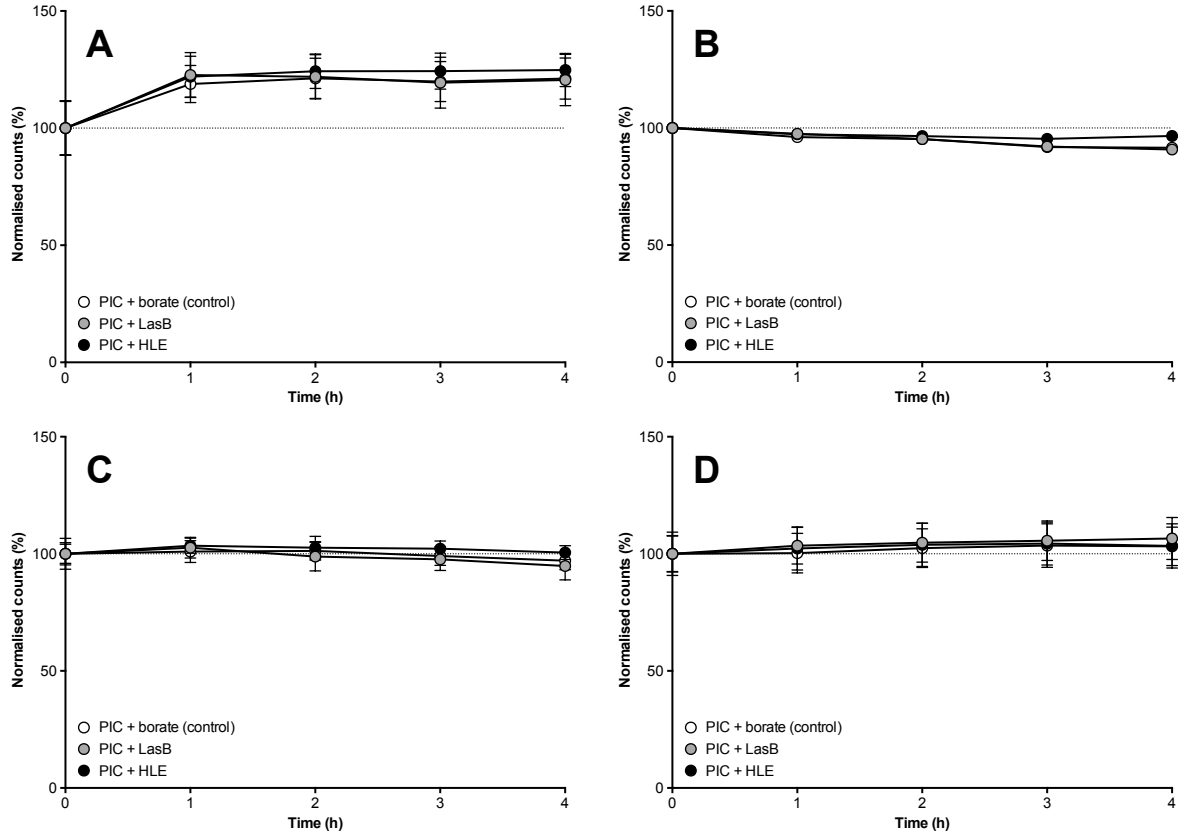

Figure S19 Normalised DLS detection counts (%) of PIC particles prepared at a [N:COOH] ratio of 1:0.3 from peptides **P2$_{SH}$** (A), **P3$_{SH}$** (B) and **P4$_{SH}$** (C), and from peptide **P3$_{SH}$** at a [N:COOH] of 1:1 (D) in the absence (○) and presence of LasB (●) and HLE (●). Data normalised to the initial counts for each of the individual experiments (100 %). *n* = 3, mean ± SD.

Enzymatic degradation of PIC particles – Fluorescamine analysis

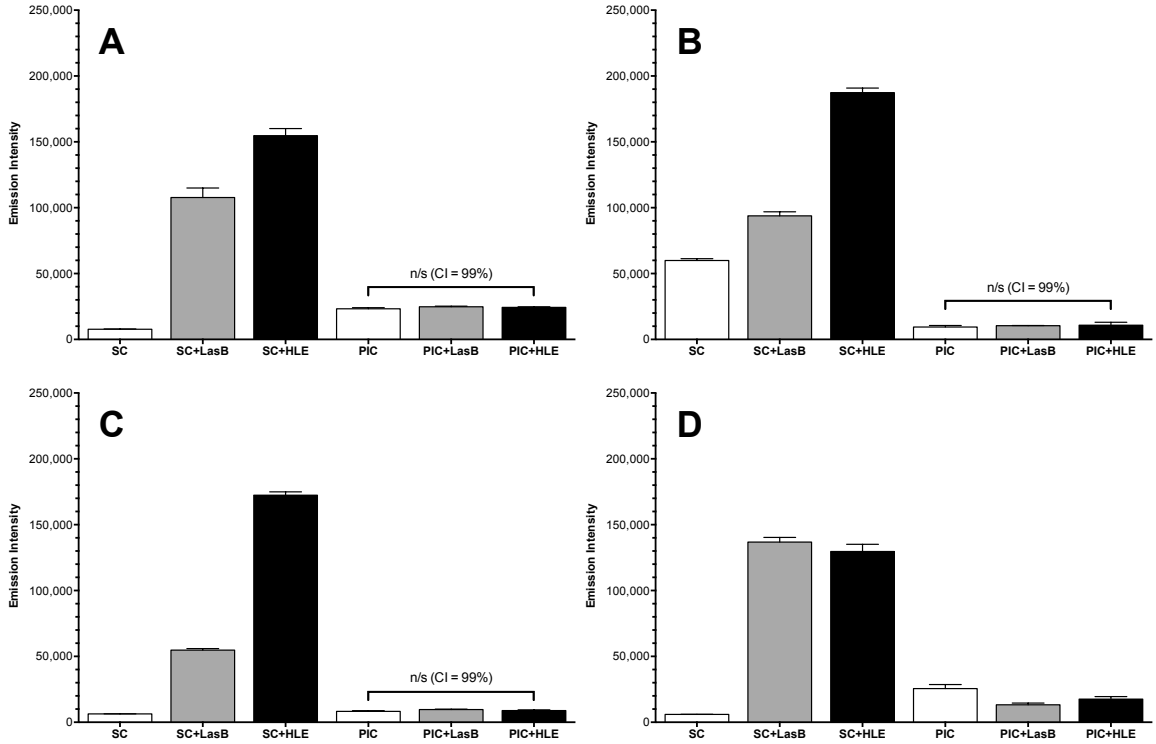

Figure S20 Emission intensity (λ_{exc} 355 nm, λ_{em} 460 nm) of fluorescamine conjugates for succinyl casein (SC) as a control for enzymatic activity and PIC particles prepared at a [N:COOH] ratio of 1:0.3 from peptides $\mathbf{P2_{SH}}$ (A), $\mathbf{P3_{SH}}$ (B) and $\mathbf{P4_{SH}}$ (C), and from peptide $\mathbf{P3_{SH}}$ at a [N:COOH] of 1:1 (D). All substrates were evaluated in the absence and presence of LasB or HLE and incubated for 4 hours. Photomultiplier (gain) values used: 1,500 (A-C) and 1,300 (D). *n* = 3, mean ± SD (One-way ANOVA).

Additional references

1 T. Vojkovsky, *Pept. Res.*, 1995, **8**, 236.

2 I. Insua, E. Liamas, Z. Zhang, A. F. A. Peacock, A. M. Krachler and F. Fernandez-Trillo, *Polym. Chem.*, 2016, **7**, 2684–2690.

CHAPTER 4

Preparation and antimicrobial evaluation of polyion complex (PIC) nanoparticles loaded with polymyxin B

Format: Paper.

Information: I. Insua, S. Majok, A. F. A. Peacock, A. M. Krachler and F. Fernandez-Trillo, *Eur. Polym. J.*, 2017, **87**, 478-486. – Published by Elsevier, shared with the Creative Commons Attribution License (CC BY): https://creativecommons.org/licenses/by/4.0/

Overview: The enzyme-responsive nanoparticles described in Chapters 2 and 3 did not have the desired antimicrobial properties they were designed for: most of these PIC particles did not display any antimicrobial effect in the presence of the targeted pathogen *Pseudomonas aeruginosa*, and even the ones that did show a pathogen-specific action, displayed very weak activities compared to that of the antimicrobial polymer loaded into them (*i.e.* PEI). At this stage, we argued that the poor antimicrobial activity of these PIC particles could due to the limited hydrolytic activity of the pathogenic enzyme LasB towards complexed peptides, which may be less accessible to LasB when aggregated into PIC particles. However, we also considered that the intrinsically weak antimicrobial activity of PEI could be limiting the results we were observing, and so it was proposed to evaluate the activity of PIC particles loaded with a stronger antibiotic.

The FDA-approved antibiotic polymyxin B (Pol-B) was selected as an alternative to PEI for its important clinical application, currently used as last resort treatment against multidrug-resistant Gram-negative infections. As such, we explored the

assembly of PIC particles from Pol-B and the anionic peptides presented in Chapters 2 and 3. Unfortunately, none of the Pol-B/peptide mixtures tested formed PIC nanoparticles, probably due to the low multivalency of both polyelectrolytes, which makes the assembly of PIC particle more difficult – as explained in Chapter 1. It must be noted that the studies to assemble Pol-B/peptide PIC particles are not described in this Chapter, written as a paper not linked to the previous work described in this thesis.

Based on the stronger binding between more multivalent polyelectrolytes (Chapter 1), we decided to approach the challenging assembly of PIC particles from small pentacationic Pol-B with an anionic polymer of very high multivalency. Thus, the low net charge of this antibiotic could be compensated with a macromolecular polyelectrolyte. We selected poly(styrene sulfonate) (PSS) to this end for being commercially available and FDA-approved, hence biocompatible.

Pol-B was successfully complexed with PSS, and the resulting PIC particles displayed tuneable physiological stabilities and antimicrobial properties based on their charge ratios (*i.e.* Pol-B/PSS blends).

Unlike the bacteria-targeted nanoparticles described in Chapters 2 and 3, these Pol-B/PSS PIC nanoparticles cannot sense bacterial enzymes, and the mechanism they follow to release the antibiotic is their unspecific swelling in physiological media and diffusion of the pre-loaded drug (*i.e*. passive release). However, although these nanoparticles cannot vectorise Pol-B to the pathogen, this system allows the preparation of PIC particles loaded with an approved antibiotic, and thus brings the development of the antimicrobial PIC particles investigated in this thesis closer to a potential clinical application. These nanoparticles can be useful tools to better control the dosing and minimise sub-inhibitory concentrations of antibiotics, which can prevent the development of new antimicrobial resistances.

Contributions: All authors contributed to the experimental set-up and discussed the results. II and FFT designed the nanoparticle synthesis and characterisation, and II, FFT and AMK designed the microbiological assays. II and SM carried out the microbiological assays, and II carried out all other experiments. II and FFT

analysed the data and wrote the paper, with all other authors contributing to the final version of the manuscript.

European Polymer Journal 87 (2017) 478–486

Contents lists available at ScienceDirect

European Polymer Journal

journal homepage: www.elsevier.com/locate/europolj

Preparation and antimicrobial evaluation of polyion complex (PIC) nanoparticles loaded with polymyxin B

Ignacio Insua [a,c], Sieta Majok [b,c], Anna F.A. Peacock [a], Anne Marie Krachler [b,c], Francisco Fernandez-Trillo [a,c,*]

[a] School of Chemistry, University of Birmingham, B15 2TT Birmingham, UK
[b] School of Biosciences, University of Birmingham, B15 2TT Birmingham, UK
[c] Institute of Microbiology and Infection, University of Birmingham, B15 2TT Birmingham, UK

ARTICLE INFO

Article history:
Received 7 July 2016
Received in revised form 23 August 2016
Accepted 24 August 2016
Available online 26 August 2016

Keywords:
PIC particles
Polyelectrolyte complexes
Antimicrobials
Drug delivery

ABSTRACT

Here, we describe novel polyion complex (PIC) particles for the delivery of Polymyxin B (Pol-B), an antimicrobial peptide currently used in the clinic as a last resort antibiotic against multidrug-resistant gram-negative bacteria. A range of conditions for the controlled assembly of Pol-B with poly(styrene sulphonate) (PSS) has been identified which let us prepare stable colloidal PIC particles. This way, PIC particles containing different Pol-B:PSS ratios have been prepared and their stability under simulated physiological conditions (*i.e.* pH, osmotic pressure and temperature) characterised. Furthermore, preliminary evaluation of the antimicrobial activity of these Pol-B containing PIC particles has been performed, by monitoring their effect on the growth of *Pseudomonas aeruginosa*, an opportunistic gram-negative bacterium.

1. Introduction

The increasing number of drug-resistant bacteria poses a serious risk to global health [1,2]. This increase in antimicrobial-resistant strains and the lack of new drugs reaching the market is encouraging the use of alternative approaches for the treatment of these infections [3,4]. One of these strategies is the resurgence of "old" antibiotics such as polymyxins, which are now prescribed more often as last-resort antimicrobials against gram-negative multidrug-resistant strains [5–7]. However, polymyxins are toxic, and therefore strategies are required to minimise this toxicity and ensure that effective dosing of the antimicrobial is achieved [8]. Moreover, with the emergence of transmittable resistance to polymyxins [9,10], strategies that can minimise systemic exposure to polymyxins are highly desirable.

Toxicity in polymyxins is associated with their amphiphilic and cationic nature. Therefore, the current strategy to minimise their toxicity is either to reduce the number of cationic residues and amphiphilic character [11], or to synthesise pro-drugs where cationic groups are masked to give a negatively-charged derivative [12,13]. However, both strategies often result in a loss of antimicrobial activity, because this activity is directly linked to the presence of these cationic charges. The synthesis of polymer-drug conjugates has been employed as an alternative [14,15], but this strategy still relies on the covalent attachment of polymyxin (or derivatives) to the polymer backbone, with the resulting loss in activity [14,16].

* Corresponding author at: School of Chemistry, University of Birmingham, B15 2TT Birmingham, UK.
E-mail address: f.fernandez-trillo@bham.ac.uk (F. Fernandez-Trillo).

http://dx.doi.org/10.1016/j.eurpolymj.2016.08.023
0014-3057/

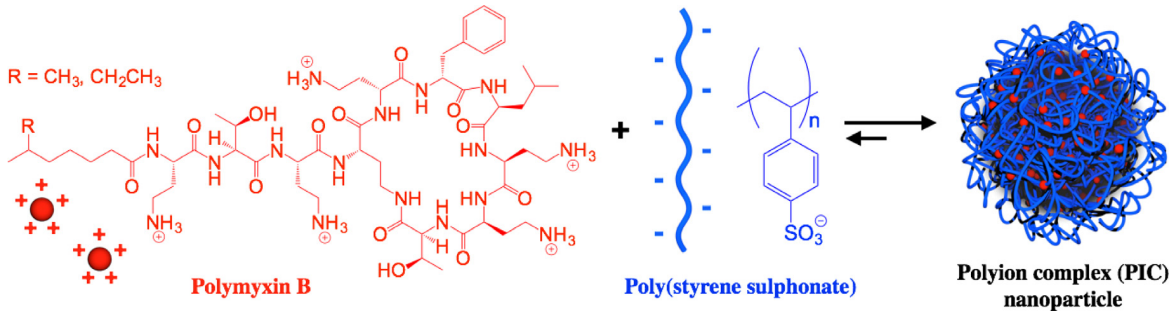

Fig. 1. Assembly of PIC nanoparticles from cationic antimicrobial polymyxin B and anionic PSS.

There are several strategies for the delivery of antimicrobial peptides and derivatives [17,18]. We and others have been exploring the use of polyion complex (PIC) nanoparticles as a platform for the delivery of this type of antimicrobials [19–24]. In this approach, the positive charge in cationic antimicrobial polymers and peptides is neutralised in the presence of a negatively charged "polymer". Under the right conditions, coacervate particles are formed upon neutralisation [25]. This way, positive charges are shielded from solution, without having to modify the structure of the antimicrobial (Fig. 1). In this article we describe the preparation of PIC nanoparticles as drug carriers for cationic polymyxin B sulphate (Pol-B), prepared by complexation of this antimicrobial with anionic poly(styrene sulphonate) (PSS). Different formulations were obtained by adjusting the Pol-B loading within these nanoparticles, and the formed PIC particles were characterised by Dynamic Light Scattering (DLS), ζ-potential and Transmission Electron Microscopy (TEM). Then, the stability of these nanomaterials was assessed under simulated physiological conditions. Finally, preliminary evaluation of the antimicrobial activity of these Pol-B:PSS PIC particles was done against *Pseudomonas aeruginosa*, an opportunistic gram-negative bacterium, and compared to that of free Pol-B to evaluate the differences in antibiotic activity of free and complexed drug.

2. Experimental

2.1. Materials

Polymyxin B sulphate (Pol-B) was purchased from Alfa Aesar®. Sodium poly(styrene sulphonate) 70 KDa average molecular weight (PSS), 4-(2-hydroxyethyl)piperazine-1-ethanesulfonic acid (HEPES), phosphotungstic acid hydrate and Luria Bertani (LB) broth (Miller) were bought from Sigma-Aldrich Co. Nylon 0.45 μm syringe filters were purchased from Camlab Ltd. Carbon-coated copper TEM grids (200 mesh) were purchased from Agar Scientific Ltd. Float-a-Lyzer® G2 (20 KDa MWCO) dialysis membranes were purchased from Spectrum Laboratories Inc. Dulbecco's phosphate buffered saline (DPBS), 9.5 mM in phosphate and without Ca^{2+} and Mg^{2+}, was bought from Lonza. Agar was purchased from Sigma-Aldrich Co.

2.2. Instrumentation

Dynamic light scattering (DLS) and ζ-potential measurements were carried out in a Zetasizer Nano ZS (Malvern Instruments Ltd.) stabilised at 37 °C. DLS was read at 173° (backscattering) for 60 s in triplicate and ζ-potentials were recorded 30 times at 140 V. TEM images of PIC nanoparticles were acquired on a JEM-1200EX (JEOL USA Inc.). PIC particle size was measured from TEM micrographs using ImageJ software (version 1.48v) and measuring each nanoparticle twice: both in their longest and shortest diameters. Reverse phase HPLC analysis was run through a Kinetex® C18-EVO column (Phenomenex®): 5 μm, 100 Å, 250 × 4.60 mm, stabilised at 35 °C and fitted to a SPD-M20A UV–vis detector (Shimadzu Co.) monitoring absorbance at 210 nm. A Loctite® LED flood array (Henkel Ltd.) operating at 405 nm was used to sterilise the samples studied in the bacterial growth experiment. A FLUOstar Omega (BMG Labtech GmbH.) microplate reader was used to incubate and measure the optical density at 600 nm (OD_{600}) in the bacterial growth experiments. Pictures of agar plates were taken on a ChemiDoc™ MP imaging system (Bio-Rad laboratories Inc.).

2.3. Preparation of PIC nanoparticles

PIC particles from Pol-B and PSS were prepared following the protocol previously described by our group [20]. The different formulations of PIC particles are defined by their [N:SO_3Na] ratio, which represents the proportion of amines in Pol-B over sulphonate groups in PSS. As an example, for the preparation of PIC particles at 0.5 [N:SO_3Na] (*i.e.* half the amount of amines compared to sulphonate groups), solutions of Pol-B (0.25 mM) and PSS (2.5 mM in monomer units) were prepared separately in 5 mM HEPES buffer at pH 7.4. Then, both stock solutions were filtered through 0.45 μm nylon syringe filters and mixed in equal amounts drop-wise under stirring. PIC nanoparticles at other [N:SO_3Na] ratios were obtained by

changing the concentration of the Pol-B stock solution and mixing with 2.5 mM PSS following the same protocol. After 24 h, samples were characterised by DLS and ζ-potential without prior dilution nor filtration.

2.4. Stability of PIC nanoparticles in simulated physiological conditions

To a sample of PIC particles (1 mL), prepared as described above, 182 μL of a 1 M solution of NaCl in water was added and the mixture was incubated at 37 °C to obtain physiological osmotic pressure and temperature. Every hour, the sample was analysed by DLS as described above.

2.5. Pol-B release from PIC particles

2.5 mL of a PIC particle sample prepared at 0.7 [N:SO_3Na] ratio were transferred into a pre-conditioned dialysis membrane (Float-a-Lyzer® G2), which was dialysed against 15 mL of DPBS at 37 °C under stirring (300 rpm). 500 μL of dialysate were taken at different time points and replaced with fresh DPBS. The dialysate samples were analysed by HPLC using an adaptation of the method previously reported by Orwa *et al.* [26], using a 50:23:22:5 mixture of 50 mM Na_2SO_4 in H_2O: H_2O: AcCN: 5% (v/v) dilution of 85% (m/m) H_3PO_4 in H_2O running at 1 mL/min. 3 replicates were studied under the same conditions. At every time point, the area under the peak of Pol-B (R_t = 2.7 min) found in each dialysate sample was normalised to the area found in a 2.5 mL sample of Pol-B prepared at the same concentration as that contained in PIC particles at 0.7 [N:SO_3Na] ratio (175 μM) diluted with 15 mL of DPBS (100% release). The same protocol was followed using a 175 μM Pol-B sample in 5 mM HEPES buffer pH 7.4 instead of PIC particles.

2.6. Growth curves of bacteria with PIC particles

50 μL aliquots of *P. aeruginosa* PAO1V cultures in LB broth (OD_{600} = 0.2) were loaded in the designated positions of a 96-well microplate. These bacterial cultures were mixed with 50 μL of PIC particles or free Pol-B in 5 mM HEPES buffer pH 7.4 to compare the antimicrobial activity of free and complexed (within PIC particles) Pol-B at the same concentration. In addition, these bacterial cultures were mixed with 50 μL of 5 mM HEPES buffer pH 7.4 as positive growth control and 1.25 mM (in monomer units) PSS in 5 mM HEPES buffer pH 7.4. Finally, 100 μL of a 1:1 mixture of the LB broth and 5 mM HEPES buffer pH 7.4 was also spotted in the microplate to confirm the sterility of the media. All samples were prepared in triplicate, with mean values and standard deviations reported. The microplate was incubated at 37 °C and orbital shaking, and the OD_{600} was monitored every 30 min for at least 15 h. The samples of PIC particles, free Pol-B, PSS and 5 mM HEPES buffer 7.4 were sterilised prior to this experiment by exposure to blue light (405 nm) for 2 h at a distance of 15 cm from the light source.

2.7. Antimicrobial assay of PIC particles: CFU counting

100 μL aliquots of a *P. aeruginosa* PAO1V culture in LB broth (OD_{600} = 0.2) were mixed with 100 μL of either PIC particles prepared at different [N:SO_3Na] ratios or Pol-B solutions at the same concentration found in the PIC particles. In addition, the *P. aeruginosa* PAO1V culture was mixed likewise with 5 mM HEPES buffer pH 7.4 and a 1.25 mM PSS solution in this same buffer as controls. All mixtures were incubated at 37 °C for 22 h. After this time, 10 μL of each sample were spotted in triplicate on an agar plates in serial dilution, from undiluted down to a 10^8-fold dilution in 10^2 increments. These agar plates were then incubated at 37 °C. After 16 h of incubation, the agar plates were photographed and bacterial concentrations in CFU/mL were calculated from the highest dilution that showed individual colonies. All samples were sterilised prior to this experiment by exposure to blue light (405 nm) for 2 h at a distance of 15 cm from the light source.

3. Results and discussion

Our aim was to develop and evaluate a novel nanoparticle system for the delivery of Pol-B, easy to prepare, inexpensive and with tuneable antimicrobial loading capacity. Based on the pentacationic structure of Pol-B, we postulated the preparation of polymeric nanoparticles by incubating this antibiotic under mild conditions with a negatively charged polyelectrolyte. We anticipated that a strong polyelectrolyte such as PSS would facilitate complexation of Pol-B, and compensate for the relative low multivalency (*i.e.* number of cationic residues) of this antibiotic: Pol-B has five amine residues derived from diaminobutanoic acid (Fig. 1). At physiological pHs, these amines should be "fully" cationic with at least 95% protonation (pK_{aH} 9–10) [27], giving Pol-B only five positive charges. Moreover, a considerably high molecular weight PSS (70 KDa) was selected to maximise the entropic gain upon PSS:Pol-B complexation. Also, PSS presents a hydrophobic styrene backbone, which could facilitate interactions with the hydrophobic residues in Pol-B and its aliphatic chain, that gives Pol-B an amphiphilic character (Fig. 1). Finally, it should be mentioned that PSS is an already approved pharmaceutical ingredient [28] and thus constituted an ideal starting point to develop our Pol-B containing PIC particles.

The preparation of Pol-B containing PIC nanoparticles was optimised by mixing stock solutions of this antimicrobial (in 5 mM HEPES buffer) with a 2.5 mM (per monomer) stock solution of PSS in the same buffer, following a protocol recently employed in our laboratories for the preparation of PIC particles containing short enzyme-responsive peptides [20]. At first,

a broad range of [N:SO_3Na] ratios was explored going from a 5-fold excess of cationic residues to a 5-fold excess of anionic groups (Fig. S1†). Not surprisingly, when equimolar amounts of ammonium and sulphonate groups were mixed, unstable suspensions were obtained that flocculated. The presence of these macroscopic aggregates suggested that neutral coacervates were being formed, which were not stable in suspension and eventually phase separated. The same result was obtained for all the formulations prepared using an excess of positive charge ([N:SO_3Na] > 1) (Fig. S1†), suggesting that the sequential adsorption of Pol-B molecules on PSS neutralises the initial negative charge in the primary complexes formed [25]. Further addition of Pol-B once these neutral flocculates are formed is redundant, as they cannot be recruited into the forming particles due to the lack of negative charge in these aggregates. This behaviour has been observed in the literature during the formation of PIC particles from small oligomeric electrolytes [20,23,25]. Interestingly, flocculation was also observed in mixtures below but very close to equimolarity (0.8 [N:SO_3Na] ratio) suggesting that not all styrene units had a sulphonate group. A commercial source of PSS was used in this work and the observed deviation from equimolarity could be explained because the industrial production of PSS from polystyrene results in different degrees of sulphonylation.

Having established that colloidal particles were only obtained at sub-stoichiometric ratios of Pol-B, this range was again explored but 10 different formulations were investigated (Fig. 2A). Again, flocculation was observed for those formulations prepared with ratios close to equimolarity (1, 0.9 and 0.8 [N:SO_3Na] ratios). Yet, we were able to obtain colloidal PIC particles from 0.7 to 0.1 [N:SO_3Na] ratios, all of which showed very similar sizes, with mean hydrodynamic diameters between 166 and 186 nm (Fig. 2B and Table S1†). All PIC particles obtained were negatively charged (ζ-potential of *ca.* −40 mV), as expected the excess of PSS present in these formulations. Particles prepared at a 0.7 [N:SO_3Na] ratio displayed a slightly smaller ζ-potential of −30 mV (Fig. 2B). While the difference in charge was small, this reduction in charge follows the expected trend towards less negatively charged particles as the formulation approaches equimolarity. TEM was performed on PIC particles prepared at a 0.4 [N:SO_3Na] ratio, selected as a representative example of all seven formulations characterised by DLS (Fig. 2C and Fig. S2†). These images confirmed the spherical shape of these nanomaterials and an average particle diameter of 140 ± 30 nm (n = 58), slightly smaller than the hydrodynamic diameter measured by DLS (174 ± 49 nm). This apparent reduction in size found by TEM can be attributed to drying upon sample preparation, which could result in these highly hydrated nanomaterials shrinking as the solvent evaporates [29].

Having identified a range of ratios from which Pol-B containing colloidal PIC particles could be prepared, the stability of these particles under simulated physiological conditions was assessed. It is well established that the presence of small electrolytes can shield the electrostatic attraction between the oppositely charged components of these nanomaterials. This screening normally results in particle swelling and can eventually lead to the disassembly of the PIC particle [25]. Since Pol-B loading dictated the number of electrostatic cross-links present in these colloids, it was anticipated that different [N:SO_3Na] ratios would behave differently in the presence of biologically relevant salt concentrations. Thus, the seven different formulations of PIC particles identified so far were incubated with 154 mM NaCl at 37 °C and analysed over time by DLS, to assess their tolerance to physiological conditions (*i.e.* osmotic pressure and temperature) (Fig. 3). Broadly, particles behaved in three different ways when challenged with physiological conditions:

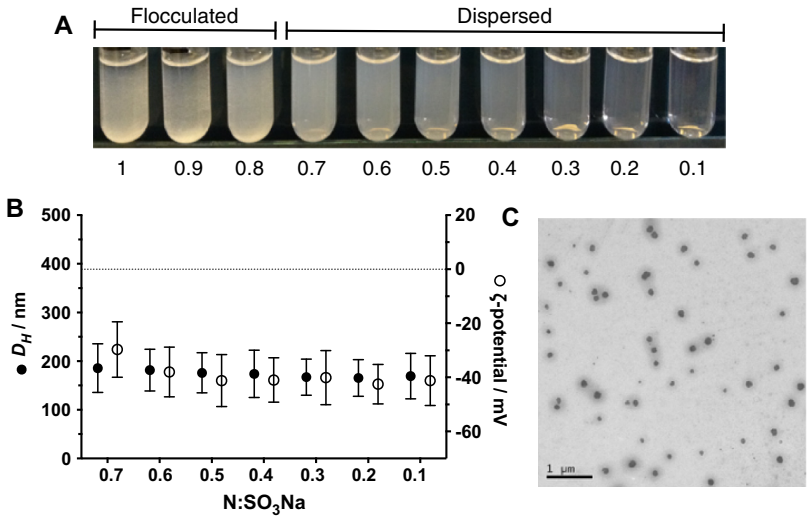

Fig. 2. (A) Macroscopic appearance of particles prepared at different [N:SO_3Na] ratios. (B) Hydrodynamic diameter (D_H, ●) and ζ-potential (○) of PIC particles prepared at different [N:SO_3Na] ratios. (C) Representative transmission electron micrograph of PIC particles prepared at a 0.4 [N:SO_3Na] ratio; Scale bar = 1 µm.

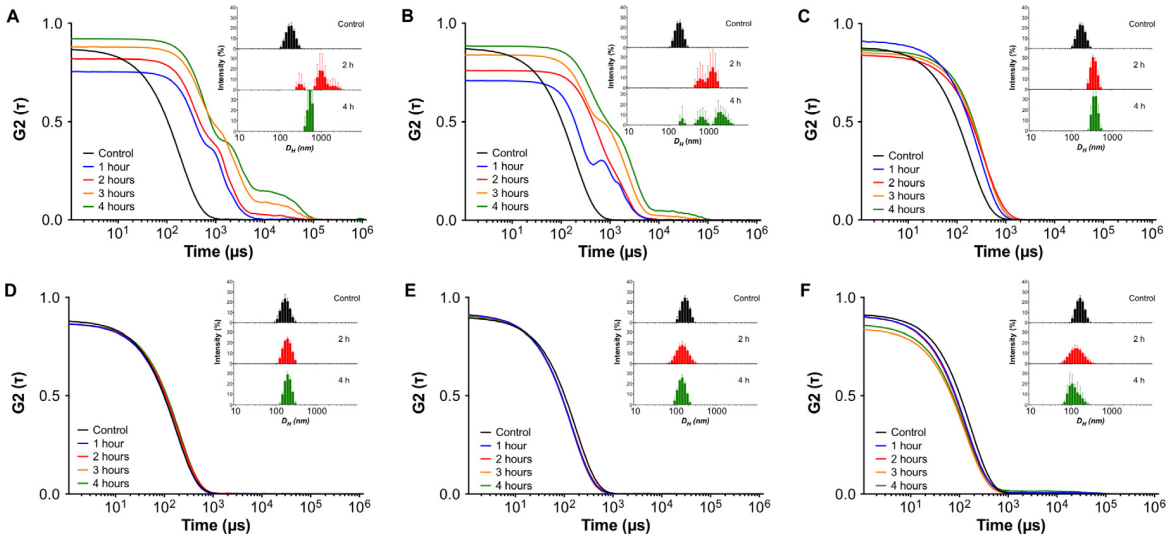

Fig. 3. Autocorrelation function (ACF) curves and representative size-intensity distributions (inset) for PIC particles prepared using six different [N:SO_3Na] ratios in the absence (control) and presence of 154 mM NaCl at 37 °C over time (1–4 h). 0.7 (A), 0.6 (B), 0.5 (C), 0.4 (D), 0.3 (E), 0.2 (F) [N:SO_3Na] ratio. Because of the dispersion in DLS measurements observed for unstable particles (*i.e.* 0.1:1 [N:SO_3Na] ratio) only representative plots are shown. 3 technical replicates were recorded for each sample.

(1) A remarkable increase in particle size was observed for those PIC particles prepared at 0.7 and 0.6 [N:SO_3Na] ratios (Fig. 3A and B). Micron-sized aggregates could be identified for these formulations, probably due to a combination of swelling and inter-particle aggregation as observed for other PIC particle systems [30].
(2) A region of high particle stability was found for formulations prepared between 0.5 and 0.2 [N:SO_3Na] ratios, for which the mean size remained almost unchanged during this experiment. For this group, only particles prepared at a 0.5 [N:SO_3Na] ratio changed their size significantly upon exposure to higher osmotic pressure, doubling their size after two hours. These particles then remained swollen and unchanged for the following hours (Fig. 3 and Fig. S4†).
(3) PIC particles prepared at a 0.1 [N:SO_3Na] ratio displayed very poor stability under these conditions, breaking into small-sized amorphous aggregates, as suggested by the loss of a sigmoidal profile in their DLS autocorrelation function curves (Fig. S3†). Overall, PIC particles at 0.1 [N:SO_3Na] exhibited the lowest tolerance to salt.

These stability experiments suggested that PIC particles could break apart in the presence of physiological conditions and therefore release the encapsulated Pol-B. To further demonstrate this release, PIC particles prepared at a 0.7 [N:SO_3Na] ratio were immersed in a dialysis tubing and this dialysis tubing suspended in DPBS buffer under mild agitation. Aliquots of the dialysate were taken at different time points and analysed by HPLC to monitor the release of Pol-B over time (Fig. S5†). Overall PIC particles were able to slow the release of Pol-B, with less than 10% of the antibiotic released after 4 h and 80% released after 48 h. However, these experiments were complicated by two main issues:

(1) There were interactions between Pol-B and the membranes used, as demonstrated by the "slow release" of free Pol-B from the dialysis tubing (Fig. S5†, black squares). Membranes of different molecular weight cut-off (MWCO) were tested to address this limitation, until significant release was observed (over 40% after 8 h) for a 20 KDa MWCO membrane. We believe this "slow release" was mainly the result of self-assembly of Pol-B, forming supramolecular aggregates with bigger hydrodynamic radius than the membrane porosity. Also, some interaction of Pol-B with the membrane was evident for the smaller MWCOs tested, with membranes turning opaque after the experiment.
(2) Under the experimental conditions used, Pol-B is a mixture of species (Fig. S6†), and only one of those (peak at 2.7 min) can be clearly identified in the dialysate.

We then evaluated the effect of encapsulating Pol-B inside these PIC nanoparticles on the activity of this antimicrobial. We anticipate that upon dilution in media, other electrolytes (*e.g.* NaCl) will screen the electrostatic interactions between Pol-B and PSS, facilitating disruption of the particle and the release of Pol-B. Towards this end, changes in optical density at 600 nm in *P. aeruginosa* cultures were monitored. This is a well-established indirect measurement of microbial growth that correlates any increase in the optical density of the culture to an increase in bacteria numbers [31]. Therefore, the effect PIC particles prepared between 0.7 and 0.1 [N:SO_3Na] ratios had on the growth of this pathogen was evaluated this way, and compared to the growth in the presence of free Pol-B and free PSS (Fig. 4). While PSS had no effect on the growth of this opportunistic pathogen (Fig. 4A–H, ◍), with changes in optical density mirroring those for *P. aeruginosa* alone (Fig. 4A–H, ●),

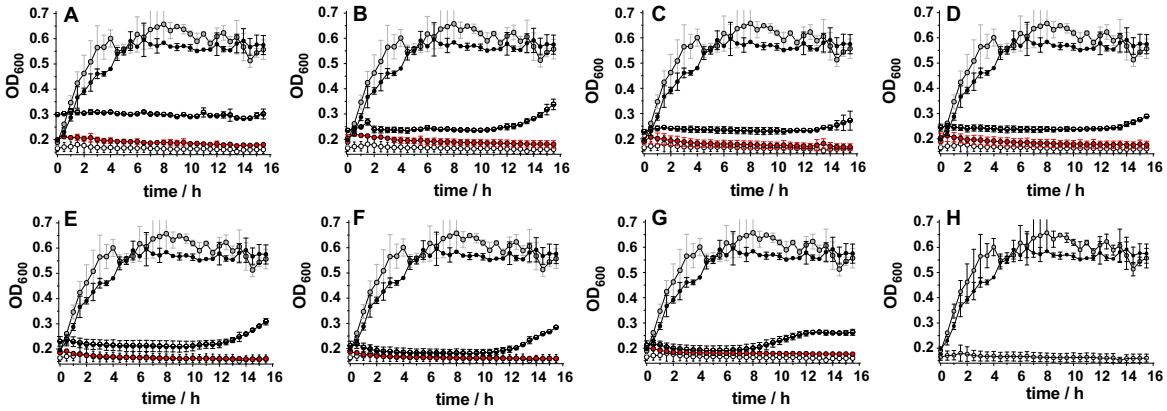

Fig. 4. Change in optical density at 600 nm (OD_{600}) for *P. aeruginosa* cultures in the absence (●) and presence of PSS (◍), Pol-B (●) and PIC particles (◒) prepared at 0.7 (A), 0.6 (B), 0.5 (C), 0.4 (D), 0.3 (E), 0.2 (F) and 0.1 (G) [N:SO_3Na] ratio. In each case, the concentration of Pol-B was adjusted to that in the PIC particles employed. Optical density of each of the controls including the media employed (1:1 LB:HEPES, ○) is shown for comparison (H). $n = 3$.

all of the concentrations of Pol-B tested (122.5–17.5 μg mL^{-1}, Fig. 4A–G, ●) inhibited *P. aeruginosa*'s growth for at least 16 h. A similar effect on growth could be observed for most of the PIC particles evaluated, with *P. aeruginosa*'s growth inhibited for at least 8 h. The antimicrobial effect of these PIC particles seemed to be formulation dependent, with those incorporating more Pol-B inhibiting the pathogen's growth for longer (*e.g.* up to 14.5 h for particles prepared at a 0.7 [N:SO_3Na] ratio).

The lower activity of these PIC nanoparticles compared to free Pol-B was expected, since these nanomaterials should act as reservoirs of Pol-B that is then slowly released from the nanoparticle. More surprising though was the fact that optical density in the presence of the particles was often higher than that in the presence of the same amount of Pol-B (◒ vs ● for each of the particles examined). This difference was more pronounced for those particles containing higher concentrations of Pol-B, with those prepared at a 0.7 [N:SO_3Na] ratio exhibiting an initial OD_{600} of 0.3, which was maintained through the duration of the experiment. Since these particles were able to scatter light (Fig. 2), and the intensity of this scattering was dependent on the formulation but also the conditions to which these particles were exposed (Fig. 3), we decided to evaluate if these particles could affect the optical density of the media in the absence of any microorganism. Incubation of particles with LB media in the absence of *P. aeruginosa* confirmed that this was the case, with particles increasing the optical density of the media in a formulation dependent fashion (Fig. 5A). No increase in optical density was observed for any of the individual components (Fig. S7A†), suggesting that the observed increase in optical density was a result of the addition of PIC particles. Particles containing more Pol-B led to higher optical densities at 600 nm, with those prepared at a 0.7 [N:SO_3Na] ratio exhibiting an initial OD_{600} of 0.28 ± 0.01, very similar to that observed in the presence of *P. aeruginosa* (Fig. 5B). Overall, this initial optical density was maintained for the duration of the experiment for most of the PIC particles evaluated, with only small changes in the optical density observed. Only particles prepared at a 0.7 and 0.6 [N:SO_3Na] ratios exhibited significant changes in OD_{600}. Both formulations increased the optical density of the media initially, but particles prepared at 0.7 [N:SO_3-Na] ratio eventually resulted in an overall reduction in optical density, with an OD_{600} of 0.23 after 15 h of incubation (Fig. 5A). This difference in behaviour may reflect the different stabilities of the PIC particles in this media (1:1 LB:HEPES), although no direct correlation should be expected with the stability observed in HEPES/NaCl buffer (Fig. 3).

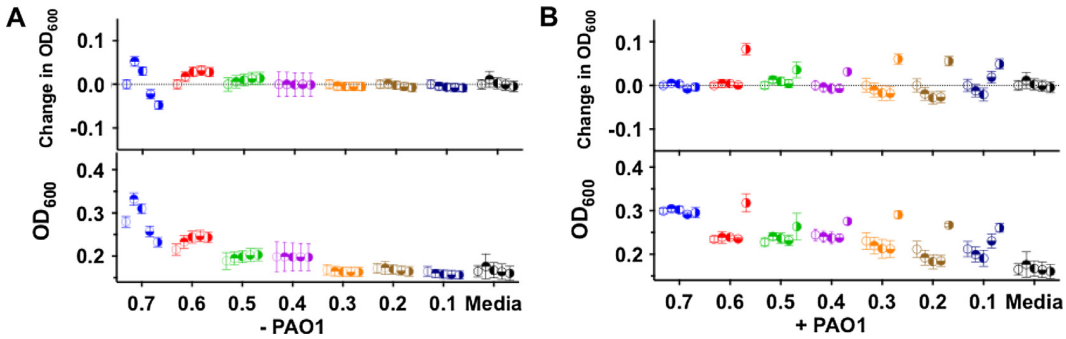

Fig. 5. Representative changes in optical density at 600 nm (OD_{600}) with time (○ 0 h, ◓ 2 h, ◐ 5 h, ◒ 10 h, ◑ 15 h) for PIC particles, prepared at different [N:SO_3Na] ratios, suspended in 1:1 LB:HEPES media in the absence (A) and presence of *P. aeruginosa* (B). Changes in OD_{600} represent the difference between the initial OD_{600} (t = 0 h) and the OD_{600} at each time point. No increase in optical density was observed for any of the individual components in the absence of *P. aeruginosa* (Fig. S7A†). $n = 3$. Each colour represents a different particle formulation.

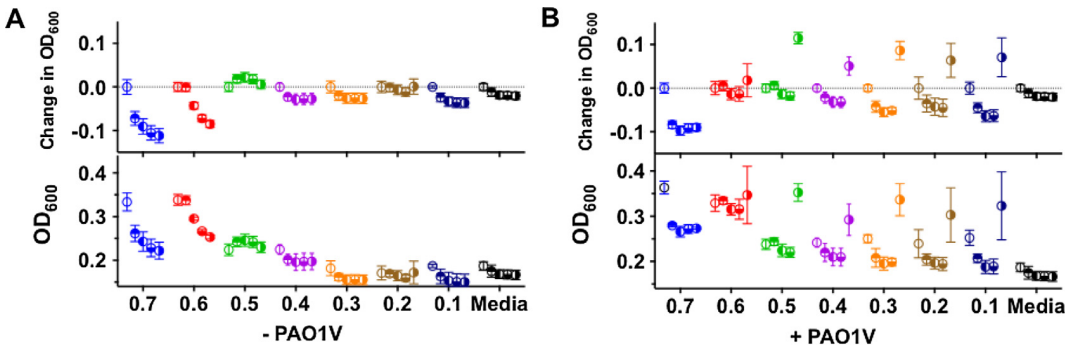

Fig. 6. Representative changes in optical density at 600 nm (OD_{600}) with time (○ 0 h, ◓ 2 h, ◐ 5 h, ◒ 10 h, ◑ 15 h) for PIC particles, prepared at different [N:SO_3Na] ratios, suspended in 1:0.4 LB:HEPES media in the absence (A) and presence of *P. aeruginosa* (B). Changes in OD_{600} represent the difference between the initial OD_{600} (t = 0 h) and the OD_{600} at each time point. No increase in optical density was observed for any of the individual components in the absence of *P. aeruginosa* (Fig. S7B†). $n = 3$. Each colour represents a different particle formulation.

To further investigate the behaviour of the particles in media, a new experiment was set-up in which particles were diluted even more in growth media (1:0.4 LB:HEPES). A similar trend was observed, both in the absence and presence of *P. aeruginosa*, although the higher content of LB media seemed to have a detrimental effect in some of the formulations (Fig. 6A). This effect was more evident for those particles that had a higher effect on the optical density of the media (0.7 and 0.6 [N:SO_3Na] ratios). As before, in the absence of bacteria, these two formulations increased the optical density of the media, in this case to an OD_{600} of approximately 0.33. However, optical density for these two formulations was then reduced, suggesting some degree of instability under these conditions. As before, inhibition of growth for *P. aeruginosa* in the presence of the particles was formulation dependent, with particles prepared at a 0.7 [N:SO_3Na] ratio sustaining the longest antimicrobial effect (Fig. 6B and Fig. S8†).

Finally, we also investigated the antimicrobial activity of these Pol-B containing particles by incubating *P. aeruginosa* with these particles and counting the resulting colony forming units (CFU). This assay correlates the amount of viable bacteria in a culture to the number of colonies that are formed after spotting an aliquot of this culture on agar plates [31]. Several dilutions were employed to spot the agar plates, to identify suitable conditions for colony counting (Fig. 7A). In agreement with the observed antimicrobial activity during growth measurements using changes in OD_{600}, all of the concentrations of free Pol-B tested inhibited the growth of *P. aeruginosa*, and no colonies were observed. Also, the antimicrobial activity of the particles was smaller than that of the free Pol-B (Fig. 7). This effect was formulation dependent but did not correlate with the amount of Pol-B incorporated in each nanoparticle. For instance, particles prepared at a 0.3 [N:SO_3Na] ratio had a higher activity than those prepared at a 0.4 [N:SO_3Na] ratio, despite having almost 25% less amount of Pol-B (Table S1†). However, particles prepared at 0.6 [N:SO_3Na] ratio had a higher activity that those prepared at 0.5 and 0.4 [N:SO_3Na] ratios, as expected from the amount of Pol-B encapsulated and the stability of the particles formed (Table S1† and Fig. 3). We believe there are several competing mechanisms affecting the observed antimicrobial activities. On the one hand, particle instability will result in "easier" release of Pol-B from unstable particles such as those prepared at 0.7, 0.6 or 0.1 [N:SO_3Na] ratios. On the other hand, the amount of Pol-B available will then strongly depend on the amount of Pol-B included in the formulation, with those prepared at a 0.1 [N:SO_3Na] ratio expected to have the lower activity. Overall, all of the concentrations tested

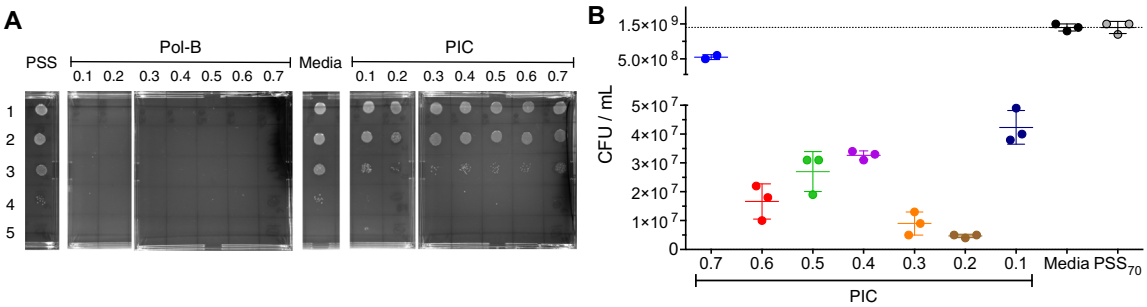

Fig. 7. (A) Representative agar plates used to evaluate antimicrobial activity of Pol-B containing PIC particles. Lane 1: No dilution, lane 2: 10^2-fold dilution, lane 3: 10^4-fold dilution, lane 4: 10^6-fold dilution, and lane 5: 10^8-fold dilution. (B) CFU/mL of *P. aeruginosa* in the absence (media, ●) and presence of PSS (◍) or PIC particles prepared at different [N:SO_3Na] ratios (dots, each colour represents a different particle formulation). Experiments were done in triplicate in 1:1 LB:HEPES media.

(except those prepared at a 0.7 [N:SO_3Na] ratio, which seems to be an outlier) were able to reduce the number of CFU/mL by approximately 2 orders of magnitude, and a relative reduction of the initial CFUs of over 97%.

4. Conclusions

Here we have presented our efforts towards the development of PIC particles for the delivery of Pol-B, an antimicrobial peptide of clinical relevance. Using 70 KDa PSS as the inert component of the formulation, we have identified a range of conditions for which Pol-B containing PIC particles can be prepared. We have evaluated the stability of these particles under simulated physiological conditions (*i.e.* pH, osmotic pressure and temperature). Preliminary evaluation of the antimicrobial activity of these PIC particles has been performed by monitoring their impact on *P. aeruginosa*'s growth. Overall, particles with a higher content of Pol-B can inhibit growth of this pathogen for longer, although this effect was formulation dependent. Finally, we report that, in the absence of bacteria, Pol-B containing particles are able to increase the optical density of the growth media in a particle-dependent fashion, an effect that can reflect the different stabilities of the PIC particles in this medium. Our efforts to optimise antimicrobial activity, including the optimisation of the polymer carrier and the development of degradable and targeted particles will be reported in due course.

Author contributions

All authors contributed to the experimental set-up and discussed the results. II and FFT designed the nanoparticle synthesis and characterisation, and II, FFT and AMK designed the microbiological assays. II and SM carried out the microbiological assays, and II carried out all other experiments. FFT and AMK secured funding. II and FFT analysed the data and wrote the paper, with all other authors contributing to the final version of the manuscript.

Acknowledgements

FFT thanks the University of Birmingham for the John Evans Fellowship. AMK thanks the University of Birmingham for a Birmingham Fellowship. FFT and AMK thank the Wellcome Trust (177ISSFPP) for funding and FFT thanks the Engineering and Physical Sciences Research Council (EPSRC) (EP/N508755/1) for funding. II thanks the University of Birmingham and the John Evans Fellowship for a PhD studentship. The authors acknowledge support from the Centre for Chemical and Materials Analysis in the School of Chemistry at the University of Birmingham. Some equipment used was obtained through Birmingham Science City: Innovative Uses for Advanced Materials in the Modern World (West Midlands Centre for Advanced Materials Project 2) and Birmingham Science City Translational Medicine: Experimental Medicine Network of Excellence project, with support from Advantage West Midlands (AWM) and part funded by European Regional Development fund (ERDF). The authors thank Dr Marie-Christine Jones and Dr Hannene Ali-Boucetta (School of Pharmacy, UoB) for the access to the DLS, and Nicolas Perez for useful discussions and help with the microbiology assays. The authors thank Prof. Suzanne M. J. Fleiszig for the kind donation of *P. aeruginosa* strain PAO1V [32].

Appendix A. Supplementary material

Supplementary data associated with this article can be found, in the online version, at http://dx.doi.org/10.1016/j.eurpolymj.2016.08.023.

References

[1] K. Hede, Antibiotic resistance: an infectious arms race, Nature 509 (2014) S2–S3, http://dx.doi.org/10.1038/509S2a.
[2] World Health Organization, Antimicrobial resistance: global report on surveillance, World Health Organization, 2014.
[3] C. Nathan, Fresh approaches to anti-infective therapies, Sci. Transl. Med. 4 (2012) 140sr2, http://dx.doi.org/10.1126/scitranslmed.3003081.
[4] B. Spellberg, J.G. Bartlett, D.N. Gilbert, The future of antibiotics and resistance, N. Engl. J. Med. 368 (2013) 299–302, http://dx.doi.org/10.1056/NEJMp1215093.
[5] A.P. Zavascki, L.Z. Goldani, J. Li, R.L. Nation, Polymyxin B for the treatment of multidrug-resistant pathogens: a critical review, J Antimicrob Chemother 60 (2007) 1206–1215, http://dx.doi.org/10.1093/jac/dkm357.
[6] D. Landman, C. Georgescu, D.A. Martin, J. Quale, Polymyxins revisited, Clin. Microbiol. Rev. 21 (2008) 449–465, http://dx.doi.org/10.1128/CMR.00006-08.
[7] E.A. Azzopardi, E.L. Ferguson, D.W. Thomas, Colistin past and future: a bibliographic analysis, J. Crit. Care. 28 (219) (2013), http://dx.doi.org/10.1016/j.jcrc.2012.04.008. e13–9.
[8] M.E. Falagas, S.K. Kasiakou, Toxicity of polymyxins: a systematic review of the evidence from old and recent studies, Crit Care. 10 (2006) R27, http://dx.doi.org/10.1186/cc3995.
[9] Y.-Y. Liu, Y. Wang, T.R. Walsh, L.-X. Yi, R. Zhang, J. Spencer, et al, Emergence of plasmid-mediated colistin resistance mechanism MCR-1 in animals and human beings in China: a microbiological and molecular biological study, Lancet Infect. Dis. 16 (2016) 161–168, http://dx.doi.org/10.1016/S1473-3099(15)00424-7.
[10] K.S. Kaye, J.M. Pogue, T.B. Tran, R.L. Nation, J. Li, Agents of last resort: polymyxin resistance, Infect. Dis. Clin. North Am. 30 (2016) 391–414, http://dx.doi.org/10.1016/j.idc.2016.02.005.
[11] K. Nakajima, Structure-activity relationship of colistins, Chem. Pharm. Bull. 15 (1967) 1219–1224. jstage.jst.go.jp/article/cpb1958/15/8/15_8_1219/_article.
[12] E.G. Beveridge, A.J. Martin, Sodium sulphomethyl derivatives of polymyxins, Br. J. Pharmacol. Chemother. 29 (1967) 125–135.

[13] J. Bergen, J. Li, C.R. Rayner, R.L. Nation, Colistin methanesulfonate is an inactive prodrug of colistin against *Pseudomonas aeruginosa*, Antimicrob. Agents Chemother. 50 (2006) 1953–1958, http://dx.doi.org/10.1128/AAC.00035-06.
[14] S.E. Bucklin, P. Lake, L. Lögdberg, D.C. Morrison, Therapeutic efficacy of a polymyxin B-dextran 70 conjugate in experimental model of endotoxemia, Antimicrob. Agents Chemother. 39 (1995) 1462–1466. aac.asm.org/content/39/7/1462.abstract.
[15] M.S. Shekhani, R.W. Schatz, C. Pugh, N. Panasik Jr., D. Stafford, Polymyxin B conjugates (2003). US6579696.
[16] P.C. Fuchs, A.L. Barry, S.D. Brown, PMX-622 (polymyxin B-dextran 70) does not alter in vitro activities of 11 antimicrobial agents, Antimicrob. Agents Chemother. 42 (1998) 2765–2767, http://dx.doi.org/10.1001/archsurg.1985.01390250044007.
[17] P. Urbán, J.J. Valle-Delgado, E. Moles, J. Marques, C. Díez, X. Fernàndez-Busquets, Nanotools for the delivery of antimicrobial peptides, Curr. Drug Targets 13 (2012) 1158–1172, http://dx.doi.org/10.2174/138945012802002302.
[18] A. Carmona-Ribeiro, L. de Melo Carrasco, Novel formulations for antimicrobial peptides, Int. J. Mol. Sci. 15 (2014) 18040–18083, http://dx.doi.org/10.3390/ijms151018040.
[19] L.D. Melo, E.M. Mamizuka, A.M. Carmona-Ribeiro, Antimicrobial particles from cationic lipid and polyelectrolytes, Langmuir 26 (2010) 12300–12306, http://dx.doi.org/10.1021/la101500s.
[20] I. Insua, E. Liamas, Z. Zhang, A.F.A. Peacock, A.M. Krachler, F. Fernandez-Trillo, Enzyme-responsive polyion complex (PIC) nanoparticles for the targeted delivery of antimicrobial polymers, Polym. Chem. 7 (2016) 2684–2690, http://dx.doi.org/10.1039/C6PY00146G.
[21] L.M. Sanches, D.F.S. Petri, L.D. de Melo Carrasco, A.M. Carmona-Ribeiro, The antimicrobial activity of free and immobilized poly (diallyldimethylammonium) chloride in nanoparticles of poly (methylmethacrylate), J. Nanobiotechnol. 13 (2015) 14, http://dx.doi.org/10.1186/s12951-015-0123-3.
[22] K.A. Les, A.H.A. Mohamed-Ahmed, S. Balan, J.-W. Choi, D. Martin, V. Yardley, et al, Poly(methacrylic acid) complexation of amphotericin B to treat neglected diseases, Polym. Chem. 5 (2014) 1037–1048, http://dx.doi.org/10.1039/C3PY01051A.
[23] K.L. Niece, A.D. Vaughan, D.I. Devore, Graft copolymer polyelectrolyte complexes for delivery of cationic antimicrobial peptides, J. Biomed. Mater. Res., Part A 101 (2013) 2548–2558, http://dx.doi.org/10.1002/jbm.a.34555.
[24] A.H.A. Mohamed-Ahmed, K.A. Les, K. Seifert, S.L. Croft, S.J. Brocchini, Noncovalent complexation of amphotericin-B with poly(α-glutamic acid), Mol. Pharm. 10 (2013) 940–950, http://dx.doi.org/10.1021/mp300339p.
[25] I. Insua, A. Wilkinson, F. Fernandez-Trillo, Polyion complex (PIC) particles: preparation and biomedical applications, Eur. Polym. J. 81 (2016) 198–215, http://dx.doi.org/10.1016/j.eurpolymj.2016.06.003.
[26] J.A. Orwa, A. Van Gerven, E. Roets, J. Hoogmartens, Liquid chromatography of polymyxin B sulphate, J. Chromatogr. A 870 (2000) 237–243, http://dx.doi.org/10.1016/S0021-9673(99)00936-X.
[27] Calculated with Marvinsketch protonation plug-in, using macro mode at 298 K. Calculated pKaH values for each of the amines: 9.07, 9.54, 9.84, 10.02 and 10.24.
[28] US Food and Drug Administration, Kayexalate®, SODIUM POLYSTYRENE SULFONATE, USP, Cation-Exchange Resin, US Food and Drug Administration. (n.d.). <http://www.accessdata.fda.gov/drugsatfda_docs/label/2009/011287s021lbl.pdf>. (accessed August 22, 2016).
[29] H. Friedrich, P.M. Frederik, G. de With, N.A.J.M. Sommerdijk, Imaging of self-assembled structures: interpretation of TEM and Cryo-TEM images, Angew. Chem., Int. Ed. Engl. (2010), http://dx.doi.org/10.1002/anie.201001493.
[30] H. Dautzenberg, G. Rother, Response of polyelectrolyte complexes to subsequent addition of sodium chloride: time-dependent static light scattering studies, Macromol. Chem. Phys. 205 (2004) 114–121, http://dx.doi.org/10.1002/macp.200350083.
[31] J.M. Willey, L. Sherwood, C.J. Woolverton, Microbial Growth, in: Prescotts Principles of Microbiology, Applied Energy, 2008, pp. 126–152.
[32] B.A. Cowell, S.S. Twining, J.A. Hobden, M.S.F. Kwong, S.M.J. Fleiszig, Mutation of lasA and lasB reduces *Pseudomonas aeruginosa* invasion of epithelial cells, Microbiology (Reading, U.K.) 149 (2003) 2291–2299, http://dx.doi.org/10.1099/mic.0.26280-0.

Preparation and antimicrobial evaluation of polyion complex (PIC) nanoparticles loaded with polymyxin B

Electronic Supplementary Information

Ignacio Insua,[a,c] Sieta Majok,[b,c] Anna F. A. Peacock,[a] Anne Marie Krachler,[b,c] and Francisco Fernandez-Trillo.[a,c]

[a] *School of Chemistry,* [b] *School of Biosciences and* [c] *Institute of Microbiology and Infection, University of Birmingham, B15 2TT Birmingham, UK*

Contents

1. PIC particles preparation and characterisation

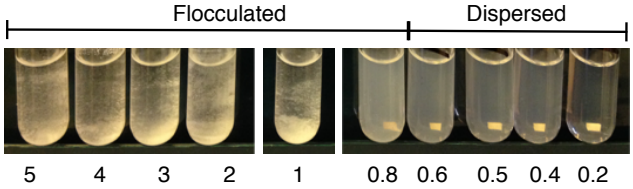

Figure S1 Macroscopic appearance of particles prepared at different [N:SO_3Na] ratios.

Table S1 Hydrodynamic diameter (D_H), ζ -potential and concentration of Pol-B of PIC particles prepared at different [N:SO_3Na] ratios. SD indicates the standard deviation found for the only size or charge population fitted by the software.

[N:SO_3Na] ratio	D_H ± SD (nm)	PdI [a]	ζ -potential ± SD (mV)	[Pol-B] (μM)
0.7	186 ± 50	0.07	-29.7 ± 10.2	175
0.6	182 ± 43	0.06	-38.0 ± 9.2	150
0.5	176 ± 41	0.05	-41.2 ± 9.6	125
0.4	174 ± 49	0.08	-41.0 ± 8.2	100
0.3	167 ± 37	0.05	-40.1 ± 10.0	75
0.2	166 ± 38	0.05	-42.5 ± 7.3	50
0.1	169 ± 47	0.08	-41.2 ± 9.2	25

[a] Polydispersity Index (PdI) calculated using the formula: PdI = $(SD/D_H)^2$.[S1]

1.1. TEM micrographs of PIC particles

5 μL of a suspension of PIC particles were deposited on the surface of the TEM grid and it was left to dry at room temperature covered from dust. Once dried, 5 μL of a 1 mg/mL solution of phosphotungstic acid in water were deposited on the grid to stain the nanoparticles for a minute, after which the excess staining solution was removed. Finally, the grid was dried as before.
For the measurement of the average PIC particle diameter, 58 nanoparticles were measured twice (in their longest and shortest diameters), giving an average of 140 nm with a standard deviation of 30 nm from a total of 116 measurements.

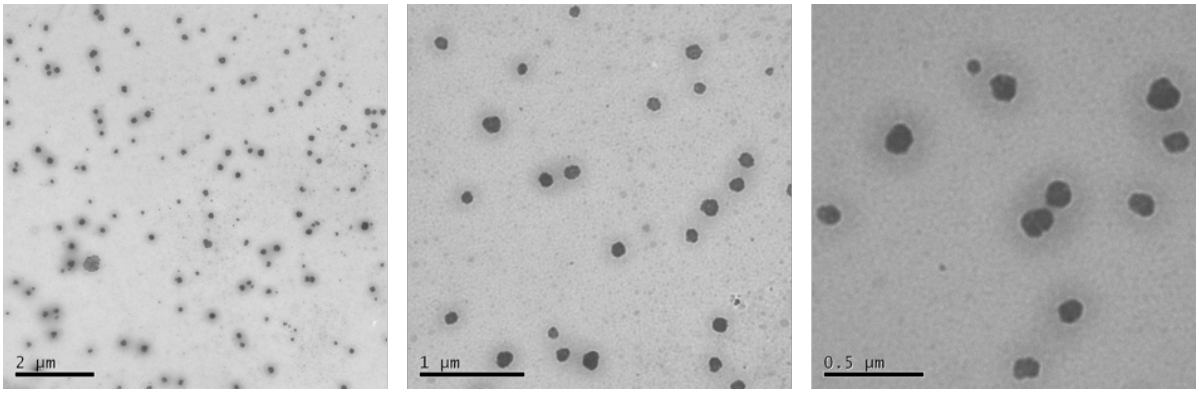

Figure S2 Representative TEM micrographs of PIC prepared at 0.4 [N:SO_3Na] ratio with increasing magnification (left to right).

1.2. Stability of PIC particles under simulated physiological conditions

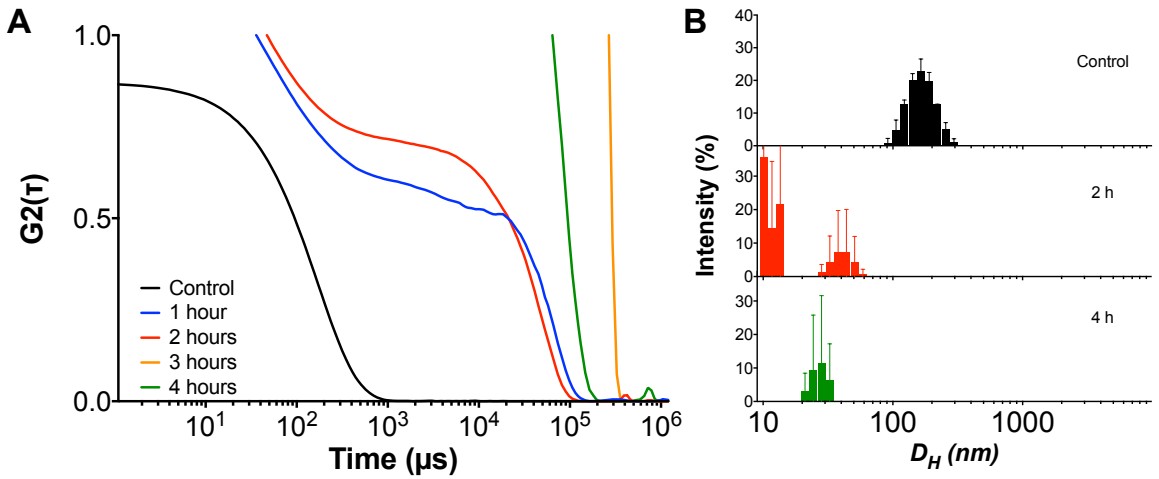

Figure S3 Autocorrelation function (ACF) curves (**A**) and representative size-intensity distributions (**B**) for PIC particles prepared at a 0.1 [N:SO_3Na] ratio in the absence (control) and presence of 154 mM NaCl at 37 °C over time (1-4 hours).

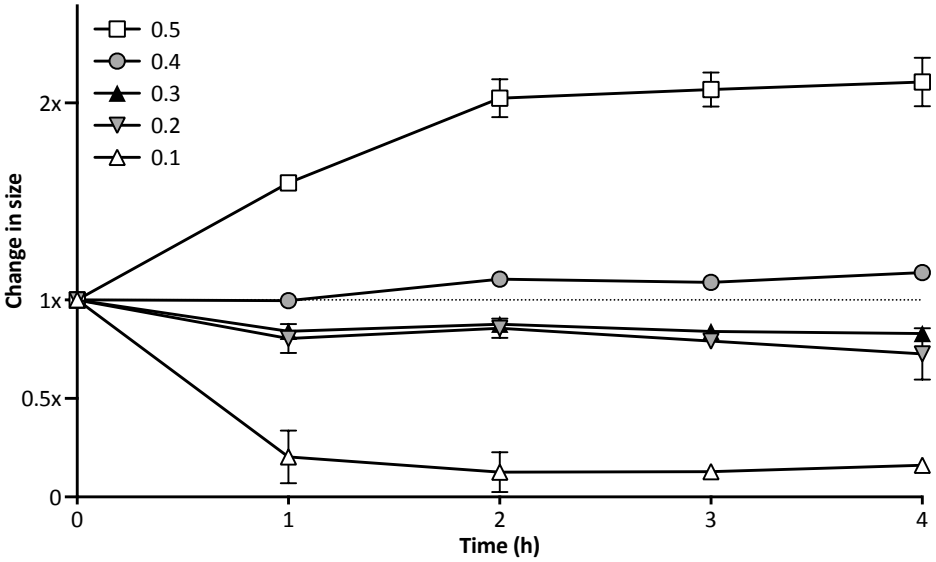

Figure S4 Evolution of PIC particle size (D_H) as measured by DLS when incubated with 154 mM NaCl at 37 ºC over time. The size of the nanoparticles was normalised to that of a control in the absence of NaCl (time point 0 h), and was monitored over 4 hours after the addition of salt (time points 1-4 h). Each symbol represents a different [N:SO_3Na] ratio.[‡] n = 3.

2. Pol-B release from PIC particles

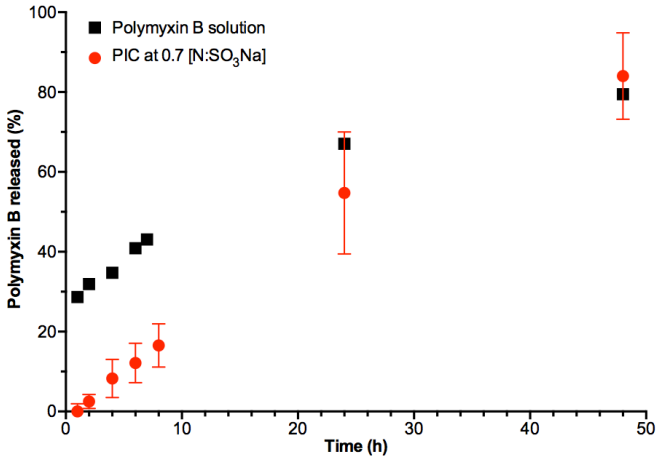

Figure S5: Pol-B content found in the dialysate of PIC particles prepared at 0.7 [N:SO_3Na] ratio (red circles) over time. Content was normalised to that found in a 175 μM Pol-B sample (drug loading in these PIC particles) diluted down to the total dialysis volume (100%) and compared to the rate of release for a Pol-B solution at the same concentration (black squares). n = 3.

[‡] PIC particles at 0.7 and 0.6 [N:SO_3H] have not been included since when these formulations were exposed to NaCl, they swelled to give more than one size distributions as indicated in **Figure 3.**

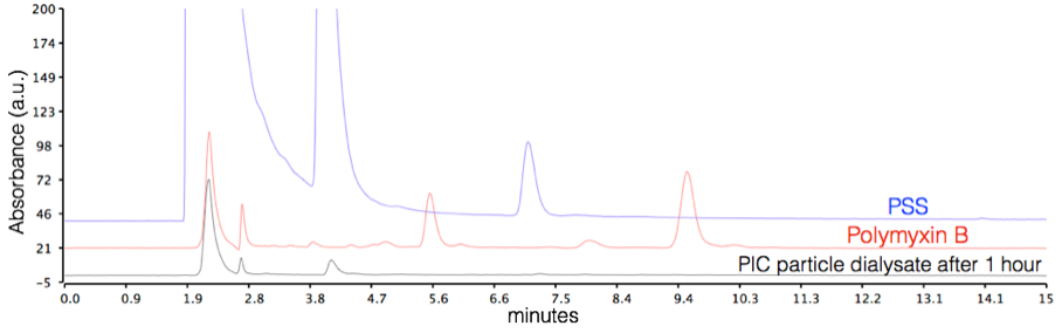

Figure S6: Representative RP-HPLC chromatograms of 70 KDa PSS (top), Pol-B (middle) and PIC particles prepared at a 0.7 [N:SO_3Na] ratio (bottom). Peak at *R*t = 2.7 min was used to monitor the release of Pol-B.

3. Antimicrobial activity of PIC particles

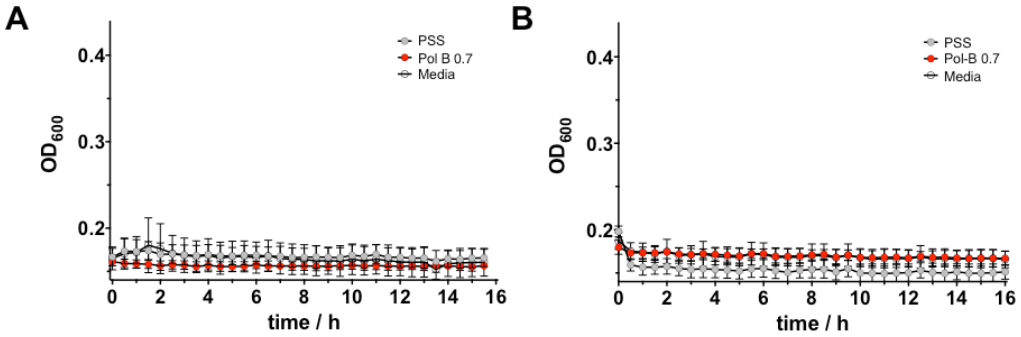

Figure S7 Change in optical density at 600 nm (OD_{600}) for media A) 1:1 LB:HEPES and B) 1:0.4 LB:HEPES; in the absence (○) and presence of PSS (◍) and Pol-B (●).

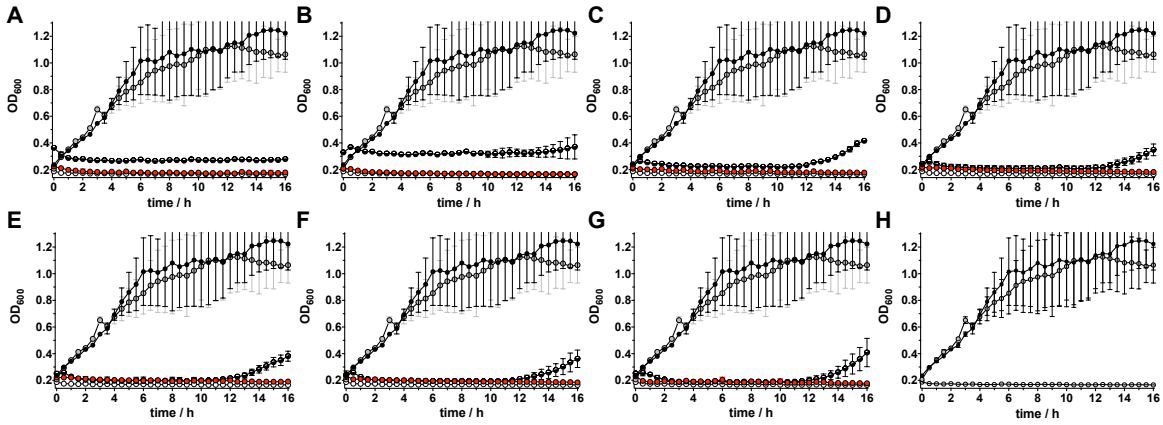

Figure S8 Change in optical density at 600 nm (OD_{600}) for *P. aeruginosa* cultures in the absence (●) and presence of PSS (◍), Pol-B (●) and PIC particles (◒) prepared at 0.7 (**A**), 0.6 (**B**), 0.5 (**C**), 0.4 (**D**), 0.3 (**E**), 0.2 (**F**) and 0.1 (**G**) [N:SO_3Na] ratio. In each case, the concentration of Pol-B was adjusted to that in the PIC particles employed. Optical density of each of the controls including the media employed (1:0.4 LB:HEPES, ○) is shown for comparison (**H**). $n = 3$.

4. Additional references

[S1] Measuring the size of nanoparticles in aqueous media using batch-mode Dynamic Light Scattering, 1st ed., NIST, U.S. Department of Commerce, 2015. doi:10.6028/nist.sp.1200-6.

4.3. Composition of commercial polymyxin B

Given the multiple peaks detected in the HPLC analysis of commercial polymyxin B (**Fig. S6**, previous page), a discussion of the identity of each of these peaks and interpretability of these results is required.

Polymyxin B is a mixture of lipopeptides naturally produced by the Gram-positive bacterium *Bacillus polymyxa*, which display antimicrobial activity towards Gram-negative bacteria.[1,2] It is commercialised as produced, containing seven main different subtypes based on a general structure with a cyclic cationic peptide and a pending aliphatic chain (**Fig. S9**).[3,4] From these subtypes, polymyxins B_1 and B_2 are the most abundant, accounting for *ca*. 50 and 24% of the total polymyxin B composition by HPLC, respectively. However, these seven subtypes only add up to 89% of the total composition of commercial polymyxin B by HPLC, and at least 14 more subtypes have been detected in small amounts.[4]

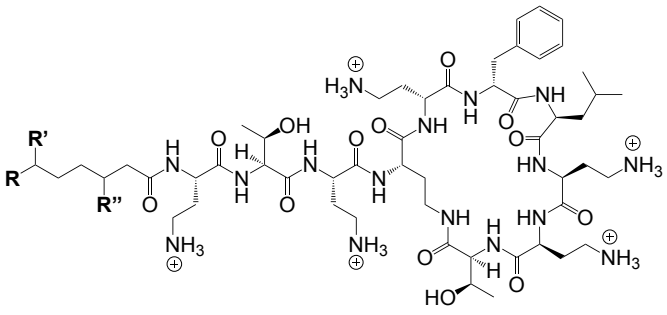

Subtype	R	R'	R''	Content (%)
B_1	C_2H_5	CH_3	H	49.9
B_2	CH_3	CH_3	H	23.8
B_3	C_2H_5	H	H	6.9
B_4	CH_3	H	H	1.6
B_5	C_3H_7	H	H	1.9
B_6	C_2H_5	CH_3	OH	2.5
Ile-B_1	Same R/R'/R'' as B_1, Ile residue instead of Leu.			2.4

Figure S9 Main polymyxin B subtypes found in commercial samples of this antibiotic and their relative peak area by HPLC analysis (*i.e.* content).[3,4]

Having established that polymyxin B consists of a mixture of similar lipopeptides, we compared our chromatograms of polymyxin B with those reported by Orwa *et al.*, who characterised the structure of the major HPLC peaks by NMR and MS.[3] Despite the slight differences between HPLC methods (**Table S2**), the traces of both chromatograms were very similar and allowed us to identify the major polymyxin B subtypes in our chromatograms with good confidence (**Fig. S10**).

Table S2 HPLC conditions used for the analysis of polymyxin B by Orwa *et al.*,[3] and those used in this thesis. Differences are highlighted in bold.

	Orwa *et al*. (see Fig. S10A)	This thesis (see Fig. S10B)
Column	C18, 5 µm, 250 x 4.6 mm, **120 Å**	C18, 5 µm, 250 x 4.6 mm, **100 Å**
Mobile phase	50 mM Na_2SO_4 : H_2O : AcCN : **6.8%** v/v H_3PO_4 (50 : **22.75** : **22.25** : 5)	50 mM Na_2SO_4 : H_2O : AcCN : **5%** v/v H_3PO_4 (50 : **23** : **22** : 5)
T (°C)	**30**	**35**
Flow rate (mL/min)	**0.5**	**1.0**

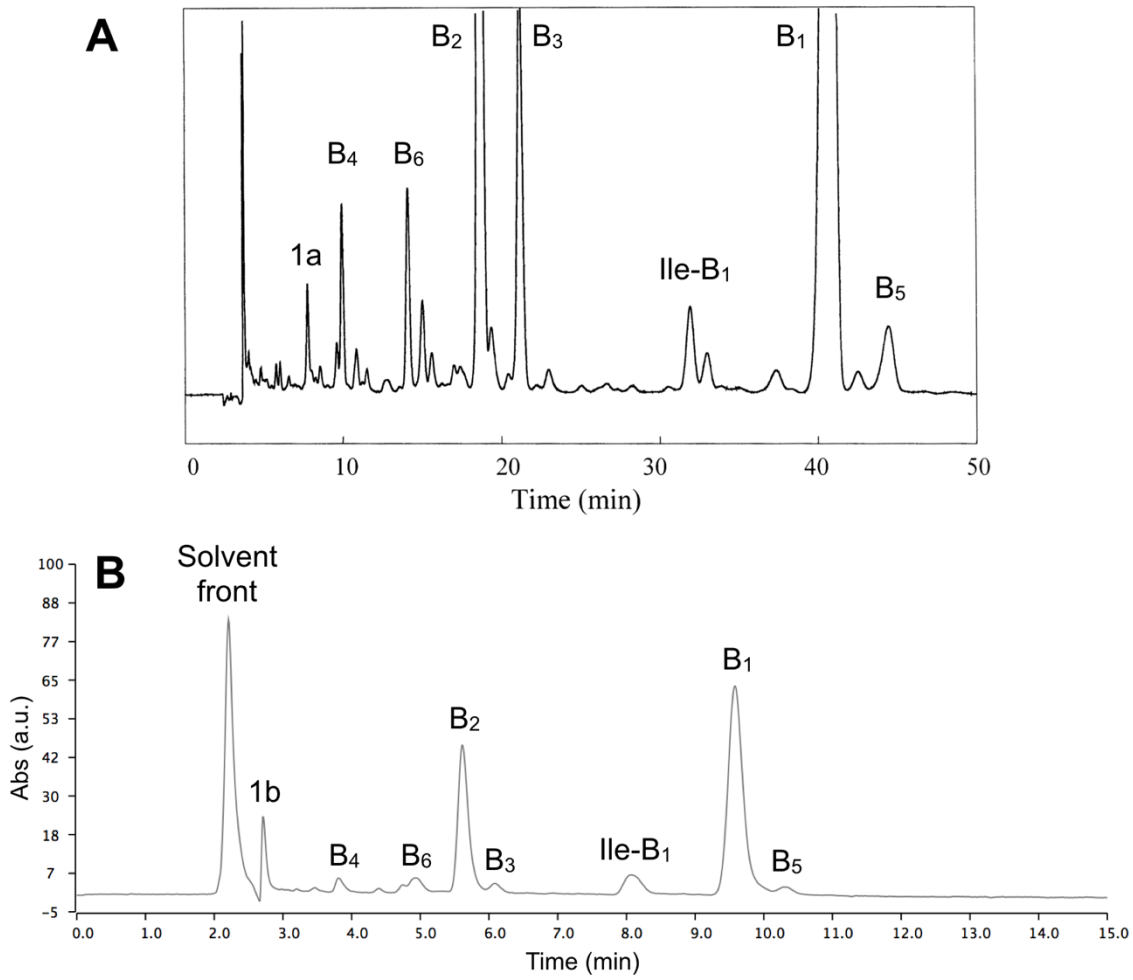

Figure S10 HPLC chromatograms of polymyxin B reported by Orwa *et al.* with the structure of each peak confirmed by MS and NMR (A),[3,5] and that reported by us as a red trace (labelled as 'Polymyxin B') in **Fig. S6** of this Chapter (B).

Based on the relative peak area and elution order, we can conclude that peak **1b**, which we monitored by HPLC in the dialysate of PIC nanoparticle samples to evaluate drug release (**Fig. S5**-**6**), does not correspond to any of the seven main polymyxin B subtypes by comparison to a reference chromatogram (**Fig. S10**). However, peak **1b** in our sample could correspond to peak **1a** in the chromatogram used as reference. Peak **1a** has been characterised previously using MS, and corresponds to a polymyxin B derivative with the general cyclic peptide linked to a $C_8H_{15}O_2$ tail, probably derived from a branched or linear hydroxylated octanoic acid, and accounts for less than 1% of the total sample by HPLC.[4,6] Whereas the relative composition of the main polymyxin B subtypes in our chromatogram (**Fig. S10B**) – 53.8 and 26.1% for polymyxin B1 and B2, respectively – is in good agreement with the values reported in the literature (**Fig. S9**),[4] the relative composition of **1b** (5.5%) is much higher than the 0.8% abundance previously reported for **1a**.[4] Therefore, although the elution order of **1a** and **1b** is similar, their very distinct relative abundance suggests they may not be the same compound. In addition, the fact that only compound **1b** could be detected by HPLC in the dialysate of PIC nanoparticles (**Fig. S6**) suggests that the structure (*i.e.* polarity and Mw) of **1b** is significantly different from the major polymyxin B subtypes, which could not diffuse through the dialysis membrane used. This 'specific membrane permeability' of **1b** suggests that this is not a polymyxin B derivative, otherwise other polymyxin B subtypes of similar structure should have also appeared in the dialysate due to similar physico-chemical interaction with the dialysis membrane. As such, and considering that **1a** has been characterised as a polymyxin B subtype,[4] we can conclude with fair confidence that **1a** and **1b** are different compounds.

The HPLC profile of a polymyxin B stock solution incubated under the same conditions as PIC nanoparticles for drug release evaluation (37°C, PBS buffer, pH 7.4) was also monitored over time. Whereas the area of the two most abundant polymyxin B subtypes (*i.e.* B1 and B2) decreased over time, the area of compound **1b** doubled from 1.7 to 3.5 a.u.·min after 20 hours of incubation (**Figure S11**). These results suggest that **1b** could be a degradation product of polymyxin

B. It is known that polymyxin B has poor stability in phosphate buffer at pH 7.4, which causes rapid drug degradation, mostly by racemisation.[7] Additionally, polymyxin B can also degrade in solution by reaction of amino acids within the peptide fraction, which happens more rapidly at pH 7.4 than in more acidic media.[8] As such, it is plausible that compound **1b** could be a degradation product of one or more of polymyxin B's species.

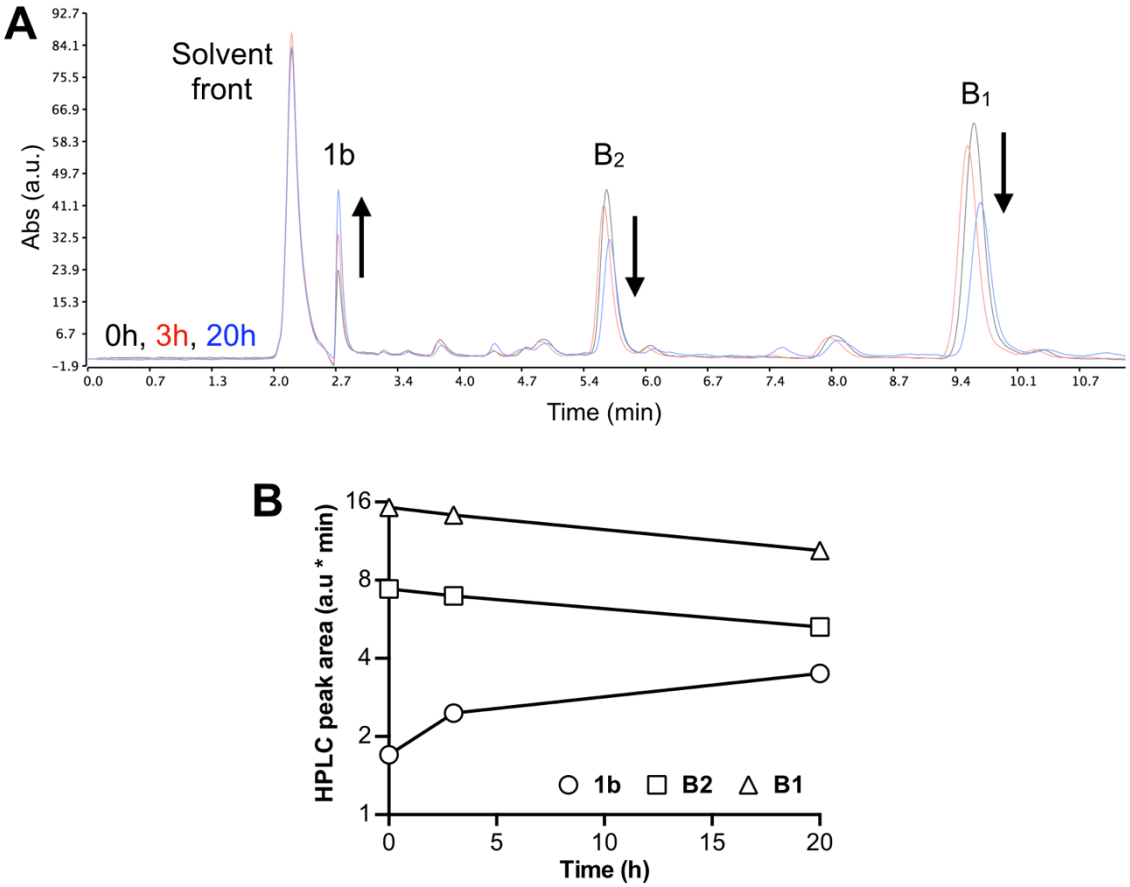

Figure S11 HPLC chromatogram of a polymyxin B solution in PBS incubated at 37°C and pH 7.4 at different time points (0, 3, 20 h; arrows indicate time evolution) (A), and the area of the three labelled peaks over time (B).

For all the above, we can conclude that the dialysis and HPLC experiments (**Fig. S5-6**) described in this Chapter to evaluate polymyxin B release from PIC nanoparticles are inconclusive. This is due to the monitoring of a peak of unknown identity by HPLC (**Fig. S10-11**; **1b**), and the absence of HPLC peaks for the most

abundant polymyxin B isoforms in the dialysate of PIC nanoparticles. Although these results may be also interpreted as if polymyxin B were not released from PIC nanoparticles, this would be in disagreement with the antimicrobial activity displayed by these nanoparticles (**Fig. 4-7**), which must stem from polymyxin B release given the lack of antimicrobial activity of the polymer PSS. Therefore, this section clarifies some of the experimental issues previously described in this Chapter regarding the drug release experiments, and supports the concerns stated before about the interpretability of this data (see page 103).

References and notes

1. T. Velkov, K. D. Roberts, P. E. Thompson and J. Li, *Future Med. Chem.*, 2016, **8**, 1017–1025.
2. S. K. Garg, O. Singh, D. Juneja, N. Tyagi, A. S. Khurana, A. Qamra, S. Motlekar and H. Barkate, *Crit. Care Res. Pract.*, 2017, DOI: 10.1155/2017/3635609.
3. J. A. Orwa, C. Govaerts, R. Busson, E. Roets, A. Van Schepdael and J. Hoogmartens, *J. Chromatogr. A*, 2001, **912**, 369–373.
4. L. Van den Bossche, A. Van Schepdael, S. Chopra, J. Hoogmartens and E. Adams, *Talanta*, 2011, **83**, 1521–1529.
5. Adapted from *J. Chromatogr. A*, 912, Orwa *et al.*, *Isolation and structural characterization of polymyxin B components*, 369-373, 2001, with permission from Elsevier.
6. C. Govaerts, J. Orwa, A. V. Schepdael, E. Roets and J. Hoogmartens, *J. Peptide Sci.*, 2002, **8**, 45–55.
7. J. A. Orwa, C. Govaerts, K. Gevers, E. Roets, A. Van Schepdael and J. Hoogmartens, *J. Pharm. Biomed. Anal.*, 2002, **29**, 203–212.
8. P. C. De Visser, C. Govaerts, P. A. V. Van Hooft, H. S. Overkleeft, A. Van Schepdael and J. Hoogmartens, *J. Chromatogr. A,* 2004, **1058**, 183–189.

CHAPTER 5

Effect of polyelectrolyte strength and degree of polymerisation on the formation, stability and activity of antimicrobial polyion complex (PIC) particles carrying polymyxin B

Format: Paper draft (unpublished).

Authors: I. Insua, A. F. A. Peacock, A. M. Krachler and F. Fernandez-Trillo.

Overview: In this Chapter, we continue the investigation of the nanoparticles for the passive release of polymyxin B (Pol-B) presented in Chapter 4. Here, we evaluate the impact of the nature and degree of polymerisation of the anionic polymer used to complex Pol-B on the properties of these PIC particles.

Since the affinity between oppositely charged polyelectrolytes is directly proportional to their multivalency, or net charge, we considered that shorter poly(styrene sulfonate) (PSS) chains than those previously explored in Chapter 4 (70 kDa in average) could lead to more weakly bound PIC particles with faster Pol-B release kinetics, and hence stronger antimicrobial activity. A collection of three PSS sources with molecular weights (*i.e*. degrees of polymerisation) below 70 kDa were explored, investigating the size, charge, saline stability and antimicrobial properties of their resulting PIC particles prepared in combination with Pol-B.

Additionally, weaker polyacids (*i.e*. those with higher pK_a values) can lead to weaker polyelectrolyte interactions when working at pH values close to their pK_a, as a result of their partial deprotonation and hence loss of multivalency. As such, weaker polyacids than PSS could also lead to more loosely bound PIC particles with faster drug release profiles, similar to the effect of the polymer's Mw described above. For this reason, we also investigated a collection of poly(acrylic

acid) (PAA) sources, a weaker polyacid than PSS, with degrees of polymerisation matching those of the PSS here reported, to evaluate the effect of the polyacid's strength on the properties of these PIC particles.

In summary, we present a dual study in this Chapter: the effect of the degree of polymerisation and acidity of six polyanions, on the assembly, saline stability and antimicrobial properties of PIC particles loaded with Pol-B.

It was found that, whereas all PSS and PAA sources allowed the assembly of PIC particles with overall very similar salt stabilities, there was a remarkable impact on their antimicrobial properties: PSS displayed stronger activities with shorter polymers, and the weaker PAA showed very strong antimicrobial effects regardless of its degree of polymerisation.

The results presented in this Chapter make a number of significant contributions to the understanding and development of PIC particles as new antimicrobial therapies: 1) Demonstrate that Pol-B can be formulated into PIC particles using polyanions of weaker affinity for Pol-B than the polymer previously explored in Chapter 4, thus further challenging the minimum net charge necessary to assemble PIC particles from small polyelectrolytes. 2) Highlight how simply the antimicrobial activity of Pol-B can be tuned when formulated into PIC particles by two means: adjusting the charge ratio of the nanoparticles and/or selecting different polymer sources. 3) Illustrate the remarkable versatility of PIC particles as drug delivery vehicles, which can be prepared in a number of different formulations from inexpensive and readily available materials, allowing the rapid development of many nanoparticle systems with distinct antimicrobial activities.

Contributions: All authors contributed to the experimental set-up and discussed the results. II and FFT designed the nanoparticle synthesis and characterisation, and II, FFT and AMK designed the microbiological assays. II carried out all experimental work. II and FFT analysed the data and wrote the paper, with all other authors contributing to the final version of the manuscript.

Effect of polyelectrolyte strength and degree of polymerisation on the formation, stability and activity of antimicrobial polyion complex (PIC) particles carrying polymyxin B

Ignacio Insua,[a,b] Anna F. A. Peacock,[a] Anne Marie Krachler[b,c] and Francisco Fernandez-Trillo[a,b,*]

[a]*School of Chemistry, University of Birmingham, B15 2TT Birmingham, UK.*
[b]*Institute of Microbiology and Infection, School of Biosciences, University of Birmingham, B15 2TT Birmingham, UK.*
[c]*Department of Microbiology and Molecular Genetics, University of Texas, 6431 Fannin. Houston (TX), USA.*
**Email: f.fernandez-trillo@bham.ac.uk*

Electronic Supplementary Information (ESI) available at the end of this article: Additional data for PIC particle characterisation, stability under simulated physiological conditions and antimicrobial results.

Here, we describe the preparation and characterisation of polymyxin B (Pol-B) containing polyion complex (PIC) particles. PIC particles were prepared with poly(styrene sulphonate) (PSS) and poly(acrylic acid) (PAA) across a range of degrees of polymerisation to evaluate the effect that the nature and multivalency of the electrolyte have on the stability and antimicrobial activity of these particles. Our results demonstrate that while particles prepared with stronger and longer polyelectrolytes (*e.g.* PSS DP 155) are more stable under simulated physiological conditions, those prepared with weaker and shorter polyelectrolytes (*e.g.* PAA DP 19) have a higher antimicrobial activity.

Introduction

Polyion complex (PIC) particles are soft colloids formed by the spontaneous aggregation of oppositely charged polyelectrolytes in aqueous media.[1] Due to their straightforward preparation and versatility, PIC particles are particularly suited for the delivery of charged (bio)molecules (*e.g.* nucleic acids and proteins), which are prevalent in nature. This way, delivery vehicles can be formulated without the need to introduce chemical modifications to these (bio)molecules and as a result, the biological activity of these therapeutics should be maintained upon release. PIC particle formation and stability are dominated by entropic effects making them ideal for the delivery of "large" and densely charged macromolecules such as nucleic acids.[2,3] More challenging is the use of PIC particles for the delivery of proteins,[4] peptides[5] or small molecules,[1] which often lack the required charge density to form stable PIC particles. However, many of the characteristics of PIC particles makes them ideally suited for the delivery of antimicrobial peptides, which are small cationic peptides that have been harnessed as last-resort antimicrobials or as alternatives to current antibiotics:[6-8] Cationic residues in antimicrobial peptides can be shielded within PIC particles,[9-12] thus minimising the toxicity towards the host, toxicity that is often associated with the cationic and amphiphilic nature of antimicrobial peptides.[6-8,13,14]

In our laboratories, we have recently developed PIC particles loaded with the clinically approved antibiotic polymyxin B (Pol-B) by complexation with poly(styrene sulphonate) (PSS).[9] These Pol-B containing particles displayed a tunable antimicrobial effect against *Pseudomonas aeruginosa*, an opportunistic gram-negative bacterium, for which Pol-B is currently used as a last resort antimicrobial. Based on the correlation between the stability of PIC particles and the net charge of their consisting polyelectrolytes, the formulation of Pol-B with shorter and/or weaker polyelectrolytes can potentially result in more permeable PIC particles with stronger antimicrobial properties. In this communication, we investigate the effect of the degree of polymerisation (*i.e.* molecular weight) and polyelectrolyte strength ($-SO_3Na$ *vs* –COONa) on the stability and biological activity of the resulting Pol-B containing particles. We believe our observations are critical and form the experimental basis for the development of polymyxin B delivery vehicles for future clinical applications.

Experimental

Materials

Polymyxin B sulphate (Pol-B) was purchased from Alfa Aesar®. Sodium poly(styrene sulphonate) (PSS) of 32, 17 and 10 kDa average Mw (GPC standards), sodium poly(acrylic acid) (PAA) of 15 (35% wt. in water), 8 (45% wt. in water) and 1.8 kDa average Mw, 4-(2-hydroxyethyl)piperazine-1-ethanesulfonic acid (HEPES), phosphotungstic acid hydrate, agar and Luria Bertani (LB) broth (Miller) were bought from Sigma-Aldrich Ltd. Nylon 0.45 µm syringe filters were purchased from Camlab Ltd. Carbon-coated copper TEM grids (200 mesh) were purchased from Agar Scientific Ltd. Dulbecco's phosphate buffered saline (DPBS), 9.5 mM in phosphate and without Ca^{2+} and Mg^{2+}, was bought from Lonza.

Instrumentation

Dynamic light scattering (DLS) and ζ-potential measurements were carried out in a Zetasizer Nano ZSP (Malvern Instruments Ltd.) stabilised at 37 °C. DLS was read at 173° (backscattering) for 60 seconds in triplicate and ζ-potentials were recorded 30 times at 140 V. Transmission Electron Microscopy (TEM) images of PIC nanoparticles were acquired on a JEM-1200EX (JEOL USA Inc.). PIC particle size was measured from TEM micrographs using ImageJ software (1.48v) and measuring

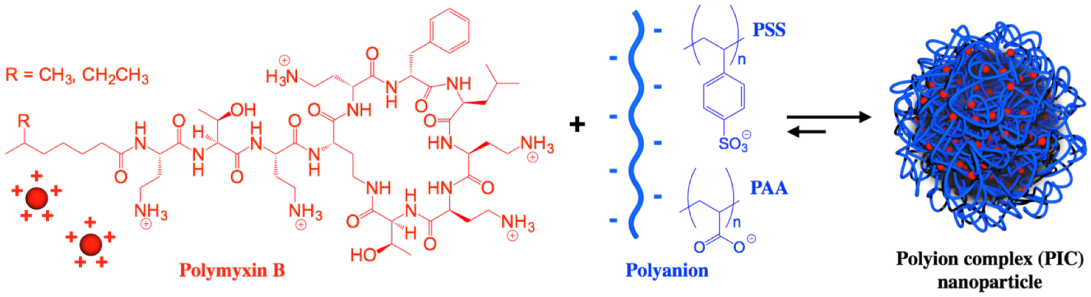

Figure 1. Formation of PIC particles by self-assembly of cationic polymyxin B with either poly(styrene sulphonate) (PSS) or poly(acrylic acid) (PAA) as polyanion.

each nanoparticle twice: both in their longest and shortest diameters. A Loctite® LED flood array (Henkel Ltd.) operating at 405 nm was used to sterilise the samples studied in the bacterial growth experiment. A FLUOstar Omega (BMG Labtech GmbH.) microplate reader was used to incubate and measure the optical density at 600 nm (OD_{600}) in the bacterial growth experiments. Pictures of agar plates were taken on a ChemiDoc™ MP imaging system (Bio-Rad laboratories Inc.).

Preparation of PIC nanoparticles.

PIC particles from Pol-B and PSS or PAA were prepared following the protocol previously described by our group.[9] The different formulations of PIC particles are defined by their [n+/n-] ratio, which represents the proportion of ammonium groups in Pol-B over acidic groups in PSS or PAA. As a representative example, for the preparation of PIC particles at 0.5 [n+/n-] ratio, solutions of Pol-B (0.25 mM) and PSS or PAA (2.5 mM in monomer units) were prepared separately in 5 mM HEPES buffer at pH 7.4. Then, both stock solutions were filtered through 0.45 µm nylon syringe filters and mixed in equal amounts drop-wise under stirring. PIC nanoparticles at other [n+/n-] ratios were obtained by changing the concentration of the Pol-B stock solution and mixing with 2.5 mM PSS or PAA following the same protocol. After 24 h, the polyion mixtures were characterised by DLS and ζ-potential without prior dilution nor filtration (**Table S1**).

TEM imaging of PIC particles.

For the preparation of the nanoparticles for TEM analysis, 5 µL of a suspension of PIC particles were deposited on the surface of the TEM grid and it was left to dry at room temperature covered from dust. Once dried, 5 µL of a 1 $mg{\cdot}mL^{-1}$ solution of phosphotungstic acid in water were deposited on the grid to stain the nanoparticles for a minute, after which the excess staining solution was removed. Finally, the grid was dried as before.

Stability of PIC nanoparticles in simulated physiological conditions.

To a sample of PIC particles (1 mL), prepared as described above, 182 µL of a 1 M solution of NaCl in water was added and the mixture was incubated at 37 °C to obtain physiological osmotic pressure and temperature. Every hour, the sample was analysed by DLS as described above.

Antimicrobial evaluation of PIC particles: Growth curves.

100 µL aliquots of *P. aeruginosa* PAO1V cultures in LB broth (OD_{600} = 0.2) were loaded in the designated positions of a 96-well microplate. These bacterial cultures were mixed with 100 µL of PIC particles or free Pol-B in 5 mM HEPES buffer pH 7.4 to compare the antimicrobial activity of free and complexed (within PIC particles) Pol-B at the same concentration. Alternatively, these bacterial cultures were mixed with 100 µL of 5 mM HEPES buffer pH 7.4 as positive growth control or 1.25 mM (in monomer units) PSS or PAA in 5 mM HEPES buffer pH 7.4. to evaluate the effect of the polymers alone. Finally, 200 µL of a 1:1 mixture of the LB broth and 5 mM HEPES buffer pH 7.4 were also loaded in the microplate to confirm the sterility of the media. All samples were prepared in triplicate, with mean values and standard deviations reported. The microplate was incubated at 37 °C and orbital shaking, and the OD_{600} was monitored every 30 min for 24 h. The samples of PIC particles, free Pol-B, PSS and 5 mM HEPES buffer 7.4 were sterilised prior to this experiment by exposure to blue light (405 nm) for 2 h at a distance of 15 cm from the light source.

Antimicrobial evaluation of PIC particles: CFU counting.

After 24 h, 10 µL of the samples from the 'growth curve' experiment (see above) were spotted in triplicate on LB agar plates in serial dilution, from undiluted to 10^2, 10^4 and 10^6-fold dilutions. These agar plates were then incubated at 37 °C. After 18 h of incubation, the agar plates were photographed and bacterial concentrations in $CFU{\cdot}mL^{-1}$ were calculated from the highest dilution that showed individual colonies.

RESULTS AND DISCUSSION

In recent work, our group reported the preparation of PIC particles via self-assembly of the cationic antibiotic polymyxin B (Pol-B) and the polyanion poly(styrene sulphonate) (PSS).[9] These nanoparticles displayed a formulation-dependent antimicrobial effect against *P. aeruginosa*, and were presented as an alternative delivery vehicle to the conventional use of antibiotics. Although the complexation of Pol-B is challenging due to its low net charge or multivalency (**Figure 1**),[15,16] this antibiotic was successfully assembled into PIC particles using a very high molecular weight PSS (70 kDa). The low multivalency of pentacationic Pol-B was compensated with PSS chains bearing *ca.* 340 charges on average, thus establishing a highly

multivalent network of electrostatic cross-links that stabilise these PIC particles.

Table 1. *Polyanions investigated in this work.*

Polymer	Code[a]	Mw[b]	DP[c]
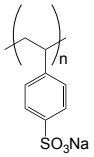	PSS_H	32,000	155
	PSS_M	17,000	82
	PSS_L	10,000	48
	PAA_H	15,000	160
	PAA_M	8,000	85
	PAA_L	1,800	19

[a] *PSS and PAA subindexes stand for high (H), medium (M) and low (L) DP.* [b] *Average Mw provided by the manufacturer.* [c] *Degree of polymerization based on the Mw.*

Since the stability of PIC particles strongly depends on the multivalency of their constituent polyelectrolytes,[1] we propose here that the complexation of Pol-B with lower DP PSS would lead to weaker polyelectrolyte complexes with potentially faster Pol-B release profiles and higher antimicrobial activities. To test this hypothesis, we investigated the assembly of PIC particles from Pol-B and PSS with average molecular weights below 70 kDa. We selected commercial PSS sources of 32 and 17 kDa to test half and a fourth of the Mw previously reported. Moreover, the shortest commercially available PSS found (10 kDa) was also tested (**Table 1**).

Pol-B was therefore mixed with each PSS in ten different proportions (*i.e.* charge ratios), denoted as [n+/n-], indicating the number of ammonium groups in Pol-B divided by the number of sulphonates in PSS present in each nanoparticle formulation. The evaluation of a range of charge ratios is critical because this parameter not only dictates the dose of antibiotic loaded inside these nanoparticles, but it can also affect their stability in solution. The range of [n+/n-] ratios explored here was selected from our previous observations with a higher DP PSS and Pol-B, which formed unstable complexes that flocculated at values of [n+/n-] ≥ 1 due to the complete neutralisation of the PSS chains by Pol-B.[9] Thus, we decided to explore [n+/n-] ratios between 1.0 and 0.1 and the resulting nanoparticle formulations were characterised by DLS and ζ-potential (**Figure 2**, **Table S1**). Colloidal particles were obtained for most of these formulations even when as little as 0.1 equivalents of Pol-B was employed. As observed for other polyelectrolytes,[17-19] we were not able to form PIC particles with any of the PSS tested at [n+/n-] ratios around equimolar range (*i.e.* 1.0, 0.9, and even 0.8 for PSS_H), which led to unstable aggregates that flocculated due to charge neutralisation (**Figure 2**).

Having identified suitable conditions for the preparation of Pol-B containing particles with as little as *ca.* 50 styrene sulphonate units, we decided next to explore the effect of changing the nature of the electrolyte. Carboxylic acids are softer electrolytes, [15,20] which will be partially protonated under physiological conditions. Softer electrolytes often result in less stable PIC particles because of their partial (de)protonation with changes in pH,[1] and as mentioned before, this reduced stability can be beneficial for the antimicrobial activity of the particles. To this end, poly(acrylic acid), a common ingredient in pharmaceutical, cosmetic and food formulations[21] was selected as a representative example. Commercially available 15 and 8 kDa PAA were chosen therefore to match the degrees of polymerisation of 32 and 17 kDa PSS, respectively (**Table 1**). Additionally, the shortest PAA commercially available (1.8 kDa) was also included in this study to evaluate the most unfavourable scenario for the preparation of PIC particles.

Like in the case of PSS, most of the formulations with PAA gave stable Pol-B containing particles (**Figure 3**). In this case, all particles prepared at equimolar [n+/n-] ratios flocculated. As expected, PAA_L gave the smallest range of successful formulations (**Figure 3**C), with flocculation observed also at 0.9 and 0.8 [n+/n-] ratios. This phase separation was possibly due to the fast shielding of such a short polymer by Pol-B, resulting in a "premature" (*i.e.* [n+/n-] < 1) neutralisation of PAA_L chains and interparticular aggregation. Moreover, PAA_L did not form nanoparticles at [n+/n-] ratios as low as 0.2 and 0.1, an effect we have also observed for other PIC particles containing small charged molecules.[22]

All particles prepared from PSS showed almost identical hydrodynamic diameters (D_H) and ζ-potentials regardless of the DP of the polymer, with average values of 192 nm (± 4%)[23] in D_H and -49.6 mV (± 6%) in charge (**Figure 2**). Similarly, PIC particles prepared from high and medium PAA showed very similar size and charge, with mean values of 147 nm (± 12%) and -34.4 mV (± 9%), respectively (**Figure 3**A,B). In contrast, PAA_L formed PIC particles with a similar size (average D_H = 149 ± 28%) but significantly higher dispersity than the other PAAs.

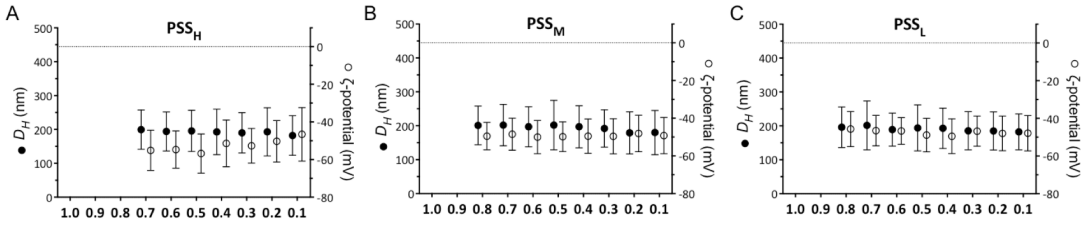

Figure 2. Hydrodynamic diameter (D_H, ●) and ζ-potential (○) of PIC particles prepared at different [n+/n-] ratios from Pol-B and PSS_H (**A**), PSS_M (**B**), and PSS_L (**C**). Each value represents the mean diameter or charge of the only size or charge population fitted by the software ± its standard deviation.

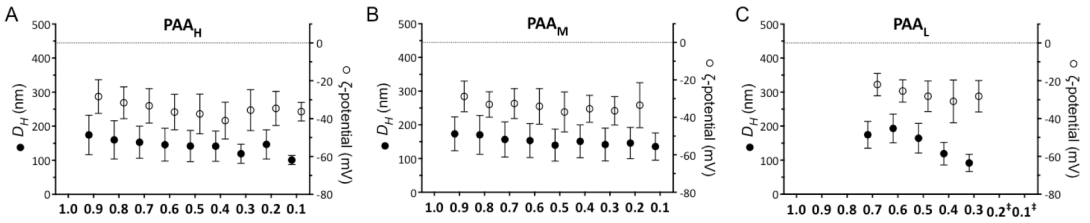

Figure 3. Hydrodynamic diameter (D_H, ●) and ζ-potential (○) of PIC particles prepared at different [n+/n-] ratios from Pol-B and PAA_H (A), PAA_M (B), and PAA_L (C). Each value represents the mean diameter or charge of the only size or charge population fitted by the software ± its standard deviation. † ζ-potential measurement polydisperse. ‡ Samples gave insufficient scattering intensities for DLS analysis.

Although overall differences were not significant, a trend towards smaller particles could be identified when lower ratios of Pol-B were used, a phenomenon also observed in the preparation of PIC particles from other small charged peptides.[22,24] Similarly, a more positive average ζ-potential of -26.9 mV (± 16%) was observed for PAA_L particles. These results for PAA_L are consistent with more loosely bound polymer chains in the PIC particles, overall yielding more polydisperse coacervates with less density of PAA chains (*i.e.* more positive ζ-potential). It is clear when comparing the results for PSS and PAA with the same DP, that the stronger affinity of PSS for Pol-B gives PIC particles with very small dispersity in size and much more negative ζ-potentials, as expected by their higher packing and hence charge density.

As explained above, PAA_L is the most challenging polyanion to complex Pol-B from the collection studied here, because it is the shortest and weakest polyelectrolyte. For this reason, PIC particles prepared from PAA_L were selected for TEM characterisation to assess whether such loose complexes would still retain morphological features of a nanoparticle. Spherical aggregates were found by TEM for particles prepared at a 0.4 [n+/n-] ratio, having a mean diameter of 67 nm (± 24%, n = 55) (**Figure 4**). The almost 50% reduction in the size of these PIC particles when analysed by TEM in comparison with their D_H in solution (119 nm ± 28%) is expected because these soft nanoparticles will collapse upon drying during sample preparation for TEM analysis.[25]

Having identified and characterised the [n+/n-] ratios that allowed the preparation of colloidal PIC particles, we then focused on assessing their stability to physiological conditions. Since small electrolytes in solution can shield the ionic networks that cross-link PIC particles, it is expected that the salts present in biological fluids can compromise the integrity of these nanoparticles. In order to test their stability, all the formulations described above were incubated in 154 mM NaCl at 37 °C and pH 7.4 to simulate physiological conditions, and DLS was monitored over time. For clarity purposes only the DLS data for PIC particles prepared at 0.7 and 0.4 [n+/n-] ratios will be discussed next, representing high and low Pol-B loading respectively. The DLS data for all the other nanoparticle formulations evaluated can be found in **Figure S1-S6**, and overall showed very similar profiles to either 0.7 or 0.4 [n+/n-] ratios, depending on the value to which they were closer. Also, regardless of the polymer used, formulations at [n+/n-] ratios of 0.1 (and also 0.2 for PAA) showed extremely poor stability to salt as expected by their low Pol-B loading and hence weak electrostatic cross-linking of the complex.

As anticipated, all PIC particles swelled in the presence of 154 mM NaCl, although this behaviour was strongly influenced by the nature of the polymer and its DP. The stability of the nanoparticles prepared from PSS was directly proportional to the DP of these polymers. Formulations containing PSS_H showed almost no changes in their autocorrelation functions (ACFs) and size distributions by DLS, with only a 2-fold increase in size after 4 hours (**Figure 5**). However, PSS_M and PSS_L experienced more pronounced swellings, increasing 7 and 20 time, respectively, their initial hydrodynamic diameters after 4 hours. Whereas PSS_H did not show any difference between [n+/n-] ratios, probably due to the strong complexation of Pol-B by this polymer, PSS_M and PSS_L formed more stable complexes at a [n+/n-] ratio of 0.4 than 0.7. This is evidenced by the loss of the characteristic sigmoidal profile in the ACF curves of these nanoparticles (*e.g.* **Figure 5**B *vs* E), which can be attributed to these particles breaking down into amorphous debris, as suggested by the smaller-size population found in their intensity plots after 4 hours (**Figure 5**B,C).

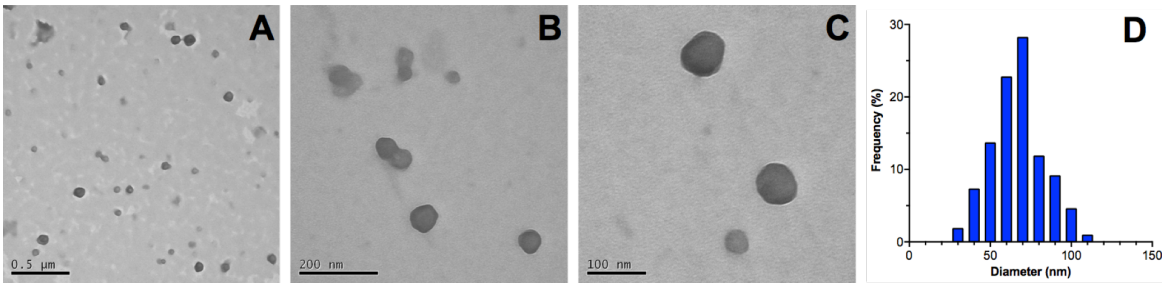

Figure 4. TEM micrographs of PIC particles prepared from Pol-B and PAA_L at a [n+/n-] ratio of 0.4 (A-C) and the size distribution of these nanoparticles found by TEM (D).

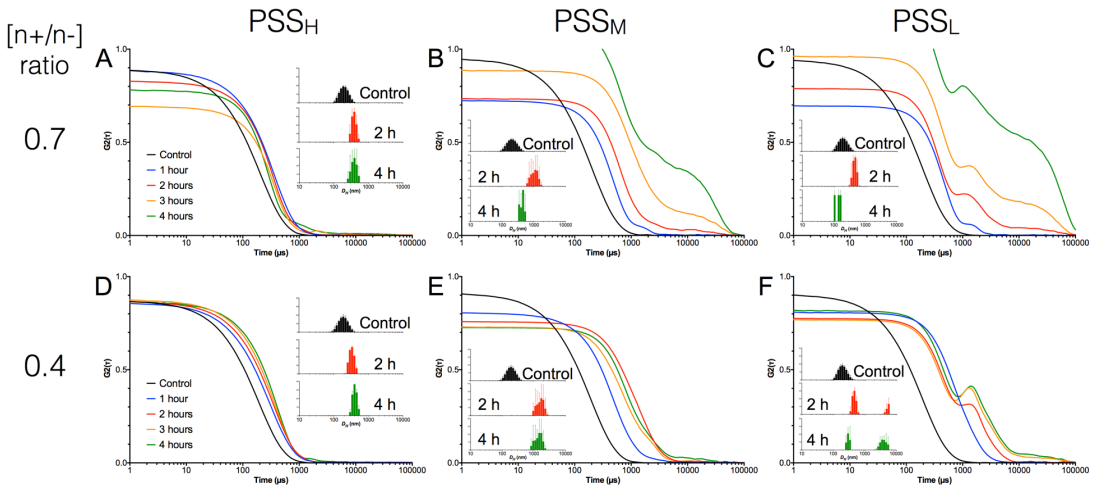

Figure 5. DLS autocorrelation function (ACF) curves and representative size-intensity plots (inset) of PIC particles prepared from PSS_H (A,D), PSS_M (B,E) and PSS_L (C,F) at [n+/n-] ratios of 0.7 (A-C) and 0.4 (D-E) in the absence (control) and presence of 154 mM NaCl (1-4 hours).

Unlike PSS, PAA did not show a clear relationship between its DP and the physiological stability of PIC particles. Surprisingly, PAA_H formulations had almost identical DLS profiles to PAA_L despite this polymer being 8 times smaller (**Figure 6**). The PIC particles prepared from these two PAAs increased up to 10-fold in size after one hour of incubation in 154 mM NaCl and remained unchanged for the rest of the experiments. However, PAA_M led to nanoparticles with less tolerance to salt, as evidenced by their ACF curves with intercepts above 1 and inconsistent size-intensity fits (**Figure 6**B,E). These results suggest that these particles were breaking apart and the Brownian motion of their debris could not be interpreted by the DLS software.

In order to analyse the effect of polyelectrolyte nature on the stability of the particles, particles prepared using polymers with matching DPs were compared. Overall, the data suggested that PSS containing particles were less likely to swell and were more stable under the conditions tested. For instance, formulations prepared with PSS_H at a 0.2 [n+/n-] ratio were stable enough to produce "good" DLS ACF curves, even after 4 hours of incubation (**Figure S1**). This was not the case for PAA_H at this [n+/n-] ratio for which particles could not be reliably measured after 1 hour (**Figure S4**). Similar trends could be observed when comparing the formulations made from polymers with the medium DP (**Figure S2** and **Figure S5**), although in this case more formulations were unstable after incubation under these simulated physiological conditions.

Interestingly, PIC particles prepared from PAA_L, despite forming particles over a smaller range of formulations, resulted in quite stable particles under physiological conditions, with 4 out of 5 formulations giving ACFs curves that could be fitted even after 4 hours of incubation. This was not the case for instance for PSS_L, for which none of the formulations were stable. This result highlights the key role the

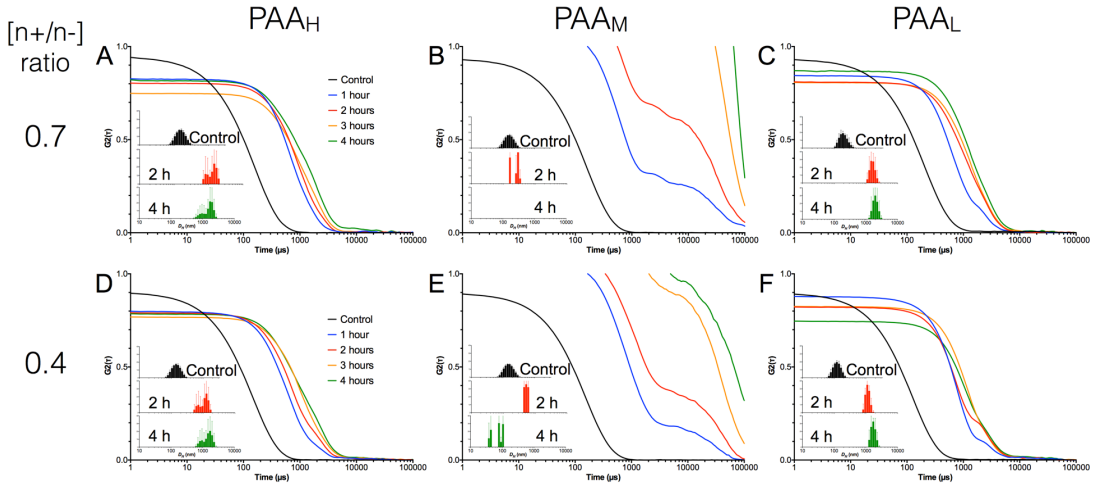

Figure 6. DLS autocorrelation function (ACF) curves and representative size-intensity plots (inset) of PIC particles prepared from PAA_H (A,D), PAA_M (B,E) and PAA_L (C,F) at [n+/n-] ratios of 0.7 (A-C) and 0.4 (D-E) in the absence (control) and presence of 154 mM NaCl (1-4 hours).

structure of the complexing polymer plays on the behaviour of PIC particles, in this particular case, possibly generating complexes with higher flexibility that results in a more efficient entanglement with Pol-B.

Having established the stability under simulated physiological conditions of the different formulations prepared, we then evaluated the antimicrobial activity of these nanoparticles against *P. aeruginosa*.[9] Experiments were focused on particles prepared at 0.7 and 0.4 [n+/n-] ratios, because the stability under physiological conditions demonstrated that these formulations were representative examples of the whole series. First, we monitored the optical density at 600 nm (OD_{600}) of *P. aeruginosa* cultures in the absence and presence of different PIC particle formulations, and their different components. This is a routine technique used in microbiology that correlates any increase in the turbidity of a sample to bacterial growth.[26] As expected, the growth of *P. aeruginosa* (●) was not inhibited by the presence of the polymers (PSS_L and PAA_L shown as representative examples) but incubation with Pol-B at the concentrations found in PIC particles at 0.7 and 0.4 [n+/n-] ratios (87.5 and 50 μM, respectively) completely inhibited the growth of this bacterium for the duration of this experiment (**Figure 7**A). Remarkably, all PIC particles prepared from PAA showed complete inhibition of growth regardless of the DP or [n+/n-] ratio tested (**Figure 7**B). We believe this is a consequence of the higher instability of the particles prepared with this weaker polyelectrolyte in biological media, as suggested by the experiments performed under simulated physiological conditions (**Figure 6**). We think PAA containing particles will also swell more in the growth media used for these experiments, leading to particles breaking apart and a potential rapid release of the antimicrobial. This way, all nanoparticles prepared from PAA showed the same antimicrobial effect as Pol-B alone (**Figure 7**A).

On the other hand, PIC particles prepared with PSS displayed different antimicrobial effects depending on the polymer's DP and Pol-B loading. Like in our previous work,[9] we observed an initial increase in the OD_{600} of the culture in the presence of these particles, an increase that was mainly dependent on the Pol-B content (**Figure 8**A vs **Figure 8**B). This increase in OD_{600} is attributed to swelling when the particles are exposed to the biological medium used in this assay, as observed with experiments performed in the absence of bacteria (**Figure 8**C). Formulations at a 0.7 [n+/n-] ratio increased the turbidity of the media much more dramatically than their analogues at 0.4.

Moreover, particles prepared with PSS_H showed a steady increase in OD_{600}, suggesting that these particles were swelling but remained stable under assay conditions. Particles prepared with PSS_M and PSS_L however showed a bigger increase in OD_{600}, but both suspensions quickly lost their turbidity, suggesting that particles were eventually breaking apart and releasing the antimicrobial. This data was in agreement with the stability observed under simulated physiological conditions (**Figure 5**), with formulations prepared with PSS_H giving more stable particles that swelled less. A similar effect was observed for PAA containing particles (**Figure S7**), although in this case formulations prepared with PAA_H resulted in similar if not higher increases in OD_{600}.

The swelling and stability in this media of the PSS containing particles also had an effect in their antimicrobial activity. For instance, nanoparticles prepared with PSS_L at a 0.7 [n+/n-] ratio, which could be expected to release most of the antibiotic after 6 hours of incubation (**Figure 8**C), inhibited the growth of *P. aeruginosa* for 24 hours (**Figure 8**D). However, the particles prepared with PSS_H and PSS_M at this [n+/n-] ratio did not have such as strong antimicrobial effect and after 13 hours growth of the pathogen was evident again (**Figure 8**A). A similar effect was observed for formulations prepared at a 0.4 [n+/n-] ratio, with particles prepared with PSS_L showing the longest inhibition effect (**Figure 8**B).

To facilitate the visual comparison of these antimicrobial results, representative data from PSS containing particles were normalised against the optical density observed at the beginning of the experiment and plotted as a function of the polymer and formulation used (**Figure 8**D). This way, we could clearly observe that only formulations prepared with PSS_L at a 0.7 [n+/n-] ratio showed a prolonged antimicrobial effect, with the turbidity at all times below that observed at the beginning of the experiment. We could also see that reducing the amount of antimicrobial in this case had a detrimental effect in the antimicrobial activity of the particles, with formulations prepared with PSS_L at a 0.4 [n+/n-] ratio having already recovered the baseline turbidity after 20 hours of incubation. This was the case for the other PSS used, with formulations prepared at a 0.7 [n+/n-] ratio having a higher antimicrobial effect than those prepared at a 0.4 [n+/n-] ratio. However, no significant differences were observed in the growth when formulations for PSS_H and PSS_M were compared across the same [n+/n-] ratio.

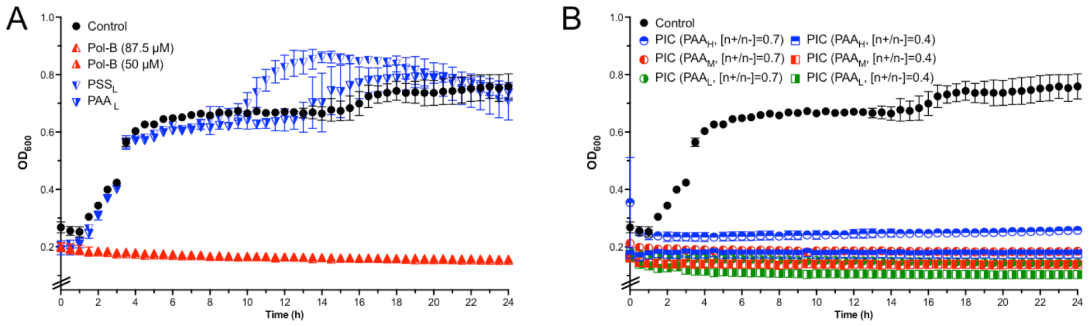

Figure 7. Change in optical density at 600 nm (OD_{600}) for *P. aeruginosa* cultures in the absence (●) and presence of Pol-B (▲ and ▲), PSS_L (▼), PAA_L (▼) (A), and PAA containing PIC particles prepared at 0.7 or 0.4 [n+/n-] ratios (B).

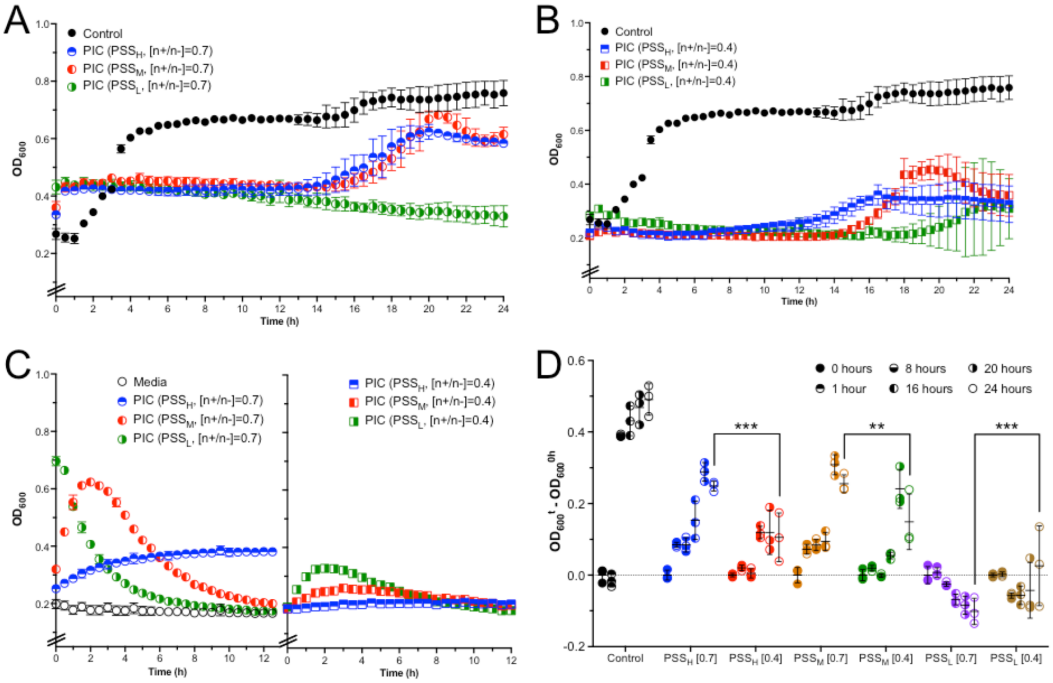

Figure 8. Change in optical density at 600 nm (OD_{600}) for *P. aeruginosa* cultures in the absence (●) and presence of PSS containing PIC particles prepared at 0.7 (A) or 0.4 (B) [n+/n-] ratios. C) Change in OD_{600} for PSS containing PIC particles suspended 1:1 LB:HEPES media in the absence of bacteria. D) Representative relative changes in OD_{600} from (A) and (B). *** $p < 0.001$, ** $p < 0.01$ (two-way ANOVA, CI = 95%). Error bars represent the standard deviation, $n = 3$.

Samples from these growth assays were collected after 24 hours of incubation and spotted on agar plates to quantify the number of viable bacteria remaining at this stage.[26] Several dilutions were spotted on the agar plates to identify suitable conditions for colony counting. *P. aeruginosa* was able to grow under these conditions and neither PSS_L or PAA_L showed any effect on this growth (**Figure 9** and **Figure S8**). Both concentrations of Pol-B used to prepare the nanoparticles completely inhibited the growth of *P. aeruginosa* (control), as expected. Interestingly, all formulations displayed some degree of antimicrobial effect as evidenced by the decrease in at least to two orders of magnitude in the number of viable bacterial colonies found in these samples. Nanoparticles prepared with PSS_L at a 0.7 [n+/n-] ratio showed a remarkable change in the number of CFU/mL of over 6 orders of magnitude (**Figure 9**B), in agreement with the turbidity assays that suggested that this was the most active formulation (**Figure 8**D). In addition, no viable colonies were observed for any of the formulations prepared for PAA (**Figure S8**), supporting the results obtained using turbidimetry assays (**Figure 7**B).

CONCLUSIONS

We have successfully prepared and characterised Pol-B containing PIC particles using six different PAA and PSS selected across a wide range of degrees of polymerisation. We have assessed the physiological stability of these nanoparticles and their antimicrobial activity against *P. aeruginosa*, an opportunistic pathogen currently treated with Pol-B. Our results indicate that nanoparticles prepared with the stronger polyelectrolyte PSS have a higher tolerance to salt than particles containing PAA of the same DP. Similarly, polymers with smaller DPs resulted in particles that swelled more under simulated physiological conditions. Our methodology allowed us to tune the antimicrobial activity of Pol-B depending on the nature of the polyanion and the [n+/n-] ratio used. In this regard, all nanoparticles prepared from PAA inhibited *P. aeruginosa*'s growth and lead to non-viable cultures of this pathogen. However, when particles were prepared with PSS, those with the shortest polyelectrolyte showed the highest antimicrobial activity. Also, the antimicrobial activity of the particles prepared with PSS of low degree of polymerisation was dependent of the [n+/n-] ratio, an effect not found in formulations prepared from longer polymers. We believe our results highlight the importance of selecting a correct polyelectrolyte and formulation in order to tune the stability and antimicrobial activity, and should be of value in the future development of these materials as a platform for the delivery of last-resort antimicrobials.

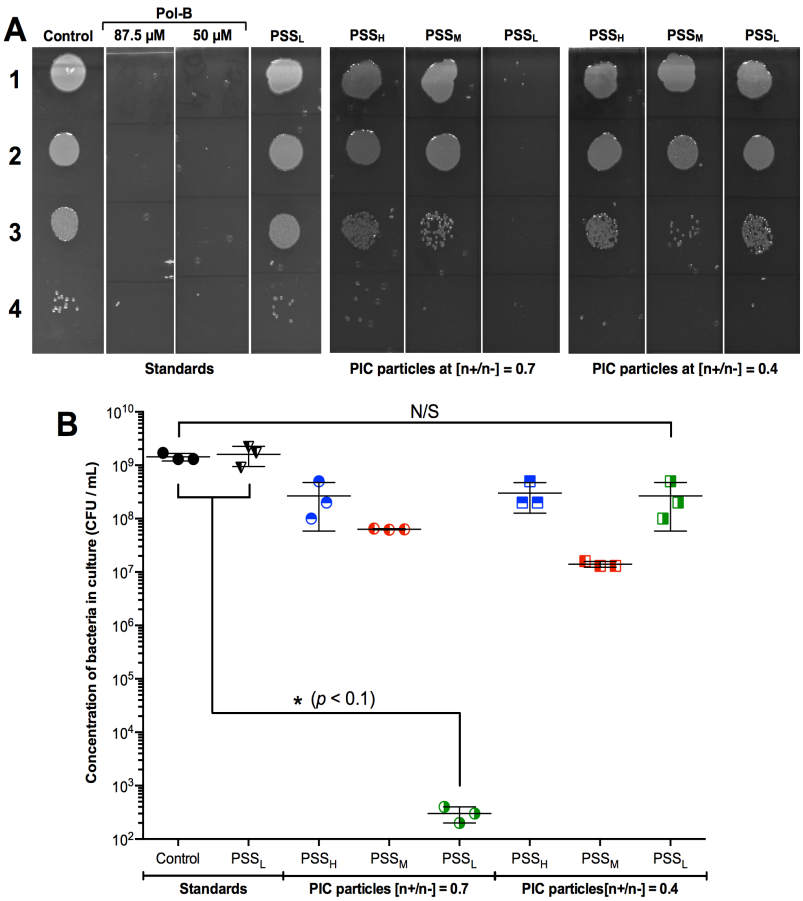

Figure 9. (A) Representative agar plates used to evaluate antimicrobial activity of PIC particles prepared from PSS and Pol-B. Lane 1: No dilution, lane 2: 10^2-fold dilution, lane 3: 10^4-fold dilution, and lane 4: 10^6-fold dilution. (B) CFU/mL of *P. aeruginosa* in the absence (control) and presence of PIC particles prepared from different PSS sources at different [n+/n-] ratios, calculated from the colonies found in the agar plates (one-way ANOVA, CI = 95%). Error bars represent the standard deviation, n = 3.

Acknowledgements

FFT thanks the University of Birmingham for the John Evans Fellowship. AMK thanks the University of Birmingham for a Birmingham Fellowship. FFT and AMK thank the Wellcome Trust (177ISSFPP) for funding and FFT thanks the Engineering and Physical Sciences Research Council (EPSRC) (EP/N508755/1) for funding. II thanks the University of Birmingham and the John Evans Fellowship for a PhD studentship. The authors acknowledge support from the Centre for Chemical and Materials Analysis in the School of Chemistry at the University of Birmingham. The authors thank Dr Marie-Christine Jones and Dr Hannene Ali-Boucetta (School of Pharmacy, UoB) for the access to the DLS, and Nicolas Perez for useful discussions and help with the microbiology assays. The authors also thank Prof. Suzanne M. J. Fleiszig for the kind donation of *P. aeruginosa* strain PAO1V.[27]

AUTHOR CONTRIBUTIONS

All authors contributed to the experimental set-up and discussed the results. II and FFT designed the nanoparticle synthesis and characterisation, and II, FFT and AMK designed the microbiological assays. II carried out all experimental work. FFT and AMK secured funding. II and FFT analysed the data and wrote the paper, with all other authors contributing to the final version of the manuscript.

REFERENCES

1 I. Insua, A. Wilkinson and F. Fernandez-Trillo, *Eur. Polym. J.*, 2016, **81**, 198–215.

2 T. Hashimoto and T. Yamaoka, in *Non-viral Gene Therapy*, Springer-Verlag, Tokyo, 2005, pp. 35–50.

3 E. Wagner, in *Nonviral Vectors for Gene Therapy Lipid- and Polymer-based Gene Transfer*, eds. L. Huang, D. Liu and E. Wagner, Academic Press, 2014, vol. 88, pp. 231–261.

4 A. B. Kayitmazer, D. Seeman, B. B. Minsky, P. L. Dubin and Y. Xu, *Soft Matter*, 2013, **9**, 2553–2583.

5 A. W. Du and M. H. Stenzel, *Biomacromolecules*, 2014, **15**, 1097–1114.

6 R. E. W. Hancock and H.-G. Sahl, *Nat. Biotechnol.*, 2006, **24**, 1551–1557.

7 J. G. Hurdle, A. J. O'Neill, I. Chopra and R. E. Lee, *Nat. Rev. Microbiol.*, 2011, **9**, 62–75.

8 A. T. Y. Yeung, S. L. Gellatly and R. E. W. Hancock, *Cell. Mol. Life Sci.*, 2011, **68**, 2161–2176.

9 I. Insua, S. Majok, A. F. A. Peacock, A. M. Krachler and F. Fernandez-Trillo, *Eur. Polym. J.*, 2016, doi: 10.1016–

j.eurpolymj.2016.08.023.
10 A. H. A. Mohamed-Ahmed, K. A. Les, K. Seifert, S. L. Croft and S. J. Brocchini, *Mol. Pharmaceutics*, 2013, **10**, 940–950.
11 K. A. Les, A. H. A. Mohamed-Ahmed, S. Balan, J.-W. Choi, D. Martin, V. Yardley, K. Powell, A. Godwin and S. J. Brocchini, *Polym. Chem.*, 2014, **5**, 1037–1048.
12 K. L. Niece, A. D. Vaughan and D. I. Devore, *J. Biomed. Mater. Res., Part A*, 2013, **101**, 2548–2558.
13 P. Urbán, J. J. Valle-Delgado, E. Moles, J. Marques, C. Díez and X. Fernàndez-Busquets, *Curr. Drug Targets*, 2012, **13**, 1158–1172.
14 A. Carmona-Ribeiro and L. de Melo Carrasco, *Int. J. Mol. Sci.*, 2014, **15**, 18040–18083.
15 F. Oosawa, *Polyelectrolytes*, Marcel Dekker, New York, 1971.
16 Y. Zhang, E. Yildirim, H. S. Antila, L. D. Valenzuela, M. Sammalkorpi and J. L. Lutkenhaus, *Soft Matter*, 2015, **11**, 7392–7401.
17 H. Dautzenberg and W. Jaeger, *Macromol. Chem. Phys.*, 2002, **203**, 2095–2102.
18 A. Drogoz, L. David, C. Rochas, A. Domard and T. Delair, *Langmuir*, 2007, **23**, 10950–10958.
19 X. Feng, R. Pelton, M. Leduc and S. Champ, *Langmuir*, 2007, **23**, 2970–2976.
20 M. Müller, Ed., *Polyelectrolyte Complexes in the Dispersed and Solid State I*, Springer Berlin Heidelberg, Berlin, Heidelberg, 2014, vol. 255.
21 U. S. Food & Administration, *Code of Federal Regulations Title 21*, vol. 3.
22 I. Insua, E. Liamas, Z. Zhang, A. F. A. Peacock, A. M. Krachler and F. Fernandez-Trillo, *Polym. Chem.*, 2016, **7**, 2684–2690.
23 The dispersion from the mean D_H and ζ-potential values indicated in brackets represent the coefficient of variation (%).
24 C. Su, M. Zhao, Z. Zhu, J. Zhou, H. Wen, Y. Yin, Y. Deng, D. Qiu, B. Li and D. Liang, *Macromolecules*, 2015, **48**, 756–763.
25 H. Friedrich, P. M. Frederik, G. de With and N. A. J. M. Sommerdijk, *Angew. Chem., Int. Ed. Engl.*, 2010.
26 *Prescotts Principles of Microbiology*, McGraw-Hill Higher Education.
27 B. A. Cowell, S. S. Twining, J. A. Hobden, M. S. F. Kwong and S. M. J. Fleiszig, *Microbiology (Reading, U. K.)*, 2003, **149**, 2291–2299.

Effect of polyelectrolyte strength and degree of polymerisation on the formation, stability and activity of antimicrobial polyion complex (PIC) particles carrying polymyxin B

Ignacio Insua,[a,c] Anna F. A. Peacock,[a] Anne Marie Krachler,[b,c,§] and Francisco Fernandez-Trillo*[a,]

[a]*School of Chemistry,* [b]*School of Biosciences and* [c]*Institute of Microbiology and Infection, University of Birmingham, B15 2TT Birmingham, UK*

† Current address: Department of Microbiology and Molecular Genetics, University of Texas McGovern Medical School at Houston, Houston, TX, 77030, USA.

Electronic Supplementary Information

Table of Contents

1. Characterisation of PIC particles: size and charge

Table S1. Hydrodynamic diameter (D_H) and ζ-potential of PIC particles prepared from six different polymers in combination with Pol-B at ten different [n+/n-] ratios.

Polymer	[n+/n-] ratio	D_H ± SD (nm) [a]	PdI [b]	ζ-potential ± SD (mV) [a]	Notes
PSS_H	1.0	-	-	-	Flocculation
	0.9	-	-	-	Flocculation
	0.8	-	-	-	Flocculation
	0.7	199 ± 58	0.08	-55.1 ± 10.7	-
	0.6	194 ± 58	0.09	-54.7 ± 9.9	-
	0.5	196 ± 61	0.10	-56.8 ± 10.4	-
	0.4	193 ± 67	0.12	-51.4 ± 12.4	-
	0.3	190 ± 60	0.10	-52.7 ± 9.2	-
	0.2	193 ± 71	0.14	-50.3 ± 11.0	-
	0.1	182 ± 58	0.10	-46.6 ± 14.2	-
PSS_M	1.0	-	-	-	Flocculation
	0.9	-	-	-	Flocculation
	0.8	201 ± 57	0.08	-49.5 ± 7.3	-
	0.7	202 ± 61	0.09	-48.5 ± 8.5	-
	0.6	197 ± 59	0.09	-50.0 ± 8.8	-
	0.5	202 ± 73	0.13	-49.8 ± 7.9	-
	0.4	197 ± 62	0.10	-49.5 ± 9.1	-
	0.3	192 ± 55	0.08	-49.6 ± 9.3	-
	0.2	179 ± 62	0.12	-48.1 ± 9.7	-
	0.1	180 ± 65	0.13	-49.2 ± 9.6	-
PSS_L	1.0	-	-	-	Flocculation
	0.9	-	-	-	Flocculation
	0.8	196 ± 60	0.09	-45.7 ± 9.3	-
	0.7	201 ± 72	0.13	-46.5 ± 8.1	-
	0.6	189 ± 49	0.07	-46.7 ± 7.1	-
	0.5	194 ± 68	0.12	-48.9 ± 8.9	-
	0.4	193 ± 60	0.10	-49.5 ± 9.2	-
	0.3	186 ± 56	0.09	-46.8 ± 8.0	-
	0.2	185 ± 56	0.09	-48.0 ± 9.2	-
	0.1	182 ± 53	0.08	-47.9 ± 9.4	-
PAA_H	1.0	-	-	-	Flocculation
	0.9	174 ± 58	0.11	-28.3 ± 8.9	-
	0.8	160 ± 56	0.12	-31.6 ± 8.4	-
	0.7	153 ± 47	0.09	-33.2 ± 9.1	-
	0.6	146 ± 48	0.11	-36.5 ± 9.4	-
	0.5	142 ± 46	0.10	-37.5 ± 10.5	-
	0.4	142 ± 44	0.10	-41.0 ± 9.7	-
	0.3	119 ± 28	0.06	-35.5 ± 10.8	-
	0.2	147 ± 43	0.09	-34.6 ± 9.0	-
	0.1	101 ± 13	0.02	-36.3 ± 4.9	-
PAA_M	1.0	-	-	-	Flocculation
	0.9	173 ± 50	0.08	-28.8 ± 8.2	-
	0.8	170 ± 58	0.11	-33.1 ± 6.8	-
	0.7	157 ± 52	0.11	-32.6 ± 8.0	-
	0.6	153 ± 50	0.11	-34.1 ± 9.5	-
	0.5	140 ± 47	0.11	-37.1 ± 10.7	-
	0.4	151 ± 49	0.10	-35.4 ± 7.2	-
	0.3	142 ± 49	0.12	-36.5 ± 7.6	-
	0.2	146 ± 46	0.10	-33.5 ± 12.0	-
	0.1	136 ± 40	0.09	Not characterised	Poor signal
PAA_L	1.0	-	-	-	Flocculation
	0.9	-	-	-	Flocculation
	0.8	-	-	-	Flocculation
	0.7	175 ± 39	0.05	-22.0 ± 5.9	-
	0.6	193 ± 42	0.05	-25.4 ± 5.9	-
	0.5	164 ± 44	0.07	-28.2 ± 8.1	-
	0.4	119 ± 33	0.08	-30.9 ± 11.3	-
	0.3	92 ± 25	0.08	-28.2 ± 8.3	-
	0.2	-	-	-	Poor signal
	0.1	-	-	-	Poor signal

[a] SD indicates the standard deviation found for the only size or charge population fitted by the software.
[b] Polydispersity Index (PdI) calculated using the formula: $PdI = (SD/D_H)^2$.

2. Stability of PIC particles under simulated physiological conditions

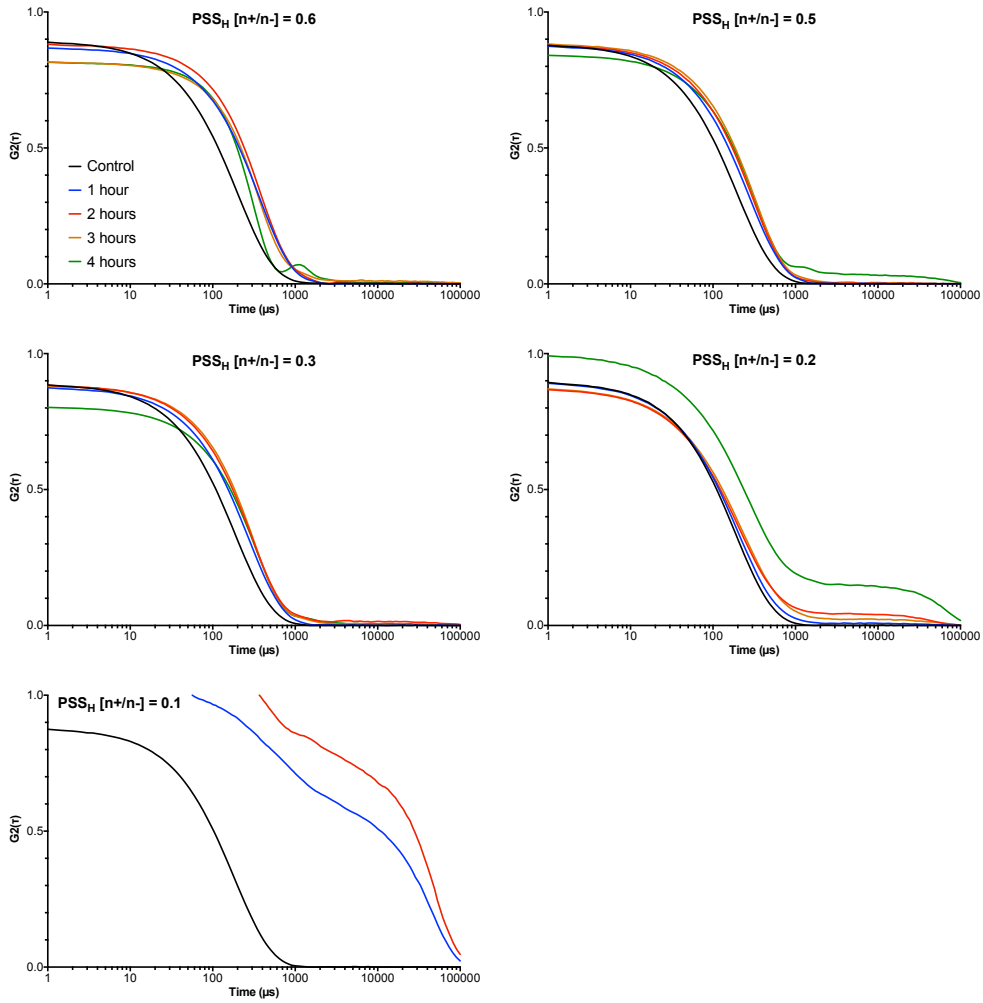

Figure S1. DLS autocorrelation function (ACF) curves of PIC particles prepared from PSS_H at different [n+/n-] ratios in the absence (control) and presence of 154 mM NaCl over time (1-4 hours).

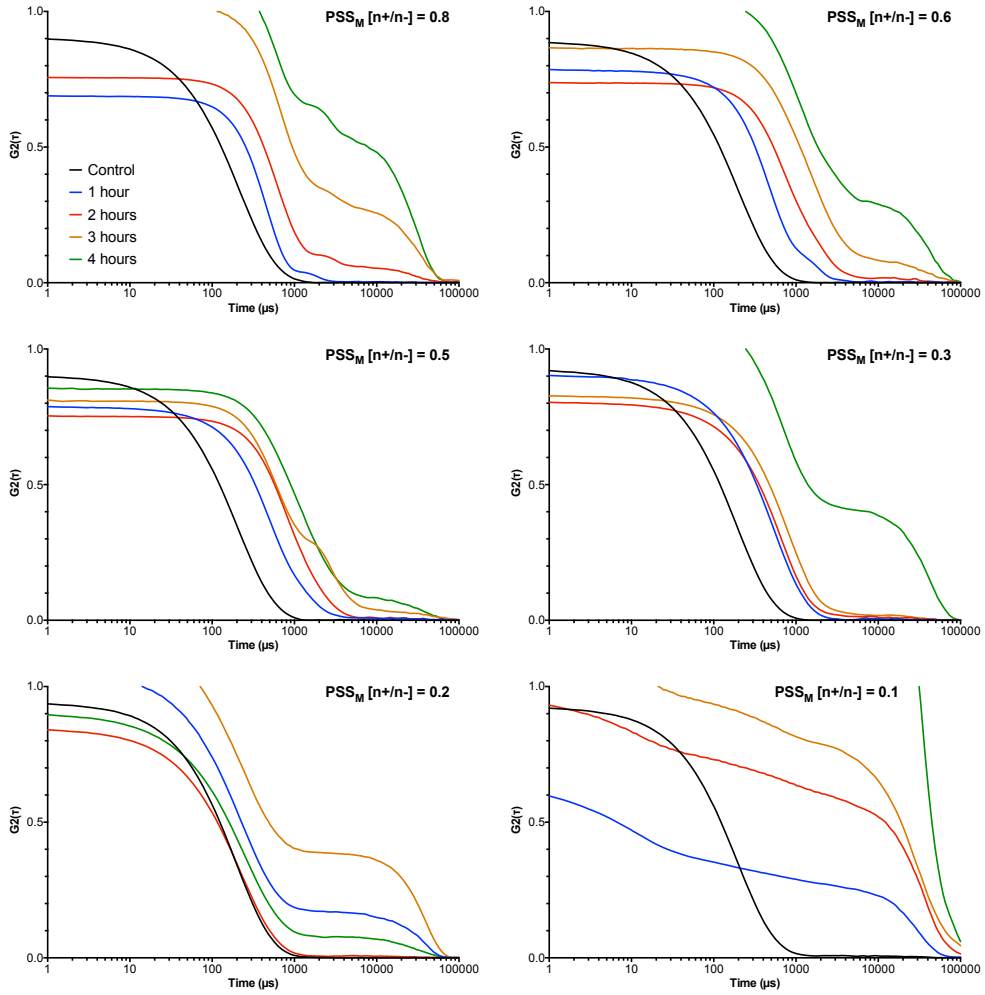

Figure S2. DLS autocorrelation function (ACF) curves of PIC particles prepared from PSS_M at different [n+/n-] ratios in the absence (control) and presence of 154 mM NaCl over time (1-4 hours).

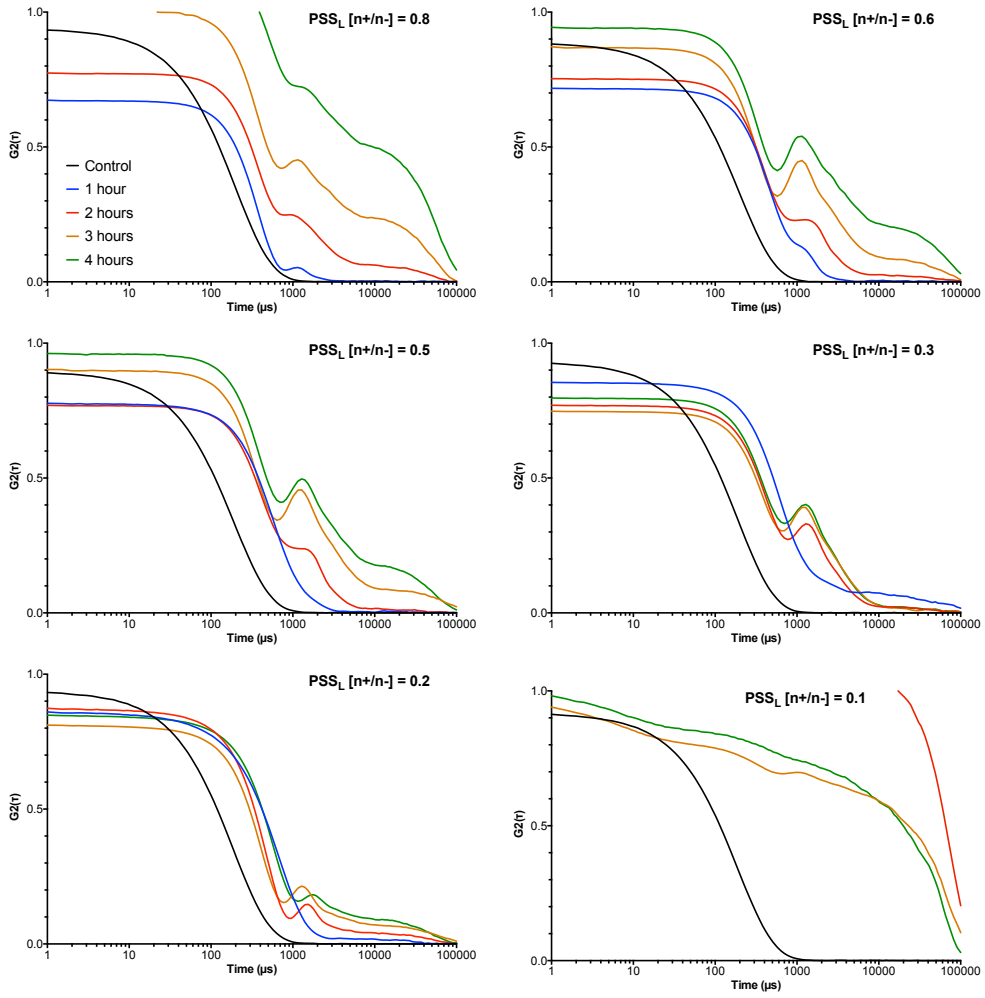

Figure S3. DLS autocorrelation function (ACF) curves of PIC particles prepared from PSS_L at different [n+/n-] ratios in the absence (control) and presence of 154 mM NaCl over time (1-4 hours).

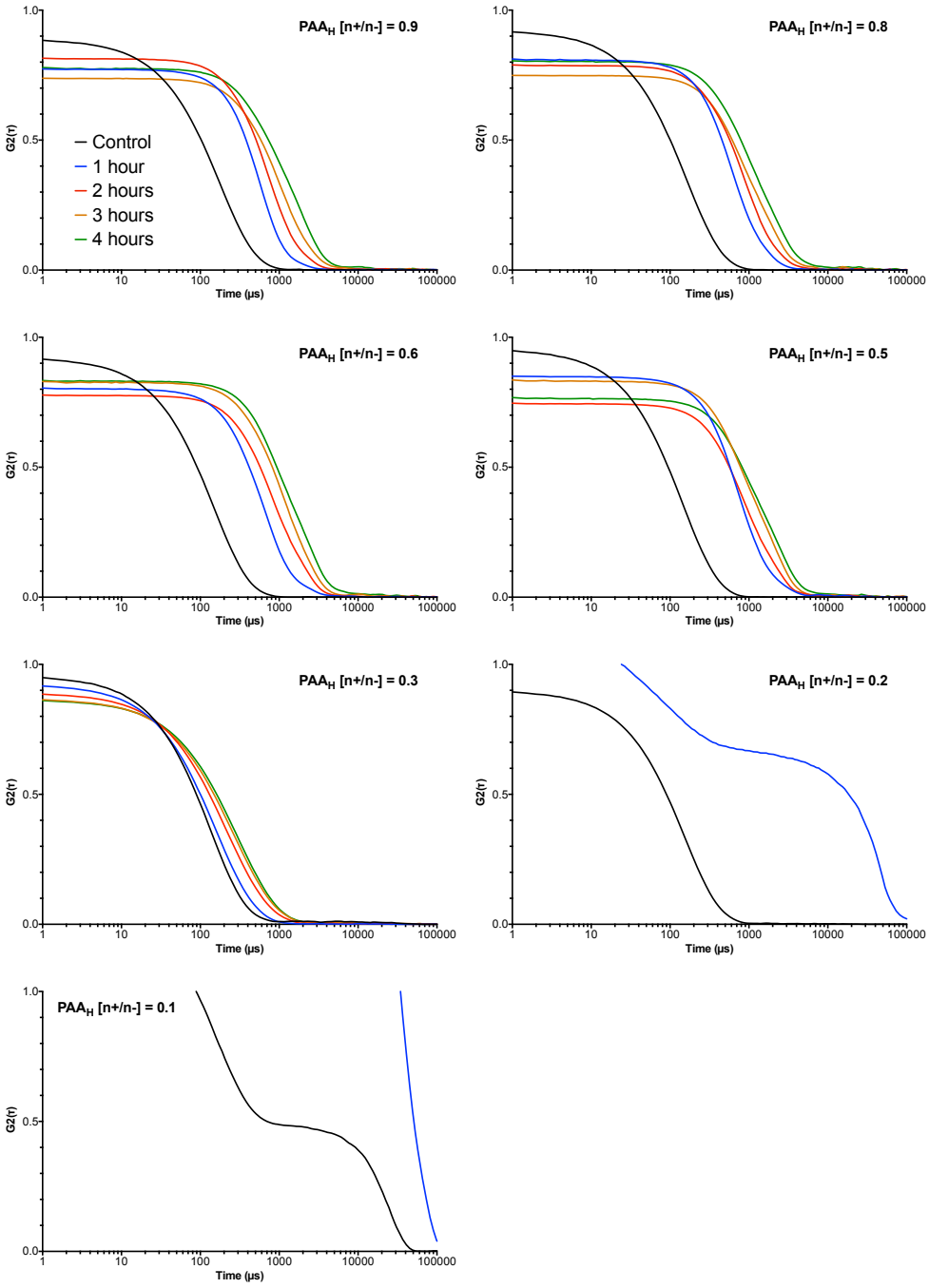

Figure S4. DLS autocorrelation function (ACF) curves of PIC particles prepared from PAA_H at different [n+/n-] ratios in the absence (control) and presence of 154 mM NaCl over time (1-4 hours).

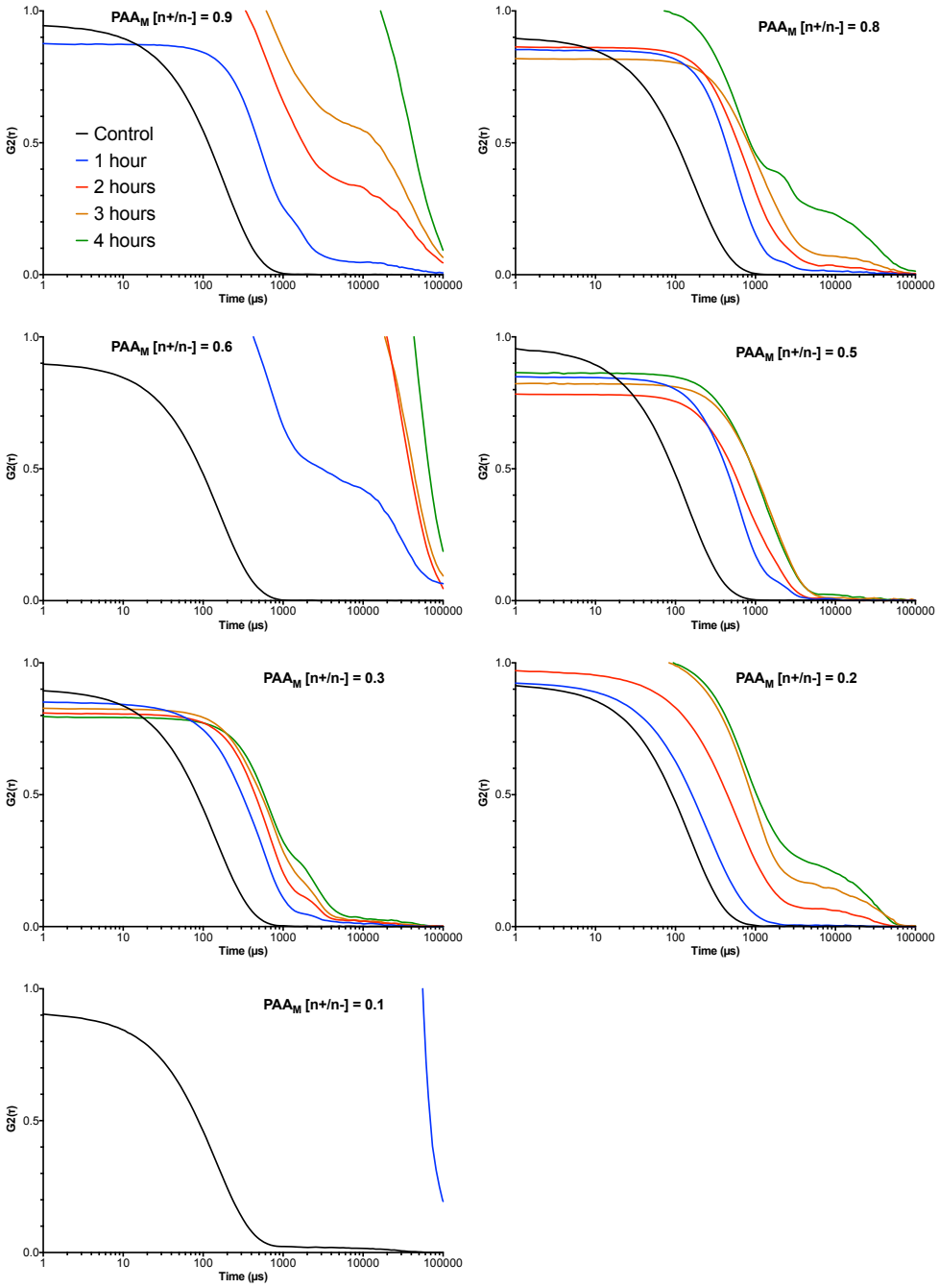

Figure S5. DLS autocorrelation function (ACF) curves of PIC particles prepared from PAA$_M$ at different [n+/n-] ratios in the absence (control) and presence of 154 mM NaCl over time (1-4 hours).

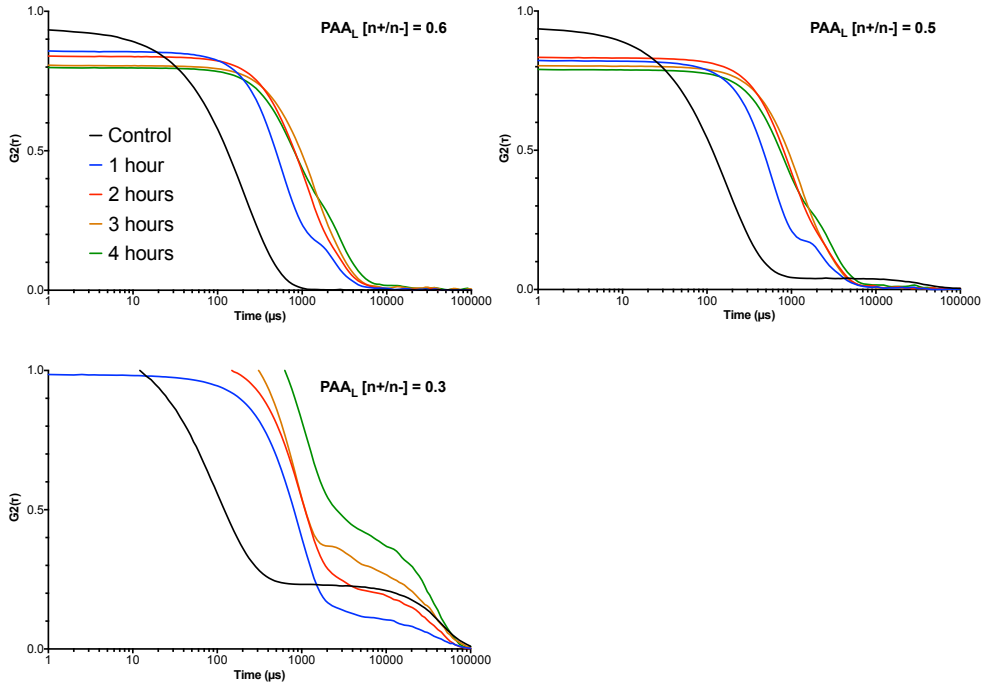

Figure S6. DLS autocorrelation function (ACF) curves of PIC particles prepared from PAA_L at different [n+/n-] ratios in the absence (control) and presence of 154 mM NaCl over time (1-4 hours).

3. Antimicrobial activity of PIC particles

3.1. Growth curves

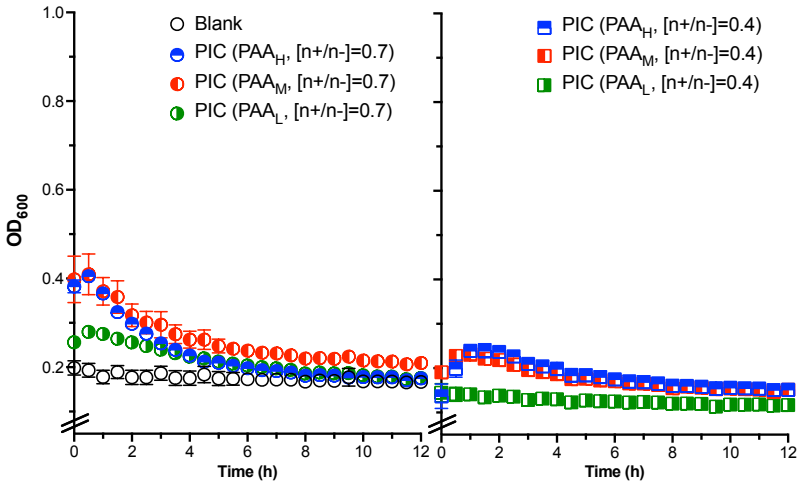

Figure S7. OD_{600} of PAA PIC particles in the absence of bacteria. Error bars represent the standard deviation, *n* = 3.

3.2. CFU counting

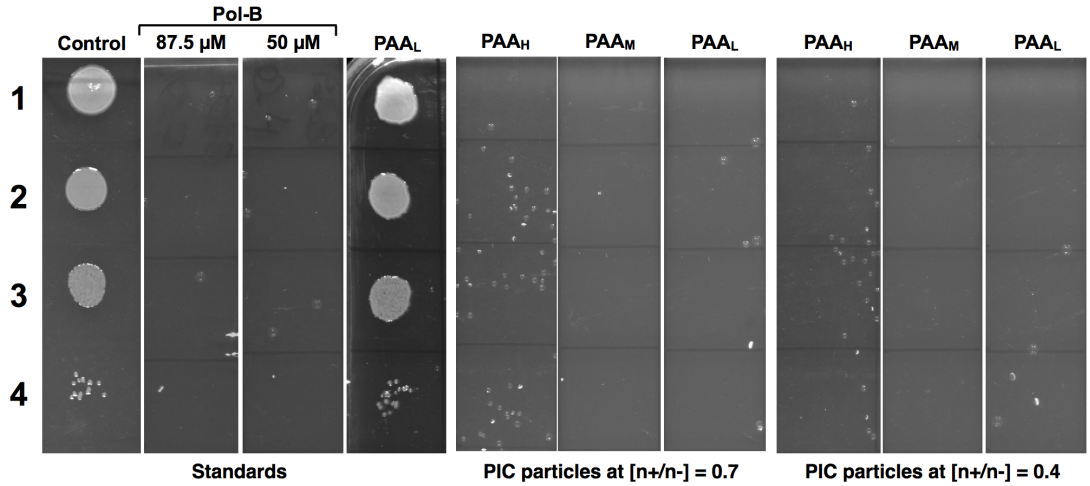

Figure S8. Representative agar plates used to evaluate antimicrobial activity of PIC particles prepared from PAA and Pol-B. Lane 1: No dilution, lane 2: 10^2-fold dilution, lane 3: 10^4-fold dilution, and lane 4: 10^6-fold dilution.

Conclusions

The overall goal of this Thesis was the study of PIC nanoparticles as targeted and passive drug delivery vehicles for antimicrobial agents. Enzyme-responsive PIC nanoparticles were developed from the antimicrobial polymer poly(ethylene imine) (PEI) in combination with peptides degradable by a bacterial protease (LasB), thus aiming to direct the degradation of these nanoparticles, and hence drug release, to bacterial niches (Chapter 2). These nanoparticles specifically degraded in the presence of LasB and not a human protease, also displaying specific antimicrobial effects towards virulent bacterial strains that produced LasB. These enzyme-responsive PIC nanoparticles showed promising properties as targeted antimicrobial agents, but their poor stability in saline media compromised their biological application. Attempts to improve the stability of these PIC nanoparticles involved the modification of the LasB-responsive peptides (*i.e*. anionic component of the nanoparticles) to include more charged and cross-linking residues (Chapter 3). These modifications allowed to access new PIC nanoparticle formulations with excellent salt compatibility, but these highly-stable complexes lost their susceptibility to LasB degradation and the resulting bacteria-targeted properties. At this point, and to improve the antimicrobial activity of the materials under development, the weak antimicrobial PEI was replaced for the more potent and FDA-approved antimicrobial peptide Polymyxin B (Pol-B). Unfortunately, the low multivalency of both Pol-B and the LasB-responsive peptides was unable to drive the assembly of these polyelectrolytes into PIC nanoparticles. Alternatively, we studied the formulation of Pol-B with the highly multivalent polyelectrolyte poly(styrene sulphonate) (PSS), which allowed the preparation of non-targeted PIC nanoparticles for passive drug release with tunable antimicrobial activities as a function of their charge ratio (Chapter 4). Finally, we evaluated the impact of the polyelectrolyte assembled with Pol-B on the stability and antimicrobial properties of the resulting PIC nanoparticles (Chapter 5). It was found that the strength (*i.e*. pKa) and multivalency (*i.e*. degree of polymerisation) of the complexing polyelectrolyte is critical to control the antimicrobial activity of Pol-B when

formulated into PIC nanoparticles, leading to stronger antimicrobial effects when using weaker and less multivalent polyelectrolytes.

The work presented in this Thesis has expanded the previous knowledge about PIC nanoparticles with regards to their design, assembly, characterisation, stability and application in antimicrobial therapy. New polyelectrolytes, analysis techniques, experimental setups and stimuli-responsive properties have been applied here for the first time to PIC nanoparticles. The key learnings derived from this Thesis are summarised below:

1) **PIC nanoparticles can be engineered to degrade in the presence of target enzymes**. The enzyme-responsive design of PIC nanoparticles has been demonstrated here for the first time. Our results cannot only guide the development of new bacteria-targeted antimicrobial agents, but also other biomedical tools for virtually any pathology mediated by enzymes.
2) **Multivalency is the most important factor that regulates the formation, stability and activity of PIC nanoparticles**. This conclusion is supported by: A) The inability of short LasB-responsive peptides and Pol-B to form PIC nanoparticles, even in the presence of cross-linking groups in the peptides. B) The requirement of a macromolecular and highly multivalent polyelectrolyte in all PIC nanoparticles presented in this Thesis to drive their assembly. C) Consistent trends in the saline stability of PIC nanoparticles with polyelectrolytes of very different nature – less multivalent polyelectrolytes leading to poorer stability –, as evidenced in Chapters 3 and 5 (see point 4 below).
3) **Cross-linking PIC nanoparticles can compensate weak multivalencies**. This was exemplified in Chapter 2, where the low multivalent peptide **P1** was unable to assemble PIC nanoparticles with poly(ethylene imine), whereas its derivative with cysteine residues $\mathbf{P1_{SH}}$, capable of cross-linking *via* disulphide bridging, led to well defined PIC nanoparticles under the same conditions. Nevertheless, $\mathbf{P1_{SH}}$ was unable to assemble PIC particles with Pol-B despite the presence of cross-linkers in this system, which reinforces the foremost importance of multivalency over other structural parameters of polyelectrolytes for PIC nanoparticle formulation.

4) **Intermediate stability is necessary in PIC nanoparticles for biological application**. Whereas poor stability in solution leads to premature and indiscriminate release of drug from PIC nanoparticles, very stable complexes have been shown in this Thesis to either lose their susceptibility to enzymes for targeted delivery (Chapter 3), or to trigger rather weak antimicrobial effects, probably due to very limited drug release (Chapter 4). As such, maximum particle stability should not be a fundamental goal when designing PIC particles for drug delivery, and a compromise between particle integrity and susceptibility should be established instead.

This Thesis has expanded the knowledge and applications of PIC nanoparticles in the biomedical field, and opens new avenues for the design of nanomaterials for the targeted and passive delivery of charged therapeutics. The optimisation of the enzyme-targeted system presented in Chapters 2 and 3 has great potential to allow localised drug delivery, and tune the therapeutic effect in response to the pathology by exploiting enzymes (*i.e*. disease markers) to adjust the release of drug. As such, future efforts should focus on the optimisation of the enzyme-responsive design of PIC nanoparticles presented here, and its application to the formulation of small charged therapeutics (*e.g*. antibiotics and anticancer drugs). To this end, the oligomerisation of the enzyme-responsive peptides introduced in Chapters 2 and 3 seems the most feasible approach to increase their multivalency, and thus aid the assembly of these responsive polypeptides with small charged drugs.